BIOACTIVE FACTORS SECRETED BY DIFFERENTIATING EMBRYONIC STEM CELLS

A Dissertation
Presented to
The Academic Faculty

by

Alyssa V. Ngangan

In Partial Fulfillment
of the Requirements for the Degree
Doctor of Philosophy in Biomedical Engineering in the
Wallace H. Coulter Department of Biomedical Engineering

Georgia Institute of Technology
August 2011

BIOACTIVE FACTORS SECRETED BY DIFFERENTIATING EMBRYONIC STEM CELLS

Approved by:

Dr. Todd C. McDevitt, Advisor
School of Biomedical Engineering
Georgia Institute of Technology

Dr. Andrés J. García
School of Mechanical Engineering
Georgia Institute of Technology

Dr. Robert E. Guldberg
School of Mechanical Engineering
Georgia Institute of Technology

Dr. Thomas Barker
School of Biomedical Engineering
Georgia Institute of Technology

Dr. Young-sup Yoon
Department of Medicine
Emory University

Date Approved: July 8, 2011

To my family – Mom, Dad, Tanya, and my husband, Brandon

ACKNOWLEDGEMENTS

My time here in the Biomedical Engineering Department at Georgia Tech and Emory has allowed me to develop my scientific knowledge as well as enjoy the other aspects of "lab life" and Atlanta. I could not have reached this point without the support of numerous people and am so grateful to have the chance to express my utmost gratitude.

First, I would like to thank my committee for their invaluable support over the past few years – Dr. Todd McDevitt, Dr. Thomas Barker, Dr. Andrés García, Dr. Robert Guldberg, and Dr. Young-sup Yoon. Their combined support and guidance has significantly impacted the success of my project, particularly through their push for scientific rigor. Dr. Barker's insight and expertise in matrix biology greatly impacted my work, especially with his suggestion to try out the CAM assay, which ultimately benefited the last studies of my research. Dr. García's guidance was not only through my committee interactions, but also as a mentor while I was an NIH Cell and Tissue Engineering Grant trainee. His straightforward and honest comments continued to challenge my scientific thinking, while making me strive to achieve a greater depth of understanding in my research. Dr. Guldberg always provided comments that influenced the big picture and made me reflect upon what I was trying to accomplish through my work. Additionally, his expertise with *in vivo* studies was quite helpful while determining my specific aims. As the clinician on the committee from Emory, Dr. Yoon always offered the therapeutic perspective and his expertise in stem cells and angiogenesis were invaluable. Each of these members of the committee has encouraged me through my research, and I thank you all for your time and commitment.

Through these nearly six years, the one person who has contributed significantly to my development as a scientist has been my advisor, Todd. I came to Tech wanting to get away from stem cell research, but I was curious to hear about Todd's newly formed lab, since it was the only ESC lab at Tech. His innovative ideas and approaches to studying stem cells was unlike what I previously encountered, so here I was again, feeding cells over the weekend. Todd always made it a point to make sure his door was open to his students, so it was not uncommon for me to stop by with some new data or discuss a number of research hurdles. Throughout the years Todd's lab has grown extensively and his schedule has achieved "rock star status" (according to Andrés García), but Todd always finds time to meet with his students. He has continued to challenge his students to work hard and think critically, in an encouraging manner, which has made him a great professor and advisor. Todd, your support and guidance as a mentor through these years have influenced me as a person and a scientist, and to you I am sincerely thankful.

There are a number of individuals in the BME department and the IBB who have contributed to this work. The bioinformatics expertise of Dr. Melissa Kemp and the statistical knowledge of Dr. Brani Vidokovic improved the gene array analysis for that particular manuscript. In the IBB core facilities, Sha'Aqua Asberry in the histology core and Steve Woodard in the microscopy core, have been tremendously helpful in training me on analytical instruments that were imperative to my research. I would also like to thank the BME academic advisors past and present - Beth Bullock Spencer, Shannon Oliver Sullivan, and Sally Gerrish; as well as the financial staff – Sandra Wilson, Penelope Pollard for their patience and helping me with all the paperwork over the years.

Not only were the members of the McDevitt lab great colleagues who challenged me scientifically, they are an entertaining group to have around during those long days n the lab. When I first joined the lab, there were four grad students – Rich Carpenedo, Ima Ebong, Rekha Nair, and Carolyn Sargent. To all of them, I thank you for setting up the lab a year earlier, which allowed me to get started in the lab once I joined. Ima was a great person who always had a smile on her face and a song in her head that she always was willing to share. At that point, Rich was the only guy in the lab who kept to himself, but came around once he found out we both shared an interest in golf and the Red Sox. Rich has not only been a great lab mate who asks those tough questions, but also has taught me quite a bit - particularly on the golf course and about strategies for competitive eating, so for those insights I must thank you. Rekha was the lucky student to pioneer the acellular EB matrix project, and I was able to build upon her work's strong foundation. In addition to being a great sounding board, Rekha, and her husband Kartik, have been good friends with whom I have enjoyed indulging in the fine foods Atlanta has to offer, as well as the other cities we visited together through the conferences we were fortunate enough to attend. Maybe we'll find out way back to Madrid one day to rectify "the incident" at the flamenco show. Rich, Rekha, and Carolyn have all inspired me to not only challenge myself scientifically, but also recreationally. Carolyn's endurance to train for a number of triathlons (and hopefully an Ironman soon!) was particularly inspiring, and she has somehow infected me with that bug. Not only was she was a great mentor while she trained Ken and I for our first triathlon, but also a good person who always lent an ear to anything I needed to vent about.

A year after I joined the lab, a cohort of three students followed: Andrés Bratt-Leal, Barbara Nsiah, and Ken Sutha. Andrés has a great sense of humor that can lighten up a long day in the lab. On numerous occasions, Todd has accidentally witnessed a few of Andrés's antics as he turns the corner in our student area. I am also thankful to Andrés for his leadership, especially in our "Pumping Iron Crew", where he ensures that we complete a hard workout before we gorge ourselves with a buffet lunch. Ken Sutha, fellow member of the "Pumping Iron Crew" and "workout husband", is always ready to lend a hand and has a smile on his face all the time – maybe it's because he is also descends from the "land of smiles" (Thailand), just like me. Barbara Nsiah, fair-weather friend of the "Pumping Iron Crew", is an independent woman who does not succumb to peer-pressure, though the lab is slowly breaking down that wall. She enjoys life the way she wants to enjoy it, and is a great shopping buddy since she knows how to find the deals. After a one year dry-spell of new grad students, Melissa Kinney, fellow Red Sox fan and Mac-user, joined our lab. Initially, Melissa started off pretty quiet, but she has acclimated to our lab quiet well and is always willing to help out. She has been very productive in her first few years, and I'm sure she will continue to do so. The latest McDevitt lab students – Kirsten Kepple, Anh Nguyen, Jenna Wilson, and Doug White are great additions to the lab, and I'm sure they will accomplish a great deal in the lab. The fellow graduate students in the lab have made my experience in the McDevitt lab a most enjoyable one with plenty of crosswords, eating challenges, and lab happy hours. So a "wicked big" thanks to you all.

The other members of the lab have been just as great as my fellow grad students. Dr. Priya Baraniak, our lab's first post-doc, has been a tremendous asset to the lab and

my work, particularly my writing. Priya has brought in a new perspective to lab and has hit the ground running during her time in the lab. The latest post-docs to join the lab – Dr. Ankur Singh and Dr. Krista Fridley, are both great additions to the lab and I'm sure they will make significant scientific contributions during their time in the lab. Marissa Cooke and Jesse McClellan are the lab managers who keep the McDevitt lab work horse running, and I appreciate all their hard work over the years to keep the lab running smoothly, especially Jesse who keeps those rotaries running. A special thanks to James Waring and Natalie Joe, two undergrads I mentored during my time at Tech. A special thanks to James, since he was the first undergrad I have ever mentored, and endured many 12-hour experimental time points. They both were very productive as undergraduate researchers in the lab, and I was impressed that they both could balance the lab work with classes, homework, and other college offerings.

Importantly, on a personal note, I want to thank my husband-to-be Brandon Kitchel. Six years ago he took a leap of faith and moved down to Atlanta with me after only dating for two years. Now after 8 years together we are finally making it official. He has been a rock through my grueling PhD journey – hearing about all the experiments gone wrong and making sure I'm taken care of as I write this dissertation. He is always making sure that I enjoy life to its fullest and that I don't give up on my dreams. He is one of the kindest souls I know, and I'm lucky to have him by my side for the rest of my life. Brandon, I am so grateful for all your support and encouragement through the years, I couldn't have done this without you.

Finally, I would like to give my greatest thanks to my family for their unwavering support throughout my life. My younger sister, Tanya, has always challenged me to be a

better person in life, in addition to making sure that I enjoy all the little things life has to offer. I am thankful and proud to be your sister. My parents have continuously pushed me to strive for excellence. My dad is one of the hardest working people I know, but he also makes sure that life doesn't just pass him by; so I thank you, dad, for making sure that I make the most of mine. The role model in my life is my mom – she is the strongest woman I know and has accomplished so much in her life. Mom, thank you for teaching me that with perseverance I can achieve anything.

TABLE OF CONTENTS

LIST OF TABLES

LIST OF FIGURES

LIST OF SYMBOLS AND ABBREVIATIONS

BMP	Bone morphogenetic protein
CM	Conditioned media
DNase	Deoxyribonuclease
ECM	Extracellular matrix
EBs	Embryoid Bodies
EBM	Embryoid body matrix
ESCs	Embryonic stem cells
FGF	Fibroblast growth factor
FT	Freeze-thaw
GAG	Glycosaminoglycan
HT	Heat treatment
IGF	Insulin-like growth factor
IPA	Ingenuity Pathway Analysis
PECAM	Platelet endothelial cell adhesion molecule
PDGF	Platelet derived growth factor
RT-PCR	Reverse transcription polymerase chain reaction
SIS	Subintestinal submucosa
VE-CAD	Vascular endothelial cadherin
VEGF	Vascular endothelial growth factor

SUMMARY

Angiogenesis is the biological process involving the expansion of existing vascular networks through the sprouting of endothelial cells from existing vasculature to grow new blood vessels. Current therapeutic strategies to stimulate endogenous angiogenic processes within injured tissue areas are typically based on introducing exogenous pro-angiogenic molecules or cell populations. Stem cell transplantation for angiogenic therapy aims to deliver populations of cells that secrete angiogenic factors and/or engraft in the new branching vasculature within the damaged tissue. Utilizing stem or progenitor cells has been shown to induce a rather robust angiogenic response despite minimal repopulation of the host vasculature, suggesting that stem cells may provide paracrine factors that transiently induce endogenous angiogenesis of tissues undergoing regeneration. Early differentiating embryonic stem cell (ESC) aggregates, referred to as embryoid bodies (EBs), can undergo vasculogenic differentiation, and also produce extracellular matrix and growth factors that induce proliferation, differentiation, and tissue morphogenesis. Taken together, the ESC extracellular environment may be an effective means by which to manipulate cell behavior. Thus, the ***objective*** of this project was to harness morphogens derived from ESCs undergoing differentiation and analyze their bioactive potential. The ***overall hypothesis*** was that the dynamic embryonic environment of EBs captured in an acellular matrix retains secreted bioactive factors and stimulates cells implemented in tissue remodeling.

Temporal patterns of phenotypic gene expression, including vasculogenesis, have been relatively well characterized during the course of differentiation; coincident patterns

of endogenous extracellular matrix (ECM) and growth factor expression that accompany pluripotent stem cell differentiation remain poorly defined. To examine the expression of extracellular factors within EBs, gene expression patterns obtained from low-density PCR arrays in conjunction with a variety of analytical tools were utilized to gain an understanding of the importance of extracellular factors in ESC differentiation. Gene expression analysis of ECM and growth factors by ESCs differentiating as EBs for up to 14 days was assessed using PCR arrays (168 unique genes total), and the results were examined by a series of different clustering and systems pathway analyses. As expected, significant decreases in molecules regulating pluripotent stem cell fate preceded subsequent increases in morphogen expression associated with differentiation. Pathway analysis indicated strong correlations between the expression patterns of ECM and growth factor genes and morphogenic cell phenomena, such as cell growth, migration, and intercellular signaling required for primitive tissue and organ developmental events. In addition, systems analysis of extracellular molecule expression alone identified key molecules and pathways potentially involved in the progression of pluripotent stem cell differentiation. Overall, these studies represented a novel framework to dissect the complex, dynamic nature of the extracellular biochemical milieu of stem cell microenvironments that regulate pluripotent cell fate decisions and morphogenesis.

Stem cells are being investigated as catalysts of tissue regeneration to either directly replace or promote cellularity due to traumatic injuries and degenerative diseases. In many instances, despite low numbers of stably integrated cells, the transient presence of cells delivered or recruited to the site of tissue remodeling globally benefited functional recovery. Such reports have motivated subsequent studies to determine how

paracrine factors secreted from transplanted cells may be capable of positively impacting endogenous repair processes. Thus, the effects of soluble factors secreted by ESCs during early stages of differentiation on exogenous cells (fibroblasts and endothelial cells) commonly involved in tissue remodeling events were investigated. The expression patterns and quantities of several growth factors involved in differentiation, including bone morphogenic protein-4 (BMP-4), insulin-like growth factors (IGFs) and vascular endothelial growth factor-A (VEGF-A), were analyzed as a function of ESC differentiation as EBs, and found to generally increase over time. Conditioned media collected from EBs at different stages of differentiation stimulated proliferation and migration of both fibroblasts and endothelial cells, based on BrdU incorporation and transwell assays, respectively. Overall, these results demonstrated that differentiating ESCs generally expressed increasing amounts of various growth factors that altogether were capable of stimulating mitogenic and motogenic activity in exogenous cells.

This soluble fraction of secreted factors contained within EB-conditioned media was compared to the matrix-associated factors produced by EBs, which led to the development of novel ESC-derived matrices via mechanical acellularization methods. Several acellularization protocols were applied to EBs, to develop a potential route to deliver ESC-derived molecules, independent of cells, to damaged tissues. Acellularization methods were developed to physically disrupt EBs via lyophilization or freeze-thaw cycling, and in combination with DNase treatment, while the efficacy of acellularization was based upon cell viability, DNA removal, and protein retention. Mechanical disruption and DNase treatment of EBs efficiently inhibited viability and removed DNA while retaining protein content to produce an acellular EB matrix.

Additionally, various batches of acellularized EBs consistently exhibited negligible amounts of endotoxin (< 0.5 EU/mL). Extraction of proteins from acellularized EBs demonstrated the presence of IGF-2 and VEGF-A growth factors retained in the acellular matrix. Biocompatibility of EB-derived acellular matrices was examined through the attachment and repopulation of the constructs by 3T3 fibroblasts in vitro. These studies demonstrated that mechanical means effectively acellularized EBs and were utilized in subsequent studies to elucidate the composition and bioactive potential of embryonic acellular matrices

The acellular embryonic stem cell-derived matrix was examined for its retention of bioactive factors that potentially could stimulate aspects of angiogenesis, including cell proliferation, chemotaxis, and structure formation as well as tissue morphogenesis. Protein extractions from EBM revealed that growth factors were harbored within the matrix in varying amounts depending on the day of EB differentiation. Following heat inactivation, BMP-4 and FGF-2 were no longer identified, contrary to IGF-2 and VEGF-A, which both showed increased amounts compared to non-heat inactivated EBM. The reaction of fibroblasts to EBM extractions was typically enhanced compared to basal level controls, in contrast to the inhibition of endothelial cells in response to EBM extractions. Endothelial cells were stimulated upon heat inactivation of EBM, especially during tube formation assays. The impact of EBMs on CAM angiogenesis was not as obvious of a response compared to EC migration and proliferation, yet altogether these bioactivity studies demonstrated the retention of bioactive factors within EBM.

In conclusion, this work has derived a novel embryonic stem cell matrix that is comprised of bioactive morphogens that further impact aspects of tissue remodeling,

particularly angiogenesis. Moreover, these studies have elucidated the modulation of extracellular factors that reflect the progression of EB differentiation, while providing a means to deliver these ESC-secreted factors in a cell-free manner. Future work will continue to elucidate the unique milieu of factors secreted by ESCs that will further advance the innovation of novel therapeutics that harness the potential of ESCs for tissue regeneration applications.

CHAPTER 1

INTRODUCTION

Tissue damage as a result of an ischemic event, such as myocardial infarction, stroke, or a chronic wound requires restoring blood flow to the area in order to rescue the injured site and prevent further injury. The biological process of angiogenesis involves the growth of new vessels through endothelial cell sprouting from existing vasculature to grow new blood vessels [1, 2]. Current therapeutic strategies to stimulate endogenous angiogenic processes within injured tissue areas are typically based on introducing exogenous pro-angiogenic molecules or cell populations. Isolated angiogenic growth factors have been examined as a potential therapeutic to stimulate an angiogenic response, with localized delivery resulting in slightly more effective blood vessel expansion in avascular areas than systemic delivery [3, 4]. However, purified growth factors are limited by the amount injected and their *in vivo* half-lives, thus a more robust reservoir of angiogenic growth factors that can be released over time would be more beneficial than a bolus injection.

Cell transplantation for angiogenic therapy is an approach to deliver exogenous cell that secrete angiogenic factors and/or integrate with the new branching vasculature in the damaged tissue. Utilizing stem or progenitor cells has been shown to induce a rather robust angiogenic response in ischemic tissues and improve overall healing by restoring normal tissue function [5-7]. However, isolating sufficient numbers of these stem cells from a primary source for transplantation has proven to be a challenge, thus necessitating their *in vitro* expansion and differentiation prior to transplantation. Although several cell

transplantation studies have been effective in rescuing injured tissues and inducing endogenous angiogenic responses *in vivo*, the number of engrafting cells is low, which has shifted the focus to paracrine effects of transplanted cells. A recent breakthrough study confirmed the importance of paracrine factors, revealing that ESCs transplanted into *Id* knockout blastocysts rescued the lethal knockout phenotype via extracellular factors secreted by the transplanted ESCs [8]. This seminal paper provided an interesting perspective on how to exploit ESCs for therapeutic applications.

Early differentiating embryonic stem cell (ESC) aggregates, referred to as embryoid bodies (EBs), generate a 3D *in vitro* environment, which mimics aspects of development, including cell proliferation, migration, differentiation, and tissue morphogenesis, including vasculogenesis. Evaluation of differentiated cell types present during EB culture has shown the presence all germ lineages, ectoderm, endoderm, and mesoderm. Furthermore, specific tissue morphogenesis within the EB, such as formation of primitive vascular structures, requires cellular response to particular matrix molecules and chemotactic gradients, which illustrates modulation of the extracellular environment due ESC differentiation.

Taken together, the ESC extracellular environment is an effective means by which to manipulate cell behavior, may it be modulating cell migration, proliferation, differentiation, or exerting a therapeutic response. Thus, the ***objective*** of this project was to harness morphogens derived from ESCs undergoing differentiation and analyze their bioactive potential. The ***overall hypothesis*** was that an acellular matrix capturing the differentiating EB embryonic environment retains secreted bioactive factors and

stimulates cells implemented in tissue remodeling. This hypothesis was tested by the following specific aims:

Specific Aim 1. Evaluate the expression of growth factors by ESCs undergoing cardiovascular differentiation within EBs. The *working hypothesis* was that progressive cardiovascular differentiation of ESCs within EBs would yield increased expression of endothelial cell markers as well as angiogenic growth factors. Investigation of EB differentiation towards the cardiovascular lineage was assessed by RT-PCR gene expression of endothelial markers, including *Flk-1*, *Flt-1*, *VE-Cadherin*, and *PECAM-1*, in addition to protein expression via immunostaining. The changes in expression of certain angiogenic growth factors were compared to the shifts in endothelial marker expression to evaluate the progression cardiovascular differentiation within EBs. Global gene expression of 168 extracellular factors, including extracellular matrix and growth factors, within EBs at days 4, 7, 10, and 14 of culture was assessed using low-density qPCR arrays and further analyzed via clustering methods (hierarchical and k-means), statistical testing, and pathway analysis. The secretion of growth factors by differentiating EBs was further examined by analyzing EB-conditioned media collected at different time points of EB culture. The content of specific growth factors, including VEGF-A, IGF-2, and BMP-4, was quantified using ELISAs while *in vitro* migration and proliferation studies were utilized to assess the bioactivity of factors contained within the EB-conditioned media.

Specific Aim 2. Develop acellularization techniques to isolate embryonic ESC-derived factors produced within EBs. The *working hypothesis* was that acellularized EB matrices would retain embryonic factors produced during EB differentiation. Mechanical acellularization techniques were developed to devitalize and remove cellular content from ECM and ECM-associated factors to yield acellular EB matrices. Two different methods of acellularization techniques were investigated, lyophilization and freeze-thaw, alone or in combination with DNase treatment. Quantitative metrics were assessed for cell viability via alamarBlue assay, total protein content using bicinchonic assay (BCA), and DNA content with PicoGreen®. More qualitative assessments on the resulting EB matrix were performed, including scanning electron microscopy (SEM), histology for overall matrix composition, and cell seeding for biocompatibility. These acellular EB matrices were tested for endotoxin content and further analyzed for specific growth factor retention using ELISAs.

Specific Aim 3. Determine the bioactivity of isolated embryonic acellular EB matrices *in vitro*. The *working hypothesis* was that ESC-derived embryonic factors isolated from EBs would stimulate exogenous cell types. The responses of NIH-3T3 fibroblasts and human umbilical vein endothelial cells (HUVECs) to ESC-derived matrix factors were analyzed via proliferation and migration assays. Proliferation assays were performed analyzed for bromodeoxyuridine (BrdU) incorporation of both cell types in response to EB matrix factors, while migration studies quantified chemoattractive cell migration as a result of EB matrix-derived factors for both cell types using a transwell insert. Additionally, the HUVEC network formation assay on growth factor-reduced

Matrigel™ was utilized to evaluate endothelial cell response to ESC-derived matrix factors.

Specific Aim 4. Evaluate the angiogenic potency of acellular EB matrices *ex ovo* using a quail chorioallantoic membrane (CAM) assay. The *working hypothesis* was that embryonic EBs undergoing vascular differentiation would yield a complex mixture of morphogens capable of promoting an angiogenic response. EB matrices (EBM) retaining growth factors were applied to quail chorioallantoic membranes (CAMs) to assess the angiogenic potency of the ESC-derived factors. Angiogenic responses were analyzed by quantifying the number of radiating vessels from the treatment location during the 48-hour treatment period. Additional analyses were performed on CAMs fixed after 48 hours to compare EBM treatments by quantifying the total percent vessel area per CAM in conjunction with a semi-quantitative measure of angiogenesis evaluated by scoring the change in blood vessel morphology surrounding the matrix graft.

This research is *significant* because it directly examines the bioactive potential of extracellular factors produced by ESCs as a mode to stimulate the different cell types involved in tissue remodeling, specifically angiogenesis. Evaluating the production and potency of angiogenic factors by differentiating EBs yielded insight into growth factors produced within an embryonic-like environment created by ESCs within EBs. These insights could advance developments in utilizing ESCs for regenerative medicine therapeutics. This work is also *innovative* because it demonstrates the ability to derive embryonic matrices to harness and deliver stem cell morphogens that in turn influence

exogenous cell and tissue responses. Ultimately, this work circumvents major issues involving ESC transplantation and exploits the benefits of ESCs by developing a novel means to deliver morphogens from an embryonic source in a cell-free manner.

CHAPTER 2

BACKGROUND

Stem Cells

Adult stem cells

The advent of stem cells several decades ago pioneered robust research that has established new frontiers in areas including biology, gene therapy, and regenerative medicine. The identification of colony-forming, self-renewing stem cells from the bone marrow [9, 10] motivated the identification of resident stem cells in a variety of somatic tissues including, but not limited to, the brain [11, 12], adipose and muscle tissue [13, 14], and the olfactory system [15]. A number of protocols have been published describing processes by which adult stem cells can be isolated, characterized, and expanded *in vitro* [16-18]. Due to the potential of adult stem cells to differentiate to a number of somatic cell lineages, these cells possess attractive therapeutic potential; yet the potency of these cells is limited based on the source.

Embryonic stem cells

The initial derivation of pluripotent embryonic stem cells (ESCs) was reported using mouse embryos a few decades after the advent of stem cells, followed by the development of culturing human embryonic stem cells in vitro 18 years later [19-21]. ESCs are the cells derived from the inner cell mass of the blastocyst that expand and differentiate to yield all somatic cell types. The pluripotency of embryonic stem cells has

been exploited to establish methods to direct ESC differentiation towards numerous somatic cell types *in vitro*. In particular, ESCs have been widely differentiated towards cells from the three germ lineages (ectoderm, endoderm, and mesoderm). Specific phenotypes achieved include: neurons (central and peripheral) [22, 23] and epithelial [24, 25] cells from the ectoderm, hepatic [26, 27] and pancreatic [28, 29] cells from the endoderm, and blood [30, 31] and muscle [32, 33] from the mesoderm. One of the extensively researched areas for *in vitro* ESC differentiation is mesoderm differentiation towards the cardiovascular lineage, especially the derivation of cardiomyocytes [34-38] and vascular endothelial cells [39, 40]. Typically, differentiation strategies involve culturing undifferentiated ESCs in an adherent culture with media containing soluble factors to direct differentiation, such as VEGF-A, BMP-4, [30, 31]. However, ESCs can also be differentiated via embryoid body (EB) formation, in which ESCs spontaneously differentiate into cells comprising the three germ lineages in a 3D environment recapitulating aspects of embryogenesis *in vitro* [41, 42]. EBs are widely used as an *in vitro* model system for embryogenesis, especially within the realm of vasculogenesis and angiogenesis [39, 43-46]. The formation of a visceral yolk sac containing blood-islands can be identified in spontaneously differentiating ESCs via EB formation in suspension culture [47]. .During *in vitro* EB culture, differentiating ESCs are capable of differentiating towards the endothelial lineage and forming vascular-like structures, [48-50]. The formation of these primitive vascular networks within the EB can typically be identified after 11 days of EB suspension culture, after which point they are capable to producing endothelial outgrowths given the proper conditions – a 3D matrix, like collagen, supplemented with angiogenic growth factors [45, 51, 52]. However, prior to

endothelial sprouting occurring, the environment within the EBs would have needed to be primed by the cells in order to induce vasculogenesis. Vascular-specific expression of phenotypic markers, including *flk-1, CD-31, tie-1, tie-2,* and *Ve-cad,* within intact EBs been well documented, thus recapitulating the progression of embryo vascular differentiation *in vitro* [48, 50, 53].

Induced-pluripotent stem cells

Unlike adult stem cells, ESCs are not capable of being patient-specific, which hinders the use of ESCs for clinical applications. Thus generating a cell that could be derived from a patient and possess the pluripotent nature of ESCs is an ideal cell source for potential therapeutic applications. Recently, the engineering of induced-pluripotent stem cells (iPSCs) has invigorated the stem cell field with numerous studies of somatic cell mimicking the pluripotent attribute of ESCs. The eminent discovery of iPSCs emerged from the Yamanaka group in 2006 using retroviral transduction of key pluripotent factors, *Oct-4, c-Myc, Sox-2,* and *Klf-4*, to reprogram mouse embryonic and adult fibroblasts [54], and was quickly followed by studies performed using human fibroblasts [55, 56]. Since then, a multitude of somatic cell types have been reprogrammed: keratinocytes [57], terminally differentiated lymphocytes [58] [59], neural cells [60-62], and liver cells [63, 64] using many methods to deliver pluripotent transcription factors: retroviral, lentiviral, transposons, adenoviral, plasmid DNA, protein, and RNA (reviewed in[65]). The recent developments concerning IPSCs have inspired stem cell biologists and bioengineers alike to exploit the therapeutic potential of IPSCs.

Angiogenesis

Angiogenesis is the sprouting of new blood vessels from existing vasculature and is present in both pathologic as well as regenerative responses. In an ischemic environment, endothelial cells (ECs) from surrounding vasculature are stimulated by angiogenic growth factors, released from macrophages or tumor cells, and expand the existing blood vessel network by proliferating and then migrating out of the vessel structure. The EC sprout continues to extend and form a tubular structure, eventually forming connections with other vessels in order to permit blood flow [1, 2]. The pathological angiogenic response has been widely researched in the realm of tumors where the development of vascular networks occurs in order to promote tumor growth. However, angiogenic responses during reparative processes are also being investigated in order to stimulate tissue regeneration. The angiogenic response within a damaged tissue, also termed revascularization, restores blood flow to compromised areas providing oxygen and nutrients to the surrounding cells in order to re-establish normal tissue function and stimulate repair. By restoring normal blood flow and oxygen levels in these compromised tissues, successful tissue regeneration can be achieved with concurrent angiogenesis, or revascularization.

Models to study angiogenesis

The process of generating new vasculature from existing vasculature primarily involves the migration and proliferation of endothelial cells. Several assays have been developed to examine the motogenic and mitogenic response of endothelial cells *in vitro* and have been reviewed to a large extent [66-69]. The proliferation of ECs can be

assayed using 3-(4,5-dimethylthiazol-2-yl)-2,5-diphenyltetrazolium bromide (MTT) assay to correlate the amount of formazan by-product with cell number [70]. An alternative mitogenic assay examines the incorporation of bromodeoxyuridine (BrdU), a thymidine analog, into the DNA during replication [71]. Furthermore, the migration of ECs as a chemotactic response can be quantified using a modified Boyden chamber assay, where ECs are plated into the top chamber, and the number of cells migrating towards the chemoattractive factors in the bottom chamber are quantified [72]. Each of these *in vitro* assays assesses more general cell behaviors; however, ECs are specialized cells and necessitate more specified tests for angiogenesis. Network formation assays examine the ability of ECs to form primitive tubular structures *in vitro* on a 3D matrix, typically Matrigel, in response to an anti- or pro-angiogenic molecule(s) [73, 74]. While organ cultures, such as the aortic ring assay [75], can evaluate the angiogenic response of endogenous ECs and other vascular cell types. Overall, these *in vitro* assays do not provide a complex angiogenic response, but are timely, efficient, and less costly compared to animal studies and provide a means to screen numerous treatment samples.

The angiogenic process is mediated by various cell types, physiological systems, and extracellular factors that cannot be thoroughly recapitulated *in vitro*, thus *in vivo* animal models are imperative in analyzing therapeutic angiogenesis. Several *in vivo* animal models have been established to examine the angiogenic response to a potential treatment. Non-injury models, such as the Matrigel plug assay and corneal angiogenesis assay, are modes to examine angiogenic stimulation by a test sample by evaluating the extent of vascular ingrowth present in the implanted material [76, 77]. Furthermore, the angiogenic and revascularization response can be analyzed in an injury model to

demonstrate the efficacy of a potential therapeutic treatment to rescue to a damaged area of tissue. One of the most widely used animal models for studying therapeutic angiogenesis is the hindlimb ischemia (HLI) model, typically performed in rabbits, rats, and mice. Inducing ischemia involves ligating and/or excising arteries in the hindlimb; however, ischemic severity is dependent on the surgical technique use, which can understate or overstate the observed results [78]. As with all *in vivo* models, animals are costly, generally span several weeks, and require technical expertise, but these models do provide the native complexity of an angiogenic response. Despite its limitations, the mouse hindlimb ischemia model is an effective and well-established *in vivo* model for evaluating angiogenic therapies within an ischemic environment.

Another *in vivo* or *ex ovo* method to examine an angiogenic response is through the use of a chorioallantoic membrane (CAM) assay. The CAM is comprised of two parts: (1) the allantois, the extra-embryonic tissue that is mesoderm-derived and contains primitive blood vessels and (2) the chorion, the membrane derived from the ectoderm surrounding the embryo [79]. Originally, CAMs were used by embryologists to study development in the chick embryo and were then utilized to examine the growth and vascularization of exogenous arterial grafts through a window created in the eggshell. However, modifications were made to permit efficient observations of the CAM using microscopy, including transferring the entire contents of the egg to a tissue culture dish and the use to quail embryos, which are smaller than chicks and permit culture in a 6-well plate format [80-82]. Upon transferring the embryo to a tissue culture dish, the embryos are typically allowed to grow between 8-10 days, at which point grafts and other angiogenic agents can be placed on the CAM to evaluate a vasoproliferative response

during a 48 – 72-hour time period [83, 84]. Numerous studies examining the angiogenic response of CAMs to purified growth factors, including FGF-2 [80, 85] or materials, including the gelatin sponge [86] and acellular tissues [87-89], have been performed. Angiogenic observations are quite noticeable, yet quantifying the angiogenic response is not as established as methods used for animal studies. The angiogenic response of the CAMs is qualitatively assessed through the use of stereomicroscopy images by observing the convergence, branching, and density of blood vessels surrounding the treatment and semiquantitaively analyzed by counting the number of converging vessels [86, 90]. The drawbacks to CAM studies are that they are performed in an avian embryonic environment that does not possess a mature immune system, which promotes inflammation-induced angiogenesis [91, 92]. Despite the drawbacks, positive aspects of the CAM assays are lower cost and shorter time studies compared to animal studies as well as the ability to screen a larger number of samples and groups.

Angiogenic therapies and growth factors

Surgical intervention to restore the vascularity of damaged tissues, particularly limbs and myocardium, involves opening up the occluded vessel via balloon angioplasty or the use of stents, bypass surgery, or excimer laser technology [93]. Recently, investigations of growth factor delivery to promote endogenous blood vessel growth have been successful with one FDA-approved growth factor-based therapeutic, [94], based on a recombinant form of PDGF, and several undergoing clinical trials, specifically assessing delivery of vascular endothelial growth factor (VEGF) and fibroblast growth factor 2 (FGF-2). Initial clinical trials have shown safety of use, but report mixed results

with respect to effectiveness [78, 95-100]. These advanced studies demonstrate the importance of extracellular factors in promoting revascularization, particularly angiogenic growth factors; however effectively delivering purified proteins *in vivo* has proven to be a challenge. Systemic delivery of growth factors for site-specific angiogenesis is not favorable due to multiple doses, off-target effects, short *in vivo* half life, and minimal effective concentration of growth factor at the in the target site [101]. Thus, localizing a source of angiogenic growth factors that can prolong release could provide a more effective means to deliver pro-angiogenic factors.

Angiogenesis and the ECM

Endogenous angiogenesis is regulated by the factors presented in the surrounding ECM [102, 103]. Not only do the matrix molecules themselves provide signals, but they can also regulate the release of soluble growth factors bound to the matrix to further enhance the response of surrounding endothelial cells. For example, several extracellular growth factors bind to heparin for stabilization and their activation or release is mediated by ECM changes, typically via enzymes, in order to stimulate certain biological processes including angiogenesis [104-107]. The importance of ECM and growth factor interactions has provided substantial motivation for bioengineering approaches to mimic the natural ECM environment [104, 108, 109]. Novel materials have been designed to function as ECM analogs with instructive bioactive sites (such as cell adhesion ligands, degradation domains, or growth factor binding sites) that can subsequently stimulate biological responses such as angiogenesis [110-113]. While engineered matrices can provide specific matrix molecules and growth factors, decellularizing native ECMs has

also been shown to be effective in retaining bioactive factors to stimulate angiogenic responses [88, 89, 114, 115]. These acellular matrices contain a more complex milieu of growth factors and matrix molecules (compared to engineered materials) that can generally work synergistically to elicit an angiogenic response.

Acellular Matrices

The ECM provides a natural scaffold for structural support of tissues and harbors a complex assembly of biochemical cues comprised of proteins, glycosylaminoglycans (GAGs), proteoglycans, and growth factors [109, 116]. Acellularization techniques provide a means to extract cells from tissues, thereby isolating the extracellular matrix (ECM) components native to the specific tissue [117, 118]. The primary criterion for successful acellularization is efficient inhibition of tissue viability coupled with preservation of native ECM composition and structure. Numerous tissues from various sources have been successfully acellularized in order to create scaffolds for tissue regeneration and include: small intestinal submucosa (SIS) [119], esophagus [120], bladder [121], cardiac valve [122, 123], dermis [124, 125], nerve [126], placenta [127], and pericardium [128]. More recently, entire organs have been acellularized, starting with the first report by Ott et al. of a whole rat heart [129]. Following the whole rat heart, rat liver [130] and rodent lungs [131-133] were then acellularized to provide intact 3D matrix structures with the vascular network preserved. These acellular organs supported cellular repopulation, demonstrating biocompatibility, and provide a potential means to tissue engineering entire organs.

As mentioned above, not only have tissues been acellularized, but several of these acellular matrices have also been utilized *in vivo*. Acellular pericardium has been used to repair rodent myocardial defects and showed infiltration of endogenous endothelial and smooth muscle cells [134]. Peripheral nerve segmentation injury in rats was treated with an acellular nerve graft that induced nerve regeneration and neovascularization [135]. Although the aforementioned examples used acellular tissues derived from the organs requiring repair, acellular tissues from one tissue source can also be successful in repairing different damaged organs. For example, SIS has been used for a number of tissue repair applications from arterial and venous grafts [136, 137], wound dressing [138], ventral hernia repair [139], to Achilles tendon repair [140]. The breadth of tissues that have been acellularized and successfully examined for tissue repair *in vitro* and *in vivo*, as well as the number of commercialized acellular matrix products currently available, attest to the utility of acellular tissue-derived materials as effective biomaterials. Nonetheless, derivation of matrices from a dynamic tissue source that not only can provide structural ECM components for cell engraftment, but are comprised of morphogens that can stimulate cellular remodeling of the matrix have yet to be examined.

Methods for acellularizing tissues

Various methods have been established to acellularize tissues using techniques that include solution-based treatments and mechanical disruption. Solution-based methods typically combine chemical treatments, such as detergents [126, 141-144], alkaline or acid solutions [145, 146], and hyper- or hypo-tonic solutions [144], as well as enzymatic reagents, including trypsin, endonucleases, and ectonucleases [147, 148].

Mechanical methods of acellularization provide a means to disrupt cells' plasma membranes, typically by repeated freeze-thaw cycles, sonication, or lyophilization [149-153]. Mechanical treatments alone are not capable of completely removing cellular content, thus a combination of physical and chemical/enzymatic methods is typically needed to successfully acellularize tissues. Additionally, perfusion systems have been used to acellularize whole organs while maintaining the original 3D structure. Solutions used to perfuse the organs via the vascular network included detergents, such as SDS, TritonX-100, or 3-[(3-cholamidopropyl)dimethylammonio]-1- propanesulfonate (CHAPs), and sometimes in combination with DNase enzymatic treatment [129-133]. The possible combinations of acellularization techniques needed are numerous due to structural variations in tissues, ranging from tissues with dense ECM content like tendons and dermis to ones with thin basement membranes like nerves and blood vessels. Furthermore, the duration of treatment/perfusion with detergents and or enzymes depends on the size and mass of tissue. Thus, there is no universal "optimal" method for acellularizing tissues, which suggests that the bioactive factors retained within the acellular matrix may vary based on the selected protocol.

Bioactive factors retained within acellular matrices

Protein characterization of acellularized tissues generally involves qualitative assessments of ECM proteins via histological staining, as well as more quantitative measure for collagens using the hydroxyproline assay, and GAGs using dimethylmethylene blue staining. Bladder and pericardial matrices acellularized using hypotonic buffers and DNase retained collagens and GAGs at levels similar to the native

tissue [128, 154, 155]. Acellular aortic valves exhibited reduced GAG, chondroitin sulfate, fibronectin, and laminin content after either Triton-X or Trypsin treatment, yet retained elastin and collagen matrix components [142]. Surprisingly, contrary to the numerous reports on tissues that have been acellularized, characterization of the growth factors retained within acellular matrices has not been as thorough. Only a few studies have demonstrated successful retention of bioactive growth factors within acellular matrices. FGF-2 was identified through immunostaining after tracheas were acellularized in 4% sodium deoxycholate and DNase [156]. Quantitative measures of two growth factors, VEGF and PDGF-BB, demonstrated preserved bioactive factors among four different acellularization treatments of porcine bladder [154, 157]. FGF-2 and TGFβ have been extracted and identified from acellular SIS, and increased cell mitogenicity *in vitro* was noted due to extracted factors [158]. The most extensive growth factor characterization was performed on acellular bladder submucosa matrix (BSM), identifying nine growth factors and comparing the efficiency of different buffers to extract these growth factors from the acellular BSM and in a bioactive form so that they could enhance cell proliferation *in vitro* [159]. All together, acellular matrices have been shown to be non-cytotoxic, permit cell infiltration, and subsequently aid in healing a number of damaged tissues, however the mechanism by which these matrices enhance tissue repair has yet to be elucidated.

Stem Cell Therapies for Cardiovascular Repair

The first clinical report of cell transplantation for angiogenic therapy emerged in 2002 from Tateishi-Yuyama et al. Injecting bone marrow-derived mononuclear cells

intramuscularly into patients with leg ischemia resulted in an increase in vessel formation and blood flow and successful limb salvage [7]. Since then, numerous stem cell therapy approaches have observed increased blood perfusion, capillary density, and improved angiogenesis utilizing a variety of cell sources to stimulate revascularization, including bone marrow-derived cells [6, 160-165], endothelial progenitor cells [166-169], and embryonic stem cells [170, 171]. In a single injury model of angiogenesis, MSCs [172] and early progenitor cells from human cord blood [173-175] have all shown revascularization induction and cytoprotective effects on endogenous cells within the hindlimb ischemia model. Additionally, differentiated cells derived from ESCs have been examined as a potential cell source for therapeutic cell transplantation, particularly ESC-derived ECs, since ECs are the primary cells involved in mediating angiogenesis and neovascularization. Endothelial-like cells derived from ESCs facilitated revascularization and inhibited muscle degeneration in ischemic models in mouse hindlimb, myocardium, and brain [171, 176, 177].

Specific negative outcomes from transplanting cells have included increased atherosclerotic lesion formation due to circulating vascular progenitor cells [178] and increased calcification within myocardium following transplantation of unselected bone marrow cells [179]. The utilization of pluripotent ESCs in angiogenic cell transplantation therapies has been investigated; however, the risk of teratoma formation *in vivo* generally outweighs the potential benefits of ESC transplantation [19]. Undifferentiated ESC populations transplanted to stimulate tissue repair typically result in teratoma formation at the site of injection due to the lack of controlled differentiation cues presented *in vivo*, [180-182]. Furthermore, the success of transplanting ESC-derived vascular cells, or any

ESC-derived cell type, depends on the ability to obtain sufficient numbers of cells for transplantation. Small rodent studies typically require on the order of 10^6 cells, which could translate to between 10^7 - 10^8 cells for human clinical trials, yet the efficiencies of directed differentiation protocols average < 5% of the total starting undifferentiated cell population. Regardless of the number of studies exhibiting cell engraftment, many have observed low incorporation of transplanted cells that differentiate and repopulate the ischemic tissue [172, 180, 183-185]. These studies suggest that upon transplantation, early multipotent cells produced extracellular factors that aid in the survival of endogenous cells needed to build new blood vessels. Thus, further studies examining the contribution of cellular versus extracellular factors during cell transplantation for tissue regeneration must be done to elicit more definitive modes of action of stem cell therapies that may lead to more innovative and effective therapies designed to target those mechanisms.

Stem Cells' Paracrine Mode of Action

One means of delivering stem cell-secreted soluble factors to injured tissues is through the use of stem cell-conditioned media (CM). To date, the release of paracrine factors into media by an array of stem cells has been characterized and analyzed for their effects on a variety of cell types and tissues. Recently a number of reports describe high-throughput analyses of extracellular molecules, or secretomes, produced by stem cell populations. Characterization of secretomes from a variety of stem/progenitor cells, including adipose-derived stem cells [186], MSCs [187], and ESCs [188], reveal the

presence of numerous factors implemented in angiogenesis and tissue repair and provide insight into mechanisms by which these cells promote overall healing.

Subsequent studies further assess the impact of stem/progenitor secretomes *in vivo*. CM generated by amniotic fluid-derived stem cells contained several pro-angiogenic molecules, such as stromal cell-derived factor (SDF)-1, IL-8, and VEGF, and promoted arteriogenesis in a murine hindlimb ischemia model [189]. Studies examining MSC-CM resulted in accelerated *in vivo* wound healing, attributed to the recruitment of macrophages and endothelial lineage cells [190], as well as improved left ventricular function after myocardial infarction [191]. Comparisons between MSC- and ESC-conditioned media perfusion following global ischemia demonstrated greater cardioprotective effect and decreased expression of proinflammatory cytokines in rat hearts treated with the ESC-CM [192].

Additional studies examining the effects of ESC-derived paracrine factors revealed positive influences on tissue regeneration. *In vitro*, ESC-CM enhanced bone marrow progenitor cell survival and decreased apoptosis, potentially due to several secreted factors including macrophage-colony stimulating factor (CSF), stem cell factor, and VEGF [193]. Additionally, inhibition of cardiomyocyte apoptosis was mediated by tissue inhibitor metalloproteinase (TIMP-1) presented in ESC-CM [194]. Furthermore, soluble ESC-secreted molecules have demonstrated efficacy, potency, and long-lasting effects on endogenous cells, most notably rescuing embryonic lethal *Id* knockout mice [8]. Overall, the factors secreted by stem cells and harbored in conditioned media retain bioactivity to promote regenerative processes. These cell-free examinations of stem cell-

secreted paracrine factors motivate alternative methods to utilize the therapeutic potential of stem cells.

CHAPTER 3

GENE EXPRESSION SIGNATURES OF EXTRACELLULAR FACTORS DURING EMBRYONIC STEM CELL DIFFERENTIATION*

Introduction

For nearly three decades, embryonic stem cells (ESCs) have been used as a model of mammalian developmental morphogenesis in order to define and characterize mechanisms of self-renewal and differentiation of pluripotent cells [20, 21, 195]. The pluripotent differentiation potential of ESCs and derivation of human ESCs have also motivated the pursuit of regenerative ESC therapies to restore endogenous cells to tissues afflicted by traumatic injuries or chronic disease [19, 42]. In recent years, an increasing emphasis has also been placed on the potent paracrine morphogenic effects of molecules synthesized and secreted by stem cells, including ESCs [8, 194, 196]. *In vitro*, ESCs are commonly induced to differentiate via the spontaneous assembly of cell aggregates in suspension referred to as embryoid bodies (EBs) [44, 197]. The temporal sequence of ESC differentiation that occurs spontaneously within EBs recapitulates several aspects of early embryogenesis, including gastrulation to yield derivatives of the three germ lineages – ecto-, endo-, and mesoderm [42, 44]. While most studies of ESC differentiation have focused on the temporal expression changes of intracellular signaling

---

* Modified from:
R Nair†, A Ngangan†, ML Kemp, and TC McDevitt. *Gene expression signatures of extracellular factors during embryonic stem cell differentiation: systems analysis approaches for evaluation low-density arrays*, in preparation. † Both authors contributed equally to this work.

molecules and phenotypic markers that accompany differentiation, the complex patterns of extracellular molecule expression by differentiating pluripotent stem cells that can significantly influence cell phenotype(s) remain less well defined.

Exogenous administration of combinations and sequences of ECM and growth factor molecules has been attempted to direct the differentiation of stem cells *in vitro* to many cell phenotypes by precisely controlling the biochemical composition of the cell microenvironment. This strategy, often based on well-established principles of developmental biology, has been successfully employed to direct pluripotent stem cell differentiation, but many protocols are not highly efficient. For example, growth factors such as bone morphogenetic proteins (BMPs), fibroblast growth factors (FGFs), and vascular endothelial growth factor (VEGF), as well as adhesive ECM proteins, such as fibronectin, collagens, and laminin, have been commonly applied to promote the differentiation of particular cell fates [198-201]. The development of high-throughput combinatorial array technologies can facilitate more rapid, parallel screening of ESC differentiation effects by a broad contingent of ECM and growth factor molecule combinations [202, 203]. Despite the wealth of information gained from studies of exogenously applied extracellular molecules, curiously much less is known about the inherent ECM and growth factors produced by ESCs as a consequence of differentiation. Some studies have begun to examine the gene expression profile of early EBs using microarrays [204-206], while others have investigated aspects of the EB transcription factor [207] and glycomics profiles [208]. In addition, the endogenous production of specific individual matrix molecules has been found to correlate with specific cell phenotypes [209-211], suggesting that the molecules produced locally within EBs can

influence ESC differentiation. Thus, globally examining the temporal profile of endogenous ECM and growth factor expression by ESCs during the course of EB differentiation could yield new insights into the extracellular factors regulating the different stages of pluripotent stem cell differentiation.

Microarrays have been widely used to screen for and identify key regulators in complex systems, resulting in the development of systems analysis approaches to dissect the molecular dynamics in cellular microenvironments. In such dynamic systems, the often-studied temporal changes drastically increase the amount of data; as a result, typically only the most significantly changing genes are reported and dominate the subsequent forms of analysis, while many potentially equally important genes and classes of molecules remain buried within the massive wealth of data obtained. As an alternative, microarrays have inspired the development of low-density array technologies that enable the investigation of a more focused subset of molecules while still capturing the dynamic changes of a system such as differentiating stem cells.

In this study, initial single RT-PCR gene expression analysis focused on the spontaneous differentiation of EBs towards a cardiovascular lineage. Previous studies have indicated that spontaneously differentiating EBs have the potential to differentiate towards more vascular cell types [50, 212]. Thus gene and protein expression analysis evaluated endothelial cell differentiation within EBs using phenotypic markers, in addition to the expression of growth factors, particularly angiogenic growth factors. The differential expression of several individually assessed growth factor genes motivated a high throughout method to examine the expression of growth factors and other extracellular factors as EBs progressively differentiated over time. Therefore, global

assessment of the dynamics of ECM and growth factor expression associated with the differentiation of ESCs within the EB microenvironment using low-density PCR arrays for gene expression and pathway analyses. Gene expression of EB differentiation focused on ECM components, including cell adhesion molecules, matricellular proteins, integrins, and proteases, as well as growth factors, including members of the BMP, FGF, transforming growth factor β (TGFβ), and interleukin (IL) families. Gene expression profiles were contrasted using hierarchical clustering, k-means clustering, and statistical mapping to identify different global patterns of expression, as well as shared profiles of independent molecules; the combination of these approaches enabled the identification of groups of molecules expressing either coincident or divergent expression patterns. Subsequent pathway analyses highlighted key signaling pathways acting on transcription factors regulating ESC phenotype at different stages of differentiation that were reconstructed solely from ECM and growth factor expression data. Thus, characterizing the dynamic relationships between ECM/growth factor expression and EB differentiation using the novel analytical framework described provides new insights into the biochemical composition of the extracellular microenvironment regulating pluripotent stem cell biology and associated with early morphogenic differentiation events.

Methods

Embryoid body culture

Mouse embryonic stem cells (ESCs; D3 cell line) were initially expanded on a feeder layer of mouse embryonic fibroblasts and were subsequently cultured feeder-free for several passages on 0.1% gelatin-coated 150 mm polystyrene cell culture dishes

(Corning) with Dulbecco's modified eagle medium (Mediatech), supplemented with 15% fetal bovine serum (HyClone), 2 mM L-glutamine (Mediatech), 1x MEM non-essential amino acid solution (Mediatech), antibiotic/antimycotics (Mediatech), and 0.1 mM β-mercaptoethanol (MP Biomedicals, LLC). Undifferentiated cells were expanded prior to EB formation in the presence of 10^3 U/mL leukemia inhibitory factor (LIF) (ESGRO), which was added to the culture media upon each re-feeding. Cells were passaged every two to three days before reaching ~70% confluence. To initiate EB culture, ESCs were trypsinized from the gelatin-coated dishes using 0.05% Trypsin/0.53 mM EDTA (Mediatech). A density of 400,000 cells/mL was used to inoculate 10 mL EB cultures in 100 mm bacteriological grade polystyrene Petri dishes (Corning) using differentiation media (ESC media without LIF). EB suspension cultures were maintained on rotary orbital shakers (Barnstead Lab-Line, Model 2314) at 40 rpm at 37°C in 5% CO_2 for the entire duration of suspension culture. Previous work from our lab has demonstrated that rotary orbital suspension culture methods result in greater yields of homogeneous populations of EBs [213]. EBs were cultured in suspension for up to 14 days and re-fed every other day after collecting independent EB cultures via gravity-induced sedimentation in 15 mL conical tubes. Spent media was aspirated, and the cultures were replenished with 10 mL of fresh differentiation media before being placed back in the Petri dishes and returned onto the rotary orbital shakers.

Microscopy and histological analysis

EB morphology was monitored daily by phase microscopy for up to 14 days of differentiation using a TE2000 microscope (Nikon) and a Spot Flex camera (Diagnostic

Instruments, Inc.). For histological analysis, EBs collected at different stages of differentiation (4, 7, 10, or 14 days) were fixed with 10% formalin for 30 minutes and embedded in Histogel® (Richard-Allan Scientific). Histogel®-embedded samples were either frozen or paraffin processed. Samples for frozen embedding were soaked in 30% sucrose solution overnight at 4°C followed by embedding in OCT (Tissue-Tek) at -80°C. Samples in histogel were prepared for paraffin embedding with a series of xylene and alcohol rinses and embedded in paraffin. Frozen sections (10μm) were obtained using a cryostat (Microm Cryo-Star HM 560MV), and paraffin sections (5μm) will be acquired using a microtome. Prior to immunostaining, frozen sections were fixed in cold acetone for 10 minutes; paraffin sections were de-paraffinized. Paraffin sections were stained with hematoxylin and eosin (H&E) using a Leica AutoStainer XL and coverslipped using low viscosity mounting medium (Cytoseal™ 60). For immunostaining, slides were blocked and permeabilized simultaneously in 2% BSA and 0.05% TritonX-100, respectively, in PBS for 45 minutes at room temperature. After 3 rinses (5 minutes each) in PBS, slides were incubated with either PECAM-1 or VE-CAD primary antibody (Santa Cruz Biotech) diluted (1:200) in blocking solution for 2 hours at room temperature. Subsequent PBS rinses (3X) were followed by incubation with FITC-conjugated secondary antibody (Southern Biotech) diluted (1:200) in blocking solution for 1 hour at room temperature, counterstained with Hoechst (1:100 dilution) for 5 minutes at room temperature, rinsed in PBS with a final wash in dI H2O. Slides were mounted and cover slipped using Gel/Mount™ with anti-fading agents (Biomeda Corp.). All slides were imaged on a Nikon 80i microscope equipped with a SPOT Flex Camera (Diagnostic Instruments).

Quantitative reverse-transcription polymerase chain reaction

RNA was extracted from undifferentiated ESCs and EBs at days 4, 7, 10, and 14 of differentiation ($n \geq 3$ for each sample) using the RNeasy Mini Kit (Qiagen). Complimentary DNA was reverse transcribed from 1 μg of total RNA using the iScript cDNA synthesis kit (Bio-Rad), and real-time RT-PCR was performed using SYBR Green technology with a MyiQ cycler (Bio-Rad). Beacon Designer software was used to design forward and reverse primers for pluripotency and differentiation markers as well as for the housekeeping gene glyceraldehyde-3-phosphate dehydrogenase (*Gapdh*), which were each independently validated with appropriate positive cell controls. Relative levels of pluripotent gene expression were calculated compared to undifferentiated ESC samples and normalized to *Gapdh* using the $\Delta\Delta C_t$ method [214], whereas gene concentrations for differentiated markers were calculated based upon standard curves and normalized to *Gapdh* expression levels [215].

For SuperArray RT^2 Profiler™ PCR array analysis, cDNA synthesis was performed using the SuperArray RT^2 First Strand kit (SABiosciences). A genomic DNA elimination mixture was prepared by first mixing 0.5 μg RNA with 5x gDNA Elimination Buffer and RNase-free water and then incubating at 42°C for 5 minutes. The RT cocktail (5x RT Buffer 3, Primer & External Control Mix, RT Enzyme Mix 3, and RNase-free water) was prepared and added to the elimination buffer mixture. Each cDNA sample was synthesized in an iCycler Thermal Cycler (Bio-Rad) (15 minutes at 42°C, 5 minutes at 95°C) and diluted with RNase-free water after synthesis was complete. RT-PCR was performed by first preparing the experimental cocktail (2x SuperArray RT^2 qPCR Master Mix, first strand cDNA synthesis reaction, and RNase-free water) and then

equally distributing the cocktail (25μL) into all of the individual wells of the PCR 96-well array (Mouse Extracellular Matrix and Adhesion Molecules array or Mouse growth factors array). Only one gene, secreted phosphoprotein 1 (*Spp1*), overlapped between both arrays besides the housekeeping genes and internal controls. Each array was tightly sealed with optical thin-wall 8-cap strips and amplified in a MyiQ cycler (Bio-Rad) with a two-step cycling program (1 cycle, 10 minutes, 95^{o}C; 40 cycles, 15 seconds, 95^{o}C; 40 cycles, 1 minute, 60^{o}C). Fold changes in gene expression were analyzed using the $\Delta\Delta C_t$ method for quantification, whereby samples of EBs from different time points (days 4, 7, 10, and 14) were compared relative to undifferentiated ESC values after individual sample values were normalized to internal *Gapdh* levels.

Gene clustering analysis: hierarchical clustering and k-means

Gene expression changes by differentiating EBs were calculated as either fold change increases or decreases at each time point examined compared to ESCs, using *Gapdh* as the normalization gene as described above. Initially, the results of the independent ECM and growth factor PCR arrays were separately analyzed by Genesis (Release 1.7.5) array analysis software. Two-dimensional hierarchical clustering of the log2-transformed data sets was performed across the different genes and time points using Euclidean distance and average linkage clustering. The clustering results were represented visually by a heat map dendrogram, with green indicating decreased expression and red indicating increased expression relative to undifferentiated ESCs. The relative color intensity values corresponding to the magnitude of fold change (either an

increase or a decrease) were set between -7.0 and 7.0 to provide a distinct color range for all log-transformed magnitudes.

Prior to all further analysis, both ECM and growth factor array data were combined and no longer examined as distinct sets of genes. The average fold change values of ESCs and EBs of each gene from the entire time course were analyzed using k-means clustering analysis in Genesis software (version 1.7.5). In order to determine the optimal number of k-means clusters that sufficiently captured the different distinct profiles of the entire data set, cluster number was varied between 4 and 20 and evaluated for a maximum of 300 iterations. Analysis with fewer clusters (4-8) did not distinguish different patterns of expression as clearly, whereas larger numbers of clusters yielded some independent groups with as a few as 1-2 genes; therefore, subsequent k-means analysis was performed using 12 clusters. In the k-means graphs, the x-axis at zero represents the undifferentiated ESC baseline, and the centroid of each cluster is indicated by a black line (Figure 3B-M).

Statistics

Significance testing was conducted using SYSTAT (Version 12) software. For individual genes, expression fold change comparisons across time points were evaluated using a one-way analysis of variance (ANOVA) with subsequent post-hoc Tukey analysis to determine significance ($p < 0.05$). Significant differences in expression fold change between consecutive time points were depicted with a branch schematic for all genes from the array, with increasing or decreasing slopes representing positive or negative fold

differences, respectively, while non-significant differences were illustrated as horizontal lines.

Ingenuity Pathway Analysis (IPA)

Pathway analysis of genes that exhibited significant changes over time was performed using Ingenuity Pathway Analysis (Version 7.5, Ingenuity® Systems) to examine the biological functions and signaling pathways that were implicated in EB development. For each time point (days 4, 7, 10, and 14), fold changes (-46.25 to -1 and 1 to +513.58) were filtered in IPA using a minimum 2-fold change threshold; from these genes, a list of "focus" genes was generated that contained molecules present in IPA's knowledge database (78% of eligible molecules). Based on the resulting eligible genes from the array ("focus genes") and IPA's database containing gene associations (via physical or biological interactions), the top biological functions and networks for each time point were assessed. Biological functions were tested for significance ($p < 0.01$) using the Benjamini-Hochberg (B-H) multiple testing correction method to account for false-positives and were then ranked in order of most to least significant (–log (B-H p-value); presented here according to day 4 EB ranking results). Based on published literature reports, IPA generated networks that included interactions between the array molecules as well as connections between array molecules and other molecules present in the IPA database. Each of the networks generated by IPA included up to 25 focus genes and was assigned a relative score by the software reflecting the probability that a given gene in a particular network was present by chance, with higher scores indicating a lower likelihood (if probability of random gene placement = 10^{-x}, then score = x).

Results

EB differentiation

The time course of EB differentiation was examined morphologically and phenotypically prior to performing semi-global gene expression analysis. Using rotary orbital suspension culture, the formation of EBs and maintenance of the EB population remained relatively uniform over the time course examined (Figure 3.1A-D), similar to previously published reports [213]. Evidence of progressive differentiation was indicated by changes in the organization and morphology of the cells within EBs (indicated by black arrows), as well as the increasing appearance of cystic cavities (red arrows) (Figure 3.1E-H). The eosinophilic (pink) staining apparent by day 10 and accumulating by day 14 was visible primarily in regions of EBs with a lower cell density, possibly suggesting an increase in matrix deposition by the cells. Over time, the average fold change of *Nanog*, a pluripotent transcription factor (Figure 3.1I), decreased from 0.701 ± 0.18 at day 4 to 0.136 ± 0.06 by day 14 of differentiation (compared to ESCs). Conversely, the endoderm differentiation marker α-fetoprotein (*Afp)* was expressed at significantly increased levels by day 14 compared to all other time points examined ($p = 0.001$; Figure 1F). In addition, several genes indicative of ectoderm (*Nestin*) and mesoderm differentiation (*Gata4*, *Nkx2.5*, myocyte enhancer factor-2c, alpha myosin heavy chain, myosin light chain-2 ventricle) increased over time (data not shown), thus further confirming the expected time course of differentiation.

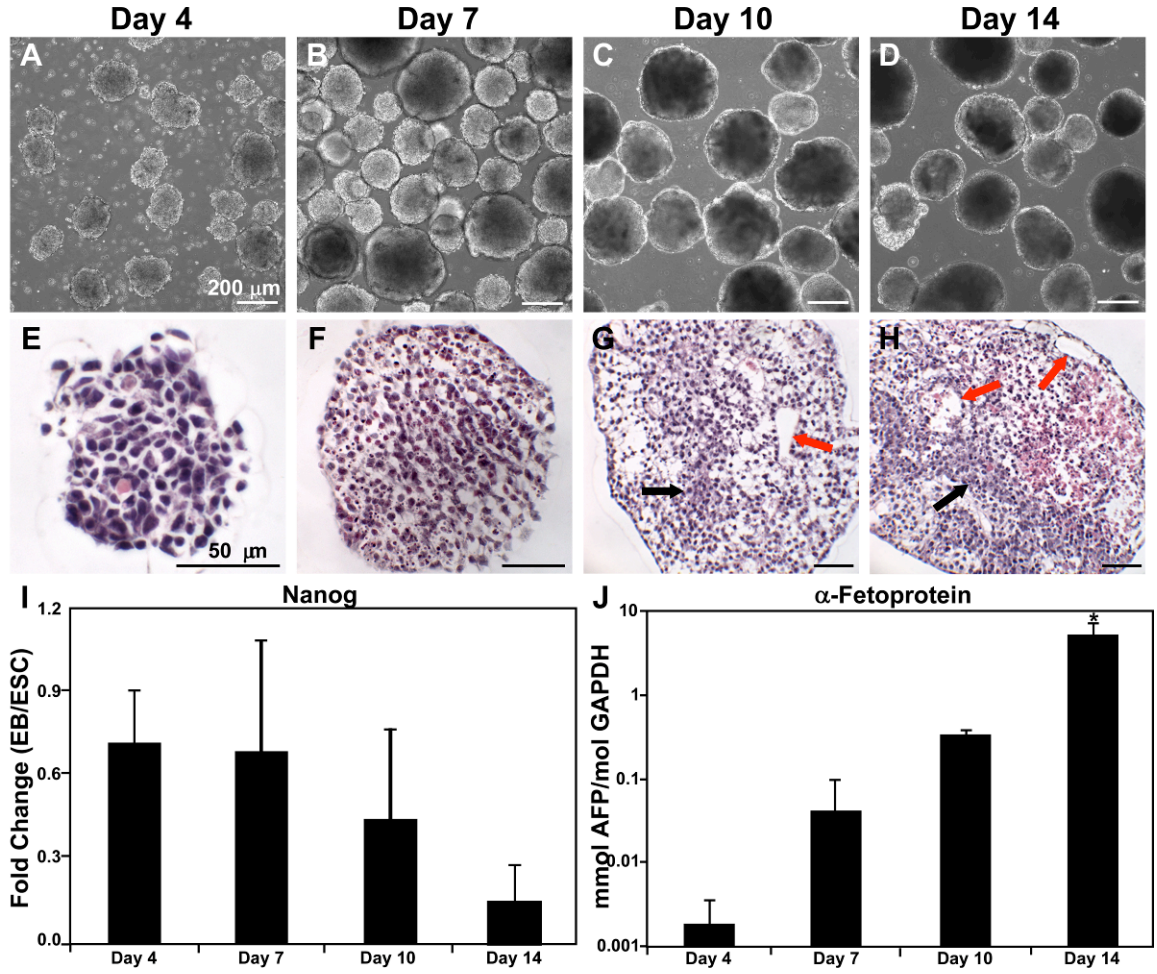

Figure 3.1. Embryoid body morphology and differentiation. (A-D) EBs cultured using rotary orbital culture maintained morphological homogeneity and increased in size over the course of differentiation. (E-H) H&E staining of EBs exhibited changes in cell organization and morphology within EBs (black arrows) and increasing appearance of cystic cavities (red arrows). (I) Gene expression of the pluripotent marker *Nanog*, relative to ESC levels, decreased as EB differentiation proceeded. (J) Conversely, gene expression of *Afp*, a marker of endoderm differentiation, increased significantly by day 14. * ANOVA: $p < 0.05$ compared to all other time points. Results indicated are mean±standard deviation (n=3).

The differentiation of EBs towards the endothelial lineage was examined over time using gene expression analysis of several phenotypic markers, including *Vegf-a* receptors *Flk-1* and *Flt-1*, and cell adhesion molecules *Pecam-1* and *VE-cadherin*. Over time, gene expression levels of endothelial cell adhesion molecules *Pecam-1* and *VE-Cad* increased from 3- and 5-fold at day 4 to 51- and 102-fold by day 10, respectively (Figure 3.2A). As for *Vegf-a* receptors *Flk-1* and *Flt-1*, gene expression levels for both remained relatively similar between days 4 and 10; however, the magnitude of the fold changes (compared to ESCs) between each gene was considerable, with *Flk-1* ~45-fold and *Flt-1* ~7-fold increases. Protein expression of both cell adhesion molecules PECAM-1 and VE-CAD was confirmed for EBs obtained at days 7 and 10, which exhibited the largest increases in gene expression during these time points. Within day 7 EBs, immunostaining demonstrated the expression both proteins was diffuse throughout the EB; whereas by day 10 the expression of both proteins was localized to the perimeter of the EB (Figure 3.2B). The coincident decrease in pluripotency and increase in germ lineage marker expression and later stage differentiation markers, as well as the EB morphological changes that occurred over 14 days of suspension culture were consistent with previous studies from our laboratory [213, 216, 217] that indicated progressive differentiation of the EBs.

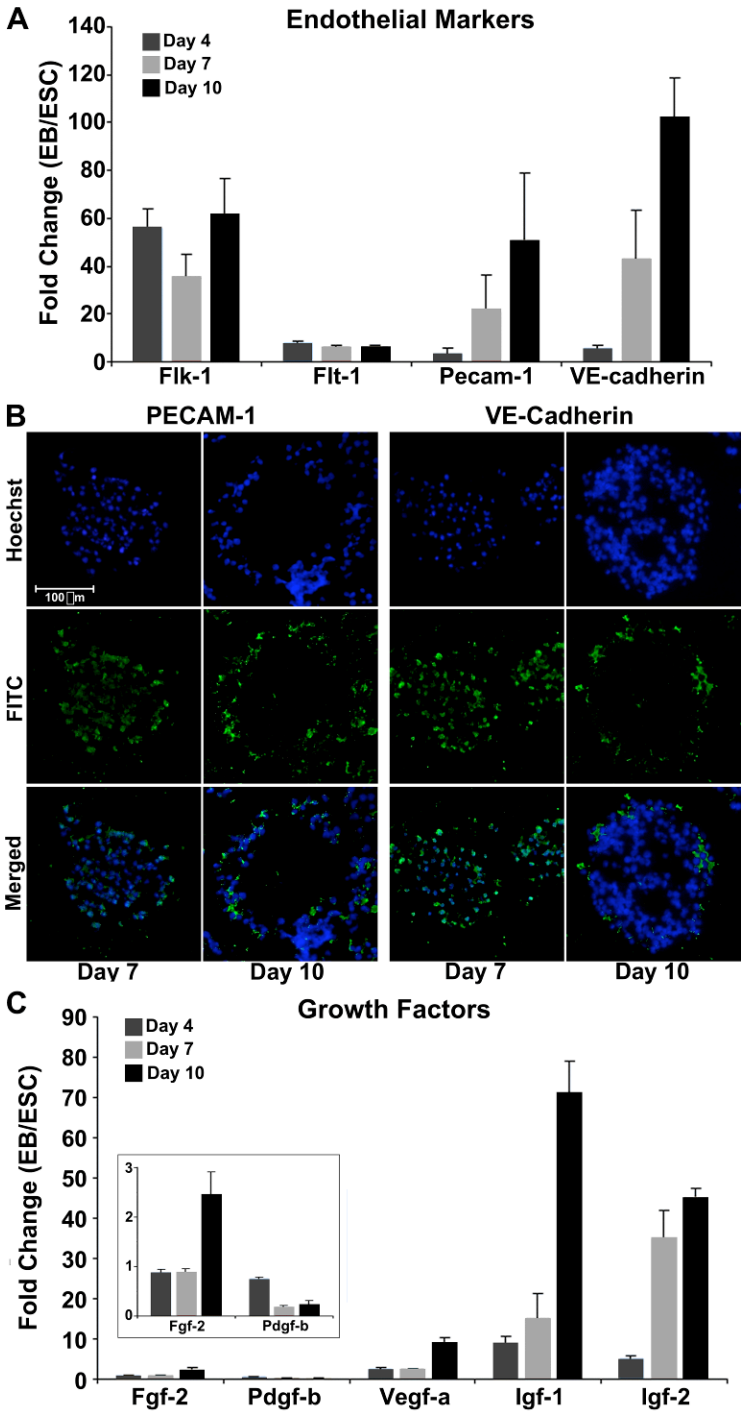

FIGURE 3.2. **Expression of endothelial phenotypic markers and growth factors.** (A) Gene expression of phenotypic markers of EC differentiation increased with EB differentiation. (B) Protein expression of endothelial markers PECAM-1 and VE-CAD (FITC) with nuclei counterstain (Hoechst). By day 10, EBs spatially regulate the expression of both endothelial markers. (C) Gene expression of several growth factors generally increased during EB differentiation. Results indicated are mean±standard deviation (n=3).

Initial insight into the expression of extracellular factors, particularly growth factors, by ESCs differentiating within EBs was evaluated on a gene-by-gene basis, including a few angiogenic growth factors, *Fgf-2, Vegf-a,* and *Pdgf-b*, as well as more development-specific growth factors, *Ifg-1* and *Igf-2* (Figure 3.2C). *Fgf-2* and *Vegf-a* were expressed at similar levels (~1-fold and 2.5-fold, respectively) between 4 and 7 days, yet increased in expression in day 10 EBs to ~2.5- and 9-fold, respectively. *Pdgf-b* was present at a slightly lower level (0.75-fold) than ESCs at day 4 and continued to decrease between 7 and 10 days (~ 0.2-fold). These three growth factors broadly affect a number of cells types, including specific roles in stimulating endothelial cells during angiogenesis. The *Igf*s were also examined for changes in gene expression during EB differentiation, particularly due to reported favorable effects of Igf-1 on angiogenesis [218, 219] and the role of *Igf-2* in up-regulating *Vegfa* and promting endothelial progenitor cell homing [220, 221]. *Ifg-1* and *Igf-2* expression levels steadily increased as EB growth progressed, starting from ~ 8.5- and 5-fold change at day 4 to 71-fold and 45-fold by 10 days, respectively. The diverse modulation of these different growth factors demonstrate the complex nature of EB differentiation within 10 days, which warranted a more global assessment of the differential expression of extracellular factors during ESC differentiation within EBs.

Gene clustering based on expression profiles

In order to visualize the general gene expression patterns exhibited by EBs and to identify any subsets of molecules undergoing coincident expression changes over time, two-dimensional hierarchical clustering was performed independently for both the

extracellular matrix and adhesion molecules array (referred to subsequently as the ECM array; Figure 3.3A) and the growth factors array (Figure 3.3B) to initially assess the clustering of genes within each array. In both the ECM and growth factor arrays, independent replicate EB samples examined at each of the individual time points clustered together; in addition, the earlier (4 and 7 days) time points clustered separately from the later (10 and 14 days) time points, altogether demonstrating the reproducibility of the independent experimental samples as well as distinct shifts in gene expression occurring over the course of differentiation. For each array, increasing (red) and decreasing (green) patterns of gene expression over time were evident, while a number of genes also appeared relatively unchanged compared to undifferentiated ESCs over the period of time examined. In the ECM array, ~18% of the molecules (16 genes) clustered together and appeared to decrease considerably over time relative to ESC levels, while ~16% (14 molecules) consistently increased over the course of differentiation and clustered together. The remaining 66% (59 molecules) exhibited nominal changes roughly equivalent to baseline values (similar to ESC levels). In contrast to the ECM array, there were a greater number of genes from the growth factor array that clustered together due to their increasing (~29%; 26 molecules) or decreasing (~31%; 28 molecules) expression patterns. Within these relatively broad classifications, visibly distinct clusters emerged from both arrays, including five sharply increasing molecules in the ECM array that exhibited 46- to 513-fold increases compared to ESCs by day 14 (indicated by the black bar, Figure 2A). In contrast, 15 molecules in the growth factor array clustered together that exhibited as much as a 25-fold decrease compared to ESCs (black bar, Figure 2B). Overall, a larger percentage of genes in the growth factor array

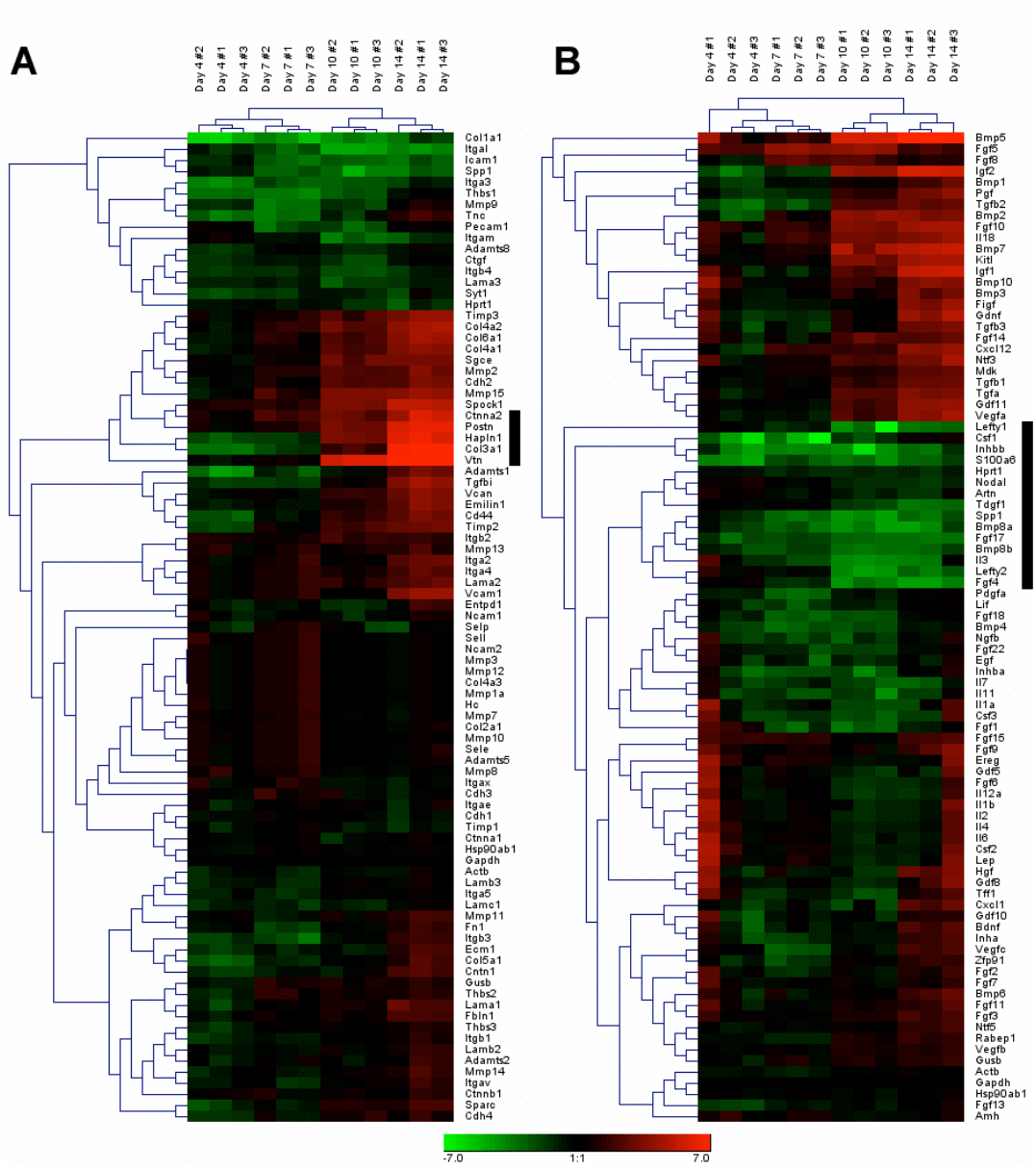

Figure 3.3. Hierarchical clustering of ECM and growth factor genes. Gene expression fold changes compared to undifferentiated ESCs were log2-transformed and analyzed using hierarchical clustering on Genesis software. Of the 84 extracellular matrix genes analyzed (A), approximately 34% of the genes demonstrated either an overall decrease (green) or increase (red) in gene expression relative to undifferentiated ESCs, whereas approximately 60% of the 84 growth factor genes (B) resulted in overall expression changes relative to ESCs. Black bars highlight noticeable gene clusters in each array set.

(~60%) exhibited either increasing or decreasing fold changes than genes contained within the ECM array (34%). Identifying such groups of genes in any data set may lead to the classification of subgroups that are similarly regulated over the given condition, but changes in the magnitude of gene expression alone are not necessarily sufficient to accurately yield insights into the key regulators of the system.

In addition to examining the ECM and growth factor arrays individually, a complete heat map of the entire set of experimental data from both arrays was generated using the average fold change values of each gene to examine how potential ECM and growth factors clustered together (Figure 3.4A). Based on hierarchical clustering, five groups of genes (labeled I – V) were identified whose expression pattern increased or decreased to varying degrees compared to ESCs (Table 3.1). Groups I and IV contained genes whose expression increased over the course of differentiation, while genes in groups II and V decreased, and those in group III remained relatively unchanged compared to ESCs. In order to more clearly define the temporal expression patterns embedded within the data, k-means analysis of the log2-transformed fold changes was performed (Figure 3.4B-M). Genes within the five groups identified in the heat map were represented in 12 k-means plots by the corresponding colors (red = group I, green = group II, grey = group III, orange = group IV, blue = group V), clearly showing the ability of k-means analysis to further distinguish subgroups embedded within the hierarchical clustering data set. As described in the methods, k-means analysis with a k-value of 12 captured an array of different expression patterns with a range of 6-29 genes per cluster (Table 3.2).

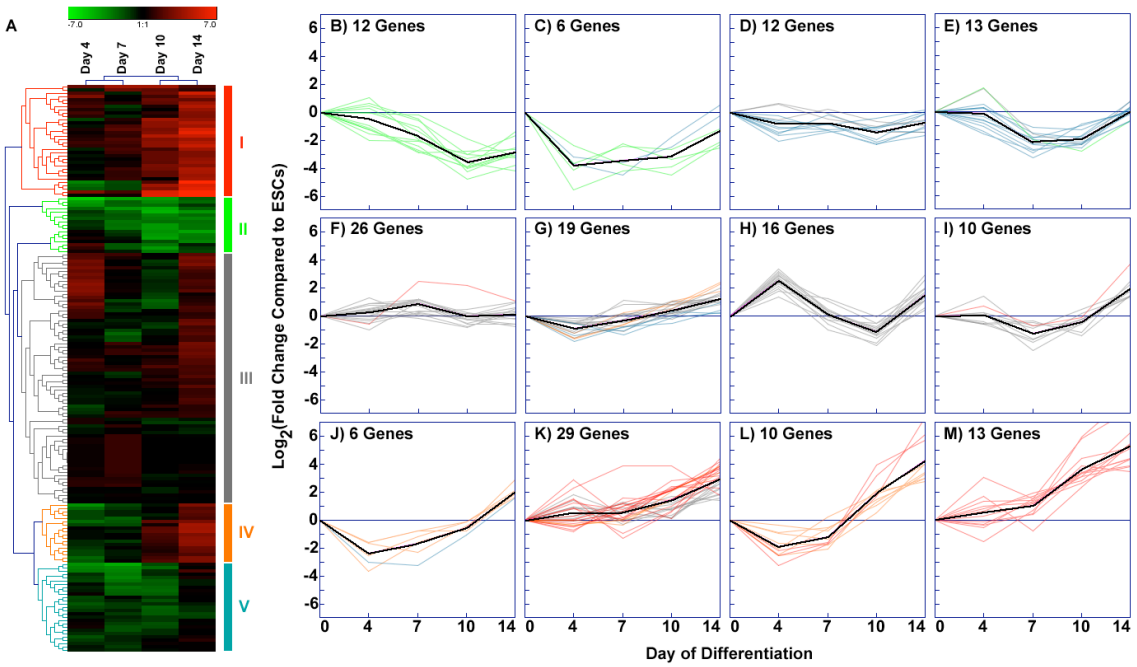

Figure 3.4. K-means clustering of combined array sets. (A) The hierarchical cluster produced by merging data from both the ECM and growth factor arrays exhibits several identifiable clusters, indicated by groups I – V. (B-M) K-means clustering of the combined data set highlights the subtle temporal changes in gene expression while clustering genes that follow similar patterns of expression over time. The expression profile for each cluster (panels B-M) is indicated by the solid black line, which connects the centroid at each time point. The colored lines in each panel correspond to genes in the color-coded groups (I – V) established by hierarchical clustering (A).

The k-means plots highlighted the dynamic nature of expression values associated with temporal changes, with few genes exhibiting continually increasing or decreasing profiles and only one centroid (black line) consistently increasing between each of the different time points examined (Figure 3.3M). Genes associated with the four k-means clusters where the centroid tended to decrease throughout differentiation (Figure 3.3B-E; 43 genes, ~25% of the total number of genes studied) came primarily from hierarchical cluster groups II and V, demonstrating the ability of k-means to distinguish additional specific groups of genes from the hierarchical clusters. In addition, genes that appeared to change nominally over time by hierarchical clustering analysis (group III) were divided into four different k-means plots (Figure 3.3F-I; 71 genes, ~41%), each containing centroids that exhibited differing profiles between the examined time points. Similarly, genes that clustered in groups I and IV were primarily distributed amongst four k-means plots (Figure 3.3J-M; 58 genes, ~34%) that almost exclusively contained genes exhibiting larger increases at later stages (post-day 7) of differentiation. Overall, the k-means cluster analysis largely sub-divided the groups initially generated by hierarchical clustering into more distinct temporal expression patterns, and thereby enabling the identification of several groups of ECM molecules and growth factors that shared similar temporal expression profiles and may therefore play coordinated roles in differentiation.

Table 3.1. Genes in each cluster represented in Figure 3.3.

Cluster I	Cluster II	Cluster III		Cluster IV	Cluster V
Fgf5	Col1a1	Fgf15	Vegfb	Adamts1	Csf1
Fgf8	S100a6	Fgf9	Ctnnb1	Col5a1	Thbs1
Igf1	Itga3	Gdf8	Fbln1	Cntn1	Tnc
Bmp10	Inhbb	Hgf	Adamts2	Ecm1	Pdgfa
Fgf14	Itgal	Ereg	Itgav	Itgb3	Mmp9
Ntf3	Bmp8b	Gdf5	Lamb2	Tgfb2	Bmp4
Gdnf	Fgf17	Il2	Ntf5	Tgfbi	Il11
Figf	Icam1	Il4	Mmp14	Gdf11	Fgf18
Bmp3	Bmp8a	Il1b	Cdh4	Vegfa	Inhba
Tgfb3	Spp1	Csf2	Thbs3	Tgfb1	Pecam1
Bmp2	Fgf4	Il6	Thbs2	Vcan	Adamts8
Kitl	Lefty1	Lep	Gusb	Pgf	Ctgf
Mmp15	Lefty2	Fgf6	Artn	Emilin1	Syt1
Ctnna2	Tdgf1	Il12a	Nodal	Lama1	Itgb4
Postn	Fgf1	Csf3	Selp	Bmp1	Lama3
Bmp7	Il3	Il1a	Cdh1	Sparc	Il7
Il18	Itgam	Tff1	Timp1	Cd44	Hprt1
Fgf10		Fgf2	Cdh3	Timp2	Egf
Spock1		Fgf7	Hc		Fgf22
Cxcl12		Gdf10	Mmp10		Ngfb
Mmp2		Bdnf	Mmp7		Lif
Cdh2		Cxcl1	Mmp1a		Lamc1
Tgfa		Entpd1	Col4a3		Fgf13
Col4a1		Inha	Mmp12		Itgb1
Sgce		Vegfc	Mmp3		Lamb3
Col4a2		Zfp91	Ncam2		Itga5
Col6a1		Fn1	Adamts5		Actb
Timp3		Itga2	Col2a1		
Vcam1		Mdk	Sele		
Col3a1		Itga4	Itgax		
Igf2		Lama2	Amh		
Hapln1		Bmp6	Mmp8		
Bmp5		Fgf11	Sell		
Vtn		Fgf3	Ctnna1		
		Itgb2	Ncam1		
		Mmp13	Itgae		
		Rabep1	Hsp90ab1		
		Mmp11	Gapdh		

Table 3.2. Genes in each k-means plot represented in Figure 3.3.

Cluster B	Cluster C	Cluster D	Cluster E	Cluster F		Cluster G
Bmp8a	Csf1	Adamts8	Egf	Fgf8	Mmp7	Rabep1
Bmp8b	Col1a1	Timp1	Fgf22	Amh	Mmp8	Lamb3
Fgf17	Itga3	Hprt1	Ngfb	Adamts5	Ncam2	Sparc
Fgf4	Thbs1	Nodal	Fgf1	Ctnnb1	Sele	Vegfb
Lefty1	S100a6	Lama3	Lif	Cdh3	Sell	Cdh4
Lefty2	Inhbb	Ctgf	Pecam1	Col2a1	Itgax	Itgb1
Tdgf1		Syt1	Csf3	Col4a3	Hsp90ab1	Lama1
Icam1		Il7	Il11	Hc	Gapdh	Lamb2
Itgal		Itgb4	Inhba	Itgae	Ctnna1	Mmp14
Itgam		Lamc1	Pdgfa	Mmp10	Selp	Thbs3
Spp1		Actb	Fgf18	Mmp12	Cdh1	Bmp1
Il3		Artn	Mmp9	Mmp1a	Ncam1	Fgf13
			Bmp4	Mmp3	Fgf7	Ntf5
						Adamts2
						Fbln1
						Itgav
						Thbs2
						Gusb
						Itga5

Cluster H	Cluster I	Cluster J	Cluster K		Cluster L	Cluster M
Gdf5	Entpd1	Adamts1	Mdk	Ntf3	Col3a1	Bmp7
Il1b	Vegfc	Col5a1	Itga2	Tgfb3	Emilin1	Ctnna2
Il2	Fn1	Ecm1	Itga4	Cdh2	Pgf	Spock1
Csf2	Mmp11	Cntn1	Itgb2	Mmp2	Tgfb2	Bmp2
Ereg	Bdnf	Itgb3	Lama2	Cxcl12	Cd44	Bmp5
Fgf15	Cxcl1	Tnc	Mmp13	Gdnf	Tgfbi	Fgf10
Fgf6	Inha		Vcam1	Tgfa	Timp2	Igf1
Gdf10	Figf		Bmp10	Tgfb1	Vegfa	Il18
Gdf8	Fgf2		Bmp3	Col4a1	Hapln1	Kitl
Hgf	Zfp91		Bmp6	Vcan	Igf2	Col4a2
Il12a			Fgf11	Sgce		Mmp15
Il1a			Fgf14	Timp3		Postn
Il4			Fgf3	Gdf11		Vtn
Il6			Fgf5	Col6a1		
Lep			Fgf9			
Tff1						

Parallel analysis of variance (ANOVA) significance testing

Although hierarchical and k-means clustering analysis enabled the identification of subgroups of genes that were similarly expressed over the course of differentiation, the correlative relationships were based upon the magnitudes of fold change relative to the starting state (ESCs), but didn't account for statistical changes occurring between each of the discrete time points examined. Parallel independent ANOVA analysis for each gene was therefore performed to evaluate significant changes in gene expression over time (Figure 3.4). In general, the number of genes exhibiting significant differences in expression between time points increased with the progression of development. Approximately 16% of the genes examined changed significantly between day 0 (ESCs) and day 4, 10% between days 4 and 7, ~22% between days 7 and 10, and ~44% between days 10 and 14. By day 4 of differentiation, ~89% of the molecules that changed significantly exhibited decreases in gene expression compared to ESCs, whereas by day 14, ~99% of genes that changed significantly increased compared to day 10. These contrasting patterns suggest that decreased expression of a small subset of extracellular factors followed by increased expression of many matrix and growth factor morphogens accompany ESC differentiation within EBs.

The ANOVA results were depicted in the form of a statistical "tree" to distinguish the numbers of genes either increasing, decreasing or not changing significantly between each of the time points of differentiation examined (Figure 3.4A). A third of the genes (58 out of 171 total) did not change significantly throughout the entire 14-day EB culture period (Figure 3.4B), including *Fgf2*, matrix metalloproteinase 2 (*Mmp2*), and the

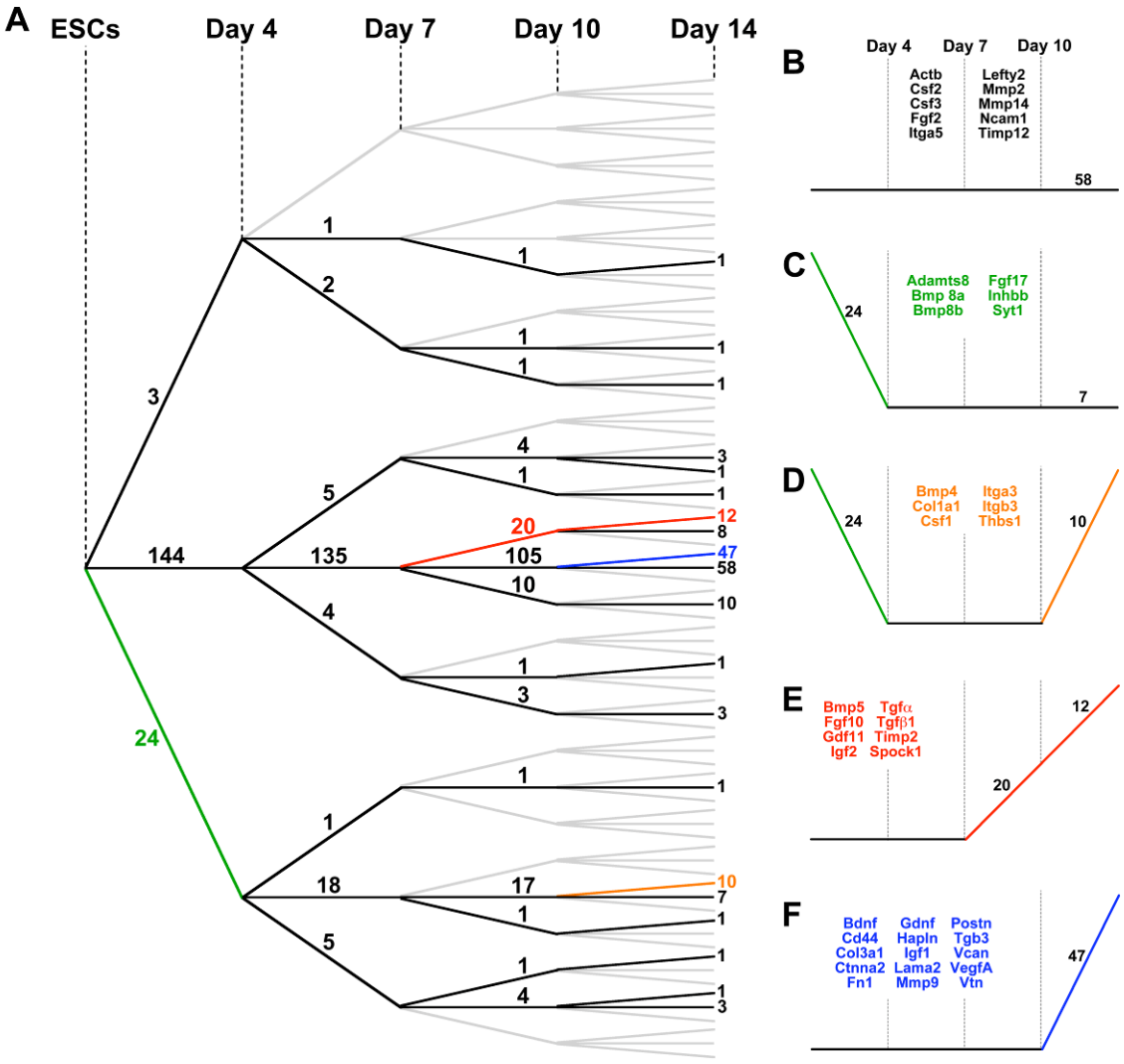

Figure 3.5. Parallel ANOVA analysis. (A) ANOVAs were performed across each time point for individual genes from both ECM and growth factor arrays. Results are depicted using a tree schematic, where the slope of the line between each time point indicates a significant increase (positive slope), significant decrease (negative slope), or no significant changes (zero slope). The number of genes in individual categories is shown on each line. A majority of the genes analyzed do not change significantly by 14 days of EB culture; however, a large number of genes significantly increase in expression between days 10 and 14. (B-F) Each graph highlights individual profiles of statistical changes in gene expression, including the number of genes encompassed in the respective profile and a sample of specific genes.

Table 3.3. List of genes represented in Figure 3.4B-F.

Figure 3.5B 57 genes		**Figure 3.5C** 24 genes	**Figure 3.5D** 10 genes	**Figure 3.5E** 12 genes	**Figure 3.5F** 47 genes	
Actb	Il18	Adamts8	Bmp4	Bmp5	Adamts1	Hapln1
Adamts2	Il1a	Bmp4	Col1a1	Fgf10	Bdnf	Igf1
Amh	Il1b	Bmp8a	Csf1	Gdf11	Bmp1	Inha
Artn	Il2	Bmp8b	Ctgf	Igf2	Bmp3	Itga2
Bmp10	Il3	Col1a1	Fgf13	Kitl	Bmp6	Itga4
Cdh1	Il4	Csf1	Itga3	Rabep1	Cd44	Lama1
Cdh2	Il6	Ctgf	Itgb3	Spock1	Cntn1	Lama2
Cdh3	Il7	Fgf13	Itgb4	Tgfa	Col3a1	Lamb2
Cdh4	Inhba	Fgf17	Lamc1	Tgfb1	Col4a1	Lif
Csf2	Itga5	Fgf18	Thbs1	Tgfb2	Col4a2	Mdk
Csf3	Itgae	Hprt1		Timp2	Col5a1	Mmp11
Ctnna1	Itgav	Icam1		Zfp91	Col6a1	Mmp9
Ctnnb1	Itgax	Inhbb			Ctnna2	Ntf5
Egf	Itgb1	Itga3			Cxcl1	Pgf
Ereg	Lefty2	Itgal			Cxcl12	Postn
Fgf11	Lep	Itgb3			Ecm1	Tgfb3
Fgf2	Mmp13	Itgb4			Emilin1	Tgfbi
Fgf22	Mmp14	Lama3			Entpd1	Timp3
Fgf6	Mmp2	Lamc1			Fbln1	Tnc
Fgf7	Mmp8	Pdgfa			Fgf3	Vcam1
Fgf9	Ncam1	S100a6			Figf	Vcan
Gdf10	Ngfb	Spp1			Fn1	Vegfa
Gdf5	Ntf3	Syt1			Gdnf	Vegfc
Gdf8	Sele	Thbs1				Vtn
Hc	Sell					
Hgf	Sparc					
Hsp90ab1	Tff1					
Il11	Thbs3					
Il12a	Timp1					

housekeeping genes heat shock protein 90kDa alpha (cytosolic), class B member 1 (*Hsp90ab1*) and β-actin (*Actb*). In the previous analyses, hierarchical and k-means clustering results similarly indicated that expression of both *Hsp90ab1* (Figure 3.3A, F) and *Fgf2* (Figure 3.3A, I) did not vary with time. In contrast, the *Mmp2* (Figure 3.3A, K) and *Actb* (Figure 3.3A,D) profiles generated by the clustering methods suggested increasing and decreasing expression over time, respectively, indicating that conventional clustering analyses alone may not accurately convey the truly significant differences that emerge with progressive differentiation. Importantly, several distinct groups of genes that did change significantly during EB differentiation could be extracted from the statistical tree results, with each containing 4-27% of the total number of the molecules contained within the arrays (Figure 3.4C-F; Table 3.3).

Interestingly, specific families of molecules often tended to appear within the same statistical "branches", suggesting that related molecules may be coordinately regulated during the course of EB differentiation. For example, cadherins (4/4 genes analyzed in the array), fibroblast growth factors (6/17 genes), interleukins (10/10 genes), and matrix metalloproteinases (4/12 genes) all appeared within the group of genes that did not change significantly between consecutive time points (Figure 3.4B), whereas members of the transforming growth factor (5/5 genes), laminin (3/6 genes), and collagen (5/8 genes) families exhibited coordinate changes, such as increasing significantly between days 10 and 14 (Figure 3.4E,F). The increasing diversity of molecular expression profiles that appeared over the entire 14-day EB time course examined was presumably reflective of the complexity of the extracellular EB environment. Mapping significant changes in gene expression over time provides a global view of matrix

signatures that can highlight subgroups of statistically related molecules, independent of magnitude changes, whose coordinated increase or decrease in expression may be related to the course of specific differentiation events.

Pathway Analysis

Network analysis was performed using only the genes that changed significantly over the course of differentiation (~67% of all genes examined) and that exhibited more than two-fold expression changes compared to ESCs. Using the IPA database, biological functions represented by these genes were generated and ranked (only the highest- (A) and lowest-ranked (B) graphs are shown in Figure 3.6). Interestingly, processes that typically occur during embryonic morphogenesis consistently appeared among the top 10 functions for each time point, including "cell growth & proliferation", "tissue development", "cell movement", and "cardiovascular system development & function". In contrast, the lowest ranking functions (Figure 3.6B) largely included disease states not conventionally related with development, such as "auditory disease", "metabolic disease", and "renal and urological disease"; bars absent from the graph were indicative of functions where no array gene met the threshold criteria. Altogether, the ranking order of these functions suggested that the gene expression analysis of extracellular factors alone were reflective of global changes that are known to accompany ESC differentiation within EBs.

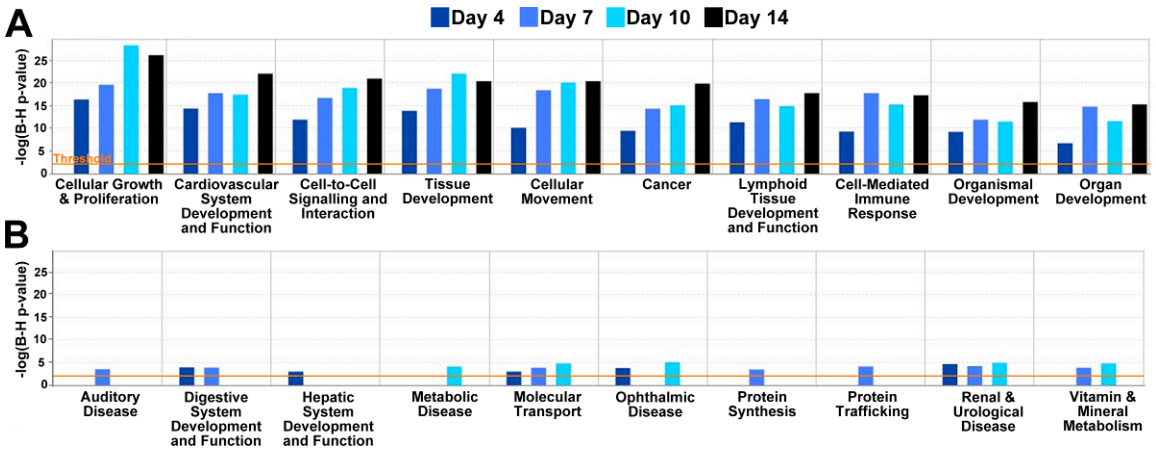

Figure 3.6. Biological functions related to global gene expression changes. Graphs of biological functions were generated using "focus" genes and the database of gene interactions present within Ingenuity Pathway Analysis software. (A) The ten highest-ranked biological functions that were significant at different differentiation time points consisted of processes typically related to development, including morphogenesis and proliferation. (B) In contrast, the ten lowest-ranked biological processes included disease states not typically associated with development.

The networks generated from the gene expression data highlighted the transition of the differentiating ESCs away from a pluripotent state (the top network for each time point is shown in Figure 3.7). Across the networks, several "hub" genes exhibited at least six network connections, including array genes fibronectin (*Fn1*; day 4), *Mmp9* (day 7), *Vegfa* (day 10), and insulin-like growth factor 1 (*Igf1*; day 14). At day 4 (Figure 3.7A), the top network was generated with 15 genes from the array (probability of random gene placement = 10^{-23}; i.e. score = 23). Many of the molecules included in the top day 4 network were related to the *p53* transcription factor that acts to suppress the pluripotent marker *Nanog* and thereby induce differentiation [222]. The top network at day 7 (Figure 3.7B) contained 17 of the array genes (score = 24) as well as several extracellular factors related to *p53*; however, there were several growth factors that act on *p53* in the day 4 network not present at day 7, indicating an emergence of different roles for growth factors by day 7. Along with the greater number of genes significantly increasing over time, the number of genes included in the networks at later time points also grew such that the top networks for days 10 (Figure 3.7C) and 14 (Figure 3.7D) contained 22 (score = 35) and 25 (score = 39) array genes, respectively. Interestingly, compared to earlier time points, the network at day 10 included several more nuclear factors, such as friend leukemia integration 1 (*Fli1*), TATA box binding protein-associated factor 4B (*Taf4b*), and cell division cycle 73 (*Cdc73*), linked to extracellular factors, but their connectivity was low (2-3 connections) compared to the number of connections formed to *p53* at days 4 and 7. This increase in the number of nuclear factors present in the day 10 network is suggestive of fewer shared nuclear targets by the

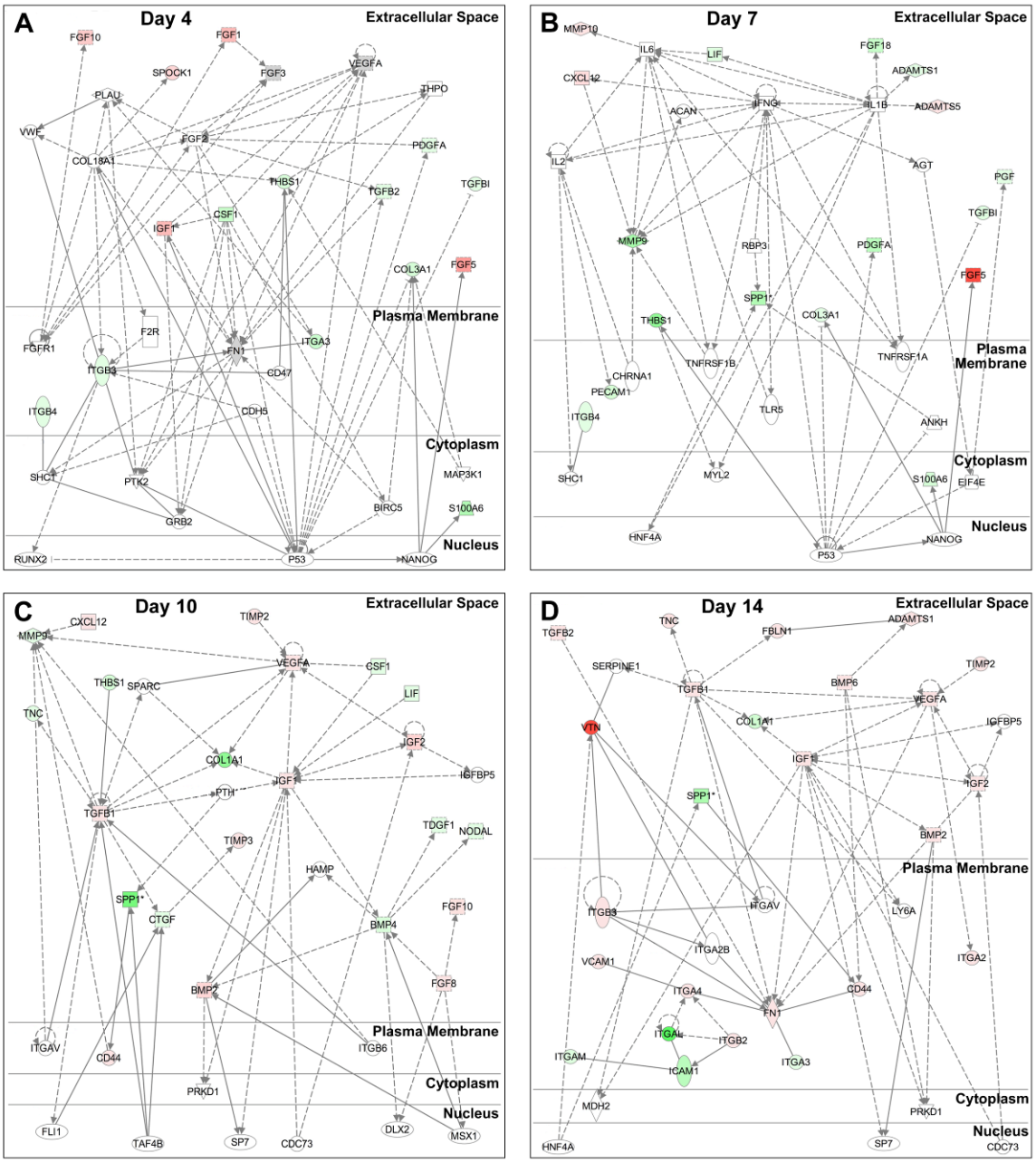

Figure 3.7. Gene networks identified during early EB differentiation. Network analysis using Ingenuity Pathway Analysis software was performed on genes that changed significantly over the course of differentiation and that exhibited at least a two-fold expression change compared to ESCs. The shift in the top networks between (A) day 4, (B) day 7, (C) day 10, and (D) day 14 demonstrates a progression from a more undifferentiated state (A) towards more differentiated ones (B-D). Relationships are divided into direct (solid line) and indirect (dashed line, - - - -) interactions, with arrow heads exhibiting the affected gene (⟶), as well as several "hub" genes. Varying intensities of green denote negative fold changes, while shades of red indicate positive fold changes over ESCs. Grey genes represent genes with fold changes less than 2 that are related to other genes in the network, while genes with no color were not contained in the array data set.

differentiating cells, possibly indicating the onset of diverging cell phenotypes. Overall, the physical and biological network connections generated using statistically significant array data highlight the ability of ECM and growth factor molecules alone to elucidate global trends in cell growth and differentiation as a function of time.

Discussion

A global view of the extracellular matrix and morphogen expression profiles of stem cells elicited the dynamic changes that occur coincidentally with differentiation. The individual assessment of specific genes of interest demonstrated the diverse expression profiles of a few genes as well as the necessity for analyzing the global changes in expression of extracellular factors. Hierarchical clustering highlighted general patterns of expression, which is useful for quick detection of subsets of genes that generally increased, decreased, or remained similar to baseline levels (in this case, undifferentiated ESCs). For the time-dependent data set presented here, two-way hierarchical clustering was useful for assessing whether non-consecutive time points exhibited any overall expression pattern similarities. K-means analysis was able to further parse out the temporal relationship across genes by isolating subsets of groups with distinct expression patterns. In order to statistically evaluate gene expression patterns, parallel ANOVAs were mapped to clearly highlight significant changes occurring between the different stages of differentiation. Finally, performing pathway analysis identified links between molecules while highlighting key regulator genes within each network.

As ESCs differentiate within the 3D EB environment, the extracellular gene expression patterns dynamically change according to the phenotypic and morphological changes occurring within the cells. Differentiation of ESCs within EBs is an increasingly complex process due to the heterogeneous differentiation of the cells to different phenotypes. By analyzing a large number of molecules simultaneously, subtle changes in expression can be used collectively to analyze the system, in contrast to the traditional approach of focusing on the gene expression changes of one molecule at a time [209]. However, results from individual gene analysis provided motivation to investigate a broad array of factors likely involved in differentiation. Importantly, ontological assessment of the extracellular genes (ECM and growth factors) included in the arrays provided links to intracellular genes, such as receptors and transcription factors, that were indicative of morphogenic changes occurring within the EB microenvironment. Analysis based on existing relationships, thus highlight overlapping roles of molecules during development in ESC differentiation *in vitro*.

In the EB system, a combination of the described analyses has provided a higher-level understanding of the influence of extracellular factors on morphogenic processes over the differentiation time course. The molecules that appear in the day 4 network primarily act upon the transcription factor *p53* that in turn decreases the pluripotent marker *Nanog*. Together, these results indicate the importance that growth factors may have in the early stages of EB culture to prime the system for differentiation or that. The ECM molecules present in the top day 7 EB network (Figure 3.7B) are largely proteases. By day 10 (Figure 3.7C), both ECM molecules and growth factors appear in the network, along with an increase in the number of connected transcription factors, suggesting the

onset of signaling related to a variety of differentiation events. Finally, the increased expression of a number of integrins by day 14 (Figure 3.7D) emphasizes the onset of cell movement and signal transduction events.

Complementary information provided from different forms of expression analysis provides an overall more comprehensive characterization of the temporal regulation of EB differentiation than individual analyses alone. Some molecules appear consistently throughout, but have different gene interactions, while others are unique to certain stages of differentiation. As an illustrative example, consider the changes occurring with *Vegfa*. This gene, which clustered with genes such as *Igf2* and *Tgfb2* within the growth factor array (Figure 3.2B, Figure 3.3L), was also found to be highly related to expression patterns of matrix proteins such as *Col3a1* and *Emilin1* (Figure 3.3L) when the two sets of array data were analyzed collectively. Furthermore, the ANOVA analysis upheld relationships with *Vegfa* when tested for statistical significance (Figure 3.4F). When visualized as a dynamically changing network, however, several additional features of *Vegfa*'s role in EB differentiation emerge. First, as indicated by the high degree of connectivity to other molecules in Figure 3.6A, signaling through this growth factor is likely important as early as day 4, even though its own expression was not higher than the 2-fold change threshold. Secondly, the high degree of clustering/statistical significance that emerges with other genes such as *Tgfb2* and *Col3a1* are due to regulation through common transcription factors (e.g. *p53*). Finally, tightly clustered proteins induce common effector molecules (e.g. *Fn1*) and one another (*Igf2* → *Vegfa*) to synergistically amplify extracellular cues associated with the EB differentiation process. Through this manner, functional relationships emerge from the data that allow for new hypothesis

generation and testing regarding exogenous molecules capable of affecting ESC differentiation.

Just as each individual analysis lends insight when examining specific molecules, the range of analyses presented is critical for extracting a more global perspective. Researchers often rely on a single method for assessing large data sets, typically either hierarchical clustering or pathway analysis, which can potentially result in overlooking molecules important to the system. For example, performing clustering (hierarchical or k-means) alone did not result in the identification of *Fn1* as an important molecule in the examined EB system, due to the fact that it didn't exhibit large fold changes over time. Further analysis using parallel ANOVAs shows that *Fn1* increases significantly by day 14 (Figure 3.5F), along with other key molecules such as *Ctnna2*, *Postn*, *Hapln1*, *Col3a1*, and *Vtn* that are highlighted in clustering analyses. Pathway analysis demonstrated that *Fn1* is a hub gene at both day 4 and day 14, suggesting its importance throughout the differentiation time course. In contrast, consider *Spock1*, which is highlighted in hierarchical clustering as exhibiting one of greatest increases in expression over time compared to ESCs, along with *Ctnna2*, *Postn*, *Hapln1*, *Col3a1*, and *Vtn*. K-means clustering also indicated an association between *Spock1* and *Postn*/*Vtn* (Figure 3M, Table 3.2), while ANOVA verified the gene's significant increase after day 7 (Figure 3.5E). However, *Spock1* was not included in the top networks at later time points of EB differentiation (days 7 – 14), although it was present in the top network at day 4 with a single connection. Analysis displayed a relationship between *Spock1* with *Col18A1*, a hub gene not included in the arrays, but highly connected to several ECM and growth factor genes contained in the arrays - *Vegfa*, *Fgf2*, and *Itgb3*, as well as other highly

connected genes - *p53* and *Fn1*. The aforementioned examples of *Fn1* and *Spock1* demonstrate that a combination of analytical tools can identify potential key regulators in the differentiation system that would have otherwise been overlooked by single forms of analysis alone.

Conclusion

The overall objective of this study was to investigate gene expression patterns obtained from low-density PCR arrays using a variety of analytical tools and to explore the utility of these assays in understanding the importance of extracellular factors in embryonic stem cell differentiation. ESCs undergo progressive differentiation within EBs and differentially express a number of ECM and growth factor genes. Although not typically used to examine differentiation patterns, variations in ECM and growth factor expression were indicative of more global changes occurring within the EB microenvironment, such as decreased pluripotency, cellular proliferation, and tissue morphogenesis. Low-density analysis of extracellular factors in dynamic environments highlights the importance of such endogenous molecules and their utility in assessing the temporal shifts in the system.

The clustering, statistical, and gene mapping tools may be critical to further understanding the role of endogenous ECM and growth factors in differentiation. Some studies have begun to elucidate the role that specific molecules play in ESC differentiation [209, 210, 223-226], although analyses that include a broader range of extracellular factors have thus far been somewhat limited [187, 208]. In order to analyze the wide spectrum of matrix molecules in this study, distinct methods were used that

either highlighted differences in expression patterns through clustering tools or focused on the relationships between the molecules via network analysis. Subsets of genes with diverging expression values (gene groups that between multiple time points had opposing signatures) emerged from k-means and statistical analyses. The simultaneous increase and decrease of different sets of molecules may be necessary for the onset of a particular differentiation event, and the identification of these sub-groups could be critical for further understanding the coincident cell phenotype specification. Studies that examine individual molecules largely remain one-dimensional and may lose the global view that contributes considerably to the fundamental understanding of the system. In contrast, the combination of clustering/statistical analyses with network mapping provides a multi-faceted approach that enables a more in-depth understanding of the dynamic EB microenvironment. Through these types of global analyses, the extracellular environment can further elucidate the ongoing biological process within EBs. Moreover, characterization of the molecules secreted by ESCs differentiating in EBs may aid in establishing the impact of ESC-derived extracellular factors.

CHAPTER 4

SOLUBLE FACTORS SECRETED BY DIFFERENTIATING EMBRYONIC STEM CELLS STIMULATE EXOGENOUS CELL PROLIFERATION AND MIGRATION*

Introduction

Tissue damage in adult mammalian species typically results in the formation of scar tissue that prohibits the recovery of normal tissue function, such as cutaneous wounds, brain and spinal cord injury, and myocardial infarction. Cellular infiltration, matrix deposition, angiogenesis, and remodeling events that transpire following tissue injury are intended to prevent further damage and preserve tissue function; however, such endogenous processes are typically insufficient to fully promote functional regeneration. Transplantation of cell populations with the ability to integrate and restore function to damaged tissues has been attempted to stimulate tissue regenerative processes in a number of different tissues [169, 227, 228], yet the percentage of cells that successfully engraft and persist within host tissues is typically very low (< 0.1-1%) [174, 229, 230].

Despite the transient presence of exogenously delivered cells, persistent macroscopic beneficial effects have been commonly observed in a variety of different tissues. The advantageous impact on the regenerative response is most likely due to the paracrine factors produced by the transplanted cells. Several studies have investigated the influence of paracrine factors secreted by cells of interest to stimulate native tissue

---

* Modified from:
AV Ngangan, JC Waring, and TC McDevitt. *Soluble factors secreted by differentiating embryonic stem cells stimulate exogenous cell proliferation and migration*, in preparation.

function in the absence of cell integration, ranging from spinal cord injury to myocardial infarction [231-234]. The remodeling of injured tissues is mediated locally by a number of cell types, including fibroblasts and endothelial cells, which are either recruited to or activated at the site of injury via the secretion of chemokines. Transplanting exogenous cells capable of secreting a potent combination of soluble factors can augment chemotaxis of host cells that participate in tissue remodeling [190, 235, 236]. Secreted factors released by a variety of cell types implemented in cell transplantation have been further characterized for growth factors and chemokines [191, 237, 238].

In addition to investigating adult stem and progenitor cells, pluripotent embryonic stem cells (ESCs) have also widely been examined for their potential to differentiate and repopulate compromised tissues following transplantation. However, paracrine modes of action appear to provide stimulatory signals for promoting tissue regeneration for a variety of tissues [8, 192, 239]. Following the establishment of a paracrine mode of action, the extracellular stem cell environment, such as the secretome and glycome, has been of interest to the scientific community [188, 193, 240]. Injured embryonic tissues are generally able to endogenously regenerate normal function, indicating that factors present in the embryonic environment are unique to promote tissue regeneration. *In vitro* differentiation of ESCs cells through the formation of small aggregates, termed embryoid bodies (EBs), mimics aspects of embryogenesis, including behaviors such as proliferation, migration, and differentiation [42, 44, 47]. As ESCs differentiate within EBs to form primitive tissues, the profile of morphogens secreted by these cells varies, and these molecules could impart a more embryonic environment that invokes endogenous tissue regeneration responses.

Hence, the objective of this study was to analyze the relative abundance of soluble factors secreted by ESCs as a function of differentiation and to elucidate the bioinductive potential of ESC-derived factors on exogenous cell types, specifically fibroblast and endothelial cells. As ESCs differentiated within EBs, the secreted growth factor profile was modulated, while the EB-conditioned media differentially affected fibroblast and endothelial cell mitogenicity and motogenicity. Characterizing the potency of growth factors secreted by differentiating ESCs on exogenous cell types may provide new insight into mechanisms of how ESC-derived cells can impact tissue regeneration.

Methods

Mouse embryonic stem cell culture

D3 murine ESCs were cultured on 0.1% gelatin-coated plates in complete medium consisting of Dulbecco's Modified Eagle Medium (DMEM, Mediatech) supplemented with 15% fetal bovine serum (FBS, Hyclone), 2mM L-glutamine (Mediatech), 1X non-essential amino acids (Mediatech), 100 U/mL penicillin (Mediatech), 100 mg/mL streptomycin (Mediatech), 0.25 mg/mL amphotericin (Mediatech), 0.1 mM β-mercaptoethanol (MP Biomedicals, LLC), and 10^3 U/mL leukemia inhibitory factor (ESCGRO, Millipore). Cells were incubated in a humidified environment at 37ºC in 5% CO_2 and passaged with 0.05% trypsin-EDTA (Mediatech) at approximately 70% confluence. To initiate ESC differentiation, embryoid bodies (EBs) were formed from a single-cell suspension of $4x10^6$ cells in 10 mL differentiation medium (complete medium without LIF) by spontaneous aggregation on a rotary orbital shaker. EBs were cultured in 100 mm Petri dishes on a rotary orbital shaker (Lab-Line

Lab Rotator, Barnstead) held constant at 40±2 rpm [213]. Rotaries were calibrated every day to ensure constant speed throughout the course of EB culture, and medium was completely exchanged every 2 days after collecting EBs via gravity-induced sedimentation in 15 mL conical tubes.

Collection of EB-conditioned media

EBs differentiated for 4, 7, or 10 days were collected (as described above), rinsed three times with phosphate-buffered saline (PBS), and cultured for an additional 2 days with a modified serum-free differentiation medium, hereafter referred to as unconditioned media (uCM), consisting of phenol red-free, low-glucose (2.8 mM) Dulbecco's Modified Eagle Medium (DMEM, Invitrogen), supplemented with 2mM L-glutamine, 1X non-essential amino acids, 100 U/mL penicillin, 100 mg/mL streptomycin, 0.25 mg/mL amphotericin, and 1 mg/ml bovine serum albumin (BSA, Fraction V, MP Biomedicals). After 48 hours of conditioning, EBs were collected by gravity-induced sedimentation and the EB-CM (~10 mL) was transferred to a fresh conical tube. The EB-CM was centrifuged for 5 minutes at 10,000 RPM at 4^{o}C to remove cellular debris and the supernatant fraction was transferred to a new 15 mL conical tube and stored at -20 ºC prior to further analysis. Conditioned media by 3T3s was also collected after 10 mL of uCM was cultured in a 100 mm plate of 3T3 fibroblasts for 48 hours.

EB count

Following EB-CM collection, EBs were washed twice with PBS and resuspended in 2 mL of PBS. From this EB suspension, two successive serial dilutions were made in

PBS (between 1:5 and 1:10) in order to reduce the density of EBs for visual counting in multiple wells of a 24-well plate. The number of EBs contained in the diluted suspensions was counted at 4X magnification using a Nikon TS100 microscope and the total number of EBs per plate was calculated based on the dilution factor used.

RNA extraction and quantitative RT-PCR

RNA was extracted from undifferentiated ESCs (day 0) and from serum-free EBs on days 6, 9, and 12 of rotary culture utilizing the RNeasy Mini Kit (Qiagen) and analyzed on the NanoDrop spectrophotometer (NanoDrop) for concentration and purity at 260 nm and 280 nm. Complimentary DNA was reverse transcribed using 1 μg of total RNA in conjunction with the iScript cDNA synthesis kit (BioRad) on the iCycler Thermal Cycler (Bio-Rad). Quantitative RT-PCR was performed using SYBR Green with the MyIQ cycler (BioRad). Primer sets were designed using Beacon Designer software for pluripotency (Octamer-4, *Oct-4*) and differentiation (α-fetoprotein, *Afp*) markers as well as for housekeeping gene glyceraldehyde-3-phosphate dehydrogenase (*Gapdh*). Additionally, growth factor primer sets were also designed, including bone morphogenetic protein-4 (*Bmp-4*), fibroblast growth factor-2 (*Fgf-2*), insulin-like growth factors 1 and 2 (*Igf-1, Igf-2*), platelet-derived growth factor B chain (*Pdgfb*), and vascular endothelial growth factor-A (*Vegfa*). Each primer pair was independently validated with appropriate positive cell controls. Relative levels of gene expression were calculated compared to undifferentiated ESC samples and normalized to *Gapdh* using the $\Delta\Delta C_t$ method [214]. All primer sequences used are shown in Table 4.1.

SDS-PAGE

EB-CM samples were analyzed using sodium dodecyl sulfate polyacrylamide gel electrophoresis (SDS-PAGE). Samples of equal volume were combined with 4X SDS-sample buffer consisting of 0.25 M Tris-HCl (pH 6.8), 8% sodium dodecyl sulfate, 40% glycerol, 8% β-mercaptoethanol, and 0.02% bromophenol blue to reach a final concentration of 1X. These samples were then loaded into precast PAGEr 10-20% Tris-glycine gels (Lonza). The gels were run in 1X running buffer consisting of glycine, Tris base, and sodium dodecyl sulfate for 2 hrs at 125V. Gels were fixed and stained using Coomassie Blue. Images were then taken using a SONY DSC-W1 digital camera.

EB-CM protein quantification

Total protein content of EB-CM was analyzed using a bicinchoninic acid (BCA) assay kit (Thermo Scientific). According to the manufacturer's protocol, 25 µl of sample was incubated with 200 uL of BCA solution for 30 minutes. Absorbance readings were taken at 562 nm using a Molecular Devices SpectraMax M2^e microplate reader and SoftMax Pro v5 microplate data acquisition software. The absorbance readings of the EB-CM samples were compared against a standard curve (0 µg/mL - 2,000 µg/mL) generated using bovine serum albumin (BSA) in order to calculate absolute protein concentrations. To determine the amount of protein secreted by the EBs during conditioning, the protein content of unconditioned medium was subtracted from all EB-CM samples.

Enzyme-linked immunosorbent assay (ELISA) kits were used to quantify the amount of proteins of interest contained within the EB-CM, specifically BMP-4, IGF-2

and VEGF-A (DuoSet, R&D Systems). Briefly, capture antibody was adsorbed onto a MaxiSorp™ Immuno 96-well plate (Nunc), followed by a blocking step, incubation with 100 μL sample, and binding of analyte to a biotinylated detection antibody. The concentrations of capture and detection antibodies used were dictated by the DuoSet protocol for each protein: 2 μg/mL and 1 μg/mL for BMP-4, 4 μg/mL and 200 ng/mL for IGF-2, and 400 ng/mL and 100 ng/mL for VEGF-A. Unconditioned medium was used as the diluent for the standard curve samples. The amount of analyte was assessed using the colorimetric reaction of peroxidase and tetramethylbenzidine (TMB) with an absorbance reading at 450 nm. The absorbances for each EB-CM sample were compared to the standard curve to establish the protein analyte content, which was normalized to EB number and reported as pg protein per 1000 EBs.

Proliferation assay

NIH-3T3 fibroblasts were cultured on tissue culture dishes in 3T3 growth medium containing DMEM supplemented with 10% bovine growth serum (BGS), 4 mM L-glutamine, 100 U/ml penicillin, 100 μg/ml streptomycin, and 0.25 μg/ml amphotericin. Human umbilical vein endothelial cells (HUVECs) were cultured on gelatin-coated tissue culture dishes in endothelial cell (EC) growth medium, consisting of MCDB131 basal medium supplemented with 5% FBS, 100 μg/ml streptomycin, 0.25 μg/ml amphotericin, 2 mM L-glutamine, 1 mg/mL hydrocortisone (Sigma), 2 ng/mL FGF-2 (PeproTech), 10 ng/mL epidermal growth factor (EGF, Gibco), 2 ng/mL IGF-1 (Gibco), 1 ng/mL VEGF-A (Sigma), and 50 mg/mL ascorbic acid (Sigma).

For proliferation studies, NIH-3T3 fibroblasts and HUVECs were cultured to approximately 50% confluence in 2-chamber glass slides (BD Bioscience), at which point growth media were removed and the cells were rinsed 3 times in PBS. Cells were then starved overnight in low-serum media, followed by an 18-hour pulse with 10 mM 5-bromo-2'-deoxyuridine in EB-CM from different time points as well as control media. After the 18-hours pulse, cells were rinsed with PBS and fixed in 70% ethanol with 2.3M HCl for 10 minutes at room temperature, rinsed in PBS 3 times, and incubated with mouse anti-BrdU primary antibody (Molecular Probes) for 1 hour at room temperature. Following primary antibody incubation, the cells were incubated with donkey anti-mouse secondary antibody conjugated to Alexafluor 488 (Invitrogen) for 2 hours at room temperature, counterstained with Hoechst, and then coverslipped using GelMount (Electron Microscopy Sciences).

Stained slides were imaged using a Nikon 80i upright microscope with a SPOTFlex digital camera and SPOT Advanced Software (Nikon) using both the FITC and DAPI filters. Nuclei counts were performed on all images using the "nuclei count" application within MetaMorph (Molecular Devices). The percentage of BrdU-positive nuclei (FITC) was calculated for all images taken (n=6 per chamber) to determine the amount of proliferation induced by the conditioned media samples compared to the control media samples.

Transwell migration assays

For migration studies, NIH-3T3 fibroblasts and HUVECs were each grown to ~80% confluence, inactivated with 10 μg/mL mitomycin-C in serum-free media (2 hours

at 37°C in 5% CO_2) and cultured overnight in growth media. Cells were also fluorescently labeled in serum-free media with 1 μM CellTracker® Green (Molecular Probes) for 20 minutes at 37ºC, followed by a 30 minute incubation in growth media prior to initiation of the migration experiment.

HTS Fluroblok transwell culture inserts (Falcon, 24-well, 8 mm pore size) were prepared with 300 μL single-cell suspension ($7.5x10^4$ 3T3s or $1x10^5$ HUVECs) in growth media (loaded in the top chamber). The bottom of the transwell chamber was filled with 800 uL of EB-CM sample or control media; cells' respective growth media were used as positive controls, while uCM served as a negative control. Transwell culture plates were incubated for 24 hours in 37°C at 5% humidity, and fluorescent microscopy images of the bottom of wells were taken every 6 hours using a Nikon TE 2000 inverted microscope with a SpotFLEX digital camera and SPOT software (Nikon). The number of cells that migrated through the porous membrane were counted for each transwell sample (fields of view = 3) using ImageJ and normalized to a unit area (mm^2).

Scratch wound assay & image analysis

In a 6-well tissue culture plate, 3T3 fibroblast cultures were allowed to reach 80% confluence before being treated with serum-free 3T3 media containing 10 μg/ml mitomycin-C for 2 hours at 37ºC in 5% CO_2. Following treatment, cells were cultured overnight in 0.5% BGS 3T3 media. Next, the monolayer was scratched using the end of a 200 μl pipette tip, washed with DPBS to remove detached cell debris, and fed with 2 ml of EB-CM sample. At 0, 12, 24, and 48 hrs media was removed and cells were rinsed with DPBS at which point phase images at 10X magnification were taken using a Nikon

TE 2000 inverted microscope with a SpotFLEX digital camera (Diagnostic Instruments, Inc.). EB-CM was replaced following imaging.

Phase images captured from scratch wound assays were analyzed using MATLAB (Simulink) programming language, in order to quantify the migration of cells across the scratch wound kinetically. Images were captured with SPOT Advanced image capturing software (Diagnostic Instruments, Inc.) at 10X magnification using a Nikon TE 2000 inverted microscope with a SpotFLEX camera at a resolution of 2048x2048 and 24-bit. Using ImageJ (NIH, Bethesda, MD), the original images were converted to an 8-bit image to enhance the contrast and subsequently converted to a binary image through threshold balance adjustment. Next, using a MATLAB script with the executable command *improfile*, an intensity average plot from 0 to 1 was calculated for a predefined portion of the image. Using the data displayed in the graph, the area under each curve was related back to the curve produced for a confluent monolayer to obtain a percent fractional coverage. Relating that percent coverage back to the starting scratch curve, the approximate percent covered after 12, 24, and 48 hours post-scratch was determined.

Statistical analysis

All experimental samples were analyzed in triplicate, with data presented as mean ± standard deviation. Statistical significance was determined using SYSTAT 12 (SYSTAT Software, Inc.) employing an analysis of variance (ANOVA) test with a post-hoc Tukey analysis to determine significance ($p < 0.05$).

Table 4.1. RT-PCR primer sequences.

Primer		Nucleotide Sequence (5' – 3')
Gapdh	**F**	GCC TTC CGT GTT CCT ACC
	R	GCC TGC TTC ACC ACC TTC
Oct-4	**F**	CCG TGT GAG GTG GAG TCT GGA G
	R	GCG ATG TGA GTG ATC TGC TGT AGG
Afp	**F**	CAC ACC CGC TTC CCT CAT CC
	R	TTC TTC TCC GTC ACG CAC TGG
Bmp-4	**F**	CTG GCC CGG AAG CTA GGT GAG TT
	R	GAG GGC CAG AGA CTG GAT CGC
Fgf-2	**F**	AGC GAC CCA CAC GTC AAA CTA C
	R	CAG CCG TCC ATC TTC CTT CAT A
Igf-1	**F**	TCC GCC AGG TTG CCT CTA G
	R	GGA AGC AGG TGG ATG GTC AG
Igf-2	**F**	TCA AAG AGT TCA GAG AGG
	R	CAA CCA TCA GTG AAT CAA A
Pdgfb	**F**	ATC GCC GAG TGC AAG ACG CG
	R	AAG CAC CAT TGG CCG TCC GA
Vegfa	**F**	TGC ACC CAC GAC AGA AGG
	R	GCA CAC AGG ACG GCT TGA

Results

Embryoid body morphology and differentiation

Preliminary studies indicated that EBs failed to initially form well in serum-free media and did not survive very well past 72 hours after being switched to serum-free conditions, especially at earlier time points of differentiation. Thus, a regimen of forming and maintaining EBs in serum-containing media before switching to serum-free media for conditioning was utilized (Figure 4.1A). As is normally observed, EBs increased in size during the course of differentiation (~250 μm diameter at day 6 compared to ~500 μm at day 12), with no significant differences in the size of EBs cultured in serum-free media for two days were observed compared to EBs in serum-containing media, thus EBs cultured for up to 48 hours with serum-free medium at different stages of differentiation were morphologically similar to their cohorts that remained in serum containing media for the same period of time (Figure 4.1B). The number of EBs per 100 mm Petri dish (on average, approximately $5x10^3$ EBs per plate) also did not vary significantly over time in serum-containing or serum-free media (Figure 4.1C). Gene expression analysis for pluripotent and differentiation markers were also performed for EBs from both culture conditions on days 6, 9, and 12 of differentiation. *Oct-4,* a pluripotent transcription factor, exhibited a similar pattern of decreasing expression for both EB culture conditions as differentiation proceeded (Figure 4.1D). At early time points, day 6 and 9, *Oct-4* gene expression levels were significantly different between serum and serum-free EB cultures ($t \leq 0.027$). By day 12, significant decreases in *Oct-4* gene expression were evident compared to day 6 for both EB cultures ($p \leq 0.025$). Increasing levels of *Afp* gene expression, a marker of primitive and definitive endoderm, were similar at each of the

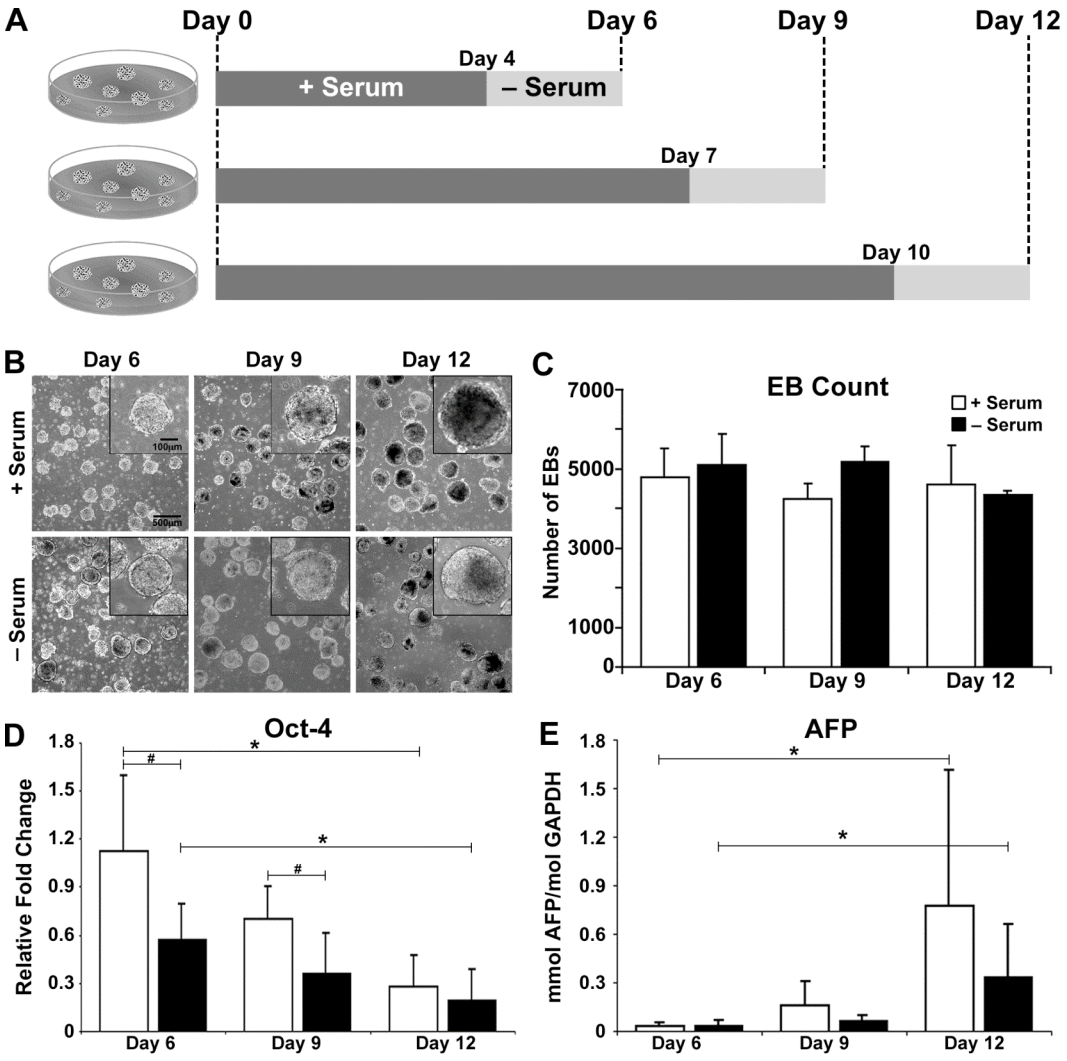

Figure 4.1. EB-conditioned media (EB-CM) collection and comparison of EB formation and differentiation in serum-containing and serum-free media. (A) EBs were cultured on a rotary orbital shaker at 40 RPM for 4, 7, and 10 days in serum-containing media, at which point the EBs were switched to serum-free media and cultured for two more days. At the end of days 6, 9, or 12 of differentiation, EB-conditioned media (CM 6, CM 9, CM 12, respectively) was collected for further analysis. (B) EBs cultured with (top row) or without (bottom row) appeared similar in size, shape, and morphology at each of the time points examined. Scale bars = 500 μm (panel) and 100 μm (inset). (C) The total number of EBs remained relatively constant (~$5x10^3$ EBs/plate) throughout EB culture for both serum-containing and serum-free conditions. (D, E) Similar EB differentiation in both media conditions was confirmed by a significant decrease in the pluripotent marker *Oct-4* by day 12 compared to day 6 and a significant increase in endoderm marker *Afp* by day 12 compared to day 6 for EBs cultured under both conditions. Results indicated are mean ± standard deviation (n=6). ANOVA: *= $p < 0.05$; Student *t*-test: # = $t < 0.05$.

time points examined between both EB culture conditions (Figure 1E). For both EB culture conditions, a significant increase in *Afp* fold change resulted at day 12 compared to day 6 EBs ($p \leq 0.034$). Thus, the switch to serum-free medium for 48 hours prior to collection did not significantly alter the differentiation progress of EBs compared to serum-containing culture. The similarities between the two EB culture conditions were examined using multiple parameters, thus suggesting minor differences during serum-free media conditioning.

In contrast, the levels of *Bmp-4*, *Fgf-2* and *Pdgfb* gene expression were significantly decreased in day 6 EBs compared to ESCs (0.3-fold, $p = 9.99\text{x}10^{-5}$; 0.02-fold, $p = 0.002$; 0.5-fold, $p = 0.015$, respectively) (Figures 4.2A, D, E). *Bmp-4* maintained similar expression at days 6 and 12 compared to ESCs, yet at day 9 expressed a signifcantly lower gene expression level compared to ESCs (0.5-fold, $p = 4\text{x}10^{-3}$). At day 9, *Fgf-2* gene expression remained significantly lower compared to ESCs (0.43-fold, $p = 0.027$), but increased by day 12 to approach a similar level to ESC expression level (Figure 4.2D). *Pdgfb* gene expression continued to increase significantly in EBs between days 9 and 12 (~1-fold) compared to day 6 ($p \leq 0.001$, Figure 4.2E) towards similar levels present in ESCs. The fold changes for *Pdgfb* remained between 0.5- and 1.3-fold, while *Fgf-2* remained between 0.2- and 1-fold. Despite the vast differences in growth factor gene expression modulation, all of the aforementioned growth factors were expressed at increasing levels as ESC differentiation progresses, suggesting functional roles in biological processes involved in differentiation, including migration and proliferation as previously described in Chapter 3.

Growth factor gene expression analysis

Overall, the gene expression levels of the six growth factors analyzed generally increased as EB differentiation progressed with serum-free media conditioning. Growth factors with the largest changes in gene expression were *Igf-1* and *Igf-2*: *Igf-1* significantly increased in fold-change by days 9 (~13-fold, $p = 0.009$) and 12 (~29-fold, $p = 6.58 \times 10^{-6}$) compared to ESCs (Figure 4.2B); whereas, *Igf-2* demonstrated significant increase in expression at day 12 (~126-fold, $p < 7.43 \times 10^{-5}$) compared to ESCs (Figure 4.2C). As for *Vegfa*, the magnitude of gene expression was modest compared to the *Igf*'s, but did increase over EB differentiation time, with significant increases at days 9 (~5-fold) and 12 (~5-fold) compared to both ESCs ($p \leq 6.37 \times 10^{-6}$) and day 6 EBs ($p \leq 9.19 \times 10^{-6}$) (Figure 4.2F). Increased expression of these growth factors progressed as EB differentiation continued, yet the magnitudes of the fold changes ranged greatly depending on the specific gene: *Igf-2* between 7- and 127-fold, *Igf-1* between 4- and 29-fold, and *Vegfa* between 2- and 5-fold differences.

Protein characterization of EB-conditioned media

The total protein content of EB-CM did not vary significantly between the different time points assessed, with a concentration range of 150-225 μg/mL (Figure 4.3B). The SDS-PAGE analysis indicated slight differences in the EB-CM content based on molecular weight, especially between to 10 – 20 kDa range (Figure 4.3A). Contrastingly, specific growth factors that exhibited large fold changes in gene expression also exhibited differences in EB-CM protein quantities. BMP-4 protein

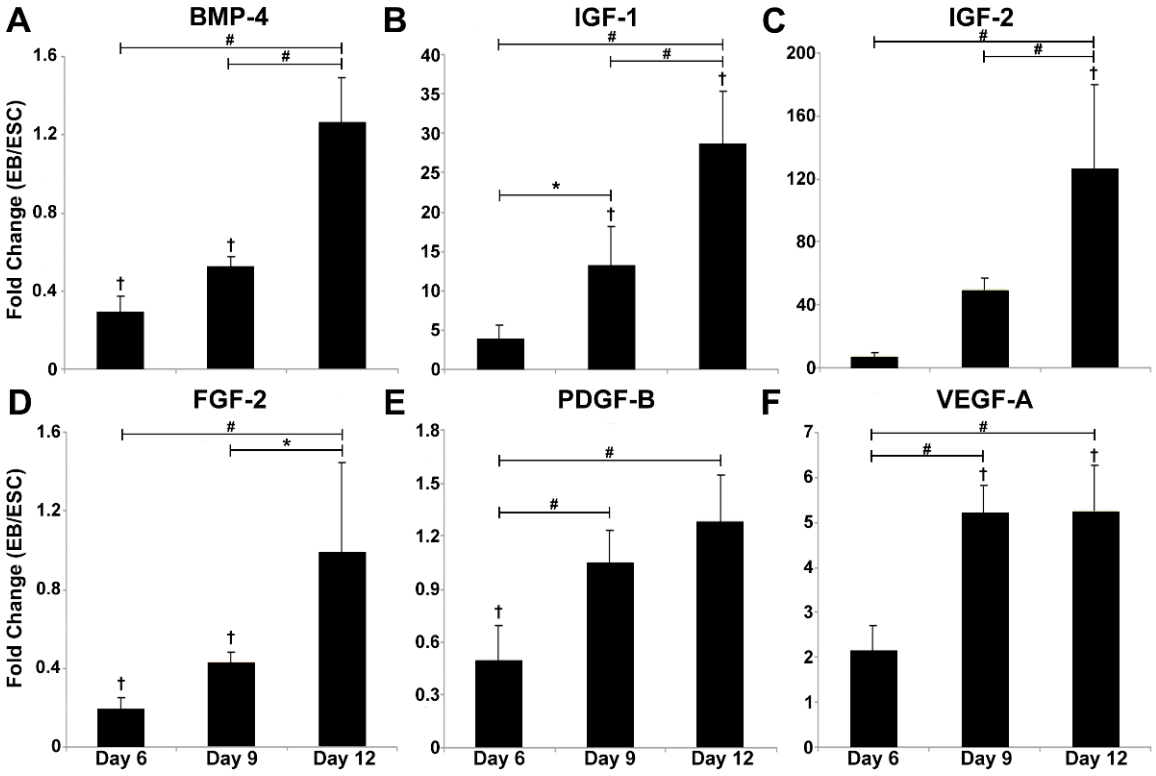

Figure 4.2. Growth factor gene expression by differentiating EBs. Overall, the expression of several growth factors increased over time during ESC differentiation within EBs. The relative values of expression are depicted as fold changes in EBs compared to the ESC starting population. Results indicated are mean ± standard deviation (n=6). ANOVA: * $p < 0.05$, # $p < 0.001$, and † $p < 0.05$ compared to ESCs.

content in CM 9 was reduced by half compared to CM 6 and 12, yet the changes in BMP-4 protein in all CM samples were not significant (Figure 4.3C). However, IGF-2 and VEGF-A both increased in protein content as EB differentiation progressed, which corresponded to their increases in gene expression (Figures 4.3D, E). Between CM 6 and 9, IGF-2 content was similar (~6 pg/1000 EBs), whereas the amount present in CM 12 was significantly increased (23.78 pg/1000 EBs) compared to both CM 6 and 9 ($p < 0.0001$). The VEGF-A protein present in the EB-CM increased by later time points of EB culture, with a significant increase in protein expression in CM 12 (2.26 pg/1000 EBs) compared to CM 6 (0.07 pg/1000 EBs; $p = 0.029$). The growth factors analyzed vary greatly in the amount contained in the EB-CM, even when the concentrations were normalized to the number of EBs per dish. Growth factors that demonstrated increased gene expression during EB differentiation, also exhibited increases in EB-CM protein content as EB differentiation progressed.

Mitogenic potential of EB-CM

Bioactive molecules contained within EB-CM stimulated fibroblast proliferation compared to uCM, but not as robustly as fibroblast growth media. CM 6 and 12 induced significantly more BrdU+ cells (~60% of fibroblasts) compared to uCM (~25%, $p \leq 4.54 \times 10^{-4}$) (Figure 4.4A), but significantly less than growth medium ($p \leq 0.004$). Comparisons between the EB-CM samples demonstrated that CM 9 stimulated significantly less proliferation (~37% of fibroblasts) compared to CM 6 and 12. As for proliferation effects on HUVECs, CM 6 and 9 elicited a similar amount of BrdU+ HUVECs, compared to uCM (~29%), yet significantly less compared to EC growth

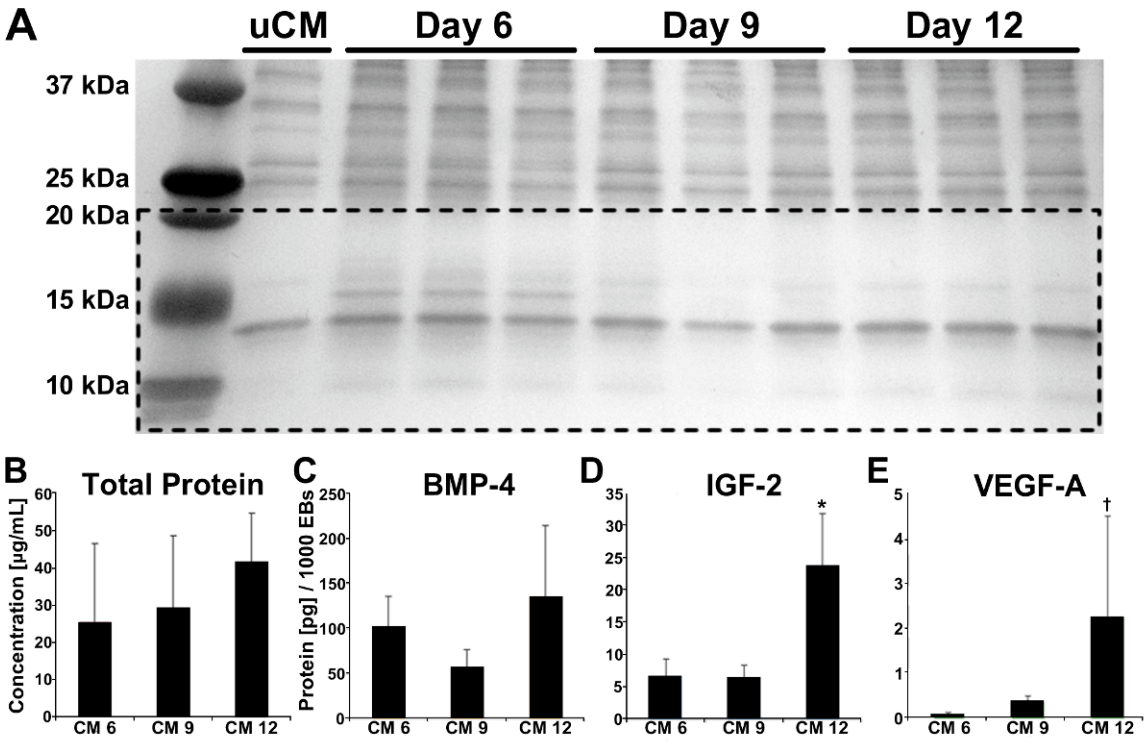

Figure 4.3. Protein analysis of EB-CM. (A) SDS-PAGE analysis illustrating the molecular weight distribution of proteins contained in EB-CM collected from different time points of EB differentiation. Proteins with differences in expression, particularly between 10-20 kDa, are highlighted within the dashed box region. (B) The total protein content of the CM collected at each time point examined did not significantly vary over time. (C) BMP-4 protein slightly increased in content as EB differentiation progressed with time, but not significantly. (D, E) Within EB-CM, IGF-2 protein increased significantly over time by CM 12 compared to CM 6 and 9; while, VEGF-A increased by CM 12 with significance compared to only CM 6. Results indicated are mean ± standard deviation (n=6). ANOVA: * $p < 0.05$ compared to CM 6 and CM 9, † $p < 0.05$ compared to CM 6.

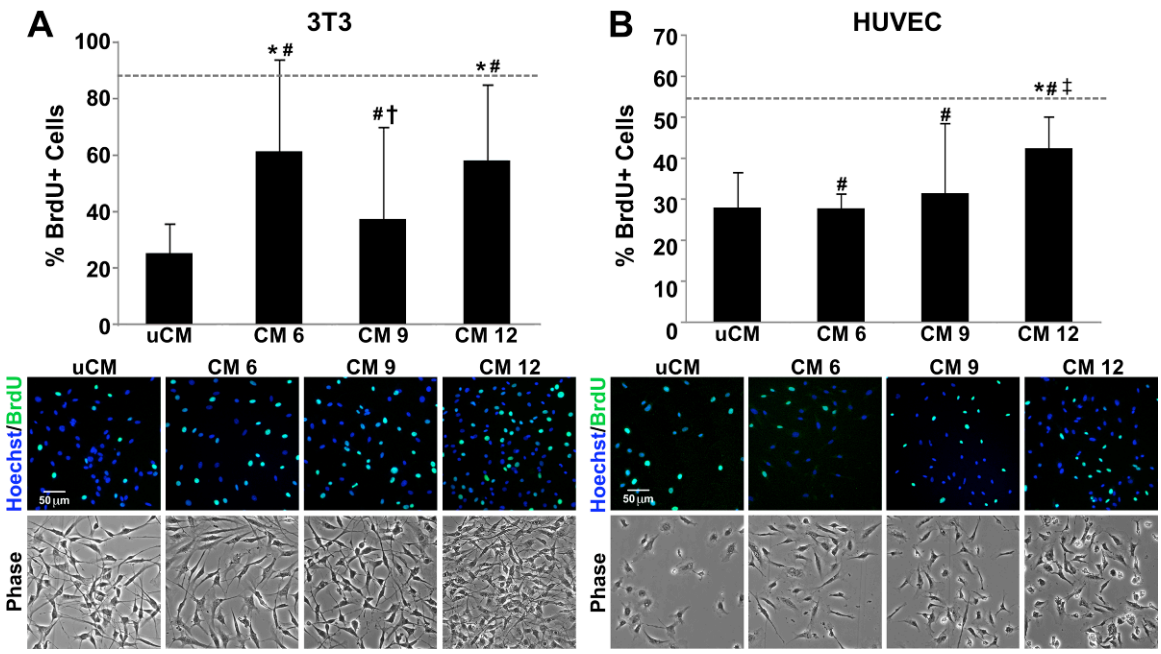

Figure 4.4. EB-CM influences mitogenic induction of exogenous cell types. (A) CM 6 and CM 12 increased fibroblast proliferation significantly compared to uCM, but remained significantly less than standard growth media. CM 9 elucidated significantly less motogenic response compared to CM 6 and CM 12. (B) Early time points of EB-CM did not significantly induce endothelial cell proliferation compared to uCM; whereas, CM 12 exhibited significantly greater proliferative response than uCM and CM 6 and CM 9. Results indicated are mean ± standard deviation (n=6). Top row images: phase images, scale bar = 50 µm. Bottom row images: fluorescent images, blue = Hoechst stain, green = BrdU-positive cells, scale bar = 50 µm. % BrdU+ cells stimulated by the respective cell type's growth media indicated as a dashed line (- - -). ANOVA: * $p < 0.05$ compared to uCM; # $p < 0.05$ compared to growth media; † $p < 0.05$ compared to CM 6 and CM 12; ‡ $p < 0.05$ compared to CM 6 and CM 9.

media (~55% of cells, $p \leq 0.001$) (Figure 4.4B). However, the CM 12 stimulated significantly more HUVEC proliferation, ~42%, compared to the other EB-CM samples ($p \leq 0.002$) and uCM ($p = 1.43 \times 10^{-4}$). Phase images illustrate the confluency differences corresponding to the mitogenic induction by the various samples, while the fluorescent images easily discern between BrdU+ and BrdU- nuclei (Figures 4.4A, B bottom rows). Between cell types, in response to CM 9 there was less proliferation in fibroblasts compared to CM 6 and 12, whereas CM9 was only less than CM 12 for EC proliferation. CM 12 enhanced proliferation in both 3T3s and HUVECs, which suggests that CM 12 contains molecular cues that can positively affect cellular proliferation. These results suggest that factor(s) present in CM 9 may suppress fibroblast proliferation, while CM12 contained factor(s) that induced EC proliferation. Overall, the mitogenic response varied based on cell type as well as the state of ESC differentiation at which the bioactive factors were collected.

Motogenic potential of EB-CM

Chemotactic migration of fibroblasts and ECs were examined in response to factors present within EB-CM. Fluorescent images of CellTracker-labeled fibroblasts (bottom-side of insert) qualitatively illustrated increased cell migration induced by EB-CM compared to uCM (Figure 4.5A). Quantitative analysis demonstrated that all CM samples stimulated significantly more cells (~27,000 – 30,000 cells) to migrate compared to uCM (~16000 cells, $p < 0.05$) and fibroblast growth medium (~7,000 cells, $p < 0.05$, data not shown) after 6 hours of incubation (Figure 4.5B). CM samples from all time points continued to yield significantly greater migration responses than uCM ($p < 0.05$)

after 12 hours (26,000 – 33,000 total migrated cells vs. 14,000 total cells). Qualitative assessment of images taken at 24 hours further illustrated differences in EB-CM treated cells compared to uCM. Fibroblasts appeared to be arranged in clusters with extended processes (stellate morphology) in EB-CM transwells compared to single rounded cells sparsely scattered in transwells containing uCM (Figure 4.5C). The results from the transwell assay corresponded to those from the fibroblast scratch wound assay - each of the EB-CM samples enhanced wound closure by 24 hours compared to uCM (Figure 4.5D). Overall, EB-CM affected migration of fibroblasts, specifically modifying cell morphology and increasing the number of migratory cells towards the EB-CM compared to uCM.

To further examine the paracrine effects of factors secreted differentiating EBs, the migrations response of endothelial cells, another cell type implicated in tissue remodeling, was evaluated. According to transwell images, individual HUVECs in EB-CM were more spread and clustered together compared to more rounded and separated HUVECs in uCM (Figure 4.6A). Over the entire 24-hour period of migration, each of the EB-CM samples stimulated HUVEC migration compared to uCM, as quantified by the fluorescent images taken of the bottom of the transwells (Figure 4.6B). All EB-CM samples significantly induced a greater number of migrated cells at each time point compared to uCM ($p < 0.05$). Comparisons between each of the different EB-CM samples at 6- and 12-hour time points indicated similar motogenic induction since the numbers of migrated cells (~4000 – 4800 cells) were not significantly different. However, by 24 hours, CM 6 and 9 samples continued to decrease in migrated cell number (~2400 and ~4000 cells, respectively), whereas CM 12 maintained a similar

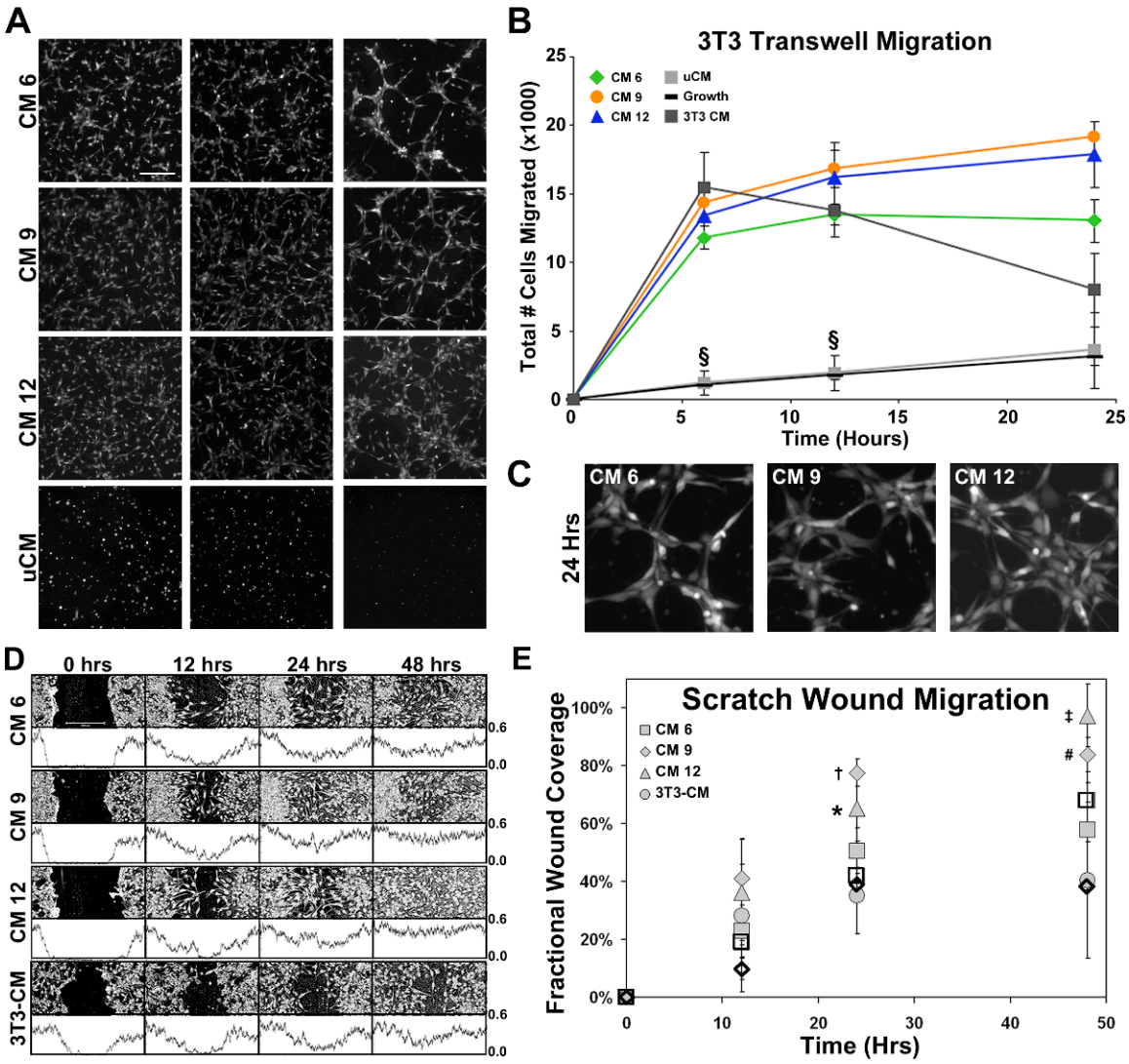

Figure 4.5. Fibroblast migration response to EB-CM. (A) Fluorescent images of the migrated fibroblasts qualitatively exhibit differences in cell number (scale bar = 150 µm). (B) Quantified migration exhibited significant number of cells were stimulated by CM collected from different days of differentiation compared to uCM (n=6). (C) At the final time point, CM influenced the appearance of fibroblasts in network structures compared to ones treated with uCM, which appeared more as single cells. (D) Binary phase images and corresponding intensity profiles (below) exhibit scratch wound closure over time. Scale bar = 500 µm. (E) The fractional coverage of the wound area was determined using MATLAB analysis on the corresponding intensity profiles. Series: □ 10% BGS 3T3 media, ◊ uCM. Results indicated are mean ± standard deviation (n=6). ANOVA: * $p < 0.05$ compared to 3T3-CM; † $p < 0.05$ compared to uCM, 3T3-CM, and 10% BGS 3T3 media; # $p < 0.05$ compared to uCM and 3T3-CM; ‡ $p < 0.05$ compared to uCM, CM 6, and 3T3-CM; § $p < 0.05$ compared to all CMs

number of migrated cells (~4800 cells) to its number at the 6- and 12-hour time points. Thus, at the 24-hour time point, the total number of migrated cells induced by CM 12 was significantly greater than the number of cells induced by CM 6 (p = 0.004). Upon examination of the HUVEC morphology after 24 hours, ECs in CM 12 were generally arranged in large clusters, while ECs in CM 6 and CM 9 remained as single cells or small clusters (Figure 4.6C).

Despite similar concentrations of total protein in EB-conditioned media collected at all time points of differentiation, different cell types responded quite differently - the number of migrated 3T3 fibroblasts was about 10-fold higher than the amount of migrated HUVECs throughout the transwell study even though the transwells were inoculated with similar numbers of cells ($7.5x10^4$ 3T3s, $1x10^5$ HUVECs). These differences may be due to fibroblasts having a mesenchymal phenotype, having the propensity to migrate, while endothelial cells have an epithelial phenotype, which are typically not migratory, unless provided with the proper cues [241]. This difference in cell phenotypes also may explain why EC growth media stimulated the majority of cells seeded in the transwell to migrate – the EGM-2 media is optimized and defined with growth factors, whereas fibroblast growth media consists of less undefined BGS. Thus, the factors contained within the EB-CM are not as stimulatory as EGM-2, but did induce EC migration compared to uCM; however, EB-CM factors were more stimulatory than BGS resulting in greater number of migrated cells compared to fibroblast growth media. Overall, the results of the migration assays revealed that EB-CM collected at different stages of EB differentiation contained chemotactic factors capable of stimulating cell migration, and in some cases greater than conventional growth medium.

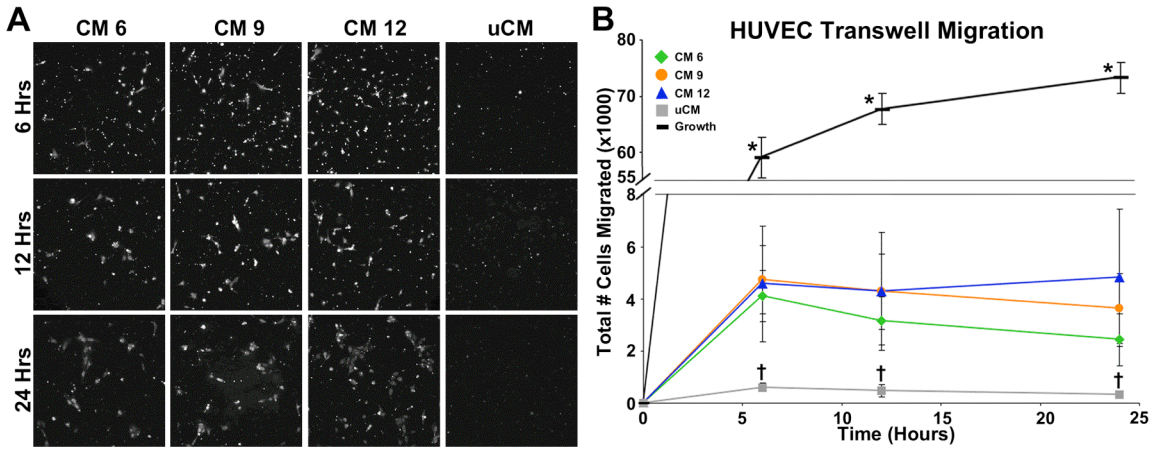

Figure 4.6. EB-CM affects endothelial migration. (A) EB-CM collections from various time points differentially affect migration of endothelial cells (scale bar = 150 μm). (B) EB-CM significantly stimulated more ECs in response all CM compared to uCM, yet significantly less than EC growth media. (C) At 24 hours, uCM did not influence the appearance of endothelial cells, mostly shown as single cells, while CM treated cells prompted cells to exist in clusters. Results indicated are mean ± standard deviation (n=6). ANOVA: * $p < 0.05$ compared to all EB-CM and uCM; † $p < 0.05$ compared to all EB-CM and growth media.

Discussion

This study elicited a number of growth factors differentially secreted by differentiating ESCs, in addition to examining the impact of this complex mixture of factors captured within the EB-CM on different cell types. ESC transplantation has been widely studied for the repopulation of tissues undergoing remodeling; however, the number of ESCs that integrate and differentiate within the host tissue is quite minimal [174, 185, 229, 230]. Several studies have demonstrated the potency of ESC-secreted molecules in inhibiting apoptosis, rescuing congenital defects, and providing a cardioprotective effect following myocardial infarction [8, 192, 239]. While ESC-secreted factors have been reported in the literature, these reports typically examined paracrine actions of undifferentiated ESCs and in monolayer culture [188, 208, 242]. When ESCs are transplanted into an injured tissue, the endogenous tissue environment will not maintain pluripotency, which will result in ESC differentiation and further modulate the paracrine factors released. Despite the loss of pluripotency, the transplanted ESCs still positively affect damaged tissue repair [243].

In this study, the change in secreted factors as a result of differentiation was analyzed for protein content and bioactivity, specifically motogenicity and mitogenicity of fibroblasts and endothelial cells. The gene expression of EBs and protein profiles of EB conditioned media demonstrated differential representation of several growth factors as EB differentiation progressed. Growth factors that decreased in gene expression relative to ESCs during EB differentiation, including *Fgf-2* and *Pdgfb*, also resulted in low levels of protein in EB-CM, which were undetectable by ELISA (data not shown). On the other hand, other growth factors' gene expression that increased steadily as ESC

differentiation progressed, particularly *Igf-2* and *Vegfa*, correlated to increased content of each protein in CM 9 and 12. The differential expression and secretion of proteins by the differentiating ESCs was elucidated not only by gene and protein analyses, but also by varied cell responses during proliferation and migration experiments comparing EB-CM collected at different days. Overall, CM 9 continued to induce significantly more fibroblast migration than uCM over the entire 24-hour period, while significantly reducing the percentage of proliferating fibroblasts compared to CM 6 and 9. Distinct fibroblast behavior in response to CM 9 demonstrates the unique combination of morphogens secreted by EBs after 9 days of differentiation – a secretome that stimulates fibroblast migration, but inhibits proliferation; whereas, days 6 and 12 EBs yield secreted factors that promote fibroblast mitogenicity. This change in promoting different cellular processes may be a reflection on the aspects of embryogenesis being mimicked within EBs. ESCs typically proliferate at a high rate, which helps establish a critical mass for EB formation. At later time points of EB differentiation, typically around 5 – 10 days, epithelial to mesenchymal transition (EMT) occurs, which is characterized by the transition of non-migratory epithelial cells to migratory mesenchymal cells to initiate tissue formation and has been identified during EB development [211, 244]. Therefore, the factors captured in the EB-CM are capable of modulating exogenous cells' responses in the same way ESCs are differentiating within the EBs. Additionally, EB-CM can provide further insight into the progression of EB development,

The factors secreted by later stage EBs were most effective in stimulating ECs, a more differentiated cell type than 3T3 fibroblasts. The migration of ECs in response to all EB-CM collections was significant compared to uCM up to 12 hours, after which

point only CM 12 was significantly increased. The proliferative capacity of ECs was also greater in response to CM 12 compared to CM 6 and 9. This increased stimulation of ECs by CM 12, corresponds to the increased differentiation of ESCs within EBs towards a more cardiovascular lineage described in Chapter 3. Day 10 EBs gene expression of endothelial markers was accompanied by increases in gene expression of angiogenic factors *Fgf-2* and *Vegfa* as well as a ~70-fold increase in *Igf-1*. Interestingly, IGF-1 protein has been shown to stimulate *in vitro* EC migration [245]. Thus, the increased differentiation of day 10 EBs towards a cardiovascular phenotype may yield an EB secretome that contains factors effective in stimulating a more differentiated vascular phenotype, such as endothelial cells.

The factors secreted into EB-conditioned media reflect the state of differentiation ESCs are undergoing, thereby providing molecular cues to which only certain cell types may respond. The expression of stimulatory molecules is typically juxtaposed with inhibitory molecules, and cellular responses are not purely based on concentrations of such factors. During the early stages of ESC differentiation EBs mimic aspects of embryogenesis: progenitors expand in number, followed by morphogenesis and cell expansion of more differentiated cell types. The growth factor profile and bioactivity results for each of the EB-CM collections at various time points demonstrate the unique combination of factors that early differentiating ESCs secrete over time and are reflected in the distinct responses from the two different cell types.

The growth factors detected in the EB-CM have been shown to promote tissue regeneration. The persistence of BMP-4 protein in the EB-CM from days 6 through 12 demonstrates the importance of this molecule during ESC differentiation, specifically

towards the mesoderm lineage, and has been shown to enhance vascular network formation within human ESC-derived EBs [198, 246]. VEGF-A is a well-documented growth factor for promoting angiogenesis in ischemic tissues [247-249]. Enhancing the re-vascularization of damaged tissues is necessary in order deliver cells and nutrients to establish a regenerating environment. As for IGF-2, many studies have shown its implication in growth and differentiation within muscle and bone tissue [250, 251]. Additionally, IGFs and BMP-4 have been shown to up-regulate VEGF expression to synergistically stimulate tissue repair. BMP-4 in concert with VEGF treatment enhanced bone formation and healing compared to single factor treatment [252]. IGF-2 and VEGF together promote homing of endothelial progenitor cells to further stimulate angiogenesis [221], and the combination of IGF-1 and VEGF can target multiple regenerative processes: angiogenesis, reinnervation, and myogenesis [253]. Taken all together, specific growth factors work in concert to effectively induce biological processes, in particular angiogenesis, to improve tissue regeneration. The increased production of these factors by EBs at days 9 and 12, suggests that early differentiating ESCs secrete factors that can promote tissue regeneration by potentially inducing angiogenesis.

Conclusion

Overall, this study demonstrates that factors secreted by ESCs undergoing morphogenic differentiation are capable of inducing proliferation and migration of exogenous cell types. The complex mixture of molecules secreted contains a number of different growth factors and morphogens whose relative abundance varies as a function of EB differentiation. Interestingly, the morphogenic events known to be associated with

EB differentiation, including cell proliferation and migration, are reflected by the endogenous expression of factors that comprise the soluble milieu. Thus, analyzing the composition and bioactivity of molecules secreted by differentiating ESCs not only provides insights into the paracrine nature environment of EB environments, but also suggests potential trophic mechanisms whereby differentiated progeny from ESCs can impact exogenous cells involved in tissue remodeling and regeneration processes.

CHAPTER 5

ACELLULARIZATION OF EMBRYOID BODIES VIA PHYSICAL DISRUPTION METHODS*

Introduction

The pluripotency of ESCs makes them an attractive cell source for regenerative cell therapies to treat a broad array of degenerative diseases and traumatic injuries. ESCs and ESC-derived cells have been transplanted into areas of damaged tissue where resultant cell repopulation and recovery of tissue function have been demonstrated [254-259]. Use of ESCs as a delivery vehicle for trophic factors has also been shown to be effective in stimulating tissue regeneration in a number of tissues [8, 260]. Notably, Fraidenraich et al. discovered that ESCs rescued embryonic lethal knockouts via secretion of soluble molecules and not by cellular repopulation [8]. Hence, ESC-derived molecular cues appear to be effective in stimulating tissue regeneration by inducing endogenous healing.

Acellularization techniques provide a means to extract cells from tissues, thereby isolating the extracellular matrix (ECM) components. The ECM provides a natural scaffold for structural support of tissues and harbors a complex assembly of biochemical cues comprised of proteins, glycosylaminoglycans, proteoglycans, and growth factors. Numerous tissues from various sources have been acellularized in order to create scaffolds for tissue regeneration, including small intestinal submucosa (SIS) [119],

---

* Modified from:
A. Ngangan and TC McDevitt. *Acellularization of embryoid bodies via physical disruption methods*. Biomaterials, 2009 30 (6): 1143-9

esophagus [120], bladder [121], cardiac valve [123, 261], dermis [124, 125], nerve [126], placenta [127], and pericardium [128]. Several methods have been developed to acellularize these tissues using techniques that include solution-based treatments and mechanical disruption. Solution-based methods typically combine chemical treatments, such as detergents [141-144, 262], alkaline or acid solutions [145, 146], and hyper- or hypo-tonic solutions [144], as well as enzymatic digests, including trypsin, endonucleases, and ectonucleases [147, 148]. While chemical and enzymatic methods effectively remove cellular content, they usually require multiple incubation and rinsing steps to ensure thorough removal or inactivation of acellularization reagents and may unintentionally remove desirable ECM components, such as GAGs, fibronectin, or laminins [141, 142]. On the other hand, mechanical methods of acellularization, including repeated freeze-thawing, sonication, or other physical means of disrupting cells' plasma membranes [149, 150], provide a direct and rapid means of acellularizing tissues, but used alone, such methods are not capable of completely removing cellular content. Thus, a combination of physical and chemical/enzymatic methods is needed to successfully acellularize tissues.

The primary criterion for acellularization is efficient inhibition of tissue viability coupled with preservation of native ECM composition and structure. Lyophilization is a mechanical acellularization method that utilizes freeze-drying to permeabilize cell membranes, as a result of intracellular ice formation during the freezing process, and subsequent removal water molecules. A number of tissues and acellular matrices have been lyophilized prior to therapeutic application, including bovine pericardium [263, 264], bone matrix [152], amniotic membrane [153], and cardiac valves [261]. Another

mechanical acellularization option uses multiple freeze-thaw cycles, which entails repeated snap-freezing of tissue by submersion in liquid nitrogen followed by thawing at room temperature in phosphate-buffered saline. Multiple freeze-thaw cycles have been utilized to render a variety of tissues acellular, including peripheral nerve grafts [149, 265], meniscal tissue [266], embryonic chick knee [267], and human dermis [268]. The aforementioned studies demonstrated that mechanical cell disruption is a mild acellularization treatment that preserves tissue components for successive tissue repair, but thus far, such methods have only been used to acellularize somatic tissues in a homeostatic state.

ESCs are commonly induced to differentiate *in vitro* by forming 3-dimensional cell spheroids, termed embryoid bodies (EBs), which recapitulate many of the molecular and cellular morphogenic events that occur during the normal pre-gastrulation stages of embryological development [41, 42, 47, 269]. Previously, our lab demonstrated that acellular matrices could be derived from EBs using solvent extraction methods in combination with DNase treatment [216, 270]. The objective of the present study was to examine the effectiveness of two separate mechanical methods, lyophilization and repetitive freeze-thaw cycles, as alternative means to efficiently acellularize matrices produced by differentiating ESCs within EBs. Acellularization was assessed based upon quantitative assays of cell viability, DNA content, and protein content compared to untreated EBs, in addition to histological analysis of acellular EB matrix structure and exogenous cell repopulation of EB-derived matrices. These studies establish novel methods by which mechanical disruption techniques effectively acellularize EBs to produce acellular matrices capable of supporting cell attachment and adhesion. Coupled

with the ability of ESCs to promote endogenous tissue regeneration *in vivo*, these naturally-derived matrices provide a novel scaffolding material for future investigations of endogenous tissue repair and regeneration, in addition to elucidating mechanisms by which ESCs promote healing and morphogenesis via the production of unique combinations of factors constituting an embryonic microenvironment.

Methods

ESC culture and differentiation

D3 murine embryonic stem cells were cultured on 0.1% gelatin-coated plates in complete media consisting of Dulbecco's Modified Eagle Medium (DMEM, Mediatech) supplemented with 15% fetal bovine serum (FBS, Hyclone), 2mM L-glutamine, 1X non-essential amino acids, 100 U/mL penicillin, 100 μg/mL streptomycin, 0.25 μg/mL amphotericin, 0.1 mM β-mercaptoethanol, and 10^3 U/mL leukemia inhibitory factor (LIF, Chemicon). To initiate ESC differentiation, embryoid bodies (EBs) were formed from a single-cell suspension of $4x10^6$ cells in 10 mL differentiation media (complete media without LIF). EBs were cultured in 100 mm Petri dishes on a rotary orbital shaker (Lab-Line Lab Rotator, Barnstead) held constant at 40±2 rpm [213]. EBs were re-fed with fresh media every 2 days by collecting individual plates of EBs via gravity-induced sedimentation in 15 mL conical tubes, aspirating the old media, and replacing with fresh differentiation media before transferring the EBs back to 100 mm Petri dishes. Rotaries were calibrated every day to ensure constant speed throughout the course of EB culture.

Acellularization of EBs

After 4, 7, or 10 days of rotary orbital suspension culture, EBs were harvested, rinsed in phosphate-buffered saline (PBS) prior to acellularization treatments, and divided into aliquots of approximately $2x10^3$ EBs per sample. To acellularize via lyophilization, EB samples in 1.5 mL microcentrifuge tubes were rinsed twice with 1 mL PBS and frozen in 1 mL dH_2O at -80°C overnight. Frozen samples were placed in the lyophilizer (Labconco) overnight and then removed for further processing. Freeze-thawed acellular samples were produced by aspirating PBS, immersing the entire tube with EBs into liquid nitrogen, and allowing the liquid nitrogen to boil off. Once the liquid nitrogen was boiled off, 1 mL PBS was added to thaw the EBs while rotating the sample for 5 minutes (LabQuake Rotisserie) at room temperature. EBs were then centrifuged for 2 minutes at 18,000 rcf at room temperature. This process of freeze-thawing was performed 1, 3, or 5 times for each sample to determine the optimal number of cycles. For comparison purposes, chemical acellularization was performed, as previously described, by treating the EB samples with 1% Triton X-100 for 30 minutes while rotating [270]. Following Triton treatment, samples were centrifuged for 2 minutes at 18,000 rcf at room temperature and rinsed three times with PBS. For DNase treatment, subsequent to mechanical and chemical permeabilization steps, samples were treated with 0.5 mL of 1 mg/mL DNase for 15 minutes while rotating, centrifuged for 2 minutes at 18,000 rcf at room temperature, and rinsed 3 times with 1 mL PBS.

Scanning electron microscopy (SEM)

Samples not dried via lyophilization (i.e. hydrated samples) were fixed in 2.5% gluteraldehyde in deionized (dI) H_2O for 1 hour while rotating. Samples were rinsed 3 times in dI H_2O and rotated in 4% osmium tetroxide in dI H_2O for 1 hour at room temperature. After 3 rinses in dI H_2O, samples were placed in acetone and dehydrated using an E3000 series critical point dryer (Quorum Technologies). Liquid CO_2 was allowed to permeate the samples for 1 hour and passed through the CO_2 critical point (31.5^{o}C, 1100 psi). Subsequently, dried samples were mounted on stubs with carbon tape and sputter-coated with gold for 120 seconds using a Polaron Sputter Coater SC 7640 (Quorum Technologies). Scanning electron microscopy images were taken using a Hitachi S-800 FE-SEM with a 10kV acceleration voltage.

Histology

Histological samples were fixed for 30 minutes in 10% formalin while rotating, washed 3 times in PBS, and embedded in Histogel®. The embedded samples were paraffin-processed and sectioned into 5 μm sections. Prior to staining, slides were de-paraffinized in a Leica Autostainer XL. Hemotoxylin and eosin (H&E) staining was performed using a Leica Autostainer XL, and slides were incubated with Hoechst dye (nuclear stain, 10 μg/ml) for 5 minutes. Slides were mounted with coverslips using either Cytoseal™ 60 for H&E (Richard-Allan Scientific) or Gel/Mount™ (Biomeda Corp.). Brightfield and fluorescent images were captured using a Nikon 80i Upright Microscope and a SPOT Flex camera (15.2 64Mp Shifting Pixel, Diagnostic Instruments) in conjunction with SPOT Advanced v.4.5 (Diagnostic Instruments) software.

Cell viability

Cell viability was analyzed using 10% alamarBlue (Biosource) in serum-free complete media without LIF. Acellular samples and untreated EBs were incubated for 2 hours in 5% CO_2 at 37^{o}C, after which 25 μl aliquots were taken from the incubated samples, and fluorescence measurements were taken (ex: 545 nm, em: 590 nm) using a SpectraMax M2e plate reader. Relative viability was determined by normalizing the acellular samples to the starting population of untreated EBs.

DNA analysis

Viable and acellular EBs were solubilized by rotating samples at room temperature for 24 hours in 6M guanidine hydrochloride in order to assess DNA content. DNA content was quantified using the Quant-iT™ PicoGreen® dsDNA Assay kit (Molecular Probes); a 1:5 volumetric ratio of solubilized sample to a solution of 1X TE buffer and 0.5X PicoGreen dye was used. The fluorescence reading (ex: 485 nm and em: 528 nm) was taken on a SpectraMax M2e plate reader, and the absolute amount of DNA (mg/mL) was quantified against a lambda DNA standard curve (0 mg/mL - 5 mg/mL). The amount of DNA present following DNase treatment was compared to untreated EBs.

Protein analysis

Total protein content was analyzed using a bicinchoninic acid (BCA) assay kit (Pierce). A 1:1 dilution of 6M guanidine hydrochloride solubilized sample (described above) in dI H_2O was used, and 25 μl of sample was incubated with BCA solution for 30 minutes. Absorbance readings were taken at 562 nm using the aforementioned plate

reader. The absorbance readings of the solubilized samples were compared against a standard curve (0 μg/mL - 2,000 μg/mL) generated using bovine serum albumin (BSA) in order to calculate absolute protein concentrations.

Enzyme-linked immunosorbent assay (ELISA) kits were used to quantify the amount of proteins of interest harbored within acellularized EB matrices, specifically IGF-2 and VEGF-A (DuoSet, R&D Systems). Acellular EBMs were solubilized using 500 μL TPER buffer (Thermo) with rotation for 2 hours at room temperature followed by 5 minutes of centrifugation at 14,000 RPM to remove particulate. Briefly, capture antibody was adsorbed onto a MaxiSorp™ Immuno 96-well plate (Nunc), followed by a blocking step, incubation with 100 μL sample, and binding of analyte to a biotinylated detection antibody. The concentrations of capture and detection antibodies used were dictated by the DuoSet protocol for each protein: 4 μg/mL and 200 ng/mL for IGF-2 and 400 ng/mL and 100 ng/mL for VEGF-A. TPER buffer was used as the diluent for the standard curve samples. The amount of analyte was assessed using the colorimetric reaction of peroxidase and tetramethylbenzidine (TMB) with an absorbance reading at 450 nm. The absorbances for each sample were compared to the standard curve to establish the protein analyte content, which was normalized to the mass of EBM (mg) and reported as pg protein per mg EBM.

Endotoxin assay

The end point chromogenic limulus amebocyte lysate (LAL) endotoxin test (Lonza) was used to assay the levels of endotoxin present in the lyophilized acellular

EBMs. Briefly, acellular EBM samples were resuspended in 500 μL sterile PBS, placed on a rotisserie for 30 minutes at room temperature, and centrifuged for 5 minutes at 14,000 RPPM to remove particulate. Endotoxin testing was performed as described in the product manual. Briefly, test samples and endotoxin standards reacted with the LAL for 10 minutes, followed by the addition of a substrate solution and incubated for 6 minutes, and then the reaction was stopped with stop reagent (25% glacial acetic acid solution). The entire reaction was performed at 37^{o}C. Absorbance readings at 405nm were taken using a SpectraMax M2e plate reader, and the endotoxin concentration (EU/mL) was calculated using the standard curve generated using the endotoxin standard supplied with the kit.

Cell seeding

NIH-3T3 fibroblasts were cultured to 80% confluence on tissue culture-treated 100 mm dishes in growth media containing DMEM supplemented with 10% bovine growth serum (BGS, Hyclone), 4 mM L-glutamine, 100 U/mL penicillin, and 100 μg/mL streptomycin. Three hours prior to seeding, 3T3s were treated with mitomycin-C (10 μM in serum-free growth media) to inhibit cell proliferation for assessment of cell invasion into the acellular matrix. Following acellularization treatments, acellular EB matrices were frozen at -80^{o}C in 1 mL dI H_2O overnight and freeze-dried. Fibroblasts were trypsinized and seeded onto the lyophilized acellular matrices at a density of 10^6 cells/mL by placing the matrices into 1 mL of 3T3 single-cell suspension and allowing them to rotate. After 3 hours of seeding in suspension, seeded matrices were gently spun down for 1 minute at 200 rcf, washed 3 times in PBS, and transferred to 48-well tissue culture

plates with 500 μl of 3T3 growth media. The seeded matrices were re-fed every two days for up to 4 days, at which point, seeded matrices were rinsed with PBS and processed for histology as previously described.

Statistics

All statistical analyses were performed using Systat software (version 12). Viability comparisons across multiple experimental groups were performed using a one-way analysis of variance (ANOVA) followed by post-hoc Tukey analysis to determine significant ($p < 0.05$) differences between the different groups. Comparisons within DNA and protein content results were done using a two-way ANOVA with significance assessed using post-hoc Tukey analysis ($p < 0.05$).

Results

Overall results exhibited efficient acellularization of EBs using mechanical permeabilization with DNase treatment. Initial studies were performed varying the number of freeze-thaw cycles (1, 3 or 5) and examined on the basis of inhibition of cell viability and retention of total protein content. Using EBs differentiated for 7 days, investigation of the number of freeze-thaw cycles indicated that 3 cycles was efficient at removing DNA while retaining protein in the final product (Figure 5.1). Successive studies were performed to assess acellularization efficiency on EBs at various stages of differentiation. Both mechanical methods, lyophilization and 3 freeze-thaw cycles, independent of EB differentiation time, significantly inhibited cell viability ($p = 5.57 \times 10^{-6}$) compared to untreated EBs; retention of total protein among EBs at different stages of

differentiation after acellularization, however, was not significantly different (Figure 5.2) from untreated EBs. Day 4 EBs generally exhibit relatively low gene expression of ECM molecules and growth factors, whereas a variety of ECM and growth factor gene expression levels begin to increase by day 7 of differentiation and continue to increase by 10 days described in Chapter 3. Thus, based on the earliest time point at which ECM and growth factors are increasingly expressed within EBs as described in Chapter 3, day 7 EBs were used for all subsequent acellularization studies.

Morphology & ultrastructure analysis

The two different mechanical disruption methods attempted yielded acellular products with very different macroscopic properties. Lyophilized EBs were maintained as distinct EBs with a "cottonball, powder-like" morphology (Figure 5.3B, C) while freeze-thawed EBs (FT) produced a single amorphous mass with a "gel-like" appearance (Figure 5.3D, E). Handling the lyophilized EBs was similar to managing a dry powder with static interaction, while the congealed, freeze-thawed EB matrix could be manipulated by collecting the entire mass using a spatula. EB matrices treated with DNase, both lyophilized (L+D) and freeze-thawed (FT+D), formed a more compact pellet compared to FT matrices and could be gently manipulated using a pair of tweezers. Compared to untreated EBs (Figure 5.4A, D), the lyophilized matrices appeared relatively smooth and largely porous (Figure 5.4B, E), whereas FT matrices consisted of a non-porous, dense particulate material, due to compaction from the centrifugation steps performed during acellularization (Figure 5.4C, F). After DNase treatment and centrifugation retrieval of the material, L+D samples were less porous and more closely

resembled the structure of the FT ± D samples (Figure 5.5). These results indicate that the sequence of the processing steps performed strongly affects the structural properties of the acellular matrices in their final forms.

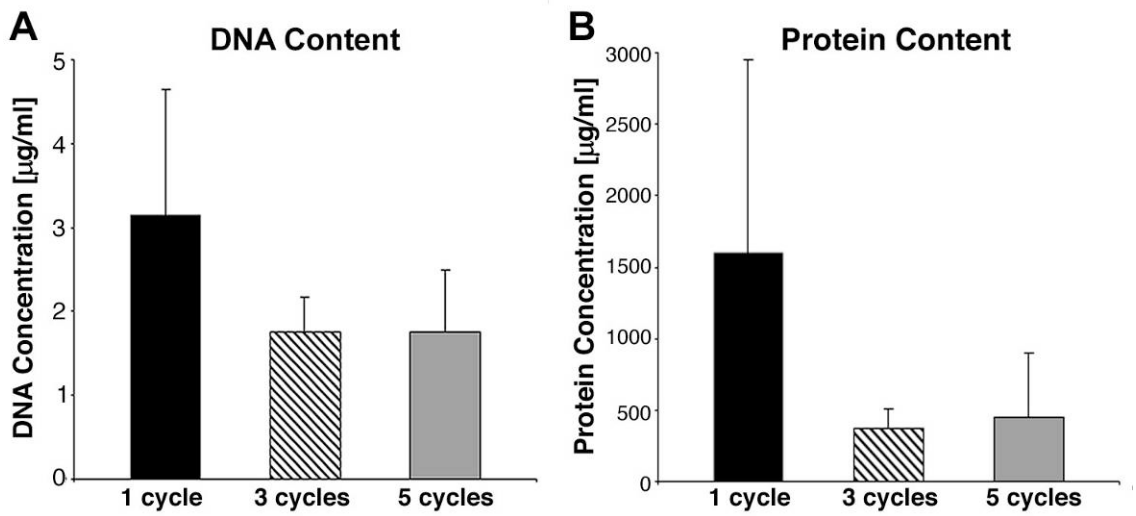

Figure 5.1. Effects of freeze-thaw cycles on acellular EB content. DNA content (A) and protein content (B) within acellular EB matrices was slightly (but not significantly) decreased after 3 or 5 cycles compared to a single freeze-thaw cycle. Results shown are mean ± standard deviation (n=3).

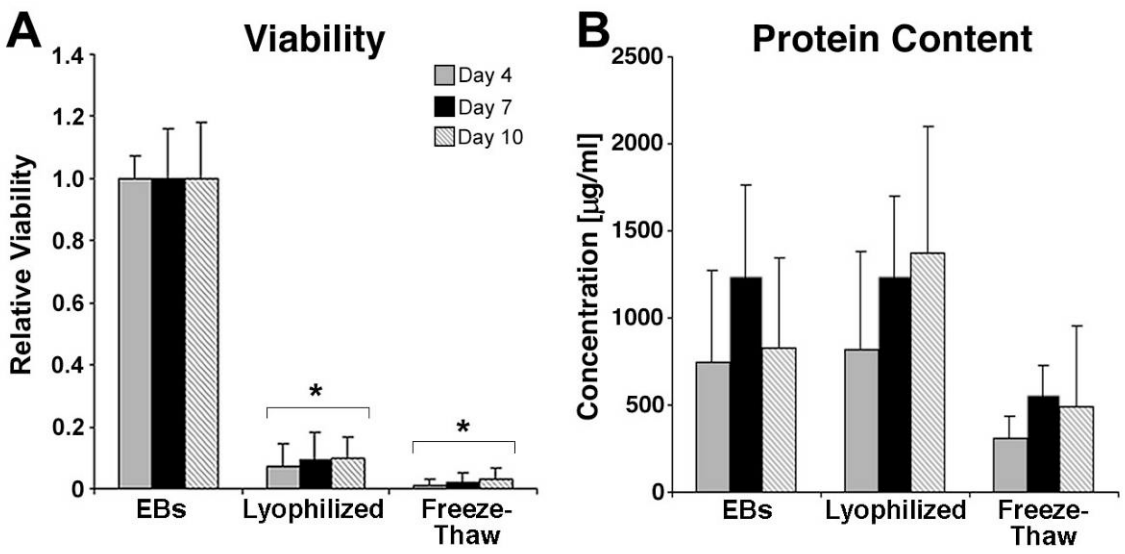

Figure 5.2. Quantitative assessment of acellular matrices derived from EBs at different stages of differentiation. (A) Significant inhibition of cell viability was achieved by mechanical acellularization of EBs at various days of differentiation. (B) The amount of protein remaining after acellularization did not change significantly after differentiation of the EBs for different periods of time. One-way ANOVA was performed for samples at the same day of differentiation (* = $p < 0.05$). Results shown are mean ± standard deviation (n=3).

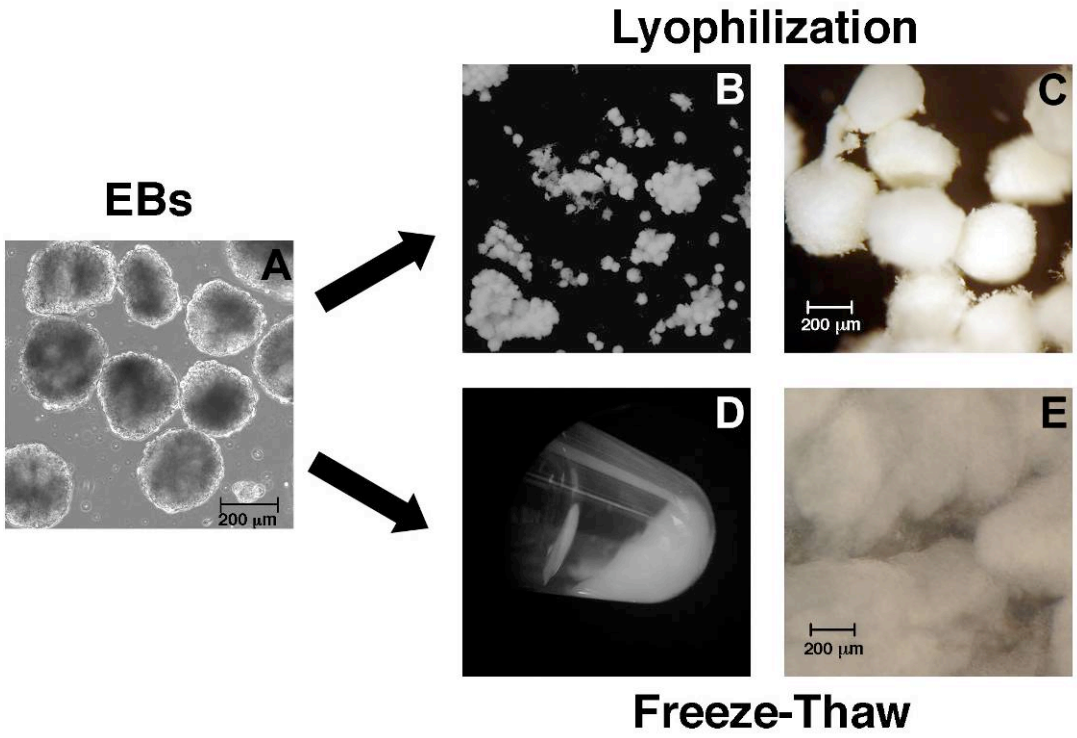

Figure 5.3. Overview of EB acellularization process. EBs differentiated for 7 days were mechanically acellularized either by lyophilization (B&C) or multiple freeze-thaw cycles (D&E) followed by DNase treatment. Phase image shows EBs cultured for 7 days (A). Digital images macroscopically exhibit EB matrix following each of the mechanical acellularization techniques (B&D), including a closer image on the far right (C&E).

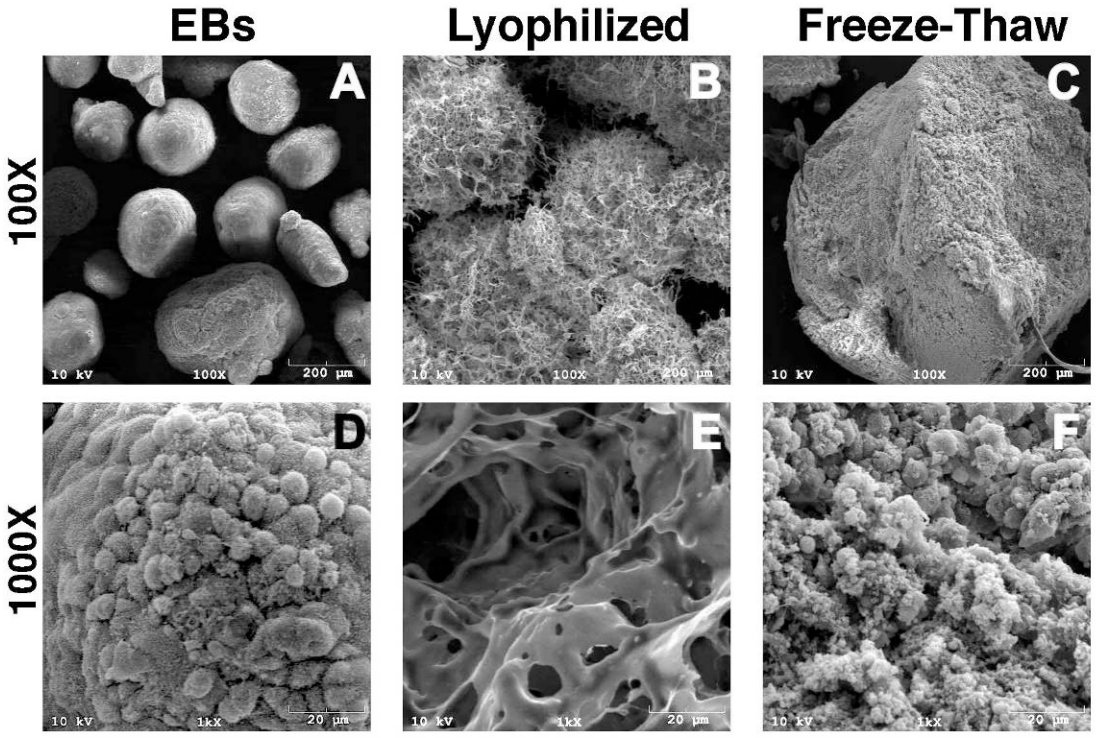

Figure 5.4. Acellular EB ultrastructure. Sample SEM images were taken before and after mechanical permeabilization at 100X (scale bar = 200 mm) and 1000X (scale bar = 20 mm) magnification. EBs (A, D) and lyophilized EBs (B, E) retain separate EB structure; however, lyophilized EBs show a more apparent porous structure compared to untreated EBs. Freeze-thawed EBs (C, F) no longer retained EB morphology and appeared to have a compact and dense structure.

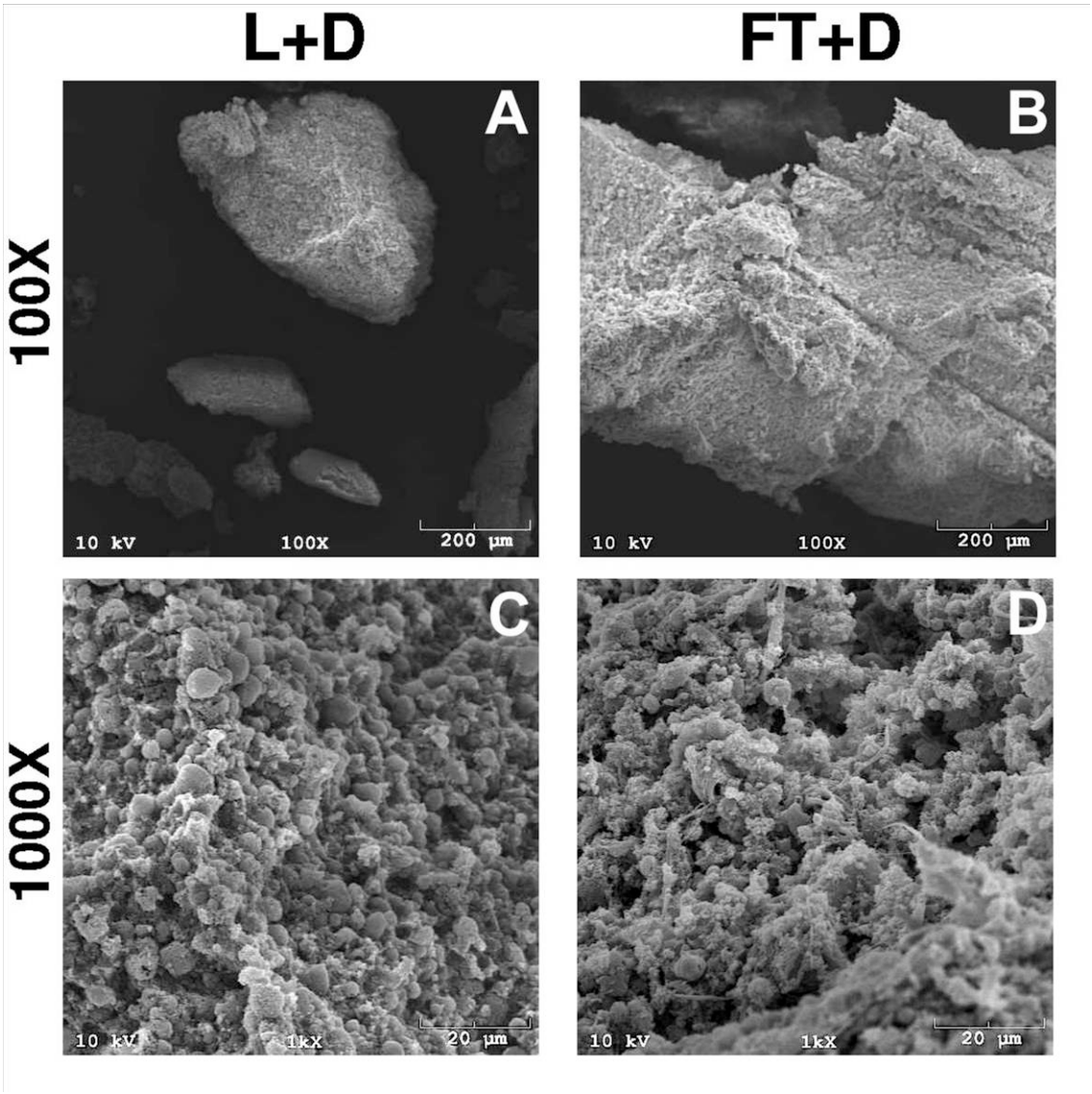

Figure 5.5. Ultrastructure of acelluar EBs with DNase treatment. Acellular sample SEM images were taken after mechanical permeabilization and DNase treatment at 100X (scale bar = 200 mm) and 1000X (scale bar = 20 mm) magnification. L+D (A, C) and FT+D (B, D) samples formed a cohesive mass of particulate material.

Histological analysis

Several notable differences in the histological appearance of lyophilized and FT EBs were also apparent. As indicated initially by SEM, lyophilized EBs were maintained as separate EBs that appeared similar in size and morphology to untreated EBs (Figure 5.6A, B), while repeated freeze-thawing caused individual EBs to agglomerate and form a cohesive mass of indistinguishable EBs (Figure 5.6C), much like Triton- or SDS-treated EBs [216, 270]. Mechanical acellularization methods alone did not remove cellular content, since nuclei were present within the resulting EB matrices (Figure 5.6A-C; 5.6A-C inserts), compared to Triton-treated samples which lacked distinct nuclei [270]. Treatment with DNase after physical permeabilization methods resulted in acellular matrices without discrete nuclei by hemotoxylin staining (Figure 5.6E, F) and little to no detectable Hoechst staining for DNA content (Figure 5.6E, F inserts), demonstrating the effectiveness of DNase treatment. In contrast, DNase alone was not able to effectively permeate untreated EBs (Figure 5.6D; 5.6D insert) to disrupt and remove DNA. Thus, the mechanical acellularization protocols produced matrices with different compositions and varying extents of cell DNA removal.

Quantitative analysis

A multi-parametric set of analyses was performed to quantitatively assess differences in cell viability, DNA removal, and residual protein content resulting from the different acellularization treatments. The viability of the cells (Figure 5.7A) was significantly inhibited to negligible levels by both mechanical acellularization methods ($p = 5.26\text{x}10^{-6}$), as well as by Triton detergent treatment ($p = 5.26\text{x}10^{-6}$), but no

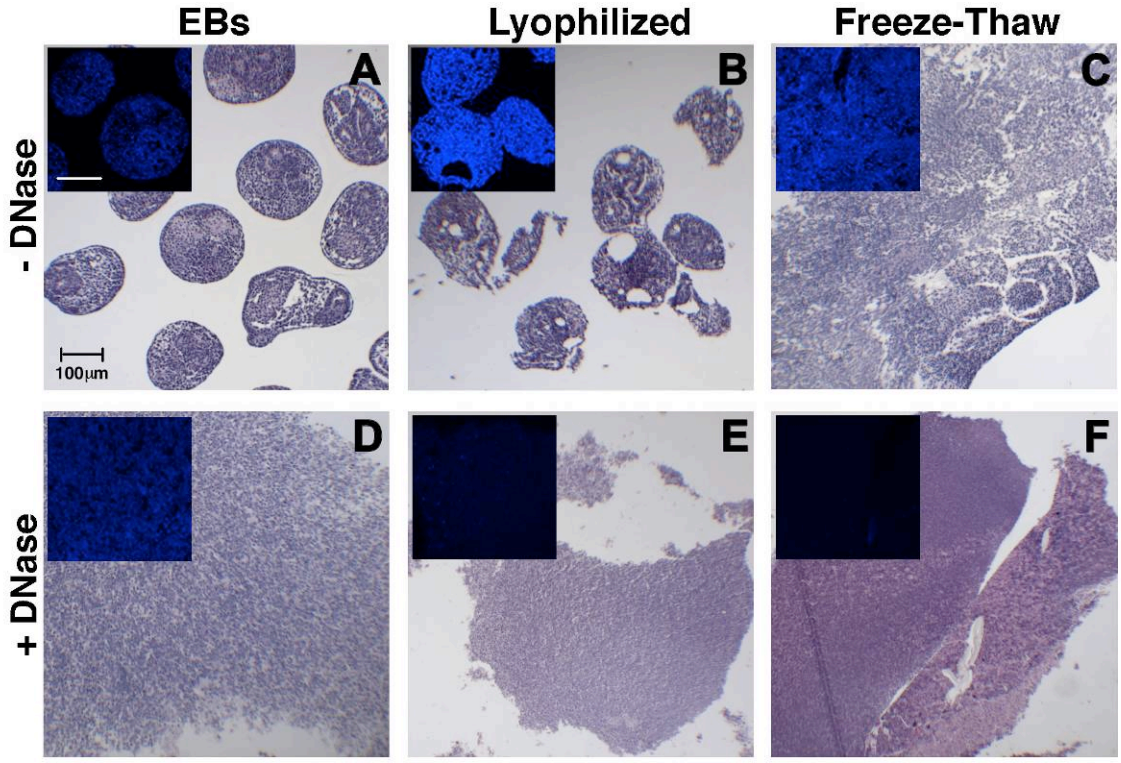

Figure 5.6. Histological analysis of mechanical acellularization. EBs and acellular samples were stained with H&E and Hoechst (inset) to qualitatively compare acellular treatments. Mechanical disruption alone (top row, A-C) was compared to mechanical disruption and DNase treatment (bottom row, D-F).

significant differences between the different permeabilization treatments were observed. Each of the relative values approached the lower sensitivity range of the assay, indicating successful complete inhibition of cell viability by each of the independent methods prior to DNase treatment. The freeze-thaw method of permeabilization allowed the most efficient removal of DNA (removing 75.02 ± 8.06% DNA), exhibited by the significant difference ($p = 1.35x10^{-5}$) in residual DNA between FT and FT+D samples (Figure 5.7B). DNA content remaining in L+D and T+D samples were not significantly reduced compared to lyophilized ($p = 0.763$) and Triton-treated ($p = 0.336$) samples, respectively. Prior to DNase treatment, overall protein content was not significantly reduced between mechanical permeabilization methods compared to untreated EBs, whereas, Triton permeabilization significantly decreased the amount of protein ($p = 0.001$) compared to untreated EBs (Figure 5.7C). With DNase treatment, mechanically permeabilized products exhibited similar protein content to chemically permeabilized samples, indicating that residual protein removal was a result of the subsequent incubation and wash steps following DNase treatment. Overall though, acellularization using mechanical disruption techniques with DNase was capable of producing acellular EB matrices with slightly increased protein content compared to acellularized EBs using detergent solvent extraction methods.

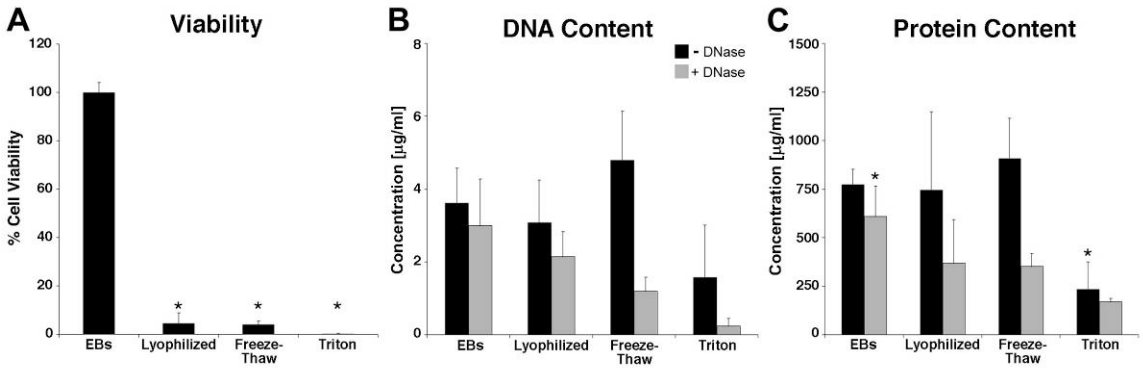

Figure 5.7. Quantitative analysis of acellular EB matrix components. (A) Cell viability of permeabilized samples. (B) Residual DNA concentration pre- and post-DNase treatment. FT permeabilization lead to significant removal of DNA following treatment with DNase. (C) Total protein content pre- and post-DNase treatment. Total protein before DNase treatment in Triton samples was significantly lower than all other treatments; whereas post-DNase treatment of mechanically permeabilized samples significantly decreased protein content compared to no DNase treatment. One-way ANOVA ($p<0.05$): * significant compared to untreated EBs. Two-way ANOVA ($p<0.05$): # significant compared to other pre-DNase samples, † significant compared to same permeabilization, post-DNase.

Acellular matrix protein characterization

The concentration of endotoxin was quantified in lyophilized matrices of day 7 and 10 EBs. The amount of endotoxin contained within the lyophilized matrices ranged between 0.03 – 0.38 EU/mL depending on the batch of EBs assessed (Figure 5.8A), which was less than the FDA guideline of 0.5 EU/mL [271]. Further characterization of two specific growth factors, IGF-2 and VEGF-A, was performed on lyophilized acellular matrix with and without DNase treatment. These samples were chosen for quantifying growth factor retention as a result of the total protein content after mechanical acellularization. The VEGF-A harbored within the lyophilized acellular EBMs was approximately 2 pg/mg for both ± DNase treatment; however, the amount of IGF-2 retained in the lyophilized EBM was 6 pg/mg, while the DNase treated EBM had undetectable levels of IGF-2 protein (Figure 5.8B). Overall, theses results indicated that these acellular EB matrices contained low levels of endotoxin while preserving growth factors content following acellularization.

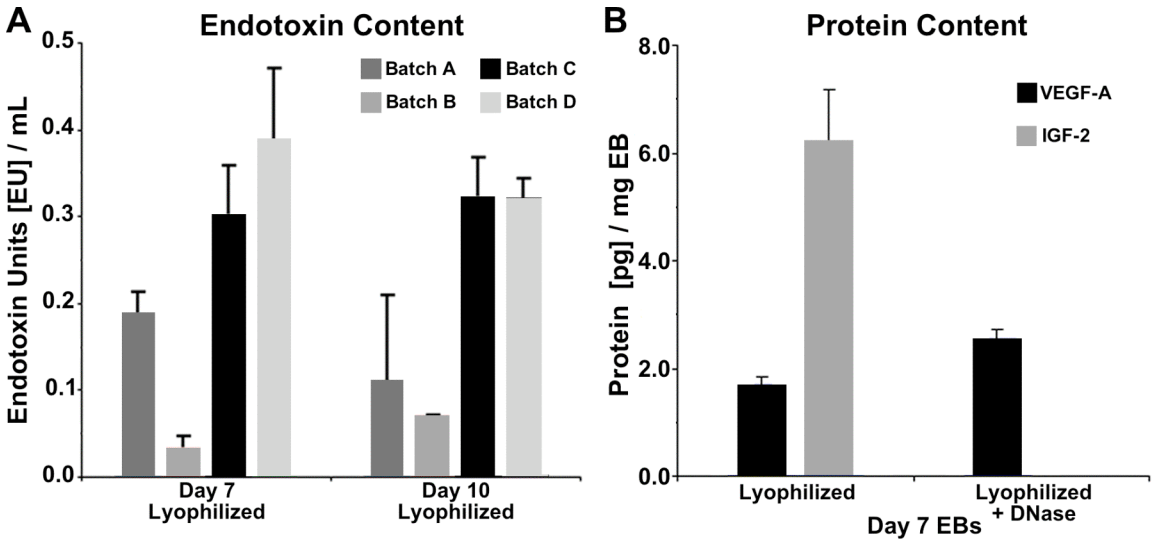

Figure 5.8. **Endotoxin and growth factor protein content.** (A) Endotoxin content present in lyophilized EB matrices remained below the FDA guideline level of 0.5 EU/mL among various batches. (B) The amount of certain growth factors retained within acellular matrices was affected the method of acellularization. Results indicated are mean ± standard deviation (n=4).

Cell repopulation of acellular EB matrices

Fibroblast (NIH-3T3) cell attachment to and repopulation of the resulting acellular EB matrices was examined 4 days after seeding the cells. As previously demonstrated, negligible Hoechst staining was observed in the unseeded acellularized matrices following DNase treatment (Figure 5.6E, F). Exogenously added fibroblasts were easily distinguished from any residual ESC nuclei based on the larger size of the fibroblast nuclei (Figure 5.9Ai, Aiv, Bi, Biv), roughly twice that of ESCs. Auto-fluorescence of the acellular matrix under the FITC channel (green) was used to distinguish the acellular matrix from the exogenously seeded cells (Figure 5.9Aii, Avi, Bii, Bvi). Fibroblasts seeded onto lyophilized matrices attached primarily to the surface of individual lyophilized EBs, but did not appear to invade the acellular matrices (Figure 5.9Aiii); similarly, FT matrices without DNase treatment did not exhibit much infiltration by 3T3 fibroblasts (Figure 5.9Biii). Although the bulk of fibroblasts were distributed throughout the exterior layers of the acellular matrices with DNase treatment, many cells were found within the acellular matrices as well (Figure 5.9Avi, Aiix, Bvi, Biix). Thus, L+D and FT+D treatments of EBs both permitted fibroblast attachment, adhesion, and repopulation of the acellular matrices.

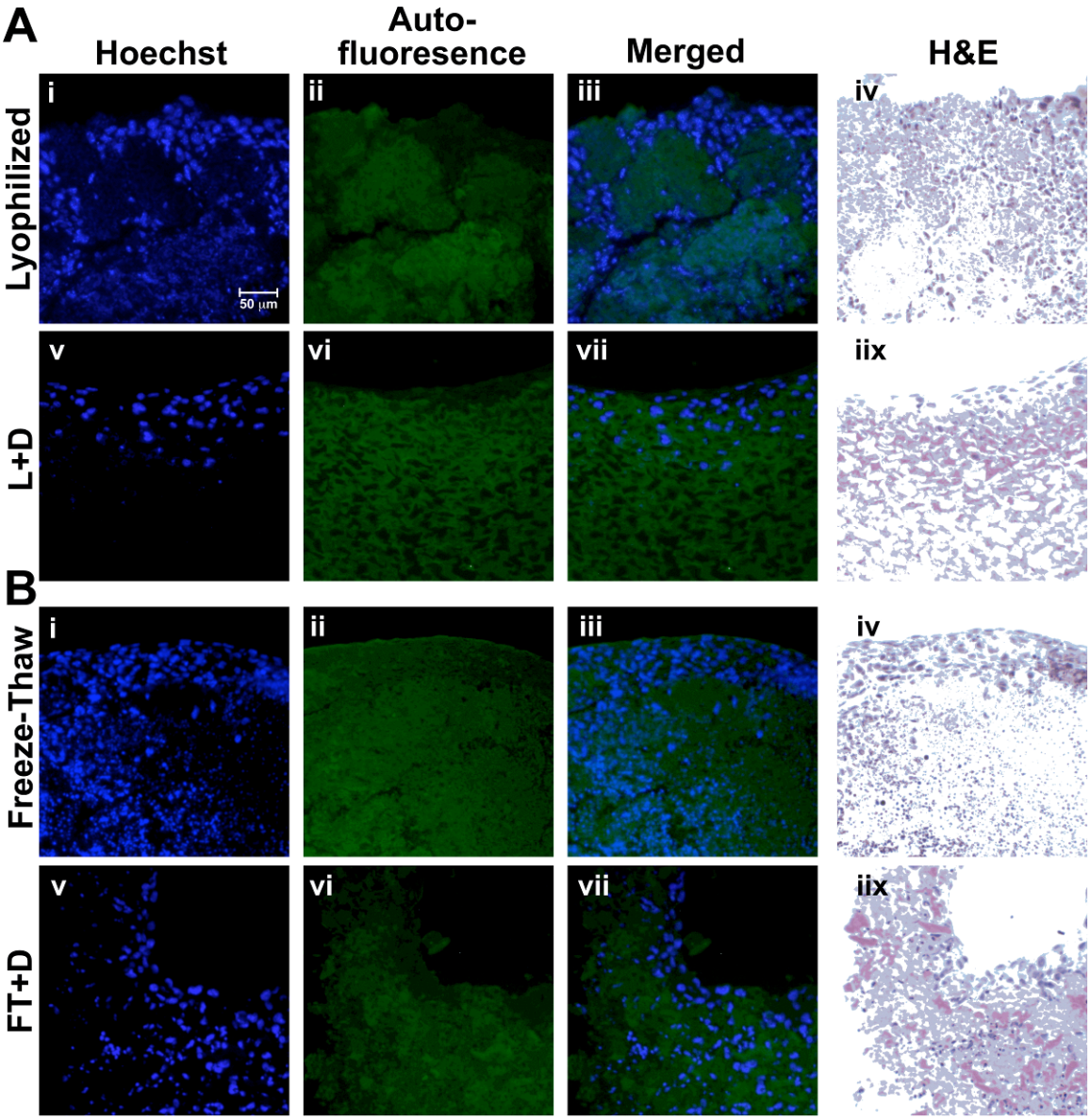

Figure 5.9. Biocompatibility of acellular EB matrices. Fibroblasts seeded on lyophilized and L+D treated matrices (A) and compared to cell seeding on FT and FT+D acellular matrices (B). DNA was stained with Hoechst (blue; first column), while the acellular matrix was visualized via auto-fluorescence (FITC channel; second column). Additionally, seeded matrices were stained with H&E to demonstrate successful repopulation (fourth column).

Discussion

The aim of this study was to develop mechanical acellularization methods to isolate ECM molecules produced by ESCs undergoing differentiation as EBs. The use of mechanical disruption techniques was investigated as an alternative approach to previously reported solvent extraction methods used to acellularize EBs [216, 270]. EBs were deemed acellular based on inhibition of cell viability, removal of DNA, and retention of protein content, thereby producing an EB-derived matrix harboring growth factors and capable of supporting exogenous cell adhesion and survival. Additionally, various batches of acellularized EBs consistently exhibited negligible amounts of endotoxin (< 0.5 EU/mL). Extraction of proteins from acellularized EBs demonstrated the presence of IGF-2 and VEGF-A growth factors retained in the acellular matrix. Isolation of acellular matrices from EBs enables further characterization of the complex assembly of ECM molecules dynamically produced by ESCs as they differentiate. These novel acellular matrices may be utilized as inductive or instructive biological scaffolds in order to determine the functional effects of ESC-derived ECM biomolecules on somatic cell phenotypes and repair and regeneration of acute and chronically wounded adult tissues.

When stem cells are utilized for tissue regenerative applications, the lasting effects typically observed do not include engraftment and stem cell differentiation, suggesting that transplanted cells exert a transient impact on tissue morphogenic processes. The transient effect could likely be due to secreted trophic factors produced by the transplanted cells that stimulate endogenous cells to repair the injured or degenerative tissue site. Previous studies have shown the ability of diffusible ESC-

secreted factors to enhance cell survival and rescue knockout phenotypes [8, 193]; furthermore, secreted factors produced by ESCs could be non-covalently associated with the ECM to modulate the local EB microenvironment. In the current study, mechanical disruption techniques, such as lyophilization and repeated freeze-thaw cycles, combined with DNase treatment resulted in acellular matrices derived from EBs. General compositional differences between acellular EB matrices and untreated EBs included the presence of intact cell nuclei in untreated EBs and indistinguishable morphology of individual EBs in most acellular matrices. Further differences between lyophilized EBs and L+D treated EBs were evident in the amount of IGF-2 extracted from the matrices - L+D treatment had resulted in undetectable levels of IGF-2. However, fibroblast seeding studies demonstrated successful cell attachment to, as well as repopulation of, the acellular EB matrices.

Acellularizing tissues has produced several naturally-derived matrices that are currently being utilized for an array of different clinical applications. Almost all existing acellularized matrices originate from adult tissues, which typically exhibit significantly less regenerative capacity than embryonic tissues. Within the developing embryo, paracrine factors, particularly morphogens and mitogens, are secreted in latent and bioactive forms into the ECM of the local microenvironment to influence and direct subsequent cell and tissue morphogenesis. As EBs differentiate, a similar cadre of morphogens and mitogens are produced within EBs, thus using EBs as the starting tissue source for acellularization provides a unique opportunity to harness complex assemblies of molecules directly from EBs mimicking embryogenesis *in vitro*. By acellularizing EBs at various stages of differentiation using different types and combinations of

permeabilization and extraction, the biomolecules associated with the differentiation of EBs and secreted into the ECM can be effectively harnessed and subsequently analyzed.

The development of acellular matrices derived from stem cells may obviate many of the potential complications encountered by using cell transplants or viable tissues constructs for tissue regeneration applications. Matrices derived from cells and tissues provide a natural scaffold material for cell adhesion and a vehicle to present instructive, morphogenic cues to cells that repopulate the scaffold. Acellular EB matrices could provide a unique, potent reservoir of morphogenic factors produced by ESCs differentiating in a 3D environment. In the future, acellular EB matrices could even be tailored for specific tissue applications by directing ESCs within EBs to differentiate towards specific cell phenotypes, which in turn could yield "tissue-specific" extracellular matrices from a single cell source. Overall, the results of this study demonstrate that mechanical acellularization of EBs is a novel route to directly obtain ESC-derived ECM molecules for potential regenerative medicine therapies.

Conclusions

The ability to harness ESC-produced molecules to stimulate tissue morphogenesis independent of the cells themselves is a novel approach in regenerative medicine. Acellularizing embryoid bodies using mechanical methods provided a means to analyze secreted molecules by ESCs in a matrix formulation that can be further tested *in vitro* to assess effects on migration, proliferation, and differentiation of exogenous cell types. Initial characterization revealed growth factor retention within the acellular EB matrix, however, global analysis of the composition of biomolecules present in the EB matrix

would elucidate the extracellular morphogens secreted by embryonic stem cells mimicking early stages of embryogenesis. Thus, the molecular cues produced during EB differentiation and harbored within the extracellular matrix could have broad applications in tissue regeneration strategies.

CHAPTER 6

ACELLULAR ESC-DERIVED MATRICES HARBOR BIOACTIVE FACTORS THAT AFFECT ASPECTS OF ANGIOGENESIS

Introduction

Cells secrete extracellular factors in order to regulate themselves in an autocrine manner or control surrounding cells in a paracrine manner. This mode of paracrine action has been studied specifically regarding the regenerative effects of secreted molecules, specifically in cell transplantation and conditioned media studies. Transplanted cells grafted into compromised tissues have been shown to yield considerable regenerative effects, however, the number of engrafted cells within the transplantation site are minimal. As of recent, there has been a wealth of literature to support the paracrine effects of transplanted cells. Studies involving MSC transplantation in the infarcted myocardium demonstrate functional benefits within 72 hours of transplantation, due to MSC paracrine factors providing a cytoprotective effect rather than cell engraftment [185, 272]. In order to alleviate the issue of transplanting cells, such as cell sourcing and obtaining sufficient quantity of cells, several studies have investigated the effects of conditioned media as a cell-free method to deliver secreted factors from a number of cell types typically utilized for cell transplantation, including adipose-derived stem cells (ASCs) [186, 273], endothelial progenitor cells (EPCs) [274], and ESCs [192, 243]. Progenitor cell-conditioned media has been demonstrated to be effective in modulating cellular responses by promoting cell survival and inhibiting apoptosis, as well as stimulating endogenous tissues in order to regenerate specific tissue

function, such as myocardium and vasculature, and overall wound healing and angiogenesis [189, 236, 275, 276]. The factors generally involved in stimulating cells in a paracrine manner are growth factors and cytokines, which typically have short *in vivo* half-lives in a soluble state [277] and would potentially require multiple injections when examining conditioned media effects *in vivo*. Additionally, the amount of factors generated in conditioned media is dilute and require concentrating down the volume to obtain growth factor concentrations at clinically relevant levels. Furthermore, administering secreted factors via conditioned media may not be clinically applicable. However, delivering growth factors associated with ECM has been used in a number of clinical settings, such as becaplermin, a recombinant form of PDGF [94] in combination with collagen products [278]. *In vivo*, growth factors are naturally associated with the extracellular matrix, potentially in latent form, and upon activation by proteases are released from the ECM to bind cell surface receptors, whereas other growth factors can bind receptors in their matrix-associated state. Therefore, the ECM acts as a reservoir for a variety of secreted growth factors by the residing cells, while the ECM proteins themselves provide binding domains for a number of adhesion receptors. The myriad of ECM and growth factors is fundamental in tissue regeneration processes, especially wound healing and angiogenesis. Several delivery strategies have been reported in order to control the release of growth factors from a variety of delivery systems, including fibrin matrices, bioartificial matrices, and decellularized tissues [279-281].

Acellularizing tissues has been a means to harness naturally derived matrices that contain a complex milieu of ECM and growth factors. Despite the number of acellular matrices derived from tissues, only a few studies have extracted and identified specific

factors retained within the matrix. Growth factors have been extracted from the extracellular matrix from a variety of tissues, including SIS, ABM, BSM, and amniotic membrane, and have been shown to retain bioactivity in a number of assays, including *in vitro* and *in vivo* studies [157-159, 282]. With all the above mentioned, only a few studies have examined acellularizing more embryonic associated tissues, such as placenta or amniotic membrane [127, 282]. Embryonic environments yield morphogens that promote proliferation, migration, self-renewal, and differentiation (reviewed in [283]), which can impact the response of fetal wound healing [284] or suppress tumor phenotypes [285]. Previous studies within our lab have established the presence of extracellular factors such as hylauronan and versican [211], among others, as well as the methods to isolate EB matrices using acellularization techniques such as chemical, mechanical, and enzymatic treatments [216, 270]. Based on results from previous chapters, including EB differentiation profile and acellular matrix protein retention, this study aims to examine the extraction of growth factors retained in acellularized EB matrices (EBMs) derived using lyophilization techniques as well as the bioactive effects on exogenous cells and tissues elicited by the morphogens harnessed within EBMs.

Methods

Cell culture

Mouse embryonic stem cells (ESCs; D3 cell line) were initially expanded on a feeder layer of mouse embryonic fibroblasts and were subsequently cultured feeder-free for several passages on 0.1% gelatin-coated 150 mm polystyrene cell culture dishes

(Corning) with Dulbecco's modified eagle medium (Mediatech), supplemented with 15% fetal bovine serum (HyClone), 2 mM L-glutamine (Mediatech), 1x MEM non-essential amino acid solution (Mediatech), antibiotic/antimycotics (Mediatech), and 0.1 mM β-mercaptoethanol (MP Biomedicals, LLC). Undifferentiated cells were expanded prior to EB formation in the presence of 10^3 U/mL leukemia inhibitory factor (LIF) (ESGRO), which was added to the culture media upon each re-feeding. Cells were passaged every two to three days before reaching ~70% confluence. To initiate EB culture, ESCs were trypsinized from the gelatin-coated dishes using 0.05% Trypsin/0.53 mM EDTA (Mediatech) and formed in AggreWell™ 400 inserts (Stem Cell Technologies) for the first 24 hours [286, 287]. A density of $6x10^6$ cells in 3 mL differentiation media (ESC media without LIF) was used to inoculate one AggreWell™ insert containing 6000 wells to form 1000 cell EBs. After allowing the cells to settle for a few minutes, inserts and cells were centrifuged for 5 minutes at 200 x g. After 24 hours of culture, EBs were transferred out of the AggreWell™ to rotary suspension culture with ~2500 EBs cultured in 1x100 mm bacteriological grade polystyrene Petri dishe (Corning) with 10 mL differentiation media. EB suspension cultures were maintained on rotary orbital shakers (Barnstead Lab-Line, Model 2314) at 40 rpm at 37°C in 5% CO_2 for the entire duration of suspension culture. Previous work from our lab has demonstrated that rotary orbital suspension culture methods result in greater yields of homogeneous populations while preventing agglomeration of EBs [213]. EBs were cultured in suspension for up to 10 days and re-fed every other day after collecting independent EB cultures via gravity-induced sedimentation in 15 mL conical tubes. Spent media was aspirated, and the

cultures were replenished with 10 mL of fresh differentiation media before being placed back in the Petri dishes and returned onto the rotary orbital shakers.

NIH-3T3 fibroblasts were cultured on tissue culture dishes in 3T3 growth medium containing DMEM supplemented with 10% bovine growth serum (BGS), 4 mM L-glutamine, 100 U/ml penicillin, 100 μg/ml streptomycin, and 0.25 μg/ml amphotericin. Human umbilical vein endothelial cells (HUVECs, Lonza) were cultured on gelatin-coated tissue culture dishes in endothelial growth medium (EGM-2), consisting of Endothelial Basal Media (EBM, Lonza) with the addition of the EGM-2 BulletKit™ consisting of 5% FBS, human EGF, hydrocortisone, gentamincin, amphotericin-B, VEGF, human FGF-2, recombinant IGF-1, ascorbic acid, and heparin.

Acellularization of EBs

Acellular EB matrices (EBMs) were obtained from EBs after days 7 and 10 of rotary culture. Day 7 and day 10 EBs were investigated based on the increased gene expression results, in particular the angiogenic growth factors, in Chapter 3 and 4. Lyophilization methods without DNase, previously described in Chapter 5 were used to acellularize these EBs. Briefly, EBs were formed for 24 hours using microwells, transferred to rotary suspension culture at 40 RPM, and re-fed every other day with fresh differentiation media. At days 7 and 10, EBs from all plates were collected as a single batch by sedimentation, rinsed 3 times with PBS, and resuspended in 1 mL of molecular biology grade water per plate of EBs. To obtain separate samples of EB matrix, 1 mL of EB suspension was aliquoted into a microcentrifuge tube, EBs were gently centrifuged at 1000 RPM for 1 minute at room temperature, and then frozen at -80^{o}C prior to

lyophilization. After lyophilizing samples for 24 hours, the mass of EB matrix was calculated by subtracting the mass of the tube alone from the mass of the EB matrix + tube. Dried EBM samples were stored in a dessicator at room temperature.

EBM extractions

Extraction of morphogens from lyophilized EB matrices (day 7 and day 10) were examined using two different extraction buffers – tissue protein extraction buffer (TPER, Thermo) and serum-free media. For both TPER and serum-free media EBM extractions, two different doses of EBM were examined for morphogen extraction - 3 mg/mL and 6 mg/mL. TPER buffer is mild enough that proteins can be assessed using reporter assays and immunoassays. Serum-free media can be readily applied to any cellular activity assay without requiring dialysis or dilutions. The appropriate volume of buffer was added to each EBM sample in a microcentrifuge tube, pipetted up and down, and placed on a rotisserie overnight at 4^{o}C. Serum-free media consisted of low glucose, phenol red-free DMEM and 0.1% bovine serum albumin (BSA, Fraction V) supplemented with 4 mM L-glutamine, 100 U/ml penicillin, 100 μg/ml streptomycin, and 0.25μg/ml amphotericin. Additionally, serum-free media extractions samples were heat treated at 95^{o}C for 5 minutes to compare bioactivity with and without heating. Before treating cells with EBM extractions, all samples (n=4 per group) were centrifuged to remove insoluble matrix for 5 minutes at 14,000 RPM at room temperature.

Protein quantification assays

The total protein content of day 7 and day 10 EBMs was determined using a bicinchonic assay (BCA, Thermo) for EBM extractions after 24 hours, as described previously. All samples were prepped and analyzed for total protein content according to the protocol provided by the BCA manufacturer. Absorbances were read on a SpectraMax M2e plate reader at 562 nm, and protein concentrations were calculated based on a BSA protein standard curve (0 – 2000 μg/mL).

As for quantifying specific growth factors extracted using TPER and serum-free media, enzyme-linked immunosorbent assays (ELISA) were performed for four growth factors: BMP-4, FGF-2, IGF-2, and VEGF-A (DuoSet, R&D Systems). FGF-2 ELISA kit was for human FGF-2, thus the cross-reactivity with mouse FGF-2 was ~30%, as reported by the manufacturer, and the results are the direct result of the ELISA. TPER extractions were not compliant with the BMP-4 ELISA kit, determined after several ELISA runs resulted the standards having a very small dynamic range unlike what is described in the product manual and the serum-free media extractions, thus BMP-4 was not analyzed for TPER extractions. Appropriate diluents (TPER or serum-free media) were used for the standard curve samples depending on the sample set, either serum-free media or TPER buffer. The amount of analyte was assessed using the colorimetric reaction of peroxidase and tetramethylbenzidine (TMB) with an absorbance reading at 450 nm. The absorbances for each sample were compared to the standard curve to establish the protein analyte content, which was normalized to the mass of EBM.

Proliferation assays

For proliferation studies, NIH-3T3 fibroblasts and HUVECs were cultured to approximately 50% confluence in 2-chamber glass slides (BD Bioscience), at which point growth media were removed and the cells were rinsed 3 times in PBS. Cells were then starved overnight in low-serum media, followed by an 18-hour pulse with 10 mM 5-bromo-2'-deoxyuridine (BrdU) in EBM extractions with the respective serum-free media as well as control media, including respective growth media (positive control) and serum-free media (negative control) (n=4 per treatment group). Matrix extractions utilized for 3T3s were conducted in serum-free 3T3 media consisting of low glucose, phenol red-free DMEM and 0.1% bovine serum albumin (BSA) supplemented with 4 mM L-glutamine, 100 U/ml penicillin, 100 μg/ml streptomycin, and 0.25 μg/ml amphotericin; whereas, EBM extractions for HUVECs used serum-free EC media which consisted of EBM and 0.1% BSA supplemented with 100 U/ml penicillin, 100 μg/ml streptomycin, and 0.25 μg/ml amphotericin. After the 18-hours pulse, cells were rinsed with PBS and fixed in 70% ethanol with 2.3M HCl for 10 minutes at room temperature, rinsed in PBS 3 times, and incubated with mouse anti-BrdU primary antibody (Molecular Probes) for 1 hour at room temperature. Following primary antibody incubation, the cells were incubated with donkey anti-mouse secondary antibody conjugated to Alexafluor 488 (Invitrogen) for 2 hours at room temperature, counterstained with Hoechst, and then coverslipped using GelMount (Electron Microscopy Sciences).

Stained slides were imaged using a Nikon 80i upright microscope with a SPOTFlex digital camera and SPOT Advanced Software (Nikon) using both the FITC and DAPI filters. Nuclei counts were performed on all images using the "nuclei count"

application within MetaMorph (Molecular Devices), which counted the number of events, between ~ 5 – 30 pixels in diameter, that were above the set intensity level. The percentage of BrdU-positive nuclei (FITC) was calculated for all images taken (n=6 fields of view per chamber) to determine the amount of proliferation induced by the EBM extraction samples compared to the heat inactivated EBM extractions as well as the control media samples, growth and serum-free media.

Migration assays

For migration studies, NIH-3T3 fibroblasts and HUVECs were each grown to ~80% confluence, inactivated with 10 μg/mL mitomycin-C in serum-free media (2 hours at 37°C in 5% CO_2) and cultured overnight in growth media. Cells were also fluorescently labeled in serum-free media with 1 μM CellTracker® Green (Molecular Probes) for 20 minutes at 37ºC, followed by a 30 minute incubation in growth media prior to initiation of the migration experiment.

HTS Fluroblok transwell culture inserts (Falcon, 24-well, 8 mm pore size) were prepared with 300 μL single-cell suspension ($7.5x10^4$ 3T3s or $1x10^5$ HUVECs) in growth media (loaded in the top chamber). The bottom of the transwell chamber was filled with 800 uL of EBM extractions in the appropriate media for each cell type (non-heat-inactivated or heat-inactivated), as described above, or control media, including cells' respective growth media (positive control) and serum-free media (negative control). Transwell culture plates were incubated for 24 hours in 37°C at 5% humidity, and fluorescent microscopy images of the bottom of wells were taken at 0, 3, 6, 12, and 24 hours using a Nikon TE 2000 inverted microscope with a SpotFLEX digital camera and

SPOT software (Nikon). Additionally, fluorescence measurements of each transwell as well as a range of known number of CellTracker™–labeled cells were taken (ex: 492 nm, em: 515 nm) using a SpectraMax M2e plate reader. The number of cells that migrated through the porous membrane was calculated based on a fluorescent cell standard curve generated for each cell type labeled with CellTracker™ ranging between 0 - 200,000 cells with cell number plotted against relative fluorescent units. At each time point, the change in relative fluorescent units from 0hr was calculated and used to determine the number of cells that migrated during that time period from the cell standard curve.

HUVEC network formation assay

Network formation assay was performed using HUVECs plated on growth factor-reduced Matrigel™ (GFRM, BD Biosciences). Two different methods of treating HUVECs on GFR Matrigel™ with EBM were studied – extracted EBM factors and lyophilized EBM. For both studies, HUVECs were each grown to ~80% confluence, fluorescently labeled in serum-free media with 1 μM CellTracker® Green (Molecular Probes) for 20 minutes at 37ºC, followed by a 30 minute incubation in growth media prior to trypsinization.

The first method introduced soluble factors contained in serum-free EC media EBM extractions (3 mg/mL and 6 mg/mL), previously described in the proliferation and migration assay. GFR Matrigel™ (200 μL per well) was allowed to gel for 30 minutes at 37^{o}C in a 24 well plate. Treatment groups included EBM extractions from either day 7 or day 10 EBM at 3 mg/mL, with a corresponding heat-inactivated sample, which was heated to 95^{o}C for 5 minutes. Prior to adding the cells to each extractions, all samples

were centrifuged for 5 minutes at 14,000 RPM. HUVEC growth media (EGM-2) was used as a positive control, while serum-free EBM was used as a negative control. After HUVECs were trypsinized and rinsed in PBS, a $1.92x10^6$ cells/mL cell suspension in serum-free EBM was used to add 48,000 HUVECs (25μL volume) to 275 μL of sample media, resulting in 300 μL total volume of sample added per well of Matrigel.

The second method assessed the EBM as a whole by embedding the lyophilized matrix into the GFR Matrigel. EBM obtained from days 7 and 10 EBs, in addition to heat-inactivated EBM from both time points, was used in the network formation assay. On ice, approximately 3mg of each type of EBM (n=3) was mixed with 50 μL of PBS to hydrate the powdery matrix followed by 150 μL of GFR Matrigel, while 50 μL of PBS with no matrix was used a control. The 200 μL mixture of Matrigel and EBM+PBS or PBS alone was added to a well of a 24 well plate and allowed to gel for 30 minutes at 37^oC. After HUVECs were CellTracker-labeled and trypsinized, a cell suspension of 160,000 cells/mL was prepared in EGM-2 and distributed among the wells at 48,000 cells (300 μL) per well.

For both network formation assay methods, fluorescent microscopy (FITC) was utilized to analyze the extent of HUVEC network formation after 18 hours using a Nikon TE 2000 inverted microscope with a SpotFLEX digital camera and SPOT software (Nikon). Images taken at 4X (n=4 per treatment) were quantified using the "Angiogensis Network Formation" application within Metamorph software (Molecular Devices) using the following parameter settings: "minimum tube width" = 1 pixel, "maximum tube width" = 7 pixels, and "grey level intensity threshold" = 16. All quantified images were assessed individually by visual inspection; if quantified images did not detect aspects of

the original image accurately, parameters were adjusted to highlight the tubes in the original image. A variety of network formation measures were expressed as a fold change compared to GFRM only controls. One-way analysis of variance (ANOVA) was used to test significance followed by a Dunnett's test ($p < 0.05$) of the treatment measures compared to control (GFRM only) measures.

Quail chorioallantoic membrane (CAM) assay

Corturnix quail eggs were obtained from Ozark Egg Company (Stover, MO) and labeled "day 0" upon arrival in the lab. Eggs were incubated overnight at 37^{o}C in a humidified chamber. On day 1, in a laminar flow hood, each egg was opened using small scissors, transferred to a well in a 6-well plate, and incubated for 7 days at 37^{o}C in a humidified incubator. Instruments used to open and transfer each egg were sonicated in 70% ethanol for ~1 minute and flamed, while each egg was sprayed with 70% ethanol prior to opening. After 7 days of incubation, each CAM was treated randomly with two samples. EBM isolated from day 7 and 10 EBs as well as respective heat-inactivated samples (negative control) and GFRM samples (positive control) were analyzed. To preserve the sterility of the EBMs and GFRM, the amount of sample for each treatment was determined prior to lyophilization. The amount of EBM per sample was normalized to a single plate of EBs, which corresponded to a dry EBM mass approximately between 1 - 2 mg, while the amount of GFRM used was similar in volume to the EBM samples, yet corresponded to a dry mass approximately half that for EBM, between 0.5 – 1 mg. Areas of the CAM with sparse vessel growth were chosen in order to easily visualize the progression of any angiogenic response. Digital images were captured at 1.25X

following sample placement at times 0, 24, and 48 hours using a Leica M165 stereoscope coupled to a Nikon Coolpix digital camera. After 48 hours of treatment, CAMs were fixed using 4% paraformaldehyde and 2% gluteraldehyde for 48 hours at 4^{o}C. The CAMs were isolated and transferred into a 35mm Petri dish and rinsed with PBS for 48 hours. Using a 10mm biopsy punch, treated areas of the CAM were isolated and placed on a microscope slide and imaged at 2X magnification using the stereoscope setup previously mentioned.

CAM image analysis

CAM images taken at 0, 24, and 48 hours prior to fixation were analyzed by quantifying the number of radiating, or anisotropic, vessels around the area of matrix treatment. In LabView's Vision Assistant software, digital RGB images were split into the three color channels (red, green, blue); the green filter was extracted and used for the vessel counts. Using the green filter images, concentric circles with two different diameters (6mm and 10mm) surrounding the matrix sample were created in Adobe Fireworks software and then imported into ImageJ to count the number of intersecting primary (large) and secondary (branching off of the primary) vessels with each of the circles. For each treatment, the Poisson count data between time points was tested for significance using the Poisson model with the Pearson's test statistic to determine if the means were equal [288]. If the means among the three time points were not equal, with a Pearson's test statistic of $p < 0.05$, then comparisons between each time point were conducted with a Bonferroni correction for alpha, such that significance between time points were determined with $p < 0.01$.

Additionally, semi-quantitative analysis was performed on fixed CAMs after 48 hours of treatment from digital images capture using a stereomicroscope, as described by Ribatti *et al*. [86]. Briefly, the angiogenic response was scored on graded scale between 0 – 5, where 0 indicates no response to the graft, 5 refers to dilated, branching vessels in a dense "spoke-wheel" pattern, and scores 2 -5 represent gradual increases in vessel density and branching resembling a "spoke-wheel" pattern. These scores can then be used to obtain a coefficient of angiogenesis by summing the scores and dividing by the highest sum possible (5 x #CAM images), thus resulting in a coefficient value between 0 and 1 [289].

Images of fixed CAMs were converted from .NRW to .TIFF format using Nikon ViewNX software. A custom LabVIEW 2010 .vi was created to isolate the vasculature from the image background and calculate the total percent vessel area. The images were converted from 32-bit RGB to 8-bit grayscale by isolating the green color plane. Further image thresholding was applied to the grayscale image using Niblack's local thresholding method in order to generate a binary image [290]. Niblack's method determined if the intensity of a pixel exceeded the mean kernal (default setting = 48 pixels x 32 pixel area). If the pixel did exceed this value, it was kept in the image; if not, it was removed. Based on visual assessment through trial and error, the default setting was used rather than a user-defined setting. Next, the resulting binary image was dilated using a 3x3 dilation matrix followed by a series of proper open and proper close algorithms, each using a 3x3 matrix. The open/close series are most easily represented in terms of their logical definitions [291]:

$$\text{Open: } A \bullet B = (A \oslash B) \blacksquare B$$

Close: $A \cdots B = (A \blacksquare B) \text{Ø } B$

$\blacksquare$ = dilation and Ø = erosion

Where 'A' is a defined region (3x3 matrix) and 'B' is the structure by which 'A' is eroded or dilated. Essentially this series of dilations and erosions fill in the holes created within a continuous vessel in the binary image resulting from the Niblack's local thresholding without exaggerating the vessel structures. The open/close series was followed by a single iteration low-pass particle filter, which removed all particles with dimensions below 5x4 pixels from the image, to produce a "clean" image. Due to the nature of the Niblack local thresholding, the centers of large vessels were deleted during the thresholding process. To correct for this loss, images were touched up manually in ImageJ; original images were used as a reference, and the centers of large vessels were filled in by hand. Images were also cropped to ensure that only the membrane area (10 mm diameter) was included. Vessel area fraction was calculated using ImageJ's histogram function (white pixels = 255 or black pixels = 0), such that:

$$\text{Vessel Area Fraction} = \#\ \text{Pixels}_{255} / \text{Total}\ \#\ \text{Pixels}_{(255+0)} \times 100$$

Statistical analysis

All experimental samples were analyzed with $n \geq 3$, with data presented as mean ± standard error. Unless otherwise stated, statistical significance was determined using SPSS® Statistics (IBM) employing an one-way analysis of variance (ANOVA) test. Levene's test was used to determine the equality of variance ($p < 0.05$) in the samples. When the Levene's test was significant, Games-Howell post-hoc analysis was used to determine significance ($p < 0.05$), but when the Levene's test was not significant, thus

equal variances among samples, Tukey post-hoc analysis was used to determine significance ($p < 0.05$).

Results

Growth factor protein extraction from acellular EBMs

In order to readily quantify several growth factors retained in the EBM and further compare the differential protein content between matrices obtained from EBs at later stages of differentiation, proteins were extracted from EBM using two different solutions – TPER buffer and serum-free media. Preliminary studies examining the use of other solutions are described in Appendix A. TPER buffer was the less mild of the two buffers used since it contained a proprietary mixture of salts and a mild detergent. To examine the efficiency of each buffer to extract proteins in general, total protein content was quantified. For TPER buffer, neither mass nor day of differentiation affected the extraction of total protein from the EBMs, since there was no significant difference between samples (~400 μg/mL, Figure 6.1A). As for serum-free media (SFM) extractions, total protein content was similar across EBM days and doses with ~400 μg/mg total protein extracted, except day 10 at 3 mg/mL yielded approximately 3-fold more total protein (~ 1000 μg/mg) (Figure 6.2A). Heat treatment (HT) of SFM extractions resulted in significantly less detection of total protein compared to non-HT counterparts, which indicated that heating the SFM extractions did impeded the detection of a significant amount of proteins present in the non-HT extractions (Figure 6.2A). Since TPER extractions were not further investigated in subsequent *in vitro* assays and heat treatment was included as a negative control for these studies, TPER extractions

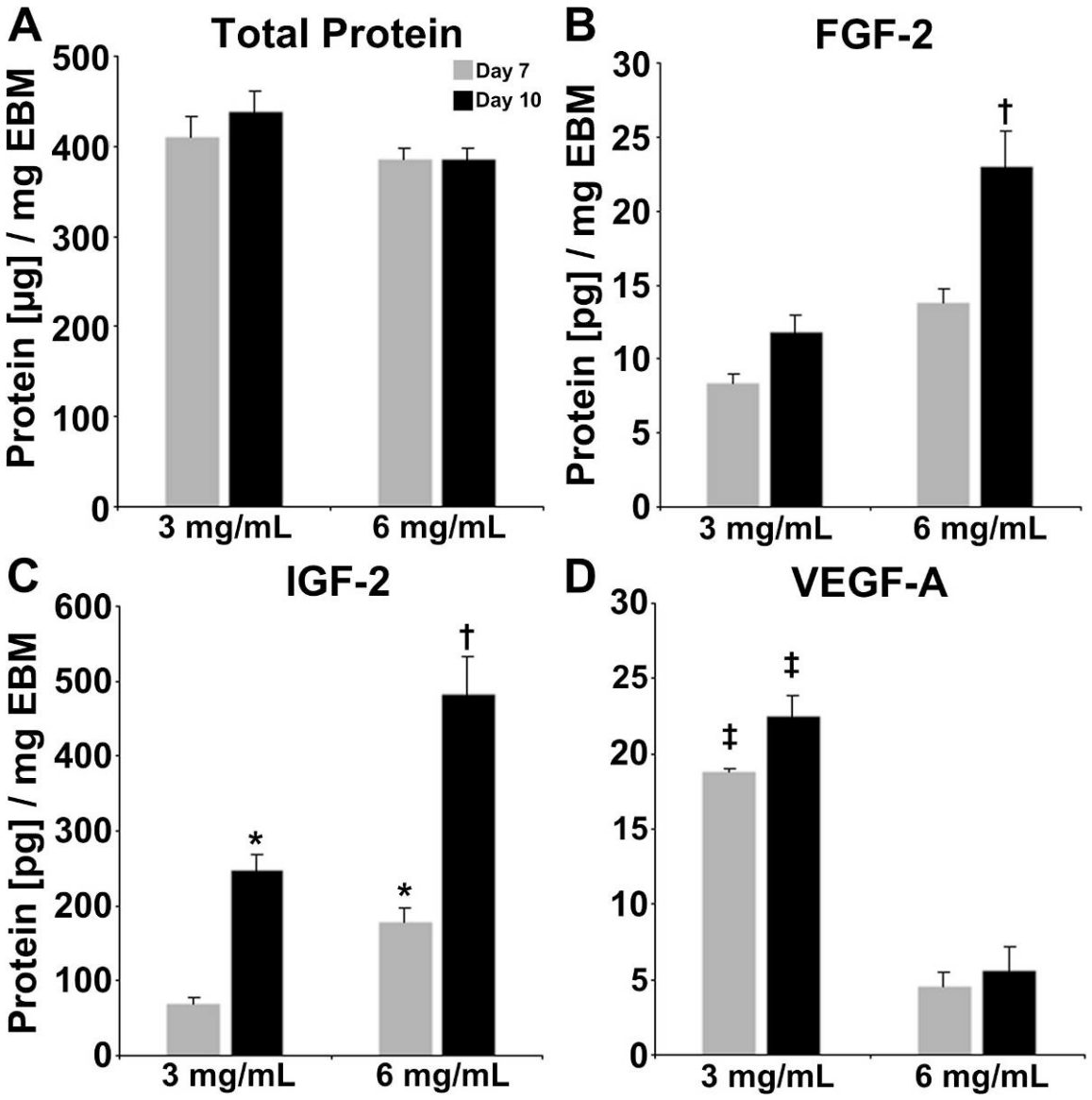

Figure 6.1. **TPER buffer extraction from EBM**. (A) Total protein extracted from EBM after 24 hours. (B-D) Specific growth factor protein components present in the TPER extraction. Results shown are mean ± standard error (n=4). ANOVA: † $p < 0.05$ compared to all other samples; ‡ $p < 0.05$ compared to 6 mg/mL day 7 and 10; *$p < 0.05$ compared to 3 mg/mL day 7.

were not heat-treated. Nonetheless, with the exception SFM extraction of 3mg/mL day 10 EBM, there appeared to be a limit to the extractable proteins from EBM using mild solutions - ~400 μg/mg which is approximately 40% of the total matrix mass. Overall, between the non-HT extractions, TPER and SFM both resulted in similar amounts of total EBM extracted protein.

In contrast to the total protein results, the extraction of specific growth factors from the EBMs for each buffer varied depending on matrix mass, day of differentiation, and heat treatment. TPER buffer extracted similar levels of FGF-2 from each matrix dose for day 7 and EBM (~8 and14 pg/mg, respectively), while day 10 at 6 mg/mL resulted in significantly more extracted FGF-2 compared to all other EBM samples. These data suggest a maximum extractable amount of FGF-2 present TPER extractions for day 7, but day 10 increases with EBM dose (Figure 6.1B). On the other hand, increases in matrix mass did affect TPER extraction of IGF-2 and VEGF-A (Figure 6.1C, D). For IGF-2, the increase in matrix mass, from 3 mg to 6 mg, resulted in significant increases (~2X) in the amount of IGF-2 extracted from both days 7 and 10 EBM. Furthermore, IGF-2 contained in TPER extractions from day 10 EBM were significantly more than day 7 EBM TPER extractions at both doses, demonstrating that day 10 EBs expressed more IGF-2 than day 7 EBs. As for VEGF-A, increases in matrix mass resulted in significant decreases (~4-fold) in TPER extraction of VEGF-A from both day 7 and 10 EBM: at 3 mg/mL both day 7 and 10 EBM extractions contained ~20 pg/mg, while at 6 mg/mL extracted VEGF-A was ~5 pg/mg for both day 7 and 10 EBM (Figure 6.1D). This decrease in VEGF-A extraction implies that the increased presence of certain

EBM molecules may inhibit VEGF-A extraction, i.e. ECM proteins that bind VEGF-A and render it insoluble.

Compared to TPER extractions, the content of specific growth factors in non-HT serum-free media (SFM) extractions were generally similar (Figure 6.2C-D). Due to ELISA incompatibility, BMP-4 could not be determined in TPER extracts; however, the amount of non-HT SFM extracted BMP-4 across all samples (mass and time point) was similar, ~40 – 57 pg/mg; following HT, the amount of BMP-4 was significantly lower, between 5 – 10 pg/mg, in each HT extraction compared to their respective non-HT sample, yet not significantly different among all HT SFM extractions (Figure 6.2B). This result indicated that a maximum extractable amount of BMP-4 was present in non-HT SFM extractions, and upon heating SFM extractions, detection of BMP-4 was hindered. Another growth factor that was present in significantly higher amounts in non-HT SFM extractions compared HT ones was FGF-2 (Figure 6.2C). Between non-HI SFM extractions, similar amounts of FGF-2 (12 – 21 pg/mg) were present and also comparable to FGF-2 levels in TPER extractions, with the exception of significantly higher levels (36.56 pg/mg) of extracted FGF-2 from day 10 EBM at 3 mg/mL compared to all other non-HI samples. The FGF-2 present in the HT SFM extractions were all significantly reduced (< 1 pg/mg) compared to their respective non-HI samples, which again exhibits the effect of heating on FGF-2 detection via ELISA. Due to the lowered cross-reactivity of mouse FGF-2 and human FGF-2, for which the ELISA was based on (~30% cross-reactivity), the ELISA extraction results may be more than the amount detected. On the other hand, detected levels of IGF-2 were significantly increased, by at least 2-fold, in all HT SFM extractions compared to their non-HT counterparts, which demonstrated that

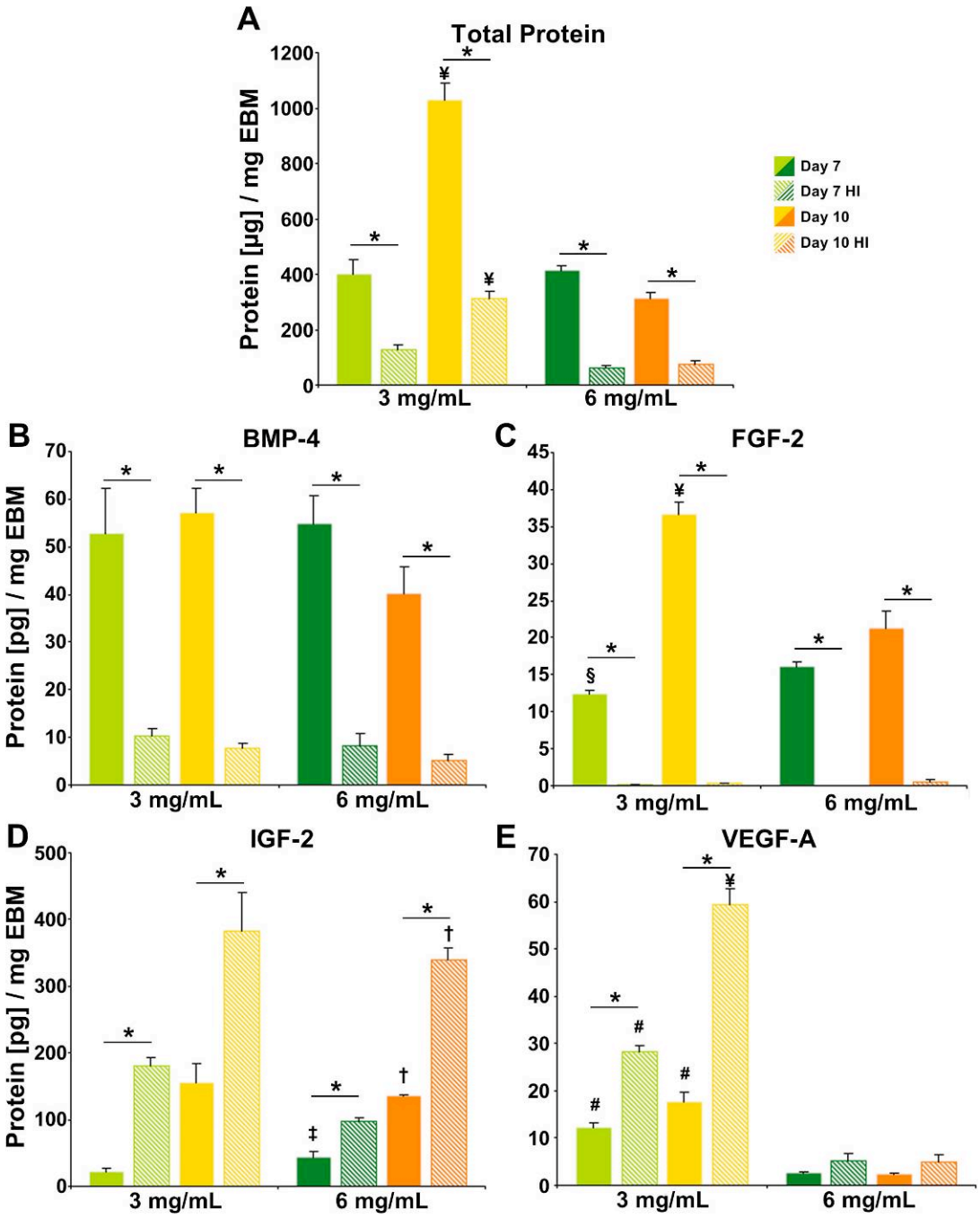

Figure 6.2. Growth factor protein extracted with serum-free media. Overall, the amount of several growth factors extracted was dependent on the time point at which the EBM was isolated as well as the matrix mass and the heat treatment. Protein content was normalized to EBM mass. Results indicated are mean ± standard error (n=4). One way ANOVA comparing among samples within the same heat treatment - ¥: $p < 0.05$ compared to all other samples, †: $p < 0.05$ compared to day 7, 3 and 6 mg/mL, #: $p < 0.05$ compared to 6 mg/mL day 7 and 10 EBM, ‡: $p < 0.05$ compared to day 7 at 3 mg/mL, §: $p < 0.05$ compared to day 7 at 6 mg/mL. Student *t*- test comparing between non-HT and HT samples * indicates $p < 0.05$.

heating SFM extraction increased the release of IGF-2 from EBM (Figure 6.2D). Also, HT SFM extractions showed comparable levels of extracted IGF-2 to TPER extractions. The increase in matrix mass yielded significantly more extracted IGF-2 from non-HT day 7 EBM, yet there was no change between non-HT or HT day 10 EBM. The comparable levels of extracted IGF-2 within the same heat treatment demonstrates that the amount of extracted IGF-2 from day 10 EBM was at maximum capacity, especially since the total protein amount for 3 mg/mL, day 10 EBM was ~3-fold more than 6 mg/mL. The effect of heat inactivation on SFM extracts also significantly increased (~2-fold higher) the level of VEGF-A present compared to non-HT SFM extracts, but only at 3mg/mL (Figure 6.2E). At higher matrix mass, SFM extracted VEGF-A levels were significantly lower compared both day 7 and day 10 EBMs of the same heat treatment. This decrease in VEGF-A extraction at high matrix mass, for both non-HT and HT, was also analogous in TPER extractions, which further supports the implication of particular molecules hampering the extraction of VEGF-A at higher matrix doses.

Overall, non-HT SFM extractions and TPER extractions resulted in comparable amounts of the majority of growth factors measured, which justified using only SFM extractions for subsequent bioactivity studies, along with the fact that undiluted TPER samples would not be conducive for cell survival compared to undiluted SFM. The differences in extraction content between matrix mass were most dramatic for VEGF-A quantities, which is a potent angiogenic factor, thus motivating the use of both matrix doses in subsequent *in vitro* assays. Moreover, the differences in SFM extractions obtained from EBMs derived from EBs at days 7 versus day 10 are parallel to the changes in quantified proteins within the EB-CM in Chapter 4 (Figure 4.3) - BMP-4

content did not change between CM9 and CM12, while IGF-2 content was significantly increased in CM12 compared to CM9. All together, not only did EBs actively secrete growth factors, but also they were retained within acellular EBMs and capable of being extracted in varying amounts depending on the time point at which the EBM was obtained.

Effects of EBM extraction on cell proliferation

The bioactive effects of the growth factors and other molecules extracted from EBMs with serum-free media, based on the extraction data previously discussed, were analyzed for their mitogenic stimulation of both fibroblasts and endothelial cells (Figure 6.3). Fibroblast proliferation in response to bioactive factors present in the EBM extractions exhibited slightly increased proliferative effects compared to SFM alone (~5%), yet significantly less than cells in fibroblast growth media (~53%) (Figure 6.3A, B). Among EBM extraction treatments, there were similar percentages of BrdU+ cells between the non-HT and HT treatments from both day 7 and 10 EBMs at 3 mg/mL (10 – 12%). However, differences in proliferation were present at 6 mg/mL EBM for both HT day 7 (19%) and day 10 (21%) compared to the non-HT, with a significantly higher proliferative response of fibroblasts from the HT treatment. This significant increase between non-HT and HT indicate, despite no significance compared to controls, suggests either the inactivation of mitogenic inhibitors of fibroblasts or the increased extraction of factors that stimulate proliferation as a result of HT.

The response of endothelial cells to the complex mixture of factors contained within EBM extractions was similar to the percent stimulated by SFM only (22%), but

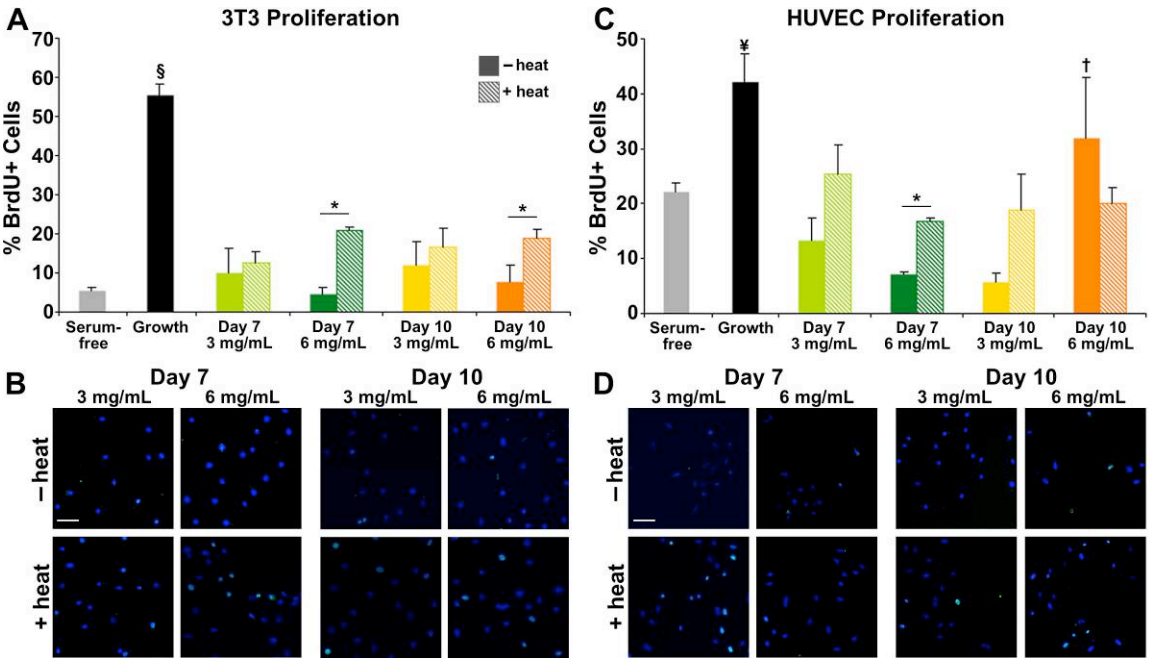

Figure 6.3. EBM effects on cell proliferation. (A, B) Fibroblast proliferation was differentially affected by EBM treatments at higher doses between the non-HT and HT matrices. (C, D) Endothelial cell proliferation was inhibited by factors contained within the non-HT treatments. Scale bar = 50 μm. Green: BrdU+ cells, blue: Hoechst. Results indicated are mean±standard deviation (n=4). One-way ANOVA comparing among samples within the same heat treatment - §: $p < 0.05$ compared to all other samples, ¥: $p < 0.05$ compared to day 7 at 3 mg/mL and 6 mg/mL (± HT), day 10 at 3 mg/mL, †: $p < 0.05$ compared to day 7 at 6 mg/mL and day 10 at 3 mg/mL. Student *t*- test comparing between non-HT and HT samples * indicates $p < 0.05$.

significantly less than growth media (42%) compared to non-HT day 7 (3 and 6 mg/mL) and day 10 (3 mg/mL) EBM, as well as HT day 7 (6 mg/mL) EBM (Figure 6.3C, D).Similar to the mitogenic response of fibroblasts to 6 mg/mL of day 7 EBM, HT stimulated significantly more (~2X) mitogenic cells compared to non-HT - an increase from 7% BrdU+ cells (non-HT) to 17% (HT). The change in mitogenic response of both fibroblasts and ECs to non-HT versus HT day 7 EBM 6 mg/mL suggests that the potential inhibitors or activators of proliferation affected by HT were not specific to either cell type. Contrastingly, significantly higher percent of BrdU+ ECs in response to day 10 EBM at 6 mg/mL compared to day 7 EBM 6 mg/mL was specific to ECs. This distinct result corresponded to significantly more IGF-2 extracted from day 10 EBM compared to day 7 (Figure 6.2D), which has been reported to stimulate angiogenesis by up-regulating *Vegfa* gene expression [292, 293]. Despite the few significant differences in EC mitogenicity in response to EBM extractions, the mitogenic bioactivity of SFM extractions was remarkably stimulating, potentially due to low concentrations of soluble growth factors, which are typically present on the order of tens of ng/mL in growth media.

EBM-induced chemotaxis

Cellular migration of two different cell types was investigated in response to potential bioactive factors present EBM extractions. The results indicated that non-HT EBM extractions stimulated chemotaxis in fibroblasts compared to HT EBM extracts (Figure 6.4A-C). Initially, 6 mg/mL treatments of day 7 and day 10 non-HT EBM stimulated the largest number of cells, ~8,700 and ~10,000 cells respectively, to migrate

by 3 hours and appeared to maintain a similar number of migrated cells throughout the 24-hour period. Fibroblast chemotaxis was stimulated significantly at 6 hours in response to non-HT, 6 mg/mL day 10 EBM extraction (16,000 cells) compared to growth media control and all HT samples (Figure 6.4B, C). By 12 hours, each of non-HT EBM extractions from both days and doses of EBM, ranging from ~7,500 to ~18,000 cells, stimulated slightly more cells than both media controls (~175 cell for serum-free media, ~1,200 cells for growth media) and HT EBMs (~1,200 - ~1,700 cells). The morphology of the cells treated with non-HT EBM extracts appeared to be larger and more stellate than the cells treated with HT EBM extracts, potentially suggesting activation of cells to migrate. (Figure 6.4A). The 3 mg/mL doses of day 7 and day 10 non-HT EBM steadily increased in the total number of migrated cells throughout the 24-hour time period, with significantly more cells migrating as an effect of 3 mg/mL of day 10 EBM (~13,500 cells) compared to serum- free media. As for HT EBM extracts, each treatment resulted in similar numbers of migrated cells compared to serum-free and growth media and continued to increase slightly in number over 24 hours. After 24 hours, 6 mg/mL day 7 EBM extraction significantly induced more fibroblast migration (~19,000 cells) compared to all other HT samples, except 6 mg/mL, HT day 10 EBM extract (Figure 6.4B, right). Overall, the factors present in the HT EBM had a minimal effect on fibroblast migration compared to the factors retained in the non-HT EBM, which induced fibroblast migration faster than the control media.

Conversely, endothelial cell migration was inhibited by factors contained in non-HT EBM extracts, while HT EBM yielded similar chemotaxis response to serum-free

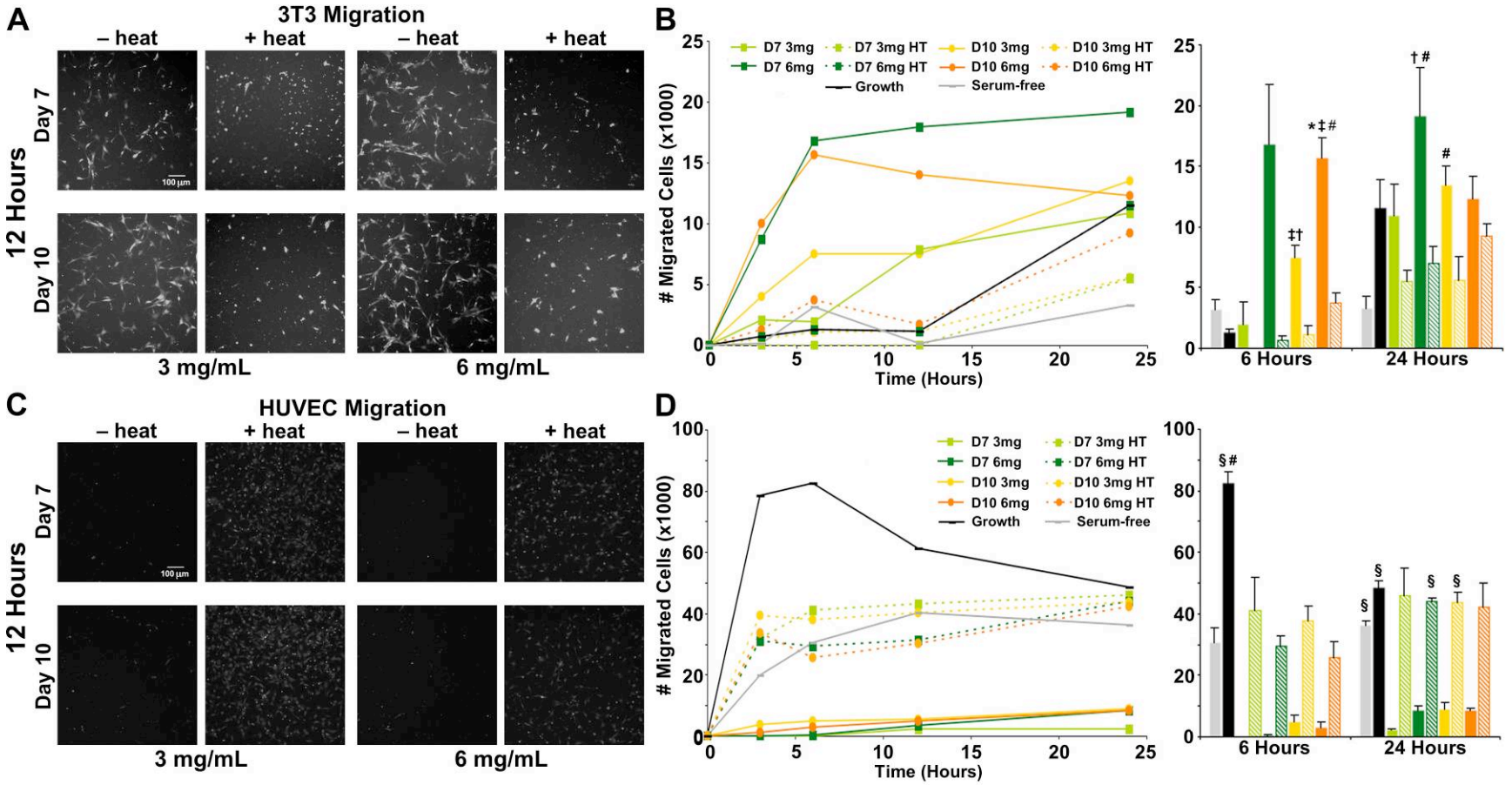

FIGURE 6.4. EBM-induced effects on cell chemotaxis. Fibroblast (A) and endothelial cell (C) morphology differences at 12 hours between non-HT and HT EBM treatments. Chemotaxis was measured by the total number of migrated fibroblasts (B) or endothelial cells (D) during 24 hours in response to EBMs (left); significance testing was conducted on the total number of migrated cells at early (6 hours) and late (24 hours) time points (right). Results indicate mean±standard error (n=4). One-way ANOVA: * $p < 0.05$ compared to all HT samples; † $p < 0.05$ compared to all HT samples except 6 mg/mL, HT day 10 EBM; ‡ $p < 0.05$ compared to growth media control; # $p < 0.05$ compared serum-free media control; § $p < 0.05$ compared to all non-HT samples.

media (Figure 6.4C, D). Initially between 3 – 6 hours, EC growth media stimulated significantly more endothelial chemotaxis (~82,000 cells) compared to non-HT EBM extracts (0 - ~5,000 cells) and serum-free media (~30,000 cells); HT EBM extractions and serum-free media stimulated a gradually increasing number of cells up to 6 hours and continued to maintain a comparable number of cells throughout 24 hours (Figure 6.4D, left). By 12 hours, the growth control decreased in the number of migrated cells (~61,000), and the non-HT EBM extractions continued to minimally stimulated chemotaxis (~2,100 – ~8,800 cells). Microscopy images taken at 12 hours validate the lack of chemotaxis in response to non-HT EBMs, and exhibit normal endothelial cell morphology of the migrated cells (Figure 6.4C). At the end of 24 hours, the number of migrated endothelial cells treated in growth media had declined (~49,000 cells) to chemotaxis levels similar to HT EBMs (~42,000 – 46,000 cells) and serum-free media (~36,000 cells). Furthermore, 6 mg/mL, HT day 7 EBM and 3 mg/mL, HT day 10 EBM had significantly stimulated a larger number of cells, ~44,000 cells each, compared to all non-HT EBMs (~2,200 – 8,900 cells) after 24 hours (Figure 6.4D, right). Interestingly, the morphogens harbored in the non-HT EBM extracts prohibited the chemotaxis of ECs over the entire 24-hour experiment; whereas, HT EBM extracts elicited similar levels of chemotaxis compared to serum-free media, suggesting the inactivation of a potential inhibitory molecule(s) for endothelial migration.

EBM impact on endothelial network formation

A more specific *in vitro* assay to specifically assess angiogenic stimulation of ECs is via Matrigel network formation assay. The formation of tubular networks by

endothelial cells was examined in response to potential bioactive factors harbored by the EBMs, particularly the soluble fraction of molecules extracted from the EBM in serum-free media in comparison to the entire matrix-associated EBM. In analyzing the soluble fraction of molecules from the EBM, non-HT and HT extractions at 3 mg/mL previously investigated in cell proliferation and migration assays were examined. In the EC network formation assay the 3 mg/mL dose was chosen based on the combination of results from extracted growth factor quantification and previously discussed EC bioactivity assays. Qualitative assessments exhibited that the formation of tubular structures was evident in the control samples of growth media and serum-free media (Figure 6.5E, F); however, network formation in day 7 (Figure 6.5A, B) and 10 (Figure 6.5 C, D) EBM extracts, non-HT. and HT, was not observed compared to the controls. Additionally, there were more rounded single ECs present in each of the EBM extracts compared to control treatments.

Overall, the soluble fraction of factors contained within EBM extractions inhibited the formation of endothelial network formation on GFR-Matrigel. These results correspond to previous EC bioactivity assays examining EBM extracts – no enhancement of EC proliferation compared to SFM only, as well as significant inhibition of EC migration in response to non-HT EBM extracts compared to SFM only. Unlike the previous EC bioactivity studies, the HT EBM extracts did not appear to result in similar levels of network formation as SFM only, thus suggesting that the inhibiting factors present in non-HT extracts were not completely inactivated upon HT.

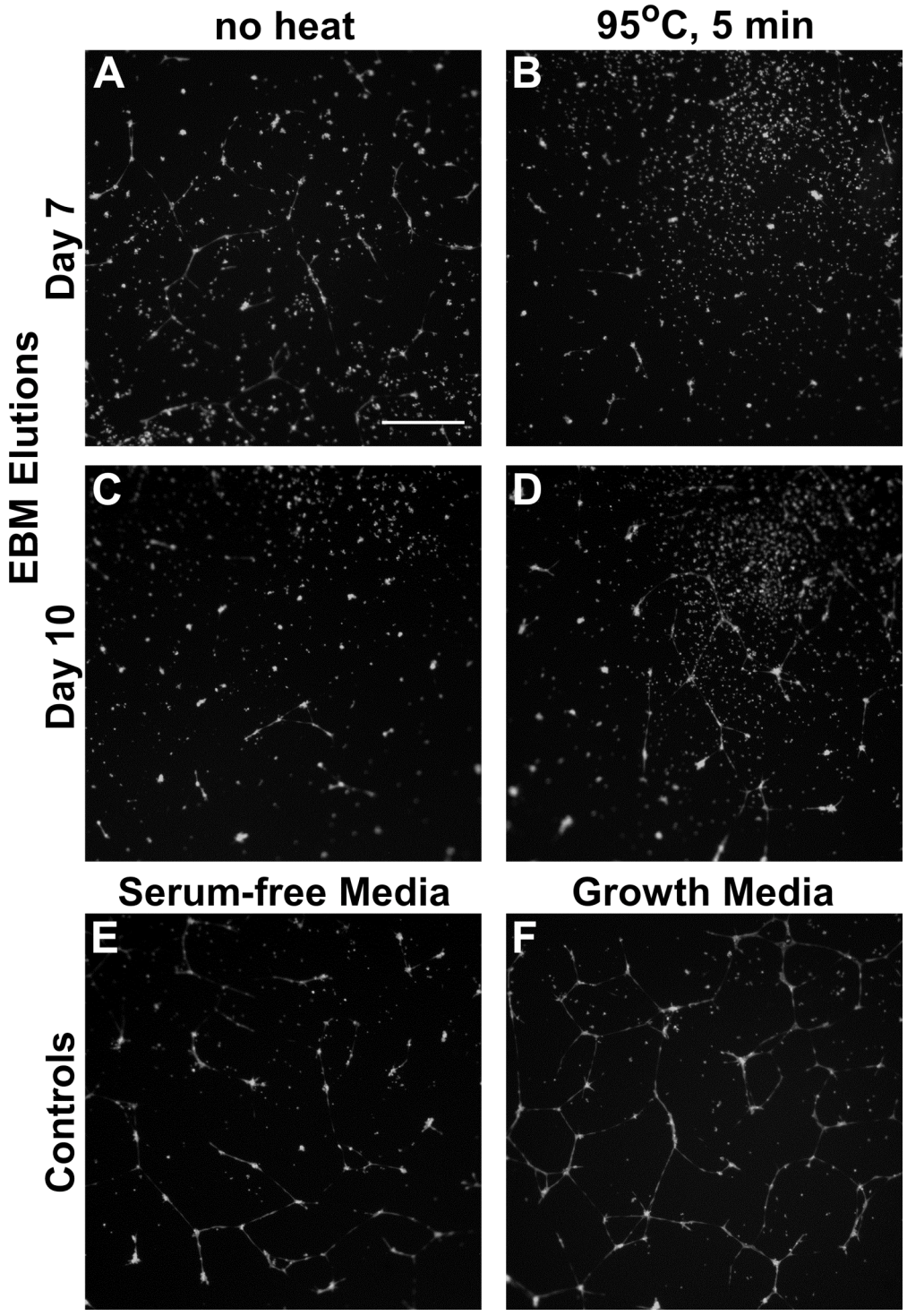

Figure 6.5. EBM extracts inhibit endothelial cell network formation. After 18 hours, the molecules in SFM extractions from in both day 7 (A, B) and day 10 (C, D) EBM elicited less network formation on GFR-Matrigel compared to both serum-free and growth media controls (E, F). Scale bar = 500 μm

In contrast to treatments with soluble factors extracted from EBMs, network formation was elicited upon addition of entire EBM (~3mg) embedded into GFR-Matrigel (GFRM) (Figure 6.6). The EBM mass of 3mg was utilized to be consistent with the 3mg/mL dose used in the EBM extracts. In addition to heating EBMs to 95°C for 5 minutes (HT_{95} EBM), EBMs were also heat inactivated at 120°C for 20 minutes (HT_{120} EBM) in order to obtain a matrix that almost completely inactivated. Qualitative evaluation of the acquired microscopy images revealed that non-HT EBM from both day 7 and 10 EBs (Figure 6.6 A, D) prohibited network formation after 18 hours compared to the various controls, including GFRM+DBM (a non-embryonic acellular matrix), GFRM+VEGF-A, and GFRM alone (Figure 6.6G-I). Qualitative comparisons of resultant tubular networks exhibit that the extent of structures formed on HT_{95} EBMs from both days 7 and 10 (Figure 6.6B, E) appeared similar to ones formed on GFRM+VEGF-A (Figure 6.6H) - a robust network of tubes and nodes compared to GFRM+DBM and GFRM only (Figure 6.6G, I). Whereas the degree of network formation on HT_{120} EBM (Figure 6.6C, F) was observed to be comparable to the frequency of nodes and tubes formed on GFRM only (Figure 6.6G, I). The qualitative differences examining the extent of network formation seen between non-HT EBMs and HT EBMs indicated the inactivation of inhibitory molecules following HT. Furthermore, the differences between HT_{95} EBM and HT_{120} EBM illustrated potential increase in stimulatory bioactive molecules in HT_{95} EBM and then subsequent inactivation of the stimulatory bioactive factors in HT_{120} EBM due to increased temperature and duration of heat.

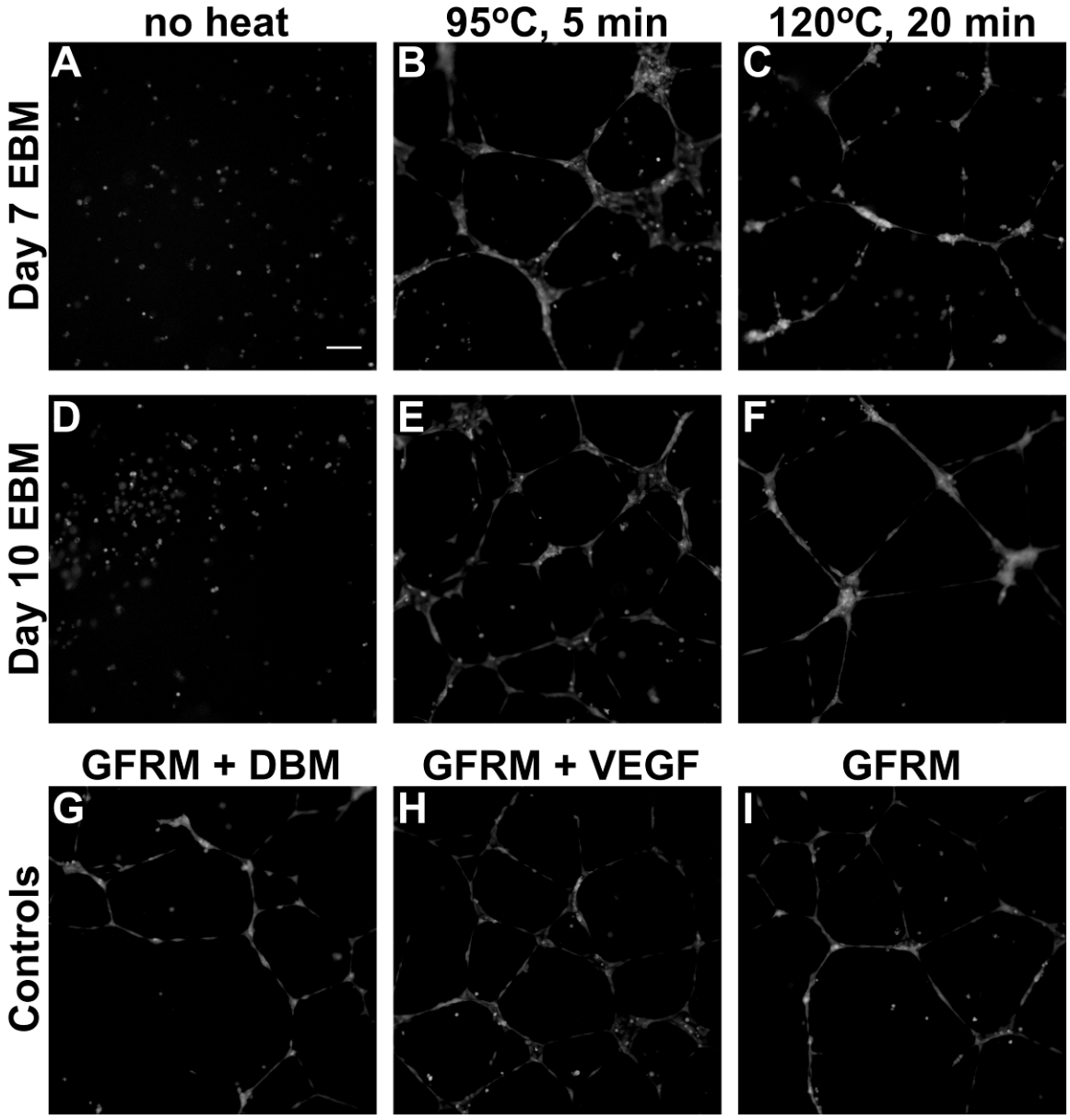

Figure 6.6. Heat-inactivated EBM-associated factors promote endothelial network formation. The formation of tubular structures was inhibited as a result of non-HT EBMs obtained from day 7 and day 10 embedded within the GFRM (A, D). Contrastingly, HT EBMs from either day 7 (B, C) or day 10 (E, F) induced network formation comparable to controls (G – I). Scale bar = 100 μm.

A more quantitative analysis of network formation in response to EBM treatments was conducted by analyzing microscopy images captured at 18 hours, including measurements of mean node and tube area, total percent area of nodes and tubes, and the number of nodes and branch points all relative to the GFRM only control. The GFRM+DBM and GFRM+VEGF-A controls both resulted in similar mean node and tube measures compared to GFRM only (Figure 6.7A). Among all the HT EBM treatments, the mean tube area for each treatment was similar to GFRM control (fold change ~1), yet the mean node area was larger than GFRM for all HT EBM treatments, with significantly increased mean node area from both day 7 HT_{95} EBM (2.4-fold) and HT_{120} EBM (1.8-fold) and day 10 HT_{95} EBM (2.1-fold) compared to GFRM (Figure 6.7A). In conjunction with the larger mean node area, day 10, HT_{95} EBM yielded significantly more total nodes (1.4-fold) and branch points (1.3-fold) compared to GFRM (Figure 6.7B). Despite the larger mean node area, day 7 HT_{120} resulted in significantly less number of total nodes (0.8-fold) and branch points (0.4-fold) compared to GFRM. The overall percent total area for each of these structures correlated to the differences observed for mean area per structure. Day 7 HT_{95} EBM and day 10 HT_{95} EBM treatments, along with controls, were not significantly different from GFRM only for total tube percent area, while day 7 HT_{120} EBM was significantly decreased by 0.4-fold (Figure 6.7C). As for total node percent area, all treatments were comparable to GFRM, except for significantly more node percent area resulting from day 7 HT_{95} EBM (2.7-fold) and day 10 HT_{95} EBM (3.0-fold) relative to GFRM. These significant differences demonstrated that day 7 HT_{95} EBM yielded greater node size and less tube area without affecting frequency; whereas, day 10 HT_{95} EBM established networks with significantly larger number and area of nodes,

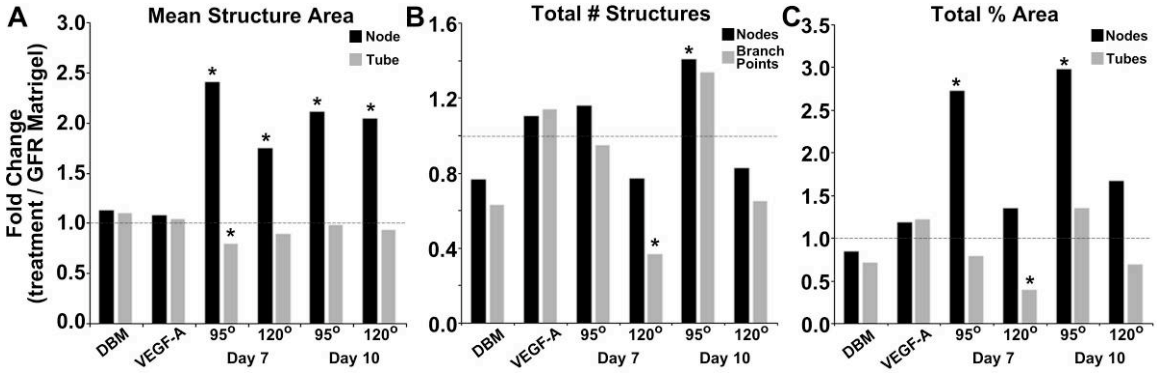

Figure 6.7. Quantitative assessment on EC network formation. The effective stimulation of network formation by ECs was measured by changes in mean structure area of nodes and tubes (A) as well as the frequency of nodes and branch points (B). All these aspects determine the total percent area of the EC network (C). Dashed line (---) indicates fold change = 1, results indicate fold change of the treatment mean/GFRM mean. Using ANOVA followed by Dunnett's test, comparisons were made between treatment measurements (n=4) and control (GFRM only) measurements (n=4), * denotes $p < 0.05$ compared to GFRM.

along with significantly more branch points to effectively stimulate endothelial network formation, thus demonstrating a significant angiogenic response compared to GFRM. Heating EBMs to 120°C for 20 minutes effectively inactivated the increased bioactive factors released in HT_{95} EBM. Embedding the EBMs within the GFRM remarkably stimulated more network formation than the EBM extracts and provided a means to effectively deliver the entire EBM. Overall, these EC network formation results indicated that the combination of ECM and its associated factors, rather than the soluble factors alone, is essential to impart a synergistic effect on *in vitro* formation of networks by endothelial cells.

CAM analysis

The angiogenic response of the vascular tissue to the lyophilized EBM was examined using the CAM assay. The entire EBM matrix, non-HT and HT, was grafted onto CAMs to observe the angiogenic stimulation of blood vessels over 48 hours. The use of the lyophilized EBM rather than EBM extractions resulted from the considerable differences in EC tube formation elicited by the EBM delivered with the GFRM. The angiogenic effects elicited by the matrix grafts was typically illustrated by the appearance of blood vessels radiating from the graft in a "spoke-wheel" pattern, with an increased density of vessels implying pronounced response, as well as changes in blood vessel morphology, including more tortuous vessels and extensive branching.

Over the 48-hour treatment, the blood vessel changes surrounding the graft area on the CAMs were assessed visually inspected (Figure 6.8). CAMs treated with GFRM or EBMs generally resulted in vessel morphologies that were indicative of angiogenesis,

such as tortuous vessels, smaller radiating vessel protruding adjacent to the graft, and extensive branching vasculature comprised of tiny vessels (Figure 6.8, bottom row). Vessel counts over 48 hours exhibited increased frequency of radiating vessels from EBM grafts (Figure 6.9). Significant differences in vessel counts at the 6mm diameter were observed over time in EBM-treated CAMs, particularly after 48 hours in the 1° and 2° vessels (Figure 6.9A), which generally corresponded with the presence of radiating vessels from the EBM graft (Figure 6.8). Day 7 EBM stimulated significantly higher number of 1° vessels by 48 hours compared to all other time points, while 2° vessels were increased at 48 hours compared to 24 hours, at 6mm. While day 10 HT EBM increased the number of vessels at 6mm by 48 hours compared to 0 hours. At the 10mm diameter, day 7 EBM had a significant increase in both 2° and 3° vessels at 24 and 48 hours compared to 0 hours; whereas day 10 HT EBM demonstrated a higher number of 3° vessels only at 24 hours compared to 0 hours, yet resulted in significantly more 2° and 3° vessels at 48 hours compared to 0 hours. The increased counts of 1° and 2° vessels suggests directional changes of the existing vascular network, while increases in tertiary vessel counts suggest more branching of the higher-order vessels, which are both features of angiogenesis. These results indicated that delivery of these ECM-associated factors stimulated vessel changes within 48 hours, and the EBM bioactive factors were able to affect aspects of angiogenesis within a distinct radial distance.

Fixed CAM images qualitatively demonstrated the angiogenic response of the vessels within the CAM as an effect of EBM treatment after 48 hours. Binary images derived from the grayscale images of fixed CAMs were used to quantify the vessel

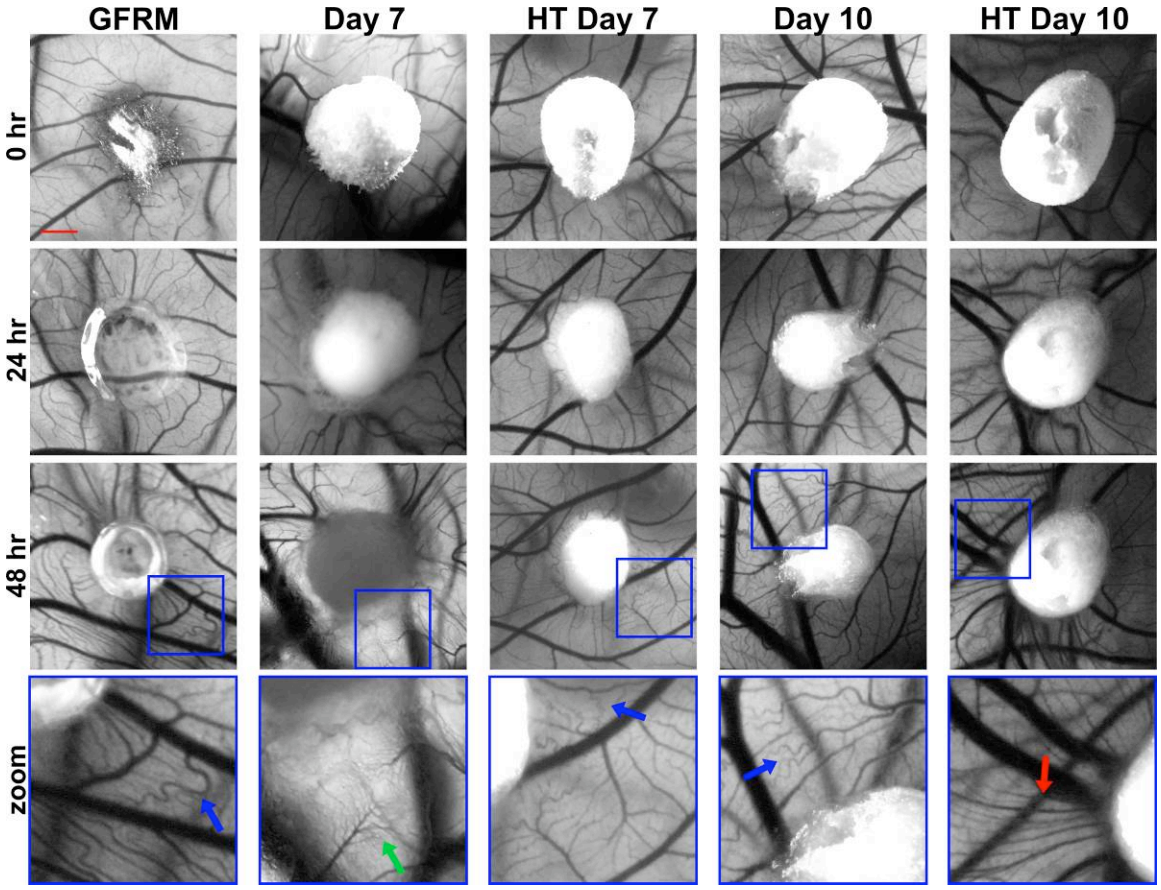

Figure 6.8. Angiogenic response of CAMs due to EBM grafts. Representative images of CAMs treated with EBMs or GFRM taken at three time points: 0 hours (top), 24 hours (second row), 48 hours (third row). Morphological changes in blood vessels indicative of angiogenesis (bottom row): tortuous vessels (blue arrow), extensive branching of tiny vessels (green arrow), and radiating vessels (red arrow). Scale bar – 1mm.

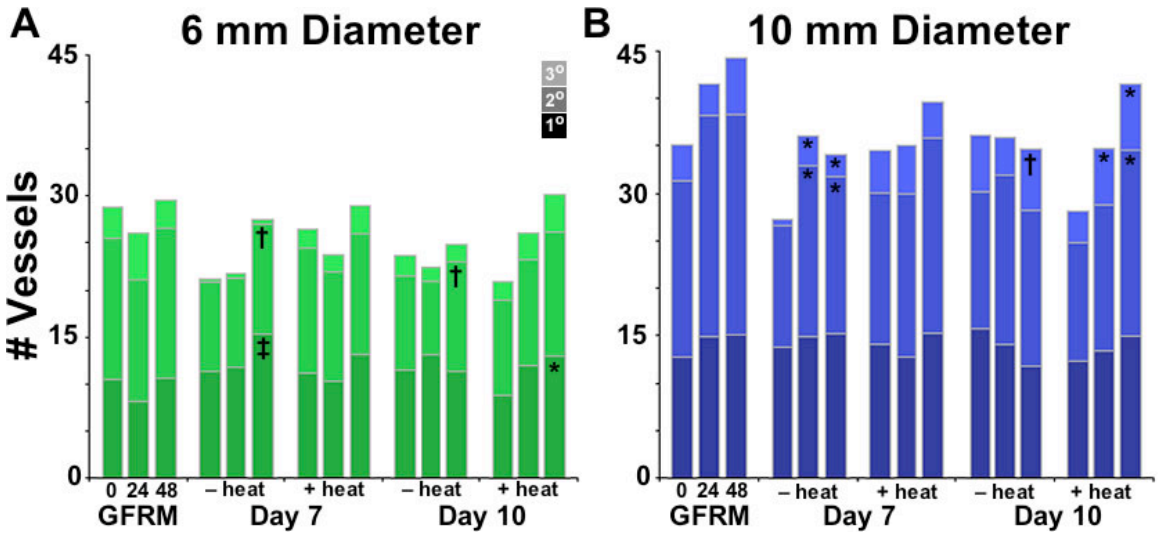

Figure 6.9. Radiating vessel counts in response to matrix grafts. The change in radiating vessel number at 0, 24, and 48 hours within a 6mm diameter (A) and 10 mm diameter (B). Tertiary (3°) vessels branched off secondary ones (2°) that sprouted from primary (1°) vessels that appeared unconnected to other vessels in the field of view. Results indicate mean count (n=7). Significance tested with Pearson's test statistic, $p < 0.01$: ‡ compared to all other time points, † compared to 24 hours, * compared to 0 hours.

density for each CAM treatment (Figure 6.10, bottom row); results ranged from ~13 to 17%, with GFRM images generating the highest total vessel area percentage (Table 6.1). The non-HT EBM images yielded higher total vessel percent areas among EBM-treated groups compared to HT EBM treatments. One caveat to measuring the total vessel percent area is that even though similar image areas were quantified, graft area size varied between CAMs, since the amount of matrix was normalized to starting EB material. Hence, grafts with larger areas typically resulted in less total vessel area. The differences in total vessel area were small, less than 5%, between each of the treatments, thus it was difficult to determine which EBMs were more effective at eliciting an angiogenic response, which suggests that total percent area alone was not an effective indicator of angiogenesis. However, taken together with other CAM data total percent vessel area could support other analytical outcomes.

Despite the previous quantitative and objective measure of angiogenesis, vessel directionality and morphology were not evident from total vessel area calculations. A more semi-quantitative image analysis readily compared the angiogenic response differences between treatments and took into account the vessel density, directionality, and morphology surrounding the grafts by calculating a coefficient of angiogenesis (Figure 6.10, top row). Treatment with GFMR (positive control) resulted in the highest coefficient at 0.725 (Table 6.1). Day 7, HT EBM and Day 10, non-HT EBM yielded the same coefficient (0.425), while Day 7, non-HT EBM was slightly higher at 0.467 and day 10, HT EBM produced the highest coefficient (0.520) compared to the other EBMs.

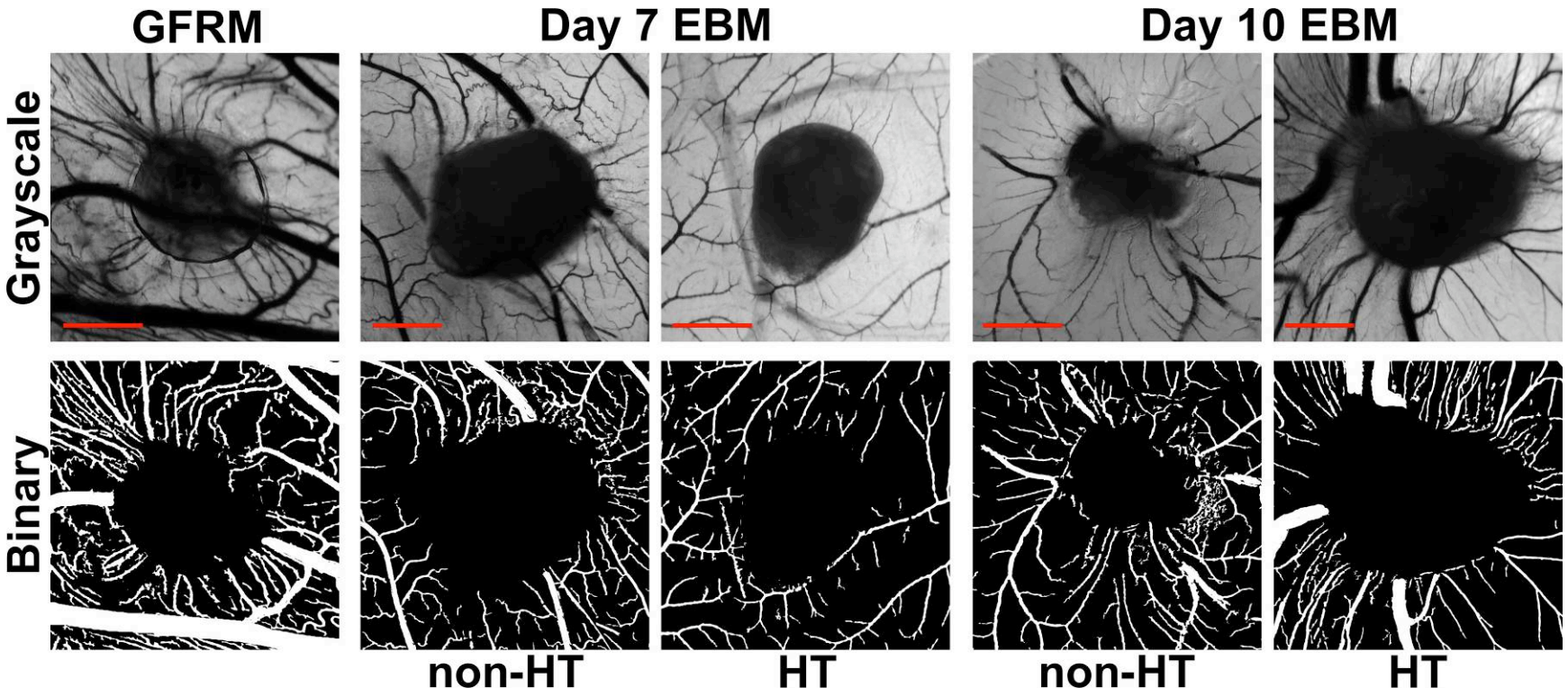

Figure 6.10. Fixed CAM images. (Top) Representative images capturing the first few millimeters surrounding the graft after fixation and used to score for angiogenesis coefficient. (Bottom) Representative binary images as a result of image processing and used to quantify the total percent vessel area. Scale bar = 1 mm.

Table 6.1 Fixed CAM image analysis values.

Treatment	GFRM	Day 7 EBM Non-HT	Day 7 EBM HT	Day 10 EBM Non-HT	Day 10 EBM HT
Total % vessel area (mean ± std. err)	16.59 ± 1.94	14.24 ± 1.13	13.60 ± 0.58	15.33 ± 1.39	12.93 ± 0.591
Coefficient of angiogenesis	0.725	0.467	0.425	0.425	0.520

Although this scoring method is not ideal by relying on the human eye, blinded scoring was used to eliminate bias. Furthermore, the human eye can detect smaller changes in vessel appearance that may go unnoticed with computer-aided analysis, especially with small vessels that may be filtered out as noise.

Overall, CAM assay analyses demonstrated that EBMs did not significantly inhibit or stimulate angiogenesis, thus the influence of EBM on inducing angiogenesis is inconclusive. In relation to GFRM treatment, EBM was less effective at stimulating angiogenesis, since the mass of GFRM applied to the CAM per sample was approximately half that of the EBM samples. The day 7 EBMs may contain some angiogenic factors due to the notable vessel changes in response to non-HT compared to day 10 non-HT, while day 10 HT EBM exhibited changes in vessel response over time compared to non-HT day 10 EBM. Altogether, these results demonstrate that EBMs are capable of eliciting morphogenic responses from exogenous tissues, due to the complex mixture of factors harnessed in the EBM.

Discussion

The bioinductive capacity of an embryonic stem cell-derived matrix was investigated for its effects on cell proliferation, chemotaxis, and structure formation as well as tissue morphogenesis, particularly CAM angiogenic induction. Protein extractions from EBM revealed that growth factors were harbored within the matrix and extracted in their active form based on the stimulatory and inhibitory *in vitro* bioactivity results. The reaction of fibroblasts to EBM extractions was typically enhanced compared to basal level controls, contrary to the inhibition of endothelial cells in response to EBM

extractions. Endothelial cells were stimulated only after EBM extractions were heat-treated, particularly during migration and tube formation assays, but only to levels similar to serum-free media only.

The influence of EBM on CAM angiogenesis based on the quantitative results was not as robust of a response compared to the significant inhibition of EC migration and tube formation. Notable angiogenic responses were consistently observed in GFRM, yet were not as consistent in response to EBMs, yet there were noticeable changes in blood vessel appearance. These observed variations seemed to affect EBM quantitative analysis, thus yielding results that were not as obvious as other bioactivity studies. Additionally, the results of different CAM analyses did not elicit any significant differences between treatments, which led to an inconclusive result as to the EBM effects on angiogenesis. Altogether, the EBM did not inhibit nor did it stimulate robust angiogenesis, which could be attributed to several factors, such as EBM dosage. The amount of EBM used in the CAM experiments was based on the EBM extraction results exhibiting higher amounts of certain growth factor compared to 6 mg/mL, as well as the *in vitro* studies demonstrating similar cellular responses between 3 and 6 mg/mL. However, in order to induce an angiogenic response, the EBM dosage may have needed to be increased since the response of a tissue, rather than isolated cells was being investigated. Granted the angiogenic responses of CAMs to EBMs were subtle, the outcomes provided insight into a more complex model of angiogenesis compared to isolated cell responses. Overall, while the EBM did not significantly affect angiogenesis with the *ex ovo* CAM assay, the *in vitro* studies demonstrated the retention of bioactive

factors within EBM that can effectively modulate specific cell behaviors essential to tissue remodeling.

The total protein quantity extracted from EBM did not vary considerably between the two buffers, yet the differences in specific growth factor content were significant comparing non-HT with HT extractions. Upon heat treatment, BMP-4 and FGF-2 were no longer detected by ELISA, in contrast to IGF-2 and VEGF-A which both showed increased levels compared to non-heat inactivated matrices, potentially indicating the effective denaturing of BMP-4 and FGF-2, but the increased extraction of IGF-2 and VEGF-A, by heat. However, during the cooling of the extractions prior to further analysis, certain proteins that do not require other protein chaperones could have re-folded alone. During the re-folding process, epitopes that are recognized by the ELISAs may be less prominent or more prominent, thus resulting in either antibody decreased or increased detection levels, respectively. Heating EBM at a high temperature for a short duration may catalyze the dissociation of matrix bound growth factors from the ECM without denaturation, thus resulting in an increased extraction of specific growth factors. However if the heat is increased and prolonged it could denature the bioactivity of the growth factors, as observed in the HT_{120} EBMs. Additionally, heating the EBMs may have permitted the release of other angiogenic growth factors as well as activated certain ones. Interestingly, members of the transforming growth factor-beta (TGF-β) family have roles in angiogenesis in a dose dependent manner and can also be thermally activated. The gene expression of several *Tgfb* genes from the array results in Chapter 3 (figure 3.5) demonstrated significantly increased expression at later time points, between days 7 and 10, as well as days 10 and 14. At low concentrations, TGF-β has a

stimulatory effect on ECs, yet at higher concentrations the effect becomes inhibitory [294, 295]. Furthermore, TGF-β is typically present in the ECM in its latent form and must be activated in order to bind to its receptors; one method to activate TGF-β is by thermal activation between 75° - 100°C for up to 5 minutes [296]. The heat treatment condition is in the temperature and time range to induce thermal activation TGF-β, which may explain the stimulation robust EC network formation seen when treated with HT_{95} EBM compared to HT_{120} EBM, which would have inactive TGF-β due to the longer duration at a higher temperature. Comparing the lack of networks formed in response to EBM extractions to the robust networks resulting from embedded EBM during EC network formation assay, these results suggest that EBM extractions potentially contained angiogenic inhibitors, which speculatively could be high levels of activated TGF-β, which are inhibitory; in contrast to, to the lower levels, stimulatory level, of activated TGF-β that could be slowly released from HT_{95} EBM when it was embedding in the GFRM. Overall, heat-treating the EBM potentially inactivates certain growth factors while thermally activating others, either stimulatory and or inhibitory, which can further influence the bioactive response of various cell types.

The amount of growth factors identified in the EBM extractions are considerably greater (~1000-fold) than previous reports of extracted growth factors from acellular matrices. Growth factors, FGF-2 and TGFβ, were identified in extractions by Westerns from acellular SIS in conjunction with comparisons to bioactivity results of the purified growth factors to the extractions [158]. Chun et al. described effective extraction of nine growth factors from acellularized bladder submucosa using acetic acid [159]: PDGF-BB had the highest reported extracted amount (~286 pg/g) and epidermal growth factor

(EGF) had the smallest (0.99 pg/g). These growth factor quantities are 1000-fold less than the quantities extracted from EBM on a mass basis. Three growth factors previously reported in the literature to be extracted and quantified from acellular matrices coincided with the ones identified in the EBM – BMP-4, FGF-2, and VEGF-A. In the non-HT EBM extractions, BMP-4 was present at ~$50x10^3$ pg/g while BSM extractions contained ~4 pg/g; FGF-2 extracted from EBM was lowest, ~30 $x10^3$ pg/g and BSM yielded ~4 pg/mg; and finally VEGF-A was present at ~$3x10^3$ pg/g in EBM extractions and at ~104 pg/g in BSM extractions. The considerable difference in growth factor quantities could potentially be due to the fact that acellularized BSM is mainly comprised of connective tissue, blood vessels, and nerves. These structures generate the extracellular environment of the BSM, however, the homeostatic nature this somatic tissue, which generally does not undergo extensive morphogenesis, could explain the low levels of growth factor present compared to the differentiating EB environment. However, these growth factor results were reported in the literature and were not conducted using the same means of extraction used for the EBM extractions. Overall, these results from literature reports compared to the EBM results suggest that embryonic environments, which are notably undergoing remarkable morphogenesis, may potentially be enriched in growth factors and morphogens and can be captured following acellularization.

The solutions used for extraction growth factors from EBMs compared TPER buffer, and serum-free media. The extractions of BSM and SIS previously described used detergents and solutions that typically denature proteins, including TritonX-100, urea, and guanidine. One recent study by Yang et al. provided evidence that VEGF and PDGF-BB were present in extracts from ABM using media [157]. The amount of growth

factors quantified were similar to other acellular matrix extracts, ranging from ~158 – 594 pg/g for PDGF-BB and ~108 – 477 pg/g for VEGF, depending on the acellularization techniques used, after 7 days of conditioning basal media with ABM. In this EBM study, basal media was conditioned for only 24 hours and the amount of VEGF present was at least 50X greater than reported ABM extracts.

Investigating the response of two different cell types to EBMs reflected the differences observed in comparing EB-CM, as described in Chapter 4. Fibroblasts are omnipresent in the body and implicated in physiological processes such as tissue remodeling and wound healing due to their primary function – producing ECM. Stimulating endothelial cells is required to elicit an angiogenic response, one of the necessary processes that accompanies wound healing and tissue repair. The factors contained in EBM extractions did not have a profound effect on stimulating cell proliferation, but did inhibit EC proliferation. The most noticeable effect was the difference in proliferation by day 7 non-HT and HT EBM extracts, which possibly demonstrates the presence of factors that inhibit proliferation in extractable EBM at day 7, which may be destroyed during heat treatment but does not permit significant proliferation increases. Interestingly, a study demonstrated the efficacy of soluble human ESC-secreted factors to inhibit growth of cancer cells, but not benign fibroblasts by delivering human ESC-conditioned media to cancer cell *in vitro* [297]. The factors (< 10 kDa) contained in the hESC-CM blocked the growth of cancer cells and were not completely inactivated upon heating.

Endothelial cells responded to the EBM in the opposite manner of fibroblasts. Fibroblasts increased in proliferation and migration in response to non-HT EB with a

decline in responses upon HT of EBM. Extracted factors from non-HT EBM presented to the ECs typically inhibited proliferation, migration, and tube formation, as opposed to the pronounced effects observed upon treating the ECs with HT EBMs. Kuzuya et al. reported that soluble heat-stable factors released from fibroblast CM did not have an effect on EC proliferation, but did increase motility and tube formation [298]. All together, these results suggest that the soluble molecules present in the extracted EBM are comprised of bioactive factors specifically inhibitory to ECs.

On the other hand, when ECs were treated with matrix-associated factors in lyophilized EBM, not just the extracted soluble factors, the effect of heat treatment on EBM was prominent. Network formation assay enabled analysis of extracted factors versus the entire matrix and clearly exhibited more profound network formation results when treated with the entire EBM compared to the extractions. The absence of tubes in non-HT EBM + GFRM further demonstrated the presence of inhibitory factors, however, HT EBM + GFRM exhibited more robust network formation than GFRM alone and similar to VEGF-A + GFRM, suggesting that heating the EBM inactivated inhibitory factors as well as presented stimulatory factors. Furthermore, CAM results, though they were not all as pronounced as EC network formation ones, indicated that day 10 HT EBM yielded the greatest angiogenic response in tissues compared to other EBM treatments. There have been several studies examining heat-stabilization of growth factors by ECM factors such as heparin. In 1986, Gospodarowicz et al. demonstrated the importance of heparin in stabilizing FGF-2 during heat treatment, which lead to increased FGF-2 bioactivity compared to no heat treatment [299]. Since there was no evidence of increased FGF-2 activity in the presence of other GAGs, including chondroitin sulfate

and HA, this result was specific to heparin. The presence of heparin in EBM was not specifically examined, although there are several studies describing the necessity of heparin expression during development and ESC differentiation [225, 300]. Additionally, increased levels of IGF2 and VEGF in EBM extractions were detected as a result of heating, potentially due to release from ECM and or binding proteins. Even though VEGF-A levels increased in HT EBM extractions, VEGF-A bound to ECM would be undetected via ELISAs performed since the insoluble fraction was removed from the extracts prior to performing the assay, and the ELISA antibodies only detected splice variants 121 and 164 that are typically found in soluble fractions. VEGF-A variant 188 binds to ECM with greater affinity than 164 and has been reported to be effective in enhancing EC signaling in its ECM-bound state [301, 302]. Thus if this VEGF-A variant was present in the HT extracts it would not have been detected, but could still be bioactive and in turn stimulate EC network formation and CAM angiogenesis. Altogether, these results suggest that increased network formation and CAM angiogenesis resulting from HT EBM treatment are in part due to ECM-bound factors enhancing endothelial behavior.

Conclusion

Overall, the complex mixture of molecules harbored within EBMs enhanced certain cell behaviors implemented in tissue remodeling and angiogenesis. The specific growth factors identified in EBM extractions exhibited retention of bioactivity that was further investigated via *in vitro* and *ex ovo* assays. Not only did this study illustrate the modulation of paracrine factors secreted by differentiating ESCs, but also demonstrated

how the modulated EBM harnessed bioactive factors capable of impacting aspects of angiogenesis. Furthermore, the differential angiogenic responses to factors presented as matrix-associated versus soluble EBM implied that the synergy of ECM and growth factors was imperative in eliciting distinct bioactive function.

CHAPTER 7

FUTURE CONSIDERATIONS

In this work, the reservoir of extracellular mediators secreted during ESC differentiation was investigated for their function in modulating embryonic morphogenesis. Strategies to isolate and characterize this novel ESC-derived matrix were developed, and the harnessed bioactive factors demonstrated significant impact on exogenous cell and tissue morphogenesis. Paracrine factors produced by stem cells have been touted as an essential means by which the cells exert therapeutic benefits; however, no reports have described capturing these factors in a naturally produced matrix for potential therapeutic applications.

With the advent of stem cells came the notion that these cells could be transplanted to enhance tissue repair by differentiating and repopulating damaged tissue. Numerous studies have transplanted a variety of stem/progenitor cell populations in order to observe this enhanced healing, particularly using *in vivo* neovascularization models [6, 7, 169, 171], yet the percent of cells that integrated into the target area were low [172, 183, 185]. Thus, these outcomes led to studies examining the paracrine effects of these transplanted cells utilizing stem cell-CM [189, 190, 193, 243], which exhibited enhanced tissue function and angiogenesis as a result. Efforts to detect regulation of the extracellular environment during stem cell growth and differentiation speak to the paradigm shift from stem cell engraftment and differentiation towards paracrine modes of action as a result of stem cell transplantation. By screening the exracellular environment using sensitive high throughput technology [303, 304] of different stem cells or

differentiated cells derived from stem cells, certain cell populations can be examined for their therapeutic capacity based on the factors they produce via the secretome [187, 188, 240], glycome [305-308], and metabolome [309-311]. Factors of interest would depend on the specific tissue application, yet the induction of neovascularization and angiogenesis has emerged as a critical aspect for successful tissue regeneration.

In parallel to the aforementioned published reports, this work has motivated further characterization of the extracellular factors secreted by differentiating EBs. Gene expression arrays and ELISAs provided insight on the modulation of EB-generated extracellular molecules during differentiation, however, a more thorough profile of the secretome using high-throughput protein detection methods may elicit unique factors present in a dynamic ESC-derived EB environment undergoing morphogenesis compared to other studies examining the maintained pluripotent or multipotent state of stem cells [190, 297]. Furthermore, these unique factors may potentially be present in low abundance thus necessitating the use of recently developed methods [303, 304] employing sensitive detection limits to fully capture the extracellular environment of the EBM that would enable studies that could potentially discover novel low-abundance factors involved in ESC differentiation that have been not been investigated due to technology limitations.

The simplest way to harness stem cell secreted factors in an acellular manner is by collecting stem cell-conditioned media. The previously mentioned reports of stem cell-derived paracrine factors enhancing tissue repair utilized stem cell-CM to deliver these factors via local injections. The benefit to injecting stem cell-CM is the synergistic response typically elicited by a complex mixture of growth factors compared to isolated

growth factor delivery. However, the *in vivo* half-life of soluble growth factors is short, on the order of hours, thus CM becomes less potent soon after injection; nevertheless, growth factors bound to ECM render them more effective due to longer half-lives. Currently, synthetic ECM analogs are being devised to capture naturally produced secreted factors from cell-conditioned media, including ESC-CM, as a vehicle to deliver factors in a cell-free manner *in vivo*. The first report of capturing stem cell-secreted factors from CM was published in 2010 by Webber et al. describing the use of a self-assembling nanofiber gel that presents biomimetic heparin to capture and deliver secreted stem cell factors *in vivo* to ischemic myocardium [234]. Soon after, another study presented in a series of two publications, examined similar CM capture again using self-assembling nanofiber gel, but with an RGD peptide, and showed renoprotective effects [312, 313]. Similar studies could investigate the capture of EB-secreted molecules that are modulated during ESC differentiation and assess the effects *in vitro* and *in vivo*, expanding the EB-CM studies in Chapter 4.

EB-CM studies demonstrated the presence of bioactive factors and established the foundation to further engineer means to exploit the EB-secreted factors. Another means to deliver ESC-secreted factors *in vivo* is by the use of microparticles that can capture secreted factors and subsequently release them. The composition of these microparticles could be tailored to capture specific fractions of molecules, just like affinity columns are used to fractionate complex mixtures. Growth factors that bind heparin, such as FGFs and VEGFs [299, 301, 314], could bind selectively to heparin microparticles added to CM, and then tested for bioactive release using angiogenesis models. Additionally, other extracellular components could be captured by tailored microparticles based on detection

technologies, such as lectin (a glycan-binding ligand) [315]. Lectin microparticles could bind naturally synthesized GAGs expressed by ESCs, or other cell types of interest, thus yielding a variety of GAG microparticles to deliver ESC-secreted GAGs, which could impact tissue repair in vivo [208, 316].

The novel means to harness naturally produced ESC factors via acellularization and the initial characterization of molecules contained within the EBM, in this work and previous work [216, 270], could also inspire investigation of acellularizing EBs undergoing directed differentiation in order to obtain a more defined matrix for specific tissue regeneration applications. For example, the propensity of EBs to spontaneously differentiate towards the mesoderm lineage using the rotary culture system [217] and the increased cardiovascular differentiation within the EB population at later days of differentiation could be further exploited to yield more homogenous cardiovascular EB differentiation. Established protocols for endothelial differentiation via EB formation and purified growth factor delivery [198, 317, 318] combined with the rotary culture system may elicit enhanced EB cardiovascular differentiation. Furthermore, these EBs could be followed by mechanical acellularization techniques to derive a more angiogenic-inducing matrix compared to EBM from spontaneously differentiating EBs.

Although EBM bioactivity was assayed in two forms, soluble extractions and lyophilized powder, delivering an exact amount of matrix was a challenge. Extracting soluble factors is a simple means to deliver the factors, however, there is likely no optimal buffer to fully solubilize and retain bioactivity for all matrix-associated factors; hence, assessing the quantity and activity of the factors extracted with a certain buffer is necessary. Preliminary studies discussed in Appendix A describe the derivation of

soluble EBM formulations using several solutions previously cited in the literature, including urea, acetic acid, and salt solutions (NaCl, $MgCl_2$) [158, 159]. The factors extracted were assayed qualitatively via SDS-PAGE; however, continuing studies are being conducted using different extractions buffers in conjunction with more sophisticated techniques to analyze the extracted factors, such as fast protein liquid chromatography (FPLC), to further separate the extractions into fractions that can be examined for bioactivity. Fractionation can be controlled by the specific column chosen to separate the solubilized matrix – size-exclusion, ion-exchange, affinity binding, or hydrophobicity. Each of these column types would generate distinct fractions that could be tested for bioactivity via *in vitro* assays and further characterized for content using previously mentioned high-throughput protein detection methods. By fractionating the solubilized EBM, mediating factors that elicit specific *in vitro* bioactivity outcomes may be more readily identified in a smaller subset of factors via inhibition assays or immunoprecipitation.

Other acellular formulations of EBM, including detergent and enzymatic techniques yield a more viscous and consolidated matrix in comparison to the powdery lyophilized matrices in this work while retaining a number of matrix proteins – collagen, laminin, and fibronectin while [216, 270]. The benefit of a lyophilized, powder matrix is the "off-the-shelf" availability - typically the longevity of lyophilized proteins is greater than proteins in a hydrated state. Consequently, methods to controllably deliver this lyophilized powdery EBM need to be considered before moving towards *in vivo* studies and are highly dependent on the animal model as well as the delivery site. Studies in progress are able to load gelatin capsules with lyophilized EBM to deliver

intramuscularly into mice. Previous studies cited in the literature report gels produced from naturally derived matrices that generally have high collagen content [319, 320], that are ideal for injectable delivery. Due to low presence of collagen present in the EBM compared to other acellularized tissues [270], EBM could be combined with purified matrices capable of gelling, such as fibrin or collagen, or self-assembling nanofibers. Delivery of EBM to ischemic tissues, such as myocardium or hindlimb, would preferably be injection for ease of administration as is most commonly used, but rather than injecting solubilized matrix, it could potentially be beneficial to deliver EBM in combination with a matrix, preliminarily exhibited in network formations in Chapter 6, that can gel at body temperature to provide more prolonged release of the reservoir of ESC-derived factors. By incorporating the lyophilized EBM within a gel, particularly one that solidifies at body temperature, the EBM can be stored as a lyophilized powder and only combined with liquid immediately prior to delivery as to maintain bioactivity.

One unexpected result from the EBM bioactivity assays was the inhibition of EC proliferation, migration, and network formation in response to non-HT EBM, while HT EBM elicited increased responses in EC migration and network formation in comparison. Although several pro-angiogenic factors were assessed for content in the EBM, anti-angiogenic factors were not. The expression of a few anti-angiogenic molecules were examined via PCR array (Chapter 3), including thrombospondin 1 and 2, and did not exhibit increased in gene expression over the course of EB differentiation; however, there are a number of ECM components that inhibit angiogenesis and could be analyzed, such as endostatin and decorin [102]. Global analysis of the secretome could provide further insight into possible anti-angiogenic components of the EBM, which could help identify

mechanisms as to how EBM significantly inhibited EC processes critical to angiogenesis. Further studies could investigate the *in vivo* effects of EBM in inhibiting angiogenesis, which is critical for anti-angiogenic therapies for ocular neovascular diseases and cancer. From these global studies, knocking down certain anti-angiogenic molecules, using ESC knock-outs or siRNA delivery, could increase the angiogenic induction of EBM. However, due to the opposing forces at play within the embryonic environment, EBs generally do not spontaneously homogenously differentiate. Thus, the observed increase in cardiovascular differentiation could most likely be met with an array of factors that are inhibiting this differentiation, which also could be knocked down to promote more cardiovascular differentiation.

Due to the complex nature of EBM, *in vitro* and *ex ovo* studies were used as initial indicators of EB retention of bioactive factors while screening EBMs that may elicit a more angiogenic response *in vivo*, which is more complex than *in vitro*. *In vivo* studies could be examined in non-injury models of angiogenesis, such as the corneal angiogenesis assay or the subcutaneous plug assay, where blood vessel infiltration and neovasculature development can be easily detected, however pathological angiogenesis is typically not present in these locations. Injury models to look at the revascularization induction by EBM could be tested to assess angiogenic effects in the presence of ischemic tissues and inflammatory response, which are aspects that were not tested *in vitro* and can greatly influence the efficacy of the EBM *in vivo*. By implanting the EBM *in vivo*, responses of local endogenous cell types can be monitored, such surrounding muscle and nerves fibers that also are damaged during tissue injury and are essential in

restoring normal function, as well as more systemic outcomes that can completely affect angiogenic response.

In conclusion, this work has contributed to establishing the foundation that ESC-derived matrices harbor potent morphogens that impact aspects of tissue remodeling. This EB matrix not only provided a novel means to investigate the paracrine factors produced by ESCs, but it delivered the therapeutic benefits of stem cells in an effective cell-free manner. Future work will continue to elucidate the unique milieu of factors secreted by ESCs that will contribute to innovating advanced treatments that harness the therapeutic potential of ESCs for regenerative medicine.

APPENDIX A
SOLUBILIZATION OF ACELLULARIZED EMBRYOID BODY MATRICES

Formulation of acellularized EB matrix was investigated in order to develop alternative means of delivering ESC-derived matrix factors. Solubilization of acellularized EB matrices was performed using different solutions to following two different methods of acellularization. Mechanically acellularized EBs (lyophilized EBM) were compared to chemically treated EBs (TritonX + DNase, T+D) using 4 different buffers – 4M guanidine hydrochloride (GuHCl), 2M magnesium chloride ($MgCl_2$), 2M sodium chloride (NaCl), and 2M urea.

Using one third of a 1x100mm plate of EBs per sample, acellular EB matrices were produced via previously established protocols [216, 270, 321]. All solutions were made in 50mM Tris-HCl (pH 7.4). Each acellular EBM sample was solubilized in 1 mL of solution overnight at 4°C, and the supernatant was collected after centrifugation at 12000xg for 30 minutes at 4°C. To remove the solubilization buffers, each supernatant sample was dialyzed for 5 days against dI H_2O at 4°C. The dialyzed supernatants were then lyophilized to concentrate the proteins. The protein extracts were analyzed for total protein content using BCA and separated via SDS-PAGE (Figure A.1), and exhibited the ability to extract different proteins from EBMs acellularized by 2 different methods.

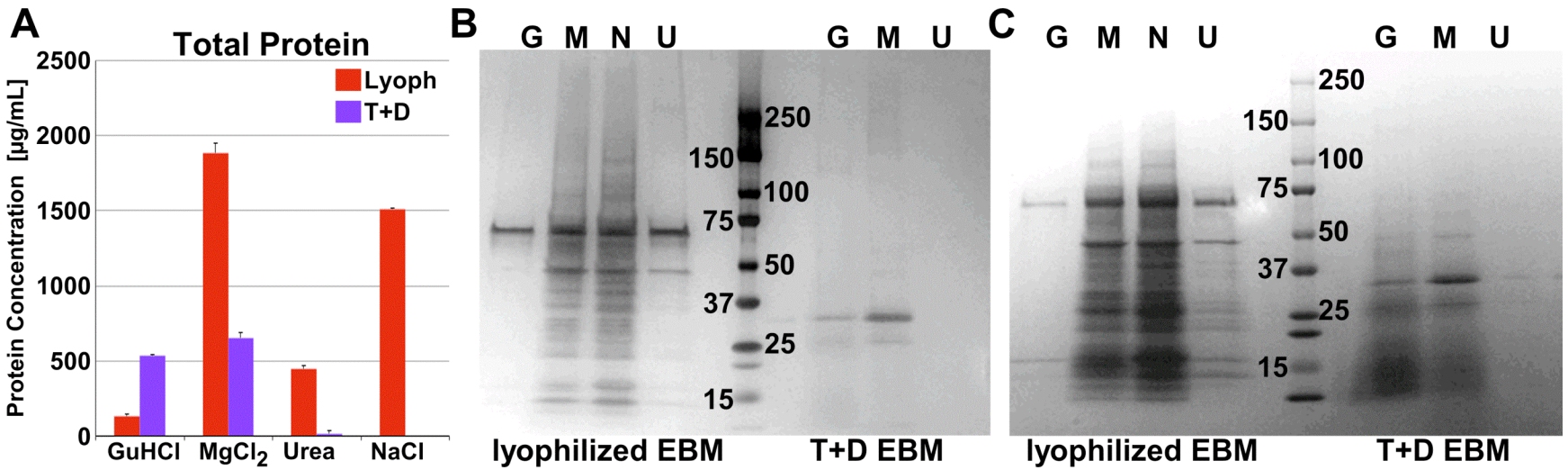

Figure A.1. Acellular EBM protein extractions. Protein extracts from two different acellularized matrices were characterized using four different solutions. Extracts were compared quantitatively (A) and qualitatively (B, C). Results indicated are mean ± standard deviation (n=3).

APPENDIX B

EVALUATION OF THE ANGIOGENIC POTENCY OF ACELLULAR EMBRYOID BODY MATRICES *IN VIVO* USING A MURINE HINDLIMB ISCHEMIA MODEL

Acellularized EBM captures the embryonic extracellular environment comprised of morphogens that induce proliferation, migration, and differentiation. While the resulting matrix contains angiogenic proteins, their ability to stimulate angiogenesis has not been tested *in vivo*. Since the acellular matrices examined will be derived from EBs with elevated expression of angiogenic factors, the activity of these factors was investigated. Acellular matrices that harnessed higher concentrations of the angiogenic factors previously assessed were examined for their angiogenic potency *in vivo* using a hindlimb ischemia mouse model.

Using a well-established HLI model, athymic male mice between weeks of age were anesthetized via intraperitoneal injection of xylazine (10 mg/kg) and ketamine (80 mg/kg) and used for all *in vivo* experiments. To create unilateral hindlimb ischemia in mice, an incision will be made in the left hindlimb to ligate and excise the femoral artery and vein. Animals were randomized into 3 groups – (1) lyophilized day 7 EBM, (2) L+D day 7 EBM, (3) untreated. EBM powder was implanted around the area of the excised artery at the time of surgery, and the dermal incision was sutured.

Laser Doppler perfusion imager (LDPI, Moor instrument) was used for serial noninvasive physiological evaluation of neovascularization. Mice were anesthetized with an intraperitoneal injection of Ketamine (40-90mg/kg) and Xylazine (10mg/kg). Each mouse was followed by a serial recording of surface blood flow of the hindlimb

immediately after surgery and on days 3, 7, 14, 21 and 28. After LDPI scanning, the stored digital color-coded images were analyzed to quantify blood flow of area and mean values of perfusion were calculated and expressed as the ratio of ischemic to non-ischemic limb.

For procedures requiring end point analysis (IHC and microCT), mice were euthanized, and the vasculature cleared using heparinized saline, perfusion fixed with 10% neutral buffered formalin, and flushed with heparinized saline. MicroCT required the vasculature to be perfused with silicone/lead chromate polymerizing contrast agent followed by removal of both hindlimbs that were treated in formic acid–based solution for 48 hours for bone decalcification. High-resolution 3D images were acquired using a microCT imaging system (vivaCT 40, Scano Medical) that assessed vasculature volume within the limb. For IHC evaluation, adductor muscles of the ischemic and control limbs were excised from perfusion-fixed mice, paraffin processed, and embedded for histological analysis. Five μm histological sections were taken and stained with H&E to examine the progression of muscle repair at days 3, 7, 14, and 28.

This pilot study was to determine the feasibility of delivering EBM to assess the angiogenic potency via a mouse HLI model. The analytical methods to investigate the angiogenic response were well defined and able to yield results (Figures B.1 – B.3); however, a means to effectively deliver a defined amount of EBM into the ischemic region needs to be devised. Additionally, the number of animals assessed (n=4 per treatment) was not sufficient to provide any concluding statements. While overall preliminary results showed differences in the EBM-treated hindlimbs compared to the untreated, future studies will need to incorporate efficient delivery vehicles as well as an

increased number of animals in order to provide increased animal numbers to sustain the entire 4-week.

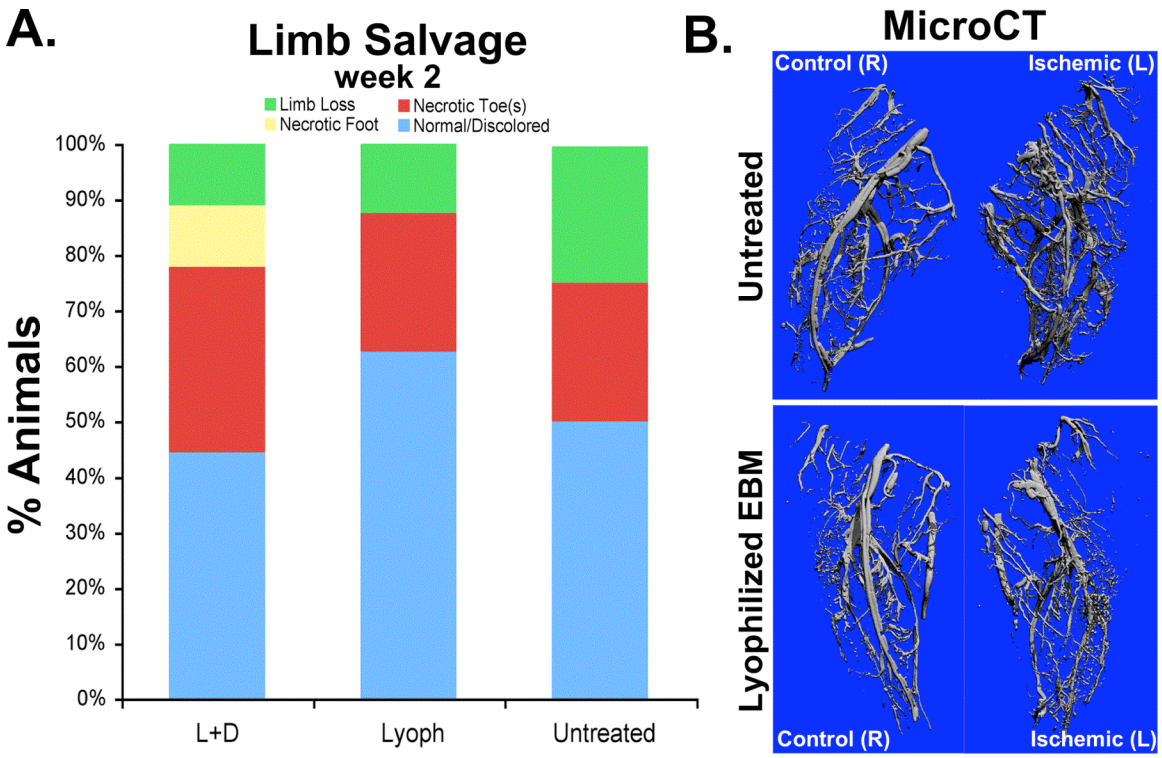

Figure B.1. Preliminary effects of EBM in ischemic hindlimb model. (A) Limb salvage observations of the ischemic hindlimb two weeks after surgery and EBM delivery. (B) MicroCT scans of limbs four weeks post-operation.

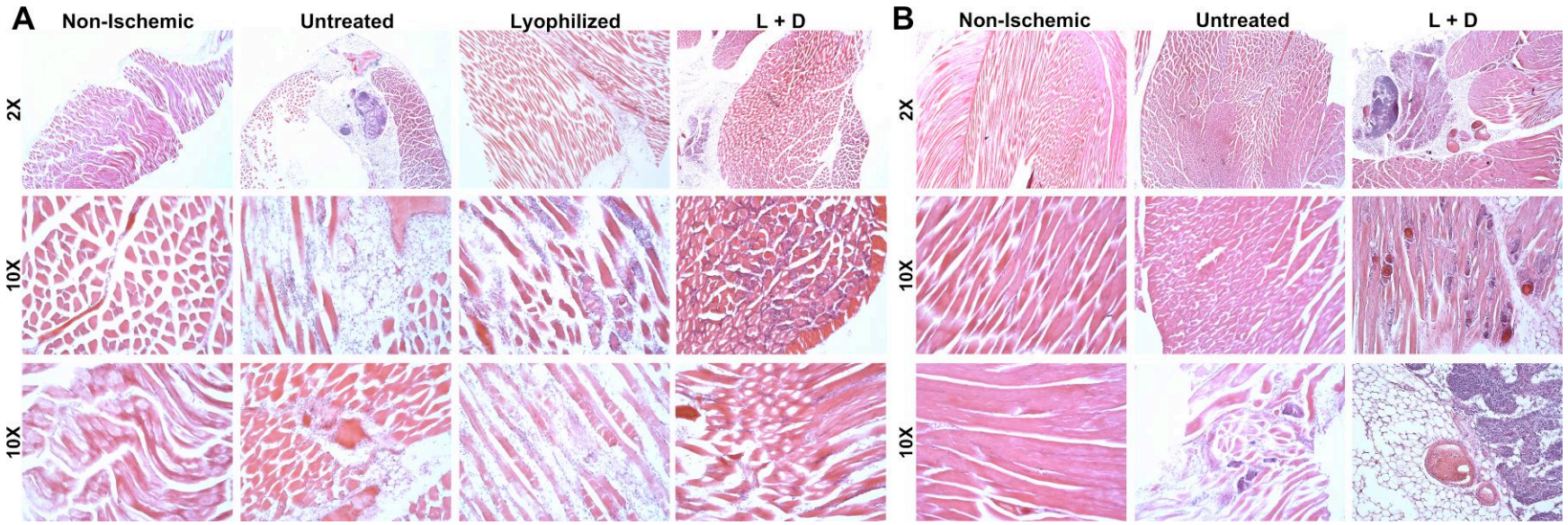

Figure B.2. Histological analysis of HLI muscle. Preliminary H&E staining of hindlimb muscles taken after 3 days (A) and 4 weeks (B) post-operation.

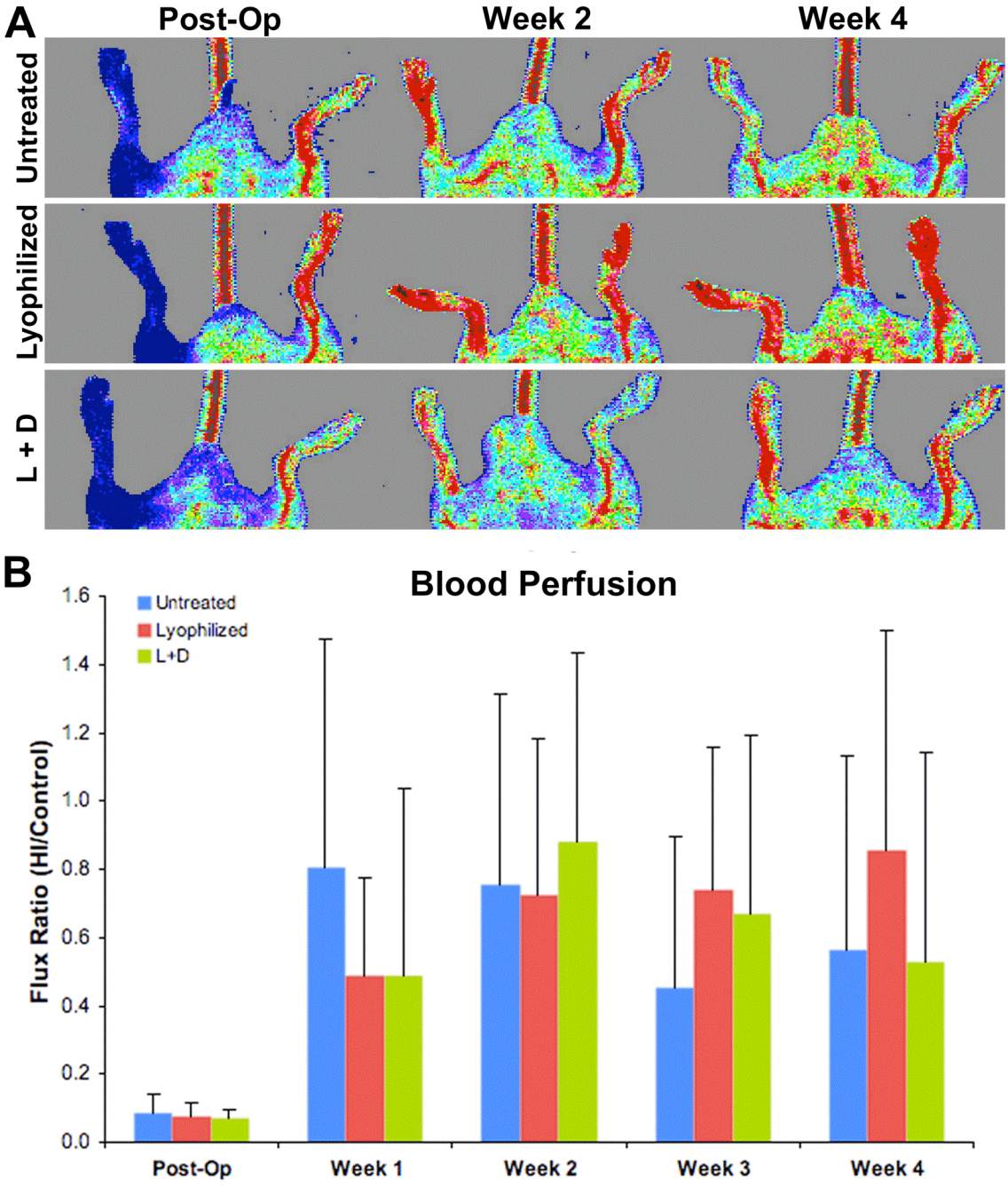

Figure B.3. Perfusion analysis of ischemic limbs. (A) LDPI assessments of blood perfusion of ischemic limbs during the 4-week study. (B) Quantitative analysis of perfusion based on the ratio of ischemic limb flux compared to control (non-ischemic) limb flux. Mean ± standard deviation.

REFERENCES

1. Folkman J, D'Amore PA. Blood vessel formation: what is its molecular basis? *Cell* 1996;87(7):1153-1155.
2. Risau W. Mechanisms of angiogenesis. *Nature* 1997;386(6626):671-674.
3. Henry TD, Rocha-Singh K, Isner JM, Kereiakes DJ, Giordano FJ, Simons M, et al. Intracoronary administration of recombinant human vascular endothelial growth factor to patients with coronary artery disease. *Am Heart J* 2001;142(5):872-880.
4. Hendel RC, Henry TD, Rocha-Singh K, Isner JM, Kereiakes DJ, Giordano FJ, et al. Effect of intracoronary recombinant human vascular endothelial growth factor on myocardial perfusion: evidence for a dose-dependent effect. *Circulation* 2000;101(2):118-121.
5. Chen S, Liu Z, Tian N, Zhang J, Yei F, Duan B, et al. Intracoronary transplantation of autologous bone marrow mesenchymal stem cells for ischemic cardiomyopathy due to isolated chronic occluded left anterior descending artery. *The Journal of invasive cardiology* 2006;18(11):552-556.
6. Fuchs S, Baffour R, Zhou YF, Shou M, Pierre A, Tio FO, et al. Transendocardial delivery of autologous bone marrow enhances collateral perfusion and regional function in pigs with chronic experimental myocardial ischemia. *J Am Coll Cardiol* 2001;37(6):1726-1732.
7. Tateishi-Yuyama E, Matsubara H, Murohara T, Ikeda U, Shintani S, Masaki H, et al. Therapeutic angiogenesis for patients with limb ischaemia by autologous transplantation of bone-marrow cells: a pilot study and a randomised controlled trial. *Lancet* 2002;360(9331):427-435.
8. Fraidenraich D, Stillwell E, Romero E, Wilkes D, Manova K, Basson C, et al. Rescue of cardiac defects in id knockout embryos by injection of embryonic stem cells. *Science* 2004;306(5694):247-252.
9. Siminovitch L, McCulloch EA, Till JE. The Distribution of Colony-Forming Cells among Spleen Colonies. *J Cell Physiol* 1963;62:327-336.
10. Becker AJ, Mc CE, Till JE. Cytological demonstration of the clonal nature of spleen colonies derived from transplanted mouse marrow cells. *Nature* 1963;197:452-454.
11. Lewis PD. Mitotic activity in the primate subependymal layer and the genesis of gliomas. *Nature* 1968;217(5132):974-975.
12. Altman J, Das GD. Autoradiographic and histological evidence of postnatal hippocampal neurogenesis in rats. *J Comp Neurol* 1965;124(3):319-335.
13. Sacco A, Doyonnas R, Kraft P, Vitorovic S, Blau HM. Self-renewal and expansion of single transplanted muscle stem cells. *Nature* 2008;456(7221):502-506.

14. Zuk PA, Zhu M, Ashjian P, De Ugarte DA, Huang JI, Mizuno H, et al. Human adipose tissue is a source of multipotent stem cells. *Mol Biol Cell* 2002;13(12):4279-4295.

15. Roisen FJ, Klueber KM, Lu CL, Hatcher LM, Dozier A, Shields CB, et al. Adult human olfactory stem cells. *Brain Res* 2001;890(1):11-22.

16. Toma JG, Akhavan M, Fernandes KJ, Barnabe-Heider F, Sadikot A, Kaplan DR, et al. Isolation of multipotent adult stem cells from the dermis of mammalian skin. *Nat Cell Biol* 2001;3(9):778-784.

17. Stemple DL, Anderson DJ. Isolation of a stem cell for neurons and glia from the mammalian neural crest. *Cell* 1992;71(6):973-985.

18. De Coppi P, Bartsch G, Jr., Siddiqui MM, Xu T, Santos CC, Perin L, et al. Isolation of amniotic stem cell lines with potential for therapy. *Nat Biotechnol* 2007;25(1):100-106.

19. Thomson JA, Itskovitz-Eldor J, Shapiro SS, Waknitz MA, Swiergiel JJ, Marshall VS, et al. Embryonic stem cell lines derived from human blastocysts. *Science* 1998;282(5391):1145-1147.

20. Martin GR. Isolation of a pluripotent cell line from early mouse embryos cultured in medium conditioned by teratocarcinoma stem cells. *Proc Natl Acad Sci U S A* 1981;78(12):7634-7638.

21. Evans MJ, Kaufman MH. Establishment in culture of pluripotential cells from mouse embryos. *Nature* 1981;292(5819):154-156.

22. Barberi T, Klivenyi P, Calingasan NY, Lee H, Kawamata H, Loonam K, et al. Neural subtype specification of fertilization and nuclear transfer embryonic stem cells and application in parkinsonian mice. *Nat Biotechnol* 2003;21(10):1200-1207.

23. Okabe S, Forsberg-Nilsson K, Spiro AC, Segal M, McKay RD. Development of neuronal precursor cells and functional postmitotic neurons from embryonic stem cells in vitro. *Mech Dev* 1996;59(1):89-102.

24. Bagutti C, Wobus AM, Fassler R, Watt FM. Differentiation of embryonal stem cells into keratinocytes: comparison of wild-type and beta 1 integrin-deficient cells. *Dev Biol* 1996;179(1):184-196.

25. Coraux C, Hilmi C, Rouleau M, Spadafora A, Hinnrasky J, Ortonne JP, et al. Reconstituted skin from murine embryonic stem cells. *Curr Biol* 2003;13(10):849-853.

26. Yamada T, Yoshikawa M, Kanda S, Kato Y, Nakajima Y, Ishizaka S, et al. In vitro differentiation of embryonic stem cells into hepatocyte-like cells identified by cellular uptake of indocyanine green. *Stem Cells* 2002;20(2):146-154.

27. Hamazaki T, Iiboshi Y, Oka M, Papst PJ, Meacham AM, Zon LI, et al. Hepatic maturation in differentiating embryonic stem cells in vitro. *FEBS Lett* 2001;497(1):15-19.

28. Colman A. Making new beta cells from stem cells. *Semin Cell Dev Biol* 2004;15(3):337-345.

29. Lumelsky N, Blondel O, Laeng P, Velasco I, Ravin R, McKay R. Differentiation of embryonic stem cells to insulin-secreting structures similar to pancreatic islets. *Science* 2001;292(5520):1389-1394.

30. Keller G, Kennedy M, Papayannopoulou T, Wiles MV. Hematopoietic commitment during embryonic stem cell differentiation in culture. *Mol Cell Biol* 1993;13(1):473-486.

31. Cerdan C, Rouleau A, Bhatia M. VEGF-A165 augments erythropoietic development from human embryonic stem cells. *Blood* 2004;103(7):2504-2512.

32. Rohwedel J, Maltsev V, Bober E, Arnold HH, Hescheler J, Wobus AM. Muscle cell differentiation of embryonic stem cells reflects myogenesis in vivo: developmentally regulated expression of myogenic determination genes and functional expression of ionic currents. *Dev Biol* 1994;164(1):87-101.

33. Vo E, Hanjaya-Putra D, Zha Y, Kusuma S, Gerecht S. Smooth-muscle-like cells derived from human embryonic stem cells support and augment cord-like structures in vitro. *Stem Cell Rev*;6(2):237-247.

34. Fijnvandraat AC, van Ginneken AC, Schumacher CA, Boheler KR, Lekanne Deprez RH, Christoffels VM, et al. Cardiomyocytes purified from differentiated embryonic stem cells exhibit characteristics of early chamber myocardium. *J Mol Cell Cardiol* 2003;35(12):1461-1472.

35. Westfall MV, Rust EM, Metzger JM. Slow skeletal troponin I gene transfer, expression, and myofilament incorporation enhances adult cardiac myocyte contractile function. *Proc Natl Acad Sci U S A* 1997;94(10):5444-5449.

36. Maltsev VA, Rohwedel J, Hescheler J, Wobus AM. Embryonic stem cells differentiate in vitro into cardiomyocytes representing sinusnodal, atrial and ventricular cell types. *Mech Dev* 1993;44(1):41-50.

37. Wobus AM, Wallukat G, Hescheler J. Pluripotent mouse embryonic stem cells are able to differentiate into cardiomyocytes expressing chronotropic responses to adrenergic and cholinergic agents and Ca2+ channel blockers. *Differentiation* 1991;48(3):173-182.

38. Robbins J, Gulick J, Sanchez A, Howles P, Doetschman T. Mouse embryonic stem cells express the cardiac myosin heavy chain genes during development in vitro. *J Biol Chem* 1990;265(20):11905-11909.

39. Yamamoto K, Sokabe T, Watabe T, Miyazono K, Yamashita JK, Obi S, et al. Fluid shear stress induces differentiation of Flk-1-positive embryonic stem cells into vascular endothelial cells in vitro. *Am J Physiol Heart Circ Physiol* 2005;288(4):H1915-1924.

40. McCloskey KE, Lyons I, Rao RR, Stice SL, Nerem RM. Purified and proliferating endothelial cells derived and expanded in vitro from embryonic stem cells. *Endothelium* 2003;10(6):329-336.

41. Keller GM. In vitro differentiation of embryonic stem cells. *Curr Opin Cell Biol* 1995;7(6):862-869.

42. Itskovitz-Eldor J, Schuldiner M, Karsenti D, Eden A, Yanuka O, Amit M, et al. Differentiation of human embryonic stem cells into embryoid bodies compromising the three embryonic germ layers. *Mol Med* 2000;6(2):88-95.

43. Nakagami H, Nakagawa N, Takeya Y, Kashiwagi K, Ishida C, Hayashi S, et al. Model of vasculogenesis from embryonic stem cells for vascular research and regenerative medicine. *Hypertension* 2006;48(1):112-119.

44. Desbaillets I, Ziegler U, Groscurth P, Gassmann M. Embryoid bodies: an in vitro model of mouse embryogenesis. *Exp Physiol* 2000;85(6):645-651.

45. Feraud O, Cao Y, Vittet D. Embryonic stem cell-derived embryoid bodies development in collagen gels recapitulates sprouting angiogenesis. *Lab Invest* 2001;81(12):1669-1681.

46. Jakobsson L, Kreuger J, Claesson-Welsh L. Building blood vessels--stem cell models in vascular biology. *J Cell Biol* 2007;177(5):751-755.

47. Doetschman TC, Eistetter H, Katz M, Schmidt W, Kemler R. The in vitro development of blastocyst-derived embryonic stem cell lines: formation of visceral yolk sac, blood islands and myocardium. *Journal of embryology and experimental morphology* 1985;87:27-45.

48. Wang R, Clark R, Bautch VL. Embryonic stem cell-derived cystic embryoid bodies form vascular channels: an in vitro model of blood vessel development. *Development* 1992;114(2):303-316.

49. Risau W, Sariola H, Zerwes HG, Sasse J, Ekblom P, Kemler R, et al. Vasculogenesis and angiogenesis in embryonic-stem-cell-derived embryoid bodies. *Development* 1988;102(3):471-478.

50. Vittet D, Prandini MH, Berthier R, Schweitzer A, Martin-Sisteron H, Uzan G, et al. Embryonic stem cells differentiate in vitro to endothelial cells through successive maturation steps. *Blood* 1996;88(9):3424-3431.

51. Gu A, Tsark W, Holmes KV, Shively JE. Role of Ceacam1 in VEGF induced vasculogenesis of murine embryonic stem cell-derived embryoid bodies in 3D culture. *Exp Cell Res* 2009;315(10):1668-1682.

52. Lange S, Heger J, Euler G, Wartenberg M, Piper H, Sauer H. Platelet-derived growth factor BB stimulates vasculogenesis of embryonic stem cell-derived endothelial cells by calcium-mediated generation of reactive oxygen species. *Cardiovasc Res* 2008.

53. Kabrun N, Buhring HJ, Choi K, Ullrich A, Risau W, Keller G. Flk-1 expression defines a population of early embryonic hematopoietic precursors. *Development* 1997;124(10):2039-2048.

54. Takahashi K, Yamanaka S. Induction of pluripotent stem cells from mouse embryonic and adult fibroblast cultures by defined factors. *Cell* 2006;126(4):663-676.

55. Yu J, Vodyanik MA, Smuga-Otto K, Antosiewicz-Bourget J, Frane JL, Tian S, et al. Induced pluripotent stem cell lines derived from human somatic cells. *Science* 2007;318(5858):1917-1920.

56. Takahashi K, Tanabe K, Ohnuki M, Narita M, Ichisaka T, Tomoda K, et al. Induction of pluripotent stem cells from adult human fibroblasts by defined factors. *Cell* 2007;131(5):861-872.

57. Aasen T, Raya A, Barrero MJ, Garreta E, Consiglio A, Gonzalez F, et al. Efficient and rapid generation of induced pluripotent stem cells from human keratinocytes. *Nat Biotechnol* 2008;26(11):1276-1284.

58. Hanna J, Markoulaki S, Schorderet P, Carey BW, Beard C, Wernig M, et al. Direct reprogramming of terminally differentiated mature B lymphocytes to pluripotency. *Cell* 2008;133(2):250-264.

59. Eminli S, Foudi A, Stadtfeld M, Maherali N, Ahfeldt T, Mostoslavsky G, et al. Differentiation stage determines potential of hematopoietic cells for reprogramming into induced pluripotent stem cells. *Nat Genet* 2009;41(9):968-976.

60. Chang MY, Kim D, Kim CH, Kang HC, Yang E, Moon JI, et al. Direct reprogramming of rat neural precursor cells and fibroblasts into pluripotent stem cells. *PLoS One*;5(3):e9838.

61. Kim JB, Greber B, Arauzo-Bravo MJ, Meyer J, Park KI, Zaehres H, et al. Direct reprogramming of human neural stem cells by OCT4. *Nature* 2009;461(7264):649-643.

62. Kim JB, Zaehres H, Wu G, Gentile L, Ko K, Sebastiano V, et al. Pluripotent stem cells induced from adult neural stem cells by reprogramming with two factors. *Nature* 2008;454(7204):646-650.

63. Liu H, Ye Z, Kim Y, Sharkis S, Jang YY. Generation of endoderm-derived human induced pluripotent stem cells from primary hepatocytes. *Hepatology*;51(5):1810-1819.

64. Li W, Wei W, Zhu S, Zhu J, Shi Y, Lin T, et al. Generation of rat and human induced pluripotent stem cells by combining genetic reprogramming and chemical inhibitors. *Cell Stem Cell* 2009;4(1):16-19.

65. Stadtfeld M, Hochedlinger K. Induced pluripotency: history, mechanisms, and applications. *Genes Dev*;24(20):2239-2263.

66. Staton CA, Reed MWR, Brown NJ. A critical analysis of current in vitro and in vivo angiogenesis assays. *Int J Exp Pathol* 2009;90(3):195-221.

67. Staton CA, Stribbling SM, Tazzyman S, Hughes R, Brown NJ, Lewis CE. Current methods for assaying angiogenesis in vitro and in vivo. *Int J Exp Pathol* 2004;85(5):233-248.

68. Auerbach R, Akhtar N, Lewis RL, Shinners BL. Angiogenesis assays: problems and pitfalls. *Cancer Metastasis Rev* 2000;19(1-2):167-172.

69. Auerbach R, Lewis R, Shinners B, Kubai L, Akhtar N. Angiogenesis assays: a critical overview. *Clin Chem* 2003;49(1):32-40.

70. Denizot F, Lang R. Rapid colorimetric assay for cell growth and survival. Modifications to the tetrazolium dye procedure giving improved sensitivity and reliability. *J Immunol Methods* 1986;89(2):271-277.

71. Gomez D, Reich NC. Stimulation of primary human endothelial cell proliferation by IFN. *J Immunol* 2003;170(11):5373-5381.

72. Alessandri G, Raju K, Gullino PM. Mobilization of capillary endothelium in vitro induced by effectors of angiogenesis in vivo. *Cancer Res* 1983;43(4):1790-1797.

73. Grant DS, Kibbey MC, Kinsella JL, Cid MC, Kleinman HK. The role of basement membrane in angiogenesis and tumor growth. *Pathol Res Pract* 1994;190(9-10):854-863.

74. Lawley TJ, Kubota Y. Induction of morphologic differentiation of endothelial cells in culture. *J Invest Dermatol* 1989;93(2 Suppl):59S-61S.

75. Burbridge MF, West DC. Rat Aortic Ring : 3D Model of Angiogenesis In Vitro. *Methods Mol Med* 2001;46:185-204.

76. Dellian M, Witwer BP, Salehi HA, Yuan F, Jain RK. Quantitation and physiological characterization of angiogenic vessels in mice: effect of basic fibroblast growth factor, vascular endothelial growth factor/vascular permeability factor, and host microenvironment. *Am J Pathol* 1996;149(1):59-71.

77. Muthukkaruppan V, Auerbach R. Angiogenesis in the mouse cornea. *Science* 1979;205(4413):1416-1418.

78. Couffinhal T, Silver M, Zheng LP, Kearney M, Witzenbichler B, Isner JM. Mouse model of angiogenesis. *Am J Pathol* 1998;152(6):1667-1679.

79. Ribatti D, Vacca A, Roncali L, Dammacco F. The chick embryo chorioallantoic membrane as a model for in vivo research on angiogenesis. *Int J Dev Biol* 1996;40(6):1189-1197.

80. Parsons-Wingerter P, Lwai B, Yang MC, Elliott KE, Milaninia A, Redlitz A, et al. A novel assay of angiogenesis in the quail chorioallantoic membrane: stimulation by bFGF and inhibition by angiostatin according to fractal dimension and grid intersection. *Microvasc Res* 1998;55(3):201-214.

81. Brooks PC, Montgomery AM, Cheresh DA. Use of the 10-day-old chick embryo model for studying angiogenesis. *Methods Mol Biol* 1999;129:257-269.

82. Auerbach R, Kubai L, Knighton D, Folkman J. A simple procedure for the long-term cultivation of chicken embryos. *Dev Biol* 1974;41(2):391-394.

83. Ribatti D, Vacca A, Bertossi M, De Benedictis G, Roncali L, Dammacco F. Angiogenesis induced by B-cell non-Hodgkin's lymphomas. Lack of correlation with tumor malignancy and immunologic phenotype. *Anticancer Res* 1990;10(2A):401-406.

84. Ausprunk DH, Knighton DR, Folkman J. Vascularization of normal and neoplastic tissues grafted to the chick chorioallantois. Role of host and preexisting graft blood vessels. *Am J Pathol* 1975;79(3):597-618.

85. Kurz H, Ambrosy S, Wilting J, Marme D, Christ B. Proliferation pattern of capillary endothelial cells in chorioallantoic membrane development indicates local growth control, which is counteracted by vascular endothelial growth factor application. *Dev Dyn* 1995;203(2):174-186.

86. Ribatti D, Nico B, Vacca A, Presta M. The gelatin sponge-chorioallantoic membrane assay. *Nature protocols* 2006;1(1):85-91.

87. Ribatti D, Conconi MT, Nico B, Baiguera S, Corsi P, Parnigotto PP, et al. Angiogenic response induced by acellular brain scaffolds grafted onto the chick embryo chorioallantoic membrane. *Brain Research* 2003;989(1):9-15.

88. Conconi MT, Nico B, Mangieri D, Tommasini M, di Liddo R, Parnigotto PP, et al. Angiogenic response induced by acellular aortic matrix in vivo. *The anatomical record Part A, Discoveries in molecular, cellular, and evolutionary biology* 2004;281(2):1303-1307.

89. Conconi MT, Nico B, Rebuffat P, Crivellato E, Parnigotto PP, Nussdorfer GG, et al. Angiogenic response induced by acellular femoral matrix in vivo. *J Anat* 2005;207(1):79-83.

90. Ribatti D, Nico B, Vacca A, Roncali L, Burri PH, Djonov V. Chorioallantoic membrane capillary bed: a useful target for studying angiogenesis and anti-angiogenesis in vivo. *Anat Rec* 2001;264(4):317-324.

91. Silvestre JS, Mallat Z, Tedgui A, Levy BI. Post-ischaemic neovascularization and inflammation. *Cardiovasc Res* 2008;78(2):242-249.

92. Arroyo AG, Iruela-Arispe ML. Extracellular matrix, inflammation, and the angiogenic response. *Cardiovasc Res*;86(2):226-235.

93. Rogers JH, Laird JR. Overview of new technologies for lower extremity revascularization. *Circulation* 2007;116(18):2072-2085.

94. Nagai MK, Embil JM. Becaplermin: recombinant platelet derived growth factor, a new treatment for healing diabetic foot ulcers. *Expert Opin Biol Ther* 2002;2(2):211-218.

95. Sellke FW, Laham RJ, Edelman ER, Pearlman JD, Simons M. Therapeutic angiogenesis with basic fibroblast growth factor: technique and early results. *Ann Thorac Surg* 1998;65(6):1540-1544.

96. Lei Y, Haider HK, Shujia J, Sim ESK. Therapeutic angiogenesis. Devising new strategies based on past experiences. *Basic Res Cardiol* 2004;99(2):121-132.

97. Evans AL, Bryant J, Skepper J, Smith SK, Print CG, Charnock-Jones DS. Vascular development in embryoid bodies: quantification of transgenic intervention and antiangiogenic treatment. *Angiogenesis* 2007;10(3):217-226.

98. Makinen K, Manninen H, Hedman M, Matsi P, Mussalo H, Alhava E, et al. Increased vascularity detected by digital subtraction angiography after VEGF gene transfer to human lower limb artery: a randomized, placebo-controlled, double-blinded phase II study. *Mol Ther* 2002;6(1):127-133.

99. Shyu KG, Chang H, Isner JM. Synergistic effect of angiopoietin-1 and vascular endothelial growth factor on neoangiogenesis in hypercholesterolemic rabbit model with acute hindlimb ischemia. *Life Sci* 2003;73(5):563-579.

100. Udelson JE, Dilsizian V, Laham RJ, Chronos N, Vansant J, Blais M, et al. Therapeutic angiogenesis with recombinant fibroblast growth factor-2 improves stress and rest myocardial perfusion abnormalities in patients with severe symptomatic chronic coronary artery disease. *Circulation* 2000;102(14):1605-1610.

101. Laham RJ, Rezaee M, Post M, Sellke FW, Braeckman RA, Hung D, et al. Intracoronary and intravenous administration of basic fibroblast growth factor: myocardial and tissue distribution. *Drug Metab Dispos* 1999;27(7):821-826.

102. Sottile J. Regulation of angiogenesis by extracellular matrix. *Biochim Biophys Acta* 2004;1654(1):13-22.

103. Madri JA, Bell L, Marx M, Merwin JR, Basson C, Prinz C. Effects of soluble factors and extracellular matrix components on vascular cell behavior in vitro and in vivo: models of de-endothelialization and repair. *Journal Of Cellular Biochemistry* 1991;45(2):123-130.

104. Chen L, He Z, Chen B, Yang M, Zhao Y, Sun W, et al. Loading of VEGF to the heparin cross-linked demineralized bone matrix improves vascularization of the scaffold. *J Mater Sci Mater Med* 2010;21(1):309-317.

105. Klagsbrun M. Mediators of angiogenesis: the biological significance of basic fibroblast growth factor (bFGF)-heparin and heparan sulfate interactions. *Seminars In Cancer Biology* 1992;3(2):81-87.

106. Mitsi M, Forsten-Williams K, Gopalakrishnan M, Nugent MA. A catalytic role of heparin within the extracellular matrix. *J Biol Chem* 2008;283(50):34796-34807.

107. Folkman J, Shing Y. Control of angiogenesis by heparin and other sulfated polysaccharides. *Adv Exp Med Biol* 1992;313:355-364.

108. Clark RAF. Synergistic Signaling from Extracellular Matrix–Growth Factor Complexes. *J Investig Dermatol* 2008;128(6):1354-1355.

109. Hynes RO. The extracellular matrix: not just pretty fibrils. *Science* 2009;326(5957):1216-1219.

110. Sun Q, Silva EA, Wang A, Fritton JC, Mooney DJ, Schaffler MB, et al. Sustained Release of Multiple Growth Factors from Injectable Polymeric System as a Novel Therapeutic Approach Towards Angiogenesis. *Pharm Res* 2009.

111. Sakiyama-Elbert SE, Hubbell JA. Controlled release of nerve growth factor from a heparin-containing fibrin-based cell ingrowth matrix. *J Control Release* 2000;69(1):149-158.

112. Sakiyama-Elbert SE, Hubbell JA. Development of fibrin derivatives for controlled release of heparin-binding growth factors. *J Control Release* 2000;65(3):389-402.

113. Lutolf MP, Hubbell JA. Synthetic biomaterials as instructive extracellular microenvironments for morphogenesis in tissue engineering. *Nat Biotechnol* 2005;23(1):47-55.

114. Zhang X, Yang J, Li Y, Liu S, Long K, Zhao Q, et al. Functional Neovascularization in Tissue Engineering with Porcine Acellular Dermal Matrix and Human Umbilical Vein Endothelial Cells. *Tissue engineering Part C, Methods* 2010.

115. Wong AK, Schonmyer BH, Schonmeyer BH, Singh P, Carlson DL, Li S, et al. Histologic analysis of angiogenesis and lymphangiogenesis in acellular human dermis. *Plastic and Reconstructive Surgery* 2008;121(4):1144-1152.

116. Badylak S. The extracellular matrix as a scaffold for tissue reconstruction. *Seminars In Cell & Developmental Biology* 2002;13(5):377-383.

117. Gilbert T, Sellaro T, Badylak S. Decellularization of tissues and organs. *Biomaterials* 2006;27(19):3675-3683.

118. Hodde J. Naturally occurring scaffolds for soft tissue repair and regeneration. *Tissue Eng* 2002;8(2):295-308.

119. McPherson T, Badylak S. Characterization of fibronectin derived from porcine small intestinal submucosa. *Tissue Engineering* 1998;4(1):75-83.

120. Bhrany A, Beckstead B, Lang T, Farwell D, Giachelli C, Ratner B. Development of an esophagus acellular matrix tissue scaffold. *Tissue Eng* 2006;12(2):319-330.

121. Bolland F, Korossis S, Wilshaw S, Ingham E, Fisher J, Kearney J, et al. Development and characterisation of a full-thickness acellular porcine bladder matrix for tissue engineering. *Biomaterials* 2007;28(6):1061-1070.

122. Curtil A, Pegg D, Wilson A. Repopulation of freeze-dried porcine valves with human fibroblasts and endothelial cells. *Journal Of Heart Valve Disease* 1997;6(3):296-306.

123. Kasimir M, Rieder E, Seebacher G, Silberhumer G, Wolner E, Weigel G, et al. Comparison of different decellularization procedures of porcine heart valves. *Int J Artif Organs* 2003;26(5):421-427.

124. Buinewicz B, Rosen B. Acellular cadaveric dermis (AlloDerm): A new alternative for abdominal hernia repair. *Annals Of Plastic Surgery* 2004;52(2):188-194.

125. Chen R, Ho H, Tsai Y, Sheu M. Process development of an acellular dermal matrix (ADM) for biomedical applications. *Biomaterials* 2004;25(13):2679-2686.

126. Hudson T, Liu S, Schmidt C. Engineering an improved acellular nerve graft via optimized chemical processing. *Tissue Eng* 2004;10(9-10):1346-1358.

127. Hopper R, Woodhouse K, Semple J. Acellularization of human placenta with preservation of the basement membrane: a potential matrix for tissue engineering. *Ann Plast Surg* 2003;51(6):598-602.

128. Mirsadraee S, Wilcox H, Korossis S, Kearney J, Watterson K, Fisher J, et al. Development and characterization of an acellular human pericardial matrix for tissue engineering. *Tissue Eng* 2006;12(4):763-773.

129. Ott HC, Matthiesen TS, Goh S-K, Black LD, Kren SM, Netoff TI, et al. Perfusion-decellularized matrix: using nature's platform to engineer a bioartificial heart. *Nature Medicine* 2008;14(2):213-221.

130. Uygun BE, Soto-Gutierrez A, Yagi H, Izamis M-L, Guzzardi MA, Shulman C, et al. Organ reengineering through development of a transplantable recellularized liver graft using decellularized liver matrix. *Nature Medicine* 2010;16(7):814-820.

131. Ott HC, Clippinger B, Conrad C, Schuetz C, Pomerantseva I, Ikonomou L, et al. Regeneration and orthotopic transplantation of a bioartificial lung. *Nature Medicine* 2010;16(8):927-933.

132. Price AP, England KA, Matson AM, Blazar BR, Panoskaltsis-Mortari A. Development of a decellularized lung bioreactor system for bioengineering the lung: the matrix reloaded. *Tissue engineering Part A* 2010;16(8):2581-2591.

133. Petersen TH, Calle EA, Zhao L, Lee EJ, Gui L, Raredon MB, et al. Tissue-engineered lungs for in vivo implantation. *Science* 2010;329(5991):538-541.

134. Chang Y, Chen S, Wei H, Wu T, Liang H, Lai P, et al. Tissue regeneration observed in a porous acellular bovine pericardium used to repair a myocardial defect in the right ventricle of a rat model. *J Thorac Cardiovasc Surg* 2005;130(3):705-711.

135. Kim B, Yoo J, Atala A. Peripheral nerve regeneration using acellular nerve grafts. *J Biomed Mater Res A* 2004;68(2):201-209.

136. Badylak S, Lantz G, Coffey A, Geddes L. Small intestinal submucosa as a large diameter vascular graft in the dog. *J Surg Res* 1989;47(1):74-80.

137. Lantz G, Badylak S, Coffey A, Geddes L, Blevins W. Small intestinal submucosa as a small-diameter arterial graft in the dog. *J Invest Surg* 1990;3(3):217-227.

138. Prevel C, Eppley B, Summerlin D, Sidner R, Jackson J, McCarty M, et al. Small intestinal submucosa: utilization as a wound dressing in full-thickness rodent wounds. *Ann Plast Surg* 1995;35(4):381-388.

139. Helton W, Fisichella P, Berger R, Horgan S, Espat N, Abcarian H. Short-term outcomes with small intestinal submucosa for ventral abdominal hernia. *Arch Surg* 2005;140(6):549-560; discussion 560-542.

140. Badylak S, Tullius R, Kokini K, Shelbourne K, Klootwyk T, Voytik S, et al. The use of xenogeneic small intestinal submucosa as a biomaterial for Achilles tendon repair in a dog model. *J Biomed Mater Res* 1995;29(8):977-985.

141. Cartmell JS, Dunn MG. Effect of chemical treatments on tendon cellularity and mechanical properties. *J Biomed Mater Res* 2000;49(1):134-140.

142. Grauss R, Hazekamp M, Oppenhuizen F, van Munsteren C, Gittenberger-de Groot A, DeRuiter M. Histological evaluation of decellularised porcine aortic valves: matrix changes due to different decellularisation methods. *Eur J Cardiothorac Surg* 2005;27(4):566-571.

143. Lin P, Chan W, Badylak S, Bhatia S. Assessing porcine liver-derived biomatrix for hepatic tissue engineering. *Tissue Eng* 2004;10(7-8):1046-1053.

144. Woods T, Gratzer PF. Effectiveness of three extraction techniques in the development of a decellularized bone-anterior cruciate ligament-bone graft. *Biomaterials* 2005;26(35):7339-7349.

145. Probst M, Dahiya R, Carrier S, Tanagho EA. Reproduction of functional smooth muscle tissue and partial bladder replacement. *British journal of urology* 1997;79(4):505-515.

146. Yoo JJ, Meng J, Oberpenning F, Atala A. Bladder augmentation using allogenic bladder submucosa seeded with cells. *Urology* 1998;51(2):221-225.

147. Bader A, Schilling T, Teebken OE, Brandes G, Herden T, Steinhoff G, et al. Tissue engineering of heart valves--human endothelial cell seeding of detergent acellularized porcine valves. *European journal of cardio-thoracic surgery : official journal of the European Association for Cardio-thoracic Surgery* 1998;14(3):279-284.

148. McFetridge PS, Daniel JW, Bodamyali T, Horrocks M, Chaudhuri JB. Preparation of porcine carotid arteries for vascular tissue engineering applications. *Journal Of Biomedical Materials Research Part A* 2004;70(2):224-234.

149. Gulati A. Evaluation of acellular and cellular nerve grafts in repair of rat peripheral nerve. *J Neurosurg* 1988;68(1):117-123.

150. Jackson D, Grood E, Arnoczky S, Butler D, Simon T. Freeze dried anterior cruciate ligament allografts. Preliminary studies in a goat model. *Am J Sports Med* 1987;15(4):295-303.

151. Aimoli CG, Nogueira GM, Nascimento LS, Baceti A, Leirner AA, Maizato MJ, et al. Lyophilized bovine pericardium treated with a phenethylamine-diepoxide as an alternative to preventing calcification of cardiovascular bioprosthesis: preliminary calcification results. *Artif Organs* 2007;31(4):278-283.

152. El-Sabban ME, El-Khoury H, Hamdan-Khalil R, Sindet-Pedersen S, Bazarbachi A. Xenogenic bone matrix extracts induce osteoblastic differentiation of human bone marrow-derived mesenchymal stem cells. *Regenerative medicine* 2007;2(4):383-390.

153. Ahn J-I, Lee D-H, Ryu Y-H, Jang I-K, Yoon M-Y, Shin YH, et al. Reconstruction of rabbit corneal epithelium on lyophilized amniotic membrane using the tilting dynamic culture method. *Artificial Organs* 2007;31(9):711-721.

154. Yang B, Zhang Y, Zhou L, Sun Z, Zheng J, Chen Y, et al. Development of a porcine bladder acellular matrix with well-preserved extracellular bioactive factors for tissue engineering. *Tissue engineering Part C, Methods* 2010;16(5):1201-1211.

155. Bolland F, Korossis S, Wilshaw SP, Ingham E, Fisher J, Kearney JN, et al. Development and characterisation of a full-thickness acellular porcine bladder matrix for tissue engineering. *Biomaterials* 2007;28(6):1061-1070.

156. Baiguera S, Jungebluth P, Burns A, Mavilia C, Haag J, De Coppi P, et al. Tissue engineered human tracheas for in vivo implantation. *Biomaterials* 2010;31(34):8931-8938.

157. Yang B, Zhou L, Sun Z, Yang R, Chen Y, Dai Y. In vitro evaluation of the bioactive factors preserved in porcine small intestinal submucosa through cellular biological approaches. *Journal Of Biomedical Materials Research Part A* 2010;93(3):1100-1109.

158. VoytikHarbin S, Brightman A, Kraine M, Waisner B, Badylak S. Identification of extractable growth factors from small intestinal submucosa. *Journal Of Cellular Biochemistry* 1997;67(4):478-491.

159. Chun SY, Lim GJ, Kwon TG, Kwak EK, Kim BW, Atala A, et al. Identification and characterization of bioactive factors in bladder submucosa matrix. *Biomaterials* 2007;28(29):4251-4256.

160. Kamihata H, Matsubara H, Nishiue T, Fujiyama S, Tsutsumi Y, Ozono R, et al. Implantation of bone marrow mononuclear cells into ischemic myocardium enhances collateral perfusion and regional function via side supply of angioblasts, angiogenic ligands, and cytokines. *Circulation* 2001;104(9):1046-1052.

161. Nishida M, Li TS, Hirata K, Yano M, Matsuzaki M, Hamano K. Improvement of cardiac function by bone marrow cell implantation in a rat hypoperfusion heart model. *Ann Thorac Surg* 2003;75(3):768-773; discussion 773-764.

162. Orlic D, Kajstura J, Chimenti S, Bodine DM, Leri A, Anversa P. Transplanted adult bone marrow cells repair myocardial infarcts in mice. *Ann N Y Acad Sci* 2001;938:221-229; discussion 229-230.

163. Perin EC, Dohmann HF, Borojevic R, Silva SA, Sousa AL, Mesquita CT, et al. Transendocardial, autologous bone marrow cell transplantation for severe, chronic ischemic heart failure. *Circulation* 2003;107(18):2294-2302.

164. Strauer BE, Brehm M, Zeus T, Kostering M, Hernandez A, Sorg RV, et al. Repair of infarcted myocardium by autologous intracoronary mononuclear bone marrow cell transplantation in humans. *Circulation* 2002;106(15):1913-1918.

165. Tse HF, Kwong YL, Chan JK, Lo G, Ho CL, Lau CP. Angiogenesis in ischaemic myocardium by intramyocardial autologous bone marrow mononuclear cell implantation. *Lancet* 2003;361(9351):47-49.

166. Assmus B, Schachinger V, Teupe C, Britten M, Lehmann R, Dobert N, et al. Transplantation of Progenitor Cells and Regeneration Enhancement in Acute Myocardial Infarction (TOPCARE-AMI). *Circulation* 2002;106(24):3009-3017.

167. Badorff C, Brandes RP, Popp R, Rupp S, Urbich C, Aicher A, et al. Transdifferentiation of blood-derived human adult endothelial progenitor cells into functionally active cardiomyocytes. *Circulation* 2003;107(7):1024-1032.

168. Kaushal S, Amiel GE, Guleserian KJ, Shapira OM, Perry T, Sutherland FW, et al. Functional small-diameter neovessels created using endothelial progenitor cells expanded ex vivo. *Nat Med* 2001;7(9):1035-1040.

169. Kocher AA, Schuster MD, Szabolcs MJ, Takuma S, Burkhoff D, Wang J, et al. Neovascularization of ischemic myocardium by human bone-marrow-derived angioblasts prevents cardiomyocyte apoptosis, reduces remodeling and improves cardiac function. *Nature Medicine* 2001;7(4):430-436.

170. Xiao Q, Zeng L, Zhang Z, Margariti A, Ali Z, Channon K, et al. Sca-1+ progenitors derived from embryonic stem cells differentiate into endothelial cells capable of vascular repair after arterial injury. *Arterioscler Thromb Vasc Biol* 2006;26(10):2244-2251.

171. Cho S-W, Moon S-H, Lee S-H, Kang S-W, Kim J, Lim JM, et al. Improvement of postnatal neovascularization by human embryonic stem cell derived endothelial-like cell transplantation in a mouse model of hindlimb ischemia. *Circulation* 2007;116(21):2409-2419.

172. Moon MH, Kim SY, Kim YJ, Kim SJ, Lee JB, Bae YC, et al. Human adipose tissue-derived mesenchymal stem cells improve postnatal neovascularization in a mouse model of hindlimb ischemia. *Cell Physiol Biochem* 2006;17(5-6):279-290.

173. Madeddu P, Emanueli C, Pelosi E, Salis MB, Cerio AM, Bonanno G, et al. Transplantation of low dose CD34+KDR+ cells promotes vascular and muscular regeneration in ischemic limbs. *FASEB J* 2004;18(14):1737-1739.

174. Koponen JK, Kekarainen T, E Heinonen S, Laitinen A, Nystedt J, Laine J, et al. Umbilical cord blood-derived progenitor cells enhance muscle regeneration in mouse hindlimb ischemia model. *Mol Ther* 2007;15(12):2172-2177.

175. Wu KH, Zhou B, Mo XM, Cui B, Yu CT, Lu SH, et al. Therapeutic potential of human umbilical cord-derived stem cells in ischemic diseases. *Transplant Proc* 2007;39(5):1620-1622.

176. Oyamada N, Itoh H, Sone M, Yamahara K, Miyashita K, Park K, et al. Transplantation of vascular cells derived from human embryonic stem cells contributes to vascular regeneration after stroke in mice. *J Transl Med* 2008;6:54.

177. Rufaihah AJ, Haider HK, Heng BC, Ye L, Tan RS, Toh WS, et al. Therapeutic angiogenesis by transplantation of human embryonic stem cell-derived CD133+ endothelial progenitor cells for cardiac repair. *Regenerative medicine* 2010;5(2):231-244.

178. Sata M. Circulating vascular progenitor cells contribute to vascular repair, remodeling, and lesion formation. *Trends Cardiovasc Med* 2003;13(6):249-253.

179. Yoon Y-S, Park J-S, Tkebuchava T, Luedeman C, Losordo DW. Unexpected severe calcification after transplantation of bone marrow cells in acute myocardial infarction. *Circulation* 2004;109(25):3154-3157.

180. Leor J, Gerecht S, Cohen S, Miller L, Holbova R, Ziskind A, et al. Human embryonic stem cell transplantation to repair the infarcted myocardium. *Heart* 2007;93(10):1278-1284.

181. Nussbaum J, Minami E, Laflamme MA, Virag JAI, Ware CB, Masino A, et al. Transplantation of undifferentiated murine embryonic stem cells in the heart: teratoma formation and immune response. *FASEB J* 2007;21(7):1345-1357.

182. Swijnenburg RJ, Tanaka M, Vogel H, Baker J, Kofidis T, Gunawan F, et al. Embryonic stem cell immunogenicity increases upon differentiation after transplantation into ischemic myocardium. *Circulation* 2005;112(9 Suppl):I166-172.

183. Ma N, Stamm C, Kaminski A, Li W, Kleine H-D, Müller-Hilke B, et al. Human cord blood cells induce angiogenesis following myocardial infarction in NOD/scid-mice. *Cardiovasc Res* 2005;66(1):45-54.

184. Iso Y, Spees JL, Serrano C, Bakondi B, Pochampally R, Song YH, et al. Multipotent human stromal cells improve cardiac function after myocardial infarction in mice without long-term engraftment. *Biochem Biophys Res Commun* 2007;354(3):700-706.

185. Gnecchi M, He H, Liang OD, Melo LG, Morello F, Mu H, et al. Paracrine action accounts for marked protection of ischemic heart by Akt-modified mesenchymal stem cells. *Nature Medicine* 2005;11(4):367-368.

186. Salgado AJBOG, Reis RLG, Sousa NJC, Gimble JM. Adipose tissue derived stem cells secretome: soluble factors and their roles in regenerative medicine. *Curr Stem Cell Res Ther* 2010;5(2):103-110.

187. Sze SK, de Kleijn DPV, Lai RC, Khia Way Tan E, Zhao H, Yeo KS, et al. Elucidating the secretion proteome of human embryonic stem cell-derived mesenchymal stem cells. *Mol Cell Proteomics* 2007;6(10):1680-1689.

188. Bendall SC, Hughes C, Campbell JL, Stewart MH, Pittock P, Liu S, et al. An enhanced mass spectrometry approach reveals human embryonic stem cell growth factors in culture. *Mol Cell Proteomics* 2009;8(3):421-432.

189. Teodelinda M, Michele C, Sebastiano C, Ranieri C, Chiara G. Amniotic liquid derived stem cells as reservoir of secreted angiogenic factors capable of stimulating neo-arteriogenesis in an ischemic model. *Biomaterials* 2011;32(15):3689-3699.

190. Chen L, Tredget EE, Wu PYG, Wu Y. Paracrine factors of mesenchymal stem cells recruit macrophages and endothelial lineage cells and enhance wound healing. *PLoS ONE* 2008;3(4):e1886.

191. Rehman J, Traktuev D, Li J, Merfeld-Clauss S, Temm-Grove CJ, Bovenkerk JE, et al. Secretion of angiogenic and antiapoptotic factors by human adipose stromal cells. *Circulation* 2004;109(10):1292-1298.

192. Crisostomo P, Abarbanell A, Wang M, Lahm T, Wang Y, Meldrum D. Embryonic Stem Cells Attenuate Myocardial Dysfunction and Inflammation After Surgical Global Ischemia via Paracrine Actions. *Am J Physiol Heart Circ Physiol* 2008.

193. Guo Y, Graham-Evans B, Broxmeyer HE. Murine embryonic stem cells secrete cytokines/growth modulators that enhance cell survival/anti-apoptosis and stimulate colony formation of murine hematopoietic progenitor cells. *Stem Cells* 2006;24(4):850-856.

194. Singla D, Lyons G, Kamp T. Transplanted Embryonic Stem Cells Following Mouse Myocardial Infarction Inhibit Apoptosis and Cardiac Remodeling. *Am J Physiol Heart Circ Physiol* 2007.

195. Wobus AM, Holzhausen H, Jakel P, Schoneich J. Characterization of a pluripotent stem cell line derived from a mouse embryo. *Exp Cell Res* 1984;152(1):212-219.

196. Grinnell KL, Bickenbach JR. Skin keratinocytes pre-treated with embryonic stem cell-conditioned medium or BMP4 can be directed to an alternative cell lineage. *Cell Prolif* 2007;40(5):685-705.

197. Höpfl G, Gassmann M, Desbaillets I. Differentiating embryonic stem cells into embryoid bodies. *Methods Mol Biol* 2004;254:79-98.

198. Boyd NL, Dhara SK, Rekaya R, Godbey EA, Hasneen K, Rao RR, et al. BMP4 promotes formation of primitive vascular networks in human embryonic stem cell-derived embryoid bodies. *Exp Biol Med (Maywood)* 2007;232(6):833-843.

199. Van Linthout S, Seeland U, Riad A, Eckhardt O, Hohl M, Dhayat N, et al. Reduced MMP-2 activity contributes to cardiac fibrosis in experimental diabetic cardiomyopathy. *Basic Res Cardiol* 2008;103(4):319-327.

200. Schenke-Layland K, Angelis E, Rhodes KE, Heydarkhan-Hagvall S, Mikkola HK, Maclellan WR. Collagen IV induces trophoectoderm differentiation of mouse embryonic stem cells. *Stem Cells* 2007;25(6):1529-1538.

201. Nourse MB, Halpin DE, Scatena M, Mortisen DJ, Tulloch NL, Hauch KD, et al. VEGF induces differentiation of functional endothelium from human embryonic stem cells: implications for tissue engineering. *Arterioscler Thromb Vasc Biol* 2010;30(1):80-89.

202. Flaim CJ, Chien S, Bhatia SN. An extracellular matrix microarray for probing cellular differentiation. *Nat Methods* 2005;2(2):119-125.

203. Flaim CJ, Teng D, Chien S, Bhatia SN. Combinatorial signaling microenvironments for studying stem cell fate. *Stem Cells Dev* 2008;17(1):29-40.

204. Kelly D, Rizzino A. DNA microarray analyses of genes regulated during the differentiation of embryonic stem cells. *Mol Reprod Dev* 2000;56(2):113-123.

205. Bhattacharya B, Cai J, Luo Y, Miura T, Mejido J, Brimble S, et al. Comparison of the gene expression profile of undifferentiated human embryonic stem cell lines and differentiating embryoid bodies. *BMC Dev Biol* 2005;5:22.

206. Mansergh F, Daly C, Hurley A, Wride M, Hunter S, Evans M. Gene expression profiles during early differentiation of mouse embryonic stem cells. *BMC Dev Biol* 2009;9(1):5.

207. Gunji W, Kai T, Sameshima E, Iizuka N, Katagi H, Utsugi T, et al. Global analysis of the expression patterns of transcriptional regulatory factors in formation of embryoid bodies using sensitive oligonucleotide microarray systems. *Biochem Biophys Res Commun* 2004;325(1):265-275.

208. Nairn AV, Kinoshita-Toyoda A, Toyoda H, Xie J, Harris K, Dalton S, et al. Glycomics of proteoglycan biosynthesis in murine embryonic stem cell differentiation. *J Proteome Res* 2007;6(11):4374-4387.

209. Chen RR, Silva EA, Yuen WW, Mooney DJ. Spatio-temporal VEGF and PDGF delivery patterns blood vessel formation and maturation. *Pharm Res* 2007;24(2):258-264.

210. Michelini M, Franceschini V, Sihui Chen S, Papini S, Rosellini A, Ciani F, et al. Primate embryonic stem cells create their own niche while differentiating in three-dimensional culture systems. *Cell Prolif* 2006;39(3):217-229.

211. Shukla S, Nair R, Rolle MW, Braun KR, Chan CK, Johnson PY, et al. Synthesis and organization of hyaluronan and versican by embryonic stem cells undergoing embryoid body differentiation. *J Histochem Cytochem* 2010;58(4):345-358.

212. Feraud O, Vittet D. Murine embryonic stem cell in vitro differentiation: applications to the study of vascular development. *Histol Histopathol* 2003;18(1):191-199.

213. Carpenedo R, Sargent C, McDevitt T. Rotary suspension culture enhances the efficiency, yield, and homogeneity of embryoid body differentiation. *Stem Cells* 2007;25(9):2224-2234.

214. Pfaffl MW. A new mathematical model for relative quantification in real-time RT-PCR. *Nucleic Acids Res* 2001;29(9):e45.

215. Warrington JA, Nair A, Mahadevappa M, Tsyganskaya M. Comparison of human adult and fetal expression and identification of 535 housekeeping/maintenance genes. *Physiol Genomics* 2000;2(3):143-147.

216. Nair R, Ngangan AV, McDevitt TC. Efficacy of solvent extraction methods for acellularization of embryoid bodies. *Journal of biomaterials science Polymer edition* 2008;19(6):801-819.

217. Sargent CY, Berguig GY, McDevitt TC. Cardiomyogenic differentiation of embryoid bodies is promoted by rotary orbital suspension culture. *Tissue Eng Part A* 2009;15(2):331-342.

218. Dobrucki LW, Tsutsumi Y, Kalinowski L, Dean J, Gavin M, Sen S, et al. Analysis of angiogenesis induced by local IGF-1 expression after myocardial infarction using microSPECT-CT imaging. *J Mol Cell Cardiol*;48(6):1071-1079.

219. Suleiman MS, Singh RJ, Stewart CE. Apoptosis and the cardiac action of insulin-like growth factor I. *Pharmacol Ther* 2007;114(3):278-294.

220. Chao W, D'Amore PA. IGF2: epigenetic regulation and role in development and disease. *Cytokine Growth Factor Rev* 2008;19(2):111-120.

221. Maeng Y-S, Choi H-J, Kwon J-Y, Park Y-W, Choi K-S, Min J-K, et al. Endothelial progenitor cell homing: prominent role of the IGF2-IGF2R-PLCbeta2 axis. *Blood* 2009;113(1):233-243.

222. Lin Z-F, Li X-K, Lin Y, Wu F, Liang L-M, Fu X-B. Protective effects of non-mitogenic human acidic fibroblast growth factor on hydrogen peroxide-induced damage to cardiomyocytes in vitro. *World J Gastroenterol* 2005;11(35):5492-5497.

223. Francis SE, Goh KL, Hodivala-Dilke K, Bader BL, Stark M, Davidson D, et al. Central roles of alpha5beta1 integrin and fibronectin in vascular development in mouse embryos and embryoid bodies. *Arterioscler Thromb Vasc Biol* 2002;22(6):927-933.

224. Li J, Yang L, Liu K, Yuan C, Tang Y, Quan Q, et al. Synergistic effects of FGF-2 and PDGF-BB on angiogenesis and muscle regeneration in rabbit hindlimb ischemia model. *Microvasc Res* 2010.

225. Li S, Harrison D, Carbonetto S, Fassler R, Smyth N, Edgar D, et al. Matrix assembly, regulation, and survival functions of laminin and its receptors in embryonic stem cell differentiation. *J Cell Biol* 2002;157(7):1279-1290.

226. Matsuoka Y, Kubota H, Adachi E, Nagai N, Marutani T, Hosokawa N, et al. Insufficient folding of type IV collagen and formation of abnormal basement membrane-like structure in embryoid bodies derived from Hsp47-null embryonic stem cells. *Mol Biol Cell* 2004;15(10):4467-4475.

227. Hofstetter CP, Schwarz EJ, Hess D, Widenfalk J, El Manira A, Prockop DJ, et al. Marrow stromal cells form guiding strands in the injured spinal cord and promote recovery. *P Natl Acad Sci Usa* 2002;99(4):2199-2204.

228. Li RK, Jia ZQ, Weisel RD, Merante F, Mickle DA. Smooth muscle cell transplantation into myocardial scar tissue improves heart function. *J Mol Cell Cardiol* 1999;31(3):513-522.

229. Jackson KA, Majka SM, Wang H, Pocius J, Hartley CJ, Majesky MW, et al. Regeneration of ischemic cardiac muscle and vascular endothelium by adult stem cells. *J Clin Invest* 2001;107(11):1395-1402.

230. Min J-Y, Huang X, Xiang M, Meissner A, Chen Y, Ke Q, et al. Homing of intravenously infused embryonic stem cell-derived cells to injured hearts after myocardial infarction. *J Thorac Cardiovasc Surg* 2006;131(4):889-897.

231. Cho HH, Kim YJ, Kim JT, Song JS, Shin KK, Bae YC, et al. The role of chemokines in proangiogenic action induced by human adipose tissue-derived mesenchymal stem cells in the murine model of hindlimb ischemia. *Cell Physiol Biochem* 2009;24(5-6):511-518.

232. Di Santo S, Yang Z, Wyler von Ballmoos M, Voelzmann J, Diehm N, Baumgartner I, et al. Novel cell-free strategy for therapeutic angiogenesis: in vitro generated conditioned medium can replace progenitor cell transplantation. *PLoS ONE* 2009;4(5):e5643.

233. Shabbir A, Zisa D, Suzuki G, Lee T. Heart Failure Therapy Mediated by the Trophic Activities of Bone Marrow Mesenchymal Stem Cells: A Non-invasive Therapeutic Regimen. *Am J Physiol Heart Circ Physiol* 2009.

234. Webber MJ, Han X, Prasanna Murthy SN, Rajangam K, Stupp SI, Lomasney JW. Capturing the stem cell paracrine effect using heparin-presenting nanofibres to treat cardiovascular diseases. *Journal of tissue engineering and regenerative medicine* 2010.

235. Kocher AA, Schuster MD, Bonaros N, Lietz K, Xiang G, Martens TP, et al. Myocardial homing and neovascularization by human bone marrow angioblasts is regulated by IL-8/Gro CXC chemokines. *J Mol Cell Cardiol* 2006;40(4):455-464.

236. Walter MNM, Wright KT, Fuller HR, MacNeil S, Johnson WEB. Mesenchymal stem cell-conditioned medium accelerates skin wound healing: an in vitro study of fibroblast and keratinocyte scratch assays. *Exp Cell Res* 2010;316(7):1271-1281.

237. Kinnaird T, Stabile E, Burnett MS, Shou M, Lee CW, Barr S, et al. Local delivery of marrow-derived stromal cells augments collateral perfusion through paracrine mechanisms. *Circulation* 2004;109(12):1543-1549.

238. Yoon BS, Moon J-H, Jun EK, Kim J, Maeng I, Kim JS, et al. Secretory profiles and wound healing effects of human amniotic fluid-derived mesenchymal stem cells. *Stem Cells Dev* 2010;19(6):887-902.

239. Singla D, Singla R, McDonald D. Factors Released from Embryonic Stem Cells inhibit Apoptosis in H9c2 cells through P1-3kinase/Akt but not ERK pathway. *Am J Physiol Heart Circ Physiol* 2008.

240. Estrada R, Li N, Sarojini H, An J, Lee M-J, Wang E. Secretome from mesenchymal stem cells induces angiogenesis via Cyr61. *Journal Of Cellular Physiology* 2009;219(3):563-571.

241. Kalluri R. EMT: when epithelial cells decide to become mesenchymal-like cells. *J Clin Invest* 2009;119(6):1417-1419.

242. LaFramboise WA, Petrosko P, Krill-Burger JM, Morris DR, McCoy AR, Scalise D, et al. Proteins secreted by embryonic stem cells activate cardiomyocytes through ligand binding pathways. *J Proteomics* 2010;73(5):992-1003.

243. Singla DK, McDonald DE. Factors released from embryonic stem cells inhibit apoptosis of H9c2 cells. *Am J Physiol Heart Circ Physiol* 2007;293(3):H1590-1595.

244. Spencer HL, Eastham AM, Merry CLR, Southgate TD, Perez-Campo F, Soncin F, et al. E-cadherin inhibits cell surface localization of the pro-migratory 5T4 oncofetal antigen in mouse embryonic stem cells. *Mol Biol Cell* 2007;18(8):2838-2851.

245. Shigematsu S, Yamauchi K, Nakajima K, Iijima S, Aizawa T, Hashizume K. IGF-1 regulates migration and angiogenesis of human endothelial cells. *Endocr J* 1999;46 Suppl:S59-62.

246. Johansson BM, Wiles MV. Evidence for involvement of activin A and bone morphogenetic protein 4 in mammalian mesoderm and hematopoietic development. *Mol Cell Biol* 1995;15(1):141-151.

247. Iwaguro H, Yamaguchi J-i, Kalka C, Murasawa S, Masuda H, Hayashi S-i, et al. Endothelial progenitor cell vascular endothelial growth factor gene transfer for vascular regeneration. *Circulation* 2002;105(6):732-738.

248. Stavri GT, Zachary IC, Baskerville PA, Martin JF, Erusalimsky JD. Basic fibroblast growth factor upregulates the expression of vascular endothelial growth factor in vascular smooth muscle cells. Synergistic interaction with hypoxia. *Circulation* 1995;92(1):11-14.

249. Yau TM, Fung K, Weisel RD, Fujii T, Mickle DA, Li RK. Enhanced myocardial angiogenesis by gene transfer with transplanted cells. *Circulation* 2001;104(12 Suppl 1):I218-222.

250. Minuto F, Palermo C, Arvigo M, Barreca AM. The IGF system and bone. *J Endocrinol Invest* 2005;28(8 Suppl):8-10.

251. Wilson EM, Hsieh MM, Rotwein P. Autocrine growth factor signaling by insulin-like growth factor-II mediates MyoD-stimulated myocyte maturation. *J Biol Chem* 2003;278(42):41109-41113.

252. Peng H, Wright V, Usas A, Gearhart B, Shen H-C, Cummins J, et al. Synergistic enhancement of bone formation and healing by stem cell-expressed VEGF and bone morphogenetic protein-4. *J Clin Invest* 2002;110(6):751-759.

253. Borselli C, Storrie H, Benesch-Lee F, Shvartsman D, Cezar C, Lichtman JW, et al. Functional muscle regeneration with combined delivery of angiogenesis and myogenesis factors. *P Natl Acad Sci Usa* 2010;107(8):3287-3292.

254. Cui L, Jiang J, Wei L, Zhou X, Fraser JL, Snider BJ, et al. Transplantation of embryonic stem cells improves nerve repair and functional recovery after severe sciatic nerve axotomy in rats. *Stem Cells* 2008;26(5):1356-1365.

255. Hodgson D, Behfar A, Zingman L, Kane G, Perez-Terzic C, Alekseev A, et al. Stable benefit of embryonic stem cell therapy in myocardial infarction. *Am J Physiol Heart Circ Physiol* 2004;287(2):H471-479.

256. Kimura H, Yoshikawa M, Matsuda R, Toriumi H, Nishimura F, Hirabayashi H, et al. Transplantation of embryonic stem cell-derived neural stem cells for spinal cord injury in adult mice. *Neurol Res* 2005;27(8):812-819.

257. Kolossov E, Bostani T, Roell W, Breitbach M, Pillekamp F, Nygren J, et al. Engraftment of engineered ES cell-derived cardiomyocytes but not BM cells restores contractile function to the infarcted myocardium. *J Exp Med* 2006;203(10):2315-2327.

258. von Unge M, Dirckx J, Olivius N. Embryonic stem cells enhance the healing of tympanic membrane perforations. *Int J Pediatr Otorhinolaryngol* 2003;67(3):215-219.

259. Wei L, Cui L, Snider BJ, Rivkin M, Yu SS, Lee C-S, et al. Transplantation of embryonic stem cells overexpressing Bcl-2 promotes functional recovery after transient cerebral ischemia. *Neurobiol Dis* 2005;19(1-2):183-193.

260. Guttinger M, Fedele D, Koch P, Padrun V, Pralong W, Brustle O, et al. Suppression of kindled seizures by paracrine adenosine release from stem cell-derived brain implants. *Epilepsia* 2005;46(8):1162-1169.

261. Curtil A, Pegg D, Wilson A. Freeze drying of cardiac valves in preparation for cellular repopulation. *Cryobiology* 1997;34(1):13-22.

262. Hudson T, Zawko S, Deister C, Lundy S, Hu C, Lee K, et al. Optimized acellular nerve graft is immunologically tolerated and supports regeneration. *Tissue Engineering* 2004;10(11-12):1641-1651.

263. Aimoli CG, Nogueira GM, Nascimento LS, Baceti A, Leirner AA, Maizato MJS, et al. Lyophilized bovine pericardium treated with a phenethylamine-diepoxide as an alternative to preventing calcification of cardiovascular bioprosthesis: preliminary calcification results. *Artificial Organs* 2007;31(4):278-283.

264. Laun A, Tonn JC, Jerusalem C. Comparative study of lyophilized human dura mater and lyophilized bovine pericardium as dural substitutes in neurosurgery. *Acta Neurochirurgica* 1990;107(1-2):16-21.

265. Ide C. Nerve regeneration and Schwann cell basal lamina: observations of the long-term regeneration. *Archivum histologicum Japonicum Nippon soshikigaku kiroku* 1983;46(2):243-257.

266. Lewis PB, Williams JM, Hallab N, Virdi A, Yanke A, Cole BJ. Multiple freeze-thaw cycled meniscal allograft tissue: A biomechanical, biochemical, and histologic analysis. *J Orthop Res* 2008;26(1):49-55.

267. Zaleske D, Peretti G, Allemann F, Strongin D, MacLean R, Yates KE, et al. Engineering a joint: a chimeric construct with bovine chondrocytes in a devitalized chick knee. *Tissue Eng* 2003;9(5):949-956.

268. Bullard KM, Banda MJ, Arbeit JM, Bergsland E, Young DM. Human acellular dermal matrix as a novel model of malignant epithelial cell invasion. *Invasion Metastasis* 1997;17(1):42-52.

269. Coucouvanis E, Martin G. Signals for death and survival: a two-step mechanism for cavitation in the vertebrate embryo. *Cell* 1995;83(2):279-287.

270. Nair R, Shukla S, McDevitt TC. Acellular matrices derived from differentiating embryonic stem cells. *Journal Of Biomedical Materials Research Part A* 2008;87(4):1075-1085.

271. Research CfDEa. Guideline on Validation of the Limulus Amebocyte Lysate Test as an End-Product Endotoxin Test for Human and Animal Parenteral Drugs, Biological Products, and Medical Devices. In: U.S. Department of Health and Human Services FaDA, editor. Rockville, 1997.

272. Gnecchi M, He H, Noiseux N, Liang OD, Zhang L, Morello F, et al. Evidence supporting paracrine hypothesis for Akt-modified mesenchymal stem cell-mediated cardiac protection and functional improvement. *FASEB J* 2006;20(6):661-669.

273. Song S-Y, Chung H-M, Sung J-H. The pivotal role of VEGF in adipose-derived-stem-cell-mediated regeneration. *Expert Opinion On Biological Therapy* 2010;10(11):1529-1537.

274. Urbich C, Aicher A, Heeschen C, Dernbach E, Hofmann WK, Zeiher AM, et al. Soluble factors released by endothelial progenitor cells promote migration of endothelial cells and cardiac resident progenitor cells. *J Mol Cell Cardiol* 2005;39(5):733-742.

275. Heil M, Ziegelhoeffer T, Mees B, Schaper W. A different outlook on the role of bone marrow stem cells in vascular growth: bone marrow delivers software not hardware. *Circulation Research* 2004;94(5):573-574.

276. Nakanishi C, Yamagishi M, Yamahara K, Hagino I, Mori H, Sawa Y, et al. Activation of cardiac progenitor cells through paracrine effects of mesenchymal stem cells. *Biochemical And Biophysical Research Communications* 2008;374(1):11-16.

277. Post MJ, Laham R, Sellke FW, Simons M. Therapeutic angiogenesis in cardiology using protein formulations. *Cardiovasc Res* 2001;49(3):522-531.

278. Stanley N. Carson ET, Karen Overall, Stephanie Lee-Jahshan. Using Becaplermin Gel with Collagen Products to Potentiate Healing in Chronic Leg Wounds. The Wound Healing Society's 13th Annual Educational Symposium and Exhibition; 2003; Seattle, WA: Wounds; 2003.

279. Brown A, Ringuette M, Prestwich G, Bagli D, Woodhouse K. Effects of hyaluronan and SPARC on fibroproliferative events assessed in an in vitro bladder acellular matrix model. *Biomaterials* 2006;27(20):3825-3835.

280. Phelps EA, Landázuri N, Thulé PM, Taylor WR, García AJ. Bioartificial matrices for therapeutic vascularization. *P Natl Acad Sci Usa* 2010;107(8):3323-3328.

281. Ehrbar M, Metters A, Zammaretti P, Hubbell JA, Zisch AH. Endothelial cell proliferation and progenitor maturation by fibrin-bound VEGF variants with

differential susceptibilities to local cellular activity. *Journal of controlled release : official journal of the Controlled Release Society* 2005;101(1-3):93-109.

282. Wolbank S, Hildner F, Redl H, van Griensven M, Gabriel C, Hennerbichler S. Impact of human amniotic membrane preparation on release of angiogenic factors. *Journal of tissue engineering and regenerative medicine* 2009;3(8):651-654.

283. Metallo C, Mohr J, Detzel C, Pablo J, Wie B, Palecek S. Engineering the stem cell microenvironment. *Biotechnol Prog* 2007;23(1):18-23.

284. Ferguson MWJ, O'Kane S. Scar-free healing: from embryonic mechanisms to adult therapeutic intervention. *Philos Trans R Soc Lond, B, Biol Sci* 2004;359(1445):839-850.

285. Postovit L-M, Margaryan NV, Seftor EA, Kirschmann DA, Lipavsky A, Wheaton WW, et al. Human embryonic stem cell microenvironment suppresses the tumorigenic phenotype of aggressive cancer cells. *P Natl Acad Sci Usa* 2008;105(11):4329-4334.

286. Ungrin MD, Joshi C, Nica A, Bauwens C, Zandstra PW. Reproducible, ultra high-throughput formation of multicellular organization from single cell suspension-derived human embryonic stem cell aggregates. *PLoS One* 2008;3(2):e1565.

287. Bratt-Leal AM, Carpenedo RL, Ungrin MD, Zandstra PW, McDevitt TC. Incorporation of biomaterials in multicellular aggregates modulates pluripotent stem cell differentiation. *Biomaterials*;32(1):48-56.

288. Vidakovic B. Statistics for Bioengineering Sciences: With MATLAB and WinBUGS Support: Springer, 2011.

289. Folkman J, Cotran R. Relation of vascular proliferation to tumor growth. *Int Rev Exp Pathol* 1976;16:207-248.

290. Niblack W. An Introduction to Digital Processing. First ed: Prentice Hall, 1986.

291. Owen R. Mathematical Morphology. 1997 [cited 2911 April 4]; Available from: http://homepages.inf.ed.ac.uk/rbf/CVonline/LOCAL_COPIES/OWENS/LECT3/node3.html

292. Bae MH, Lee MJ, Bae SK, Lee OH, Lee YM, Park BC, et al. Insulin-like growth factor II (IGF-II) secreted from HepG2 human hepatocellular carcinoma cells shows angiogenic activity. *Cancer Lett* 1998;128(1):41-46.

293. Kim HJ, Kim TY. Regulation of vascular endothelial growth factor expression by insulin-like growth factor-II in human keratinocytes, differential involvement of mitogen-activated protein kinases and feedback inhibition of protein kinase C. *Br J Dermatol* 2005;152(3):418-425.

294. Pepper MS. Transforming growth factor-beta: vasculogenesis, angiogenesis, and vessel wall integrity. *Cytokine Growth Factor Rev* 1997;8(1):21-43.

295. Goumans MJ, Valdimarsdottir G, Itoh S, Rosendahl A, Sideras P, ten Dijke P. Balancing the activation state of the endothelium via two distinct TGF-beta type I receptors. *EMBO J* 2002;21(7):1743-1753.

296. Brown PD, Wakefield LM, Levinson AD, Sporn MB. Physicochemical activation of recombinant latent transforming growth factor-beta's 1, 2, and 3. *Growth Factors* 1990;3(1):35-43.

297. Giuffrida D, Rogers IM, Nagy A, Calogero AE, Brown TJ, Casper RF. Human embryonic stem cells secrete soluble factors that inhibit cancer cell growth. *Cell Prolif* 2009;42(6):788-798.

298. Kuzuya M, Kinsella JL. Induction of endothelial cell differentiation in vitro by fibroblast-derived soluble factors. *Exp Cell Res* 1994;215(2):310-318.

299. Gospodarowicz D, Cheng J. Heparin protects basic and acidic FGF from inactivation. *Journal Of Cellular Physiology* 1986;128(3):475-484.

300. Holley RJ, Pickford CE, Rushton G, Lacaud G, Gallagher JT, Kouskoff V, et al. Influencing hematopoietic differentiation of mouse embryonic stem cells using soluble heparin and heparan sulfate saccharides. *J Biol Chem*;286(8):6241-6252.

301. Hutchings H, Ortega N, Plouët J. Extracellular matrix-bound vascular endothelial growth factor promotes endothelial cell adhesion, migration, and survival through integrin ligation. *FASEB J* 2003;17(11):1520-1522.

302. Chen TT, Luque A, Lee S, Anderson SM, Segura T, Iruela-Arispe ML. Anchorage of VEGF to the extracellular matrix conveys differential signaling responses to endothelial cells. *J Cell Biol* 2010;188(4):595-609.

303. Lawlor K, Nazarian A, Lacomis L, Tempst P, Villanueva J. Pathway-based biomarker search by high-throughput proteomics profiling of secretomes. *J Proteome Res* 2009;8(3):1489-1503.

304. Luchansky MS, Bailey RC. Silicon photonic microring resonators for quantitative cytokine detection and T-cell secretion analysis. *Anal Chem*;82(5):1975-1981.

305. Heiskanen A, Hirvonen T, Salo H, Impola U, Olonen A, Laitinen A, et al. Glycomics of bone marrow-derived mesenchymal stem cells can be used to evaluate their cellular differentiation stage. *Glycoconj J* 2009;26(3):367-384.

306. Piecewicz S, Sengupta S. The Dynamic Glycome Microenvironment and Stem Cell Differentiation into Vasculature. *Stem Cells Dev* 2011.

307. Satomaa T, Heiskanen A, Mikkola M, Olsson C, Blomqvist M, Tiittanen M, et al. The N-glycome of human embryonic stem cells. *BMC Cell Biol* 2009;10:42.

308. Tateno H, Toyoda M, Saito S, Onuma Y, Ito Y, Hiemori K, et al. Glycome diagnosis of human induced pluripotent stem cells using lectin microarray. *J Biol Chem* 2011.

309. Cezar GG, Quam JA, Smith AM, Rosa GJM, Piekarczyk MS, Brown JF, et al. Identification of small molecules from human embryonic stem cells using metabolomics. *Stem Cells Dev* 2007;16(6):869-882.

310. Rubakhin SS, Romanova EV, Nemes P, Sweedler JV. Profiling metabolites and peptides in single cells. *Nat Methods*;8(4 Suppl):S20-29.

311. Yanes O, Clark J, Wong DM, Patti GJ, Sánchez-Ruiz A, Benton HP, et al. Metabolic oxidation regulates embryonic stem cell differentiation. *Nat Chem Biol* 2010;6(6):411-417.

312. Bakota EL, Wang Y, Danesh F, Hartgerink JD. Injectable Peptide Nanofiber Hydrogel as Delivery Agent for Stem Cell Secretome. *Biomacromolecules* 2011.

313. Wang Y, Bakota E, Chang BHJ, Entman M, Hartgerink JD, Danesh FR. Peptide nanofibers preconditioned with stem cell secretome are renoprotective. *J Am Soc Nephrol* 2011;22(4):704-717.

314. Benezra M, Vlodavsky I, Ishai-Michaeli R, Neufeld G, Bar-Shavit R. Thrombin-induced release of active basic fibroblast growth factor-heparan sulfate complexes from subendothelial extracellular matrix. *Blood* 1993;81(12):3324-3331.

315. Katrlík J, Svitel J, Gemeiner P, Kozár T, Tkac J. Glycan and lectin microarrays for glycomics and medicinal applications. *Med Res Rev* 2010;30(2):394-418.

316. Li B, Liu H, Zhang Z, Stansfield HE, Dordick JS, Linhardt RJ. Analysis of glycosaminoglycans in stem cell glycomics. *Methods Mol Biol* 2011;690:285-300.

317. Gerecht-Nir S, Dazard J-E, Golan-Mashiach M, Osenberg S, Botvinnik A, Amariglio N, et al. Vascular gene expression and phenotypic correlation during differentiation of human embryonic stem cells. *Dev Dyn* 2005;232(2):487-497.

318. Balconi G, Spagnuolo R, Dejana E. Development of endothelial cell lines from embryonic stem cells: A tool for studying genetically manipulated endothelial cells in vitro. *Arterioscler Thromb Vasc Biol* 2000;20(6):1443-1451.

319. Singelyn J, Dequach J, Seif-Naraghi S, Littlefield R, Schup-Magoffin P, Christman K. Naturally derived myocardial matrix as an injectable scaffold for cardiac tissue engineering. *Biomaterials* 2009.

320. Dai W, Wold LE, Dow JS, Kloner RA. Thickening of the infarcted wall by collagen injection improves left ventricular function in rats: a novel approach to preserve cardiac function after myocardial infarction. *J Am Coll Cardiol* 2005;46(4):714-719.

321. Ngangan AV, McDevitt TC. Acellularization of embryoid bodies via physical disruption methods. *Biomaterials* 2009;30(6):1143-1149.